PRODUCTION OF ACTIVATED CARBON FROM SOUTH AFRICAN SUGAR-CANE BAGASSE

By

Prathisha Baruth Devnarain

[BSc. (Eng.)]

submitted in fulfillment of the academic requirements for the degree of Master of Science in Engineering in the Department of Chemical Engineering, University of Natal, Durban.

Durban 2003

ABSTRACT

The South African sugar industry generates excessive amounts of sugar cane bagasse (~ 25 wt% of feed) as a byproduct during the extraction of sugar juice from cane. Although bagasse is extensively consumed in various processes, a substantial amount remains unexploited. The industry's core business is the production of refined sugar which involves among others, a step of decolourising raw sugar liquor. Activated carbons are well known adsorbents and their excellent decolourisation capabilities have been established since 1800 in the sugar industry. The possibility of making suitable in-house activated carbons from sugar cane bagasse to aid the decolourisation process of raw sugar liquor is of interest to the growing South African sugar industry.

The purposes of this research study were to develop an understanding on the manufacture of activated carbons from sugar cane bagasse, produce suitable activated carbons on a laboratory scale, characterize them and subsequently determine their sugar decolourisation capabilities under simulated conditions.

The application of the two-step physical method of processing was found to be the most effective and feasible route to produce activated carbons from sugar cane bagasse for the purposes of decolorizing unrefined sugar. A semi-batch process was developed whereby compressed sugar cane bagasse was pyrolysed under a nitrogen atmosphere at a heating rate of 10 °C/min to the final pyrolysis temperature for a desired hold time resulting in bagasse chars with a rudimentary pore structure. These bagasse chars were subsequently subjected to partial and controlled gasification with a steam/nitrogen mixture at higher temperatures to produce the final activated carbon product. Both pyrolysis and activation were carried out in a pyrolysis furnace that was modified to represent a fixed bed reactor system. The process was designed such that it included a steam supply and a gas cleaning system.

Feasible processing conditions were established by varying the temperature, hold time and partial pressure of steam in the pyrolysis furnace. The bagasse chars and final activated carbons were characterized with respect to surface area, pore volume, pore size distribution, methylene blue number, iodine number and molasses number. The optimum pyrolysis conditions were found to be at heating rate of 10 °C/min to the final pyrolysis temperature of 680 °C for a hold time of 1 hour, which gave rise to microporous carbons. Increasing the steam partial pressure and activation temperature during activation of bagasse chars resulted in the gasification reaction proceeding at a much faster rate leading to well developed mesoporous activated carbons having high adsorption capacity for large colour bodies present in molasses and sugar

liquor. This was achieved by activating bagasse chars at a temperature of 900 °C for 2 hours with a steam / nitrogen mixture of 1:0.6 which resulted in 50% burn-off being reached.

Excellent powder and granular activated carbons were produced from sugar cane bagasse fibres by the established process with the latter being mixed with refined sugar prior to pyrolysis and activating for half an hour extra. A typical final activated carbon produced in this research possessed a BET surface area of 995 m^2/g, pore volume of 0.82 cm^3/g, iodine number of 994 mg/g, molasses number of 700 and methylene blue number of 256 mg/g. High ash content in the bagasse raw material tends to decrease the surface area and pore volume for adsorption of the final activated carbon.

Both granular and low ash bagasse activated carbons possess high adsorption capacity to remove large colour bodies from molasses and brown liquor solutions and compare well with commercial Norit N2 carbon. Approximately 80% colour removal was achieved using 0.5 g carbon/ 100g brown liquor. The bagasse activated carbons were stable in acidic and basic brown liquor solution and maintained their high decolourisation potential. The ability of bagasse activated to replace commercial activated carbons has been proven in this study.

The option of producing both granular and powder activated carbons provide flexibility of the sugar industry to choose between batch and continuous adsorption systems during sugar decolourisation.

This research has established that the fact that excellent sugar decolourising activated carbons can be produced from South African sugar cane bagasse fibres. However, more research needs to be carried out in order for the sugar industry to take this project to the commercial stage and it is suggested that a pilot study and an economic study be carried out.
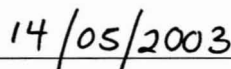
PREFACE

The research work presented in this thesis was performed at the University of Natal, Durban from February 2000 to February 2002. This project was supervised by Professor D. Arnold and Professor B. K. Loveday.

This thesis is presented as a full requirement for the degree of Master of Science in Chemical Engineering at the University of Natal. All work presented in this thesis is original unless otherwise stated and has not been submitted in part or whole to any other university as part of a degree. Sections of chapter 5 and 6 in this thesis have been published in the open literature and cited accordingly.
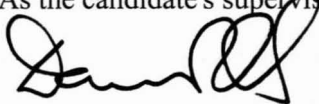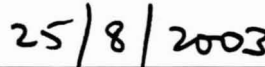
P.B. Devnarain   14/05/2003

P.B. Devnarain   Date

As the candidate's supervisor I have/have not approved this thesis/dissertation for submission

D.R. Arnold   25/8/2003

D.R. Arnold   Date

ACKNOWLEDGEMENTS

TABLE OF CONTENTS

LIST OF FIGURES

Chapter 2

Overview on Activated Carbon Production

Chapter 3

Bagasse

Chapter 4

Characterization of Activated Carbons

Appendix C

Characterization

LIST OF TABLES

Chapter 6

Results & Discussion

Appendix A

Molecular Dimensions

NOMENCLATURE

Symbol	Description
A	Absorbance of filtrate of the test activated carbon.
A_s	Absorbance of filtrate from the standard activated carbon
B	An empirical constant
c	BET constant
C	Concentration of reactant, moles
C_{av}	Average concentration of reactant, moles
C_b	Colour of blank
C_c	Integration constant
C_s	Colour of sample
D, D_{pore}	Pore diameter
E_a	Activation energy, kJ/mol
F	Final sample methylene blue concentration (mg/l) from graph x dilution
H_1	Molar adsorption of enthalpy in the first layer, kJ/mol
H_L	Molar enthalpy for condensation, kJ/mol
I	Initial methylene blue concentration, mg/l
k	Boltzmann constant, 1.38408×10^{-23} J/K
K	Reaction rate constant, min^{-1}
K_a	Adsorption capacity of adsorbent
K_o	Arrenhuis rate constant
L	Total pore length, nm or Å
L_k	Pore width, nm of Å
L_{pore}	Pore length, nm or Å
R	gas constant , 8.314 J/molK
M	Mass of adsorbent, g
$MBno.$	Methylene blue number, mg/g
MW	Molecular weight of the adsorbate
M_t	Molasses number of standard activated carbon (usually 400)
n	Moles adsorbate adsorbed on 1g adsorbent
n_c	Effect of concentration on adsorption capacity
n_m	monolayer capacity
N_A	Avagrado's number, 6.022×10^{23} number/mole
P	Partial pressure of the adsorbate
P_d	Pressure at which a cylindrical pore of radius r_k is desorbed

P_g	Pressure of gas
P_{Hg^-}	Pressure of Mercury
P_i	Pressure of component i
P_o	Saturation pressure of the liquid adsorbate at temperature T
P/P_o	Relative pressure
r_k	Kelvin radius, nm or Å
r_p	Pore radius, nm or Å
S_{BET}	BET surface area of the adsorbent , m^2/g
S_{cum}	Cumulative surface area, m^2/g
S_{ext}	External surface area, m^2/g
S_{micro}	Micropore surface area, m^2/g
S_{pore}	Pore Surface Area, m^2/g
t	Time of reaction in minutes
th	Statistical thickness, Å
t_l	Desorption layer of thickness
T	Temperature in Kelvin or °C
V	Volume adsorbed per gram of adsorbent
V_i	Molar volume of the gas at STP = 22.4litres/mol
V_m	Monolayer adsorption capacity in terms of volume, cm^3 gas/g adsorbent
V_{meso}	Mesopore Volume, cm^3/g
V_{micro}	Micropore Volume, cm^3/g
V_p, V_{pore}	Pore Volume, cm^3/g
V_{total}	Total pore volume, cm^3/g
V_s	Volume of contacting stock solution (acetic acid), litres
w_o	Initial weight of sample
w_t	Weight of the sample after time t
w_∞	Weight of sample left at the end of heating
w_{aa}	Dry weight after activation
w_{ba}	Dry weight before activation
w_{rm}	Dry weight of raw material after activation
X	Mass of solute adsorbed
ρ	Adsorbate liquid density
σ	Average area occupied by the adsorbate molecule, $Å^2$
θ	Contact angle between the solid and mercury
γ	Surface tension of the liquid adsorbate, 8.72 mN/m for nitrogen at 78 K

Å	Angstroms

Abbreviation	Description
BET	Brunauer –Emmet-Teller
BJH	Barett-Joyner-Halenda
nm	nanometers

INTRODUCTION

Activated carbon is the generic term referring to a wide range of amorphous carbon-based products having a high degree of porosity and an extensive intraparticulate surface area. Activated carbons are produced either chemically or physically from carbonaceous raw materials by thermal decomposition or pyrolysis followed by combustion or partial and controlled gasification with steam or carbon dioxide at high temperatures (700 – 1100 ^{o}C). These products can be found either in the powder or granular form. Activated carbons are unique and versatile adsorbents used extensively in industries such as food processing, pharmaceuticals, chemical, petroleum, mining, nuclear, automobile, water treatment and vacuum manufacturing. They are used to purify, decolourise, deodorise, dechlorinate, detoxicate, filter, recover salts by concentration and separation and used as catalysts and catalyst supports [Bansal et al, 1988].

These outstanding properties were discovered as early as 1550 BC by the Egyptians who used activated carbons in the form of carbonised wood to purify oils and store drinking water in charred wooden barrels on ships [Allen et al, 1998]. In India the ancient Hindus filtered their drinking water through charcoal [Bansal et al, 1988]. In 1773 Scheele [Dietz, 1944] recognised the adsorptive powers of carbon and charcoal by experiments with gases followed by Lowitz [Lowitz, 1786] in 1786, who discovered their ability to decolourise solutions. Wood char was used to purify cane sugar in 1808 [Hassler, 1974] and was applied to the developing sugar beet industry but Figuers in 1811 [Dietz, 1944] found that bone char had a much greater decolourising potential and thus was adopted by sugar industries. During the 19th century many studies were performed to produce activated carbons from various types of raw materials [Hassler, 1974]. In 1822 Busy [Busy, 1822] heated blood with potash in laboratory studies and produced carbons with 20 to 50 times the decolourising capacity of bone char. Hunter [Hunter, 1865] in 1865 revealed that coconut char had great gas-adsorbing power and Stenhouse

[Stenhouse, 1872] made a decolourising carbon from a mixture of flour, tar and magnesium carbonate. Stenhouse [Stenhouse, 1856] in 1854 described the forerunner to the modern gas mask using activated carbon for the protection against poisonous gases, which were used during World War I [Mackay *et al*, 1982]. In the late 1930s, activated carbons were produced from sawdust by chemically activating with zinc chloride for solvent recovery and removal of benzene from tower gas [Bansal *et al*, 1988]. As the demand for better adsorbents in industry increased so too did the development, manufacture and market for activated carbons from different precursors on an industrial scale. Currently, activated carbons are produced commercially from precursor materials such as coconut shells, coal, peat, nutshells, wood and lignite by either chemical or physical activation or a combination of both these methods [Bansal *et al*, 1988].

Activated carbons are manufactured such that they possess a large surface area, high degree of surface reactivity, universal adsorption effect and favourable pore size, which adds to the carbon's adsorptive properties such that the internal surface is accessible and the adsorption rate and mechanical strength are enhanced. These characteristics are also dependent on the type of raw material used. Commercial carbons have specific surface areas in the range of 800-1500m^2/g predominately contributed by the pores less than 2nm in diameter (micropores). Basically, an active carbon consists of a tortuous network of pores that can be differentiated into micropores (diameters less than 2nm), mesopores (diameters between 2 and 50nm) and macropores (diameters greater than 50nm). The macropores do not add significantly to the surface area property, but act as passageways to the micro and meso pores. The manufacturing process can be manipulated to obtain a specific pore size distribution of an activated carbon.

Activated carbons are used for both gas and liquid phase applications with 60000 tons/year (1988) being consumed for gas phase applications and 220000 tons/year for the latter. The per capita consumption of active carbon per year is [Bansal *et al*, 1988]:
- 0.5kg in Japan
- 0.4kg in United States
- 0.2kg in Europe
- 0.03kg in the rest of the world

The South African sugar industry produces large quantities of bagasse at about 51% moisture, after the extraction of sucrose from sugar cane. This fibrous by-product is utilised in several processes such as energy generation, papermaking, furfural and animal feed production, and landfill. However, excess bagasse still remains on some sugar mills and has to be removed.

Since bagasse is a highly carbonaceous material it can be perceived as a potential raw material in the production of activated carbon. Activated carbon has an extensive history in the sugar industry and is currently used on a large scale in USA and France for decolourisation of brown liquor in order to produce refined sugar. Another major contributing factor leading to research in manufacturing activated carbon from bagasse, is that all activated carbon used in South Africa is imported at a relatively high cost. Thus, manufacturing activated carbon locally from this waste material would add value to a no-value by-product and thereby provide a significant competitive advantage to the South African sugar industry.

South African bagasse is rather unique as it is generated via the diffuser process whereas most sugar cane bagasse material is produced through the conventional milling process. Powder and granular activated carbons have in fact been successfully produced from milled sugar cane bagasse material in other countries. The option of producing powder activated carbons from South African sugar bagasse offers the flexibility of burning spent powder activated carbon as fuel in the boilers instead of regenerating them, thereby reducing costs and harm to the environment.

Hence the objectives of this study were to:
- review the literature and the "state-of-the-art" manufacture of activated carbon from bagasse,
- produce suitable activated carbons on a laboratory scale, and subsequently characterize them,
- test the activated product under simulated conditions in the sugar environment and
- determine the activated carbon requirements of a local sugar-milling industry in terms of specific volumes.

Consequently the body of this thesis encompasses all work carried out in meeting these objectives, such that the next two chapters are dedicated to a literature survey on producing activated carbon from bagasse and other precursors including various types of process methods and equipment. The characterisation of activated carbon with respect to surface area, pore volumes, pore size distribution, and their ability to adsorb methylene blue, iodine, and molasses and decolourise sugar are also discussed together with their fundamental theories. A pyrolysis furnace has been modified such that both pyrolysis and partial gasification take place batch-wise in a single unit. A method has been established and adopted to produce high surface area powder and granular activated carbon by varying process conditions and is described in the rest

of this work accompanied by characterisation of the resulting activated carbons produced from bagasse. Their applicability in the sugar industry has been tested and is presented in this work.

OVERVIEW ON ACTIVATED CARBON PRODUCTION

Activated carbons are generally manufactured from carbonaceous raw materials in two main steps, the thermal decomposition of the raw material in an oxygen depleted atmosphere at temperatures below 800 °C and the activation of the resulting carbonised product [Bansal *et al*, 1988]. The final activated carbon product depends on the nature of the carbonaceous raw material, the history of the carbonisation / pyrolysis process, the activating agent and the conditions of the activating process. Figure 2.1 below illustrates a general flow diagram summarised by Bansal *et al* [1988] for the production of activated carbon from any carbonaceous raw material.
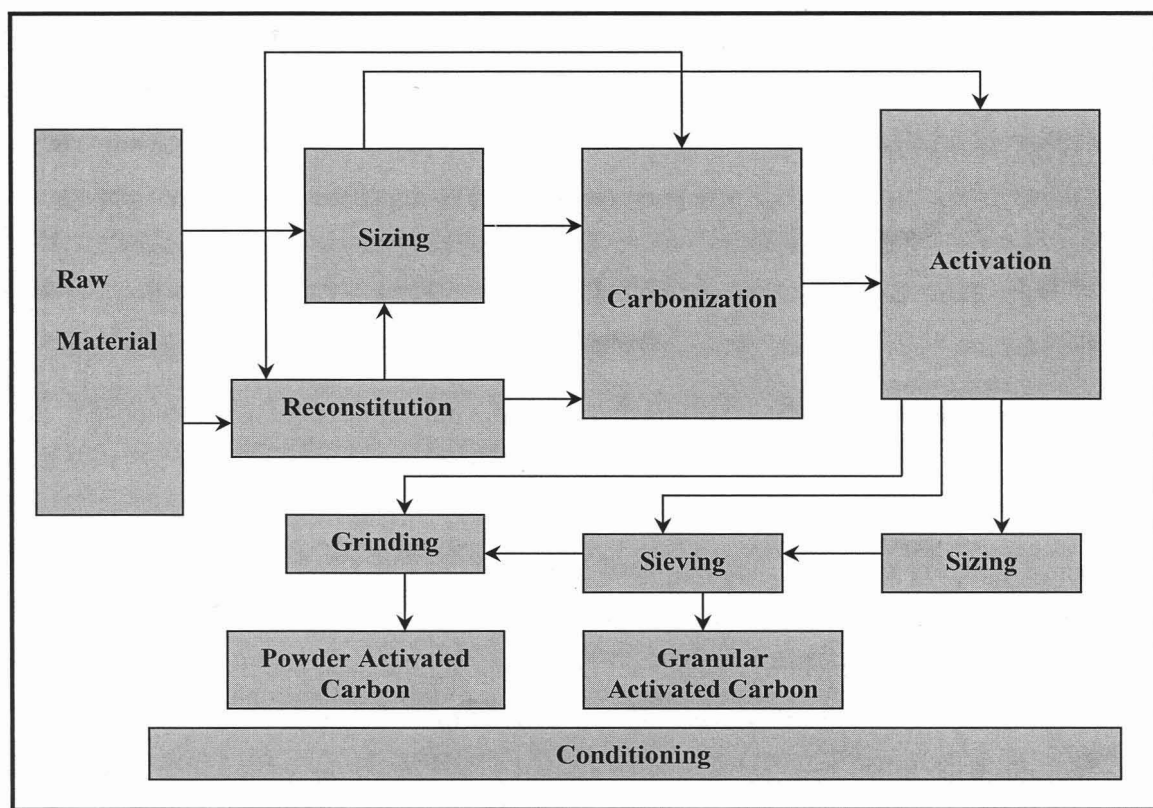
Fig 2.1: Basic process flow sheet for the production of activated carbon [Bansal *et al*, 1988]

Sizing involves the breakdown of the raw material into lumps or granules to ensure effective handling in the subsequent operations. In some cases the raw material is first pulverised and then agglomerated by extrusion, briquetting or tableting in the reconstitution stage. During carbonisation, most of the non-carbon elements such as hydrogen and oxygen are removed as volatile gaseous products; leaving behind low surface area chars having a rudimentary pore structure [Lua and Guo, 1999]. The pore structure is further enhanced in the activation section by oxidising the resultant carbons with an oxidising agent at elevated temperatures.

The activation can be carried out using either a physical or chemical method or sometimes a combination of both these methods [Mattson and Marck, 1971]. Physical activation subjects the carbonised products to partial and controlled gasification at higher temperatures (above 800 °C) with mild oxidising gases like steam, carbon dioxide (CO_2), air, or a mixture of these to produce final products with well developed porosities and high surface area. During chemical activation, inorganic additives and metallic chlorides such as zinc chloride ($ZnCl_2$), sulphuric acid (H_2SO_4), phosphoric acid (H_3PO_4) and potassium hydroxide (KOH) are incorporated into the starting material prior to carbonisation [Allen *et al*, 1998]. These additives act as dehydrating agents as well as oxidants so that carbonisation and activation takes place simultaneously around 250- 650°C.

Factors that also affect the pore volume, pore size distribution, surface area and mean pore diameter of the final activated carbon product [Bansal *et al*, 1988] are:
- the heating rate during carbonisation,
- the final carbonisation temperature and hold-time,
- the temperature and length of the activation period.

2.1 Raw Materials

Any inexpensive raw material having a high carbon and low inorganic content can be used as a precursor for the preparation of activated carbon [Bansal *et al*, 1988]. In early production processes high quality activated carbons were produced from wood, peat, wastes of vegetable origin (fruit stones, nutshells and sawdust) and bone material. The most common commercial feedstocks for the production of activated carbons are wood, anthracite and bituminous coal, lignite, coconut shell and peat, with wood having the greatest production capacity [Pollard *et al*, 1992]. Environmental awareness and the demand for low-cost carbons introduced the concept of using agricultural by–products such as sugar cane bagasse, rice straw, soybean hulls, rice hulls, olive and grape bagasse, palm wastes, etc.

As can be seen in figure 2.1 activated carbons can exist in powder or granular form. The properties and form of activated carbon produced, as well as its application in industry depend very much on the nature of the raw material. Raw materials having low inorganics will reduce the ash content in terms of percentage in the final product as the ash percentage increases many times during the manufacturing process due to the loss of volatiles and carbon. Density and volatile content tends to affect the manufacturing process [Bansal *et al*, 1988]. Soft compressible raw materials having low density and high volatile content such as rice hulls, rice straw and sugar-cane bagasse produce large pore volume and low density activated carbons and are used as a source of powder activated carbons for liquid phase applications [Pollard *et al*, 1992;, Yousseff and Mostafa, 1992; Teker *et al*, 1997; Lavarack, 1997; Bernado *et al*, 1997; Mackay and Roberts, 1982a]. According to Johns *et al* [1998] these materials can be good precursors for the production of granular activated carbon by being mixed with suitable binders and compressed into pellets or briquettes thereby increasing their density before pyrolysis and activation. Studies carried out by Morgan and Fink in 1946 [Morgan and Fink, 1946] on different binders and base materials for granular activated carbon production indicated that the characteristics before activation were due to the binder and after activation the characteristics were of the raw material.

In contrast coconut shells, fruit pits and nutshells are hard, dense, not easily compressed and have high volatile contents which produce hard, granular activated carbons with high micropore volume and are used especially for vapour phase and some liquid phase applications usually involving gold recovery in mineral processing.

Volume, cost, storage life and workability of the raw material are other vital factors that contribute to producing high quality activated carbons. Raw materials, used to produce activated carbons on a commercial scale, together with their properties and uses presented by Bansal *et al* [1988] are tabulated in table 2.1.

Bansal *et al* [1988], by his illustration clearly reinforces the concept that raw materials with high carbon content and low ash content irrespective of their density produce activated carbons with unique properties dependent on their applications in industry.

Table 2.1: Properties of some raw materials used in the production of activated carbon [Bansal *et al*, 1988]

Raw Material	Carbon %	Volatiles %	Density kg/litres	Ash %	Texture of activated Carbon	Uses of Activated Carbon
Soft wood	40-45	55-60	0.4-0.5	0.3-1.1	Soft, large pore volume	Aqueous phase adsorption
Hard wood	40-42	55-60	0.55-0.8	0.3-1.2	Soft, large pore volume	Aqueous phase adsorption
Lignin	35-40	58-60	0.3-0.4	-	Soft, large pore volume	Aqueous phase adsorption
Nutshells (Coconut)	40-45	55-60	1.4	0.5-0.6	Hard, large micropore volume	Vapour phase application
Lignite	55-70	25-40	1-1.35	5-6	Hard, small pore volume	Waste water treatment
Soft coal	65-80	20-30	1.25-1.5	2-12	Medium hard, medium micropore volume	Liquid and vapour phase adsorption
Hard coal	85-95	5-10	1.5-1.8	2-15	Hard, large pore volume	Gas vapour adsorption
Petroleum coke	70-85	15-20	1.35	0.5-0.7	Medium hard, medium pore volume	Waste water treatment

2.2. Carbonisation

The carbonisation step involves the thermal decomposition of the carbonaceous raw material in an inert atmosphere. During this stage all-volatile, non-carbon elements are removed, and a non-graphitisable char with a fixed carbon skeleton made up of aromatic sheets and strips, giving rise to a rudimentary pore structure, are produced. This process is usually carried out at temperatures below 800°C in units like multiple hearth furnaces or rotary kilns using an inert gas [Bansal *et al*, 1988].

The quality of the resulting char depends on the following pyrolysis parameters:

- the nature and physical state of the raw material (as discussed above in Section 2.1)
- the heating rate to the final pyrolysis temperature
- the final pyrolysis temperature and
- the hold-time at the final pyrolysis temperature.

Different raw materials with varying carbonisation conditions result in carbons with unique characteristics and adsorption properties.

MacKay and Roberts, [1982] concluded in their studies that lower heating rate results in lower volatilisation and higher carbon yields due to increased dehydration and more stable polymeric components. In further studies they also found that the basic microporous structure of the char was already created by 500 ^{O}C, even though some of these pores become blocked with pyrolysis products because these could become available when the carbons are further subjected to high temperature treatment.

Zulkarnain *et al* [1993] found that by varying the pyrolysis heating times and temperature for mangrove wood, the optimum pyrolysis conditions were at a final pyrolysis temperature of 500°C and hold time of 3hours with respect to surface area and pore diameters. Their results were based on the iodine number which is a relative indictor of porosity and surface area. The resulting carbons possessed a higher iodine number (503m^2/g) and larger pore diameters (>10μm) compared to a coconut carbon produced under the same set of conditions.

2.2.1. Effect on Activation

The history of the pyrolysis process has a profound effect on the activation step and the quality of the activated carbon. Smisek *et al* [1970] investigated the effects of pyrolysis conditions on the activation process and the final product. They found that the reactivity of the activating gas in the activation stage was influenced by:

- the pyrolysis heating rate below 500 ^{O}C,
- the period of exposure to the pyrolysis temperature near 900 ^{O}C and
- the nature of the oxidising atmosphere.

Thus, during the initial stages of the activation process, chars produced a temperatures lower than 500°C gasify at a faster rate due to the chars undergoing further pyrolytic decomposition during activation resulting in weight loss independent of the activating gas. When the weight loss reaches above 20-30%, the low temperature chars gasify at the same rate as the high temperature chars. However, chars prepared at low heating rates reacted more slowly during the activation step.

Preparing chars at low heating rates to final pyrolysis temperatures above 500°C would possibly enable better control of the gasification reactions and increase reactivity of the activating gas

during the activation step such that the desired properties of the final activated carbon can be achieved.

2.2.2. Reactions during Pyrolysis

Smisek *et al* [1970], from their study also describe the phenomena that occur with increasing temperature as carbonisation proceeds for the case of wood carbonisation. Dehydration of the feedstock occurs up to a temperature of $170^{O}C$, followed by partial degradation above this temperature such that carbon dioxide (CO_2), carbon monoxide (CO) and acetic acid ($C_2H_4O_2$) are evolved. Between 270 and 280 ^{o}C, exothermal decomposition occurs and a large amount of tar, methanol and other substances are released. Carbonisation is almost complete around 400-600 ^{o}C. During this process, the resulting char has a carbon content of approximately 80%. The carbonisation process is generally carried out at a fast enough rate to minimise the contact between the pyrolysed and volatile product.

2.2.3. Effect on Final Product

According to Bansal *et al*,[1988], the pyrolysis step comprises of two stages having a great effect on the final product. The first is the softening period whereby temperature control has a major impact on the type of char obtained, followed by the second stage where the char begins to harden and shrink. Shrinkage of the char influences the development of porosity in the char. In the case of soft coal, a slow heating rate in the softening period will allow the gases to escape through the pores without collapsing or deforming them. For wood, lignin and petroleum coke (hard materials), low heating rate can produce denser and harder chars. During the softening stage, compression can be applied to chars for the low-density materials in order to obtain activated carbons with properties comparable to those prepared from dense materials (example coconut carbon.) Low heating rates can promote shrinkage, which reduces pore volume, but this can be later developed in the activating step.

Addition of other materials prior to carbonisation also influences the final product. Drozhalina *et al* [1984], added peat to brown coal prior to carbonisation at 800-900 ^{o}C and discovered that the strength of the carbon improved, porosity developed and as the temperature increased there was an increase in micropore and macropore volume.

Chars developed under specific pyrolysis conditions can also be used successfully without any further processing, but their adsorptive potential (surface area, porosity and surface oxide groups) can be increased by activation [Allen *et al*, 1998].

2.3. Activation

Activation aims at enhancing the pore volume and enlarging the diameter of the pores, which were created during the pyrolysis process and also to create new porosities. The large surface area of an active carbon is the result of the activation process in which the char with little internal surface area is oxidised at temperatures between 750-1000 $^{\circ}$C. Here again it is re-emphasised that the type of raw material and the carbonisation process predetermines the pore structure and pore size distribution of the activated carbon. During the first phase of the activation step, the active oxygen in the activating agent burns away the tarry pyrolysis off-products trapped within the pores, thereby initialising porosity development (development of a microporous structure). In the latter phase, the significant effect is the formation of large-sized pores by the widening of existing pores or by the total burnout of the walls between adjacent pores. The latter phase brings about a reduction in volume of micopores and an increase in meso- and macropore volume [Allen *et al*, 1998].

The degree of activation is measured by the extent of burn-off the carbon material. The type of pores generated by the degree of activation is shown in table 2.2 [Dubnin and Zaverina, 1949].

Table 2.2: Pore types as function of degree of burn-off [Dubnin and Zaverina, 1949]

Degree of burn-off /(%)	Pore Type	Pore size
< 50	Micropores	< 2nm
> 75	Macropores	> 5nm
50-75	Mixed pores	All types

The precise activation method of carbons are not known since they are mainly "kept under lock and key" by each manufacturer.

Generally, there are two methods of activation, physical and chemical activation. Chemical activation is a single step process incorporating both carbonisation and activation by thermal decomposition of the raw material that has been impregnated with the chemical activating agents. In contrast, physical activation is a two-step process involving partial and controlled

gasification of the chars produced after the pyrolysis step with oxidising gases such as steam or carbon dioxide in the temperature range of 800-1100 $^{\circ}$C.

2.3.1. Chemical Activation

Chemical activation is a single-stage process and is carried out by the raw material being impregnated with the activating agent in the form of a concentrated solution usually by mixing or kneading followed by extruding and then pyrolysing in a rotary kiln between 400 and 800 $^{\circ}$C in an oxygen depleted atmosphere. The most widely used chemical activating agents are phosphoric acid (H_3PO_4), zinc chloride ($ZnCl_2$), sulphuric acid ($H2SO_4$), chloride salts of magnesium (Mg) and ferric iron, sodium carbonate (Na_2CO_3), sodium and calcium hydroxide, and potassium sulphide. These chemicals act as dehydrating agents and influence the pyrolytic decomposition and inhibit the formation of tars as well as decrease the formation of acetic acid, methanol, etc. and increase the yield of carbon [Allen et al, 1998, Bansal et al, 1988]. After calcination, the activated carbon product is cooled and washed to remove the activating agent, which is recycled (see fig.2.2).
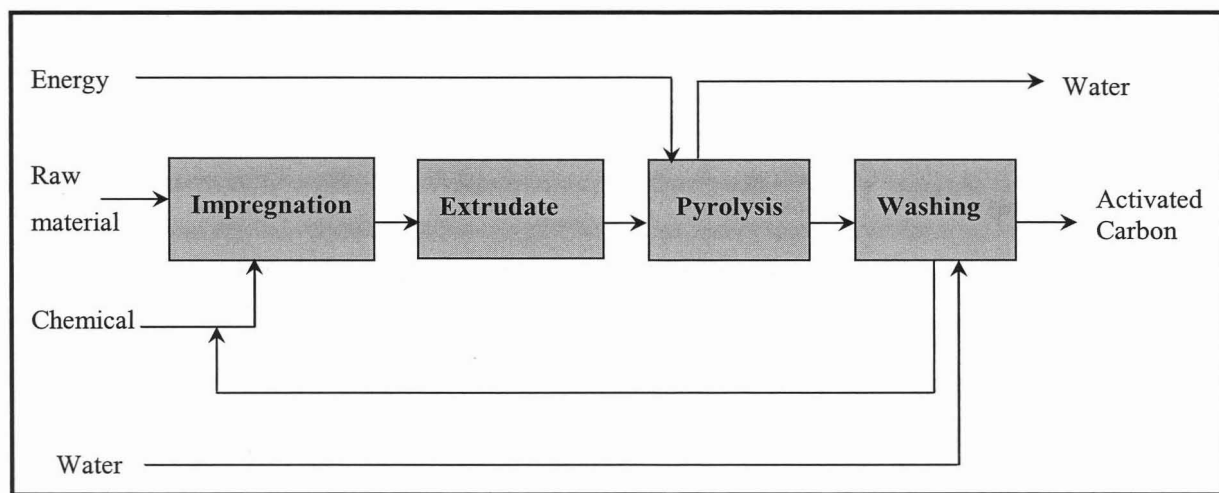
Figure 2.2: Process flow diagram for chemical activation

There have been claims that since activated carbons produced by chemical activation require a lower temperature (400–800 $^{\circ}$C) than physical activation (800-100 $^{\circ}$C) and fewer stages; they have a more developed porous structure [Rodriguez-Reinoso and Molina-Sabio, 1992, Allen et al, 1998]. However, this developed pore structure is associated with wide micropores and narrow mesopores [Allen et al, 1998] and its adsorption capacity seems to be limited towards molecules in this particular range. The developed pore structure is also determined by the type and amount of chemical activating agent used. Therefore, chemical activation is associated with

high operating costs due the high cost of chemicals and the extra washing step needed in the process.

2.3.1.1 Effects of Chemical Activators

Rodriguez-Reinoso and Molina-Sabio [1992], after working with zinc chloride ($ZnCl_2$) as the activating agent to produce activated carbons concluded from their observations of weight loss, departure of volatiles, weakening of the structures and increased elasticity, that during impregnation the chemical activator accesses the interior of the raw material and causes hydrolysis reactions to occur. They also noticed that particle swelling accompanies these hydrolysis reactions and the formation of tars was prevented during pyrolysis. $ZnCl_2$ causes hydrogen and oxygen atoms to be stripped away as water instead of hydrocarbons or oxygenated organic compounds leading to a high carbon yield. Furthermore, from their study they were able to conclude that zinc chloride ($ZnCl_2$) tends to produce an activated carbon consisting of mainly of meso and micropores.

The degree of impregnation determines the pore size distribution in the final product. The greater the degree of impregnation, the less ordered the distribution of the chemical within the particle becomes thus, resulting in a heterogeneous pore size distribution. Teng *et al* [1999] also found with his studies using potassium hydroxide (KOH) that the porosity development was affected by the degree of impregnation.

Bansal *et al*, [1988] relates that in the case of sawdust, phosphoric acid was used as the activator and the final product depended on the degree of impregnation, the heating rate of wood-acid mixture, the temperature at which the wood-acid mixture was kept in the oven and the composition of the combustion gases used for heating. *et al*, [1999] proved in their studies that at a 50 % phosphoric acid concentration and temperature of 500°C mesoporous activated carbons from cotton stalks could be prepared. Laine *et al* [1991] suggested that during phosphoric acid activation, a "skin" of phosphate is formed protecting the internal carbon structure and in so doing protects the carbon from excessive burn-off.

Hu *et al*, [1996] found that the surface area and porosity can be specifically modified by the use of potassium hydroxide (KOH) activation and are dependent on the soak time and impregnation ratios. Adding to this deduction Otowa *et al*, [1995] showed that an active carbon with a surface area in excess of $3000m^2/g$ could be prepared by mixing petroleum coke with excess potassium hydroxide (KOH) prior to pyrolysis.

Ahmadpour et al, [1998] did a comparative study using zinc chloride ($ZnCl_2$) and potassium hydroxide (KOH) to produce activated carbons from macadamia nutshells and found that carbons activated with potassium hydroxide (KOH) resulted in a more microporous structure while those activated with zinc chloride ($ZnCl_2$) were more mesoporous. Hence, the type of chemical activator is important in producing an activated carbon with a specific pore size distribution.

2.3.2. Physical Activation

Physical or thermal activation generally follows the carbonisation process whereby the resultant chars from pyrolysis develop an extended surface area and enhanced porosity of molecular dimensions in this stage. The carbonisation stage is a pre-requisite as it dehydrates the precursor material, thereby preparing it for activation [Allen, et al, 1998]. Activation is carried out at elevated temperatures between 800 and 1100°C with oxidising gases such as steam, carbon dioxide (CO_2), and air and sometimes by a combination of these gases in process units such as rotary kilns, multiple hearth furnaces or fluidised beds. Activation initialises porosity development and then develops the microporous structure by partial and controlled gasification of the pyrolysis off-products (tarry matter) that were trapped in the pores during pyrolysis and the more reactive parts of the carbon skeleton to carbon monoxide (CO) and carbon dioxide(CO_2) [Bansal et al, 1988; Allen et al, 1998]. Buczek et al [1999] in his studies state that activation is a heterogeneous gas-solid reaction that can be limited by diffusion, which brings about the burning of the particle at the periphery rather the interior.

The oxidation reactions that occur with the oxidising gases steam, carbon dioxide and air are as follows:
Steam:

$$C + H_2O \rightarrow CO + H_2 \qquad \Delta H = -121.42 \text{ kJ} \qquad (2.1)$$

This is accompanied by the water-shift-gas reaction that occurs on the solid surface [Tsai, 1982]:

$$CO + H_2O \leftrightarrow CO_2 + H_2 \qquad \Delta H = +41.87 \text{ kJ} \qquad (2.2)$$

Carbon dioxide:

$$C + CO2 \rightarrow 2CO \qquad \Delta H = -163.29 \text{ kJ} \qquad (2.3.)$$

Air:

$$C + O_2 \rightarrow CO_2 \qquad \Delta H = +386.86 \text{ kJ} \qquad (2.4)$$

and

$$C \ + O_2 \qquad \rightarrow \quad 2CO \qquad \qquad \Delta H = +225.67 \text{ kJ} \qquad (2.5)$$

In activation with oxidizing agents, the properties of the activated carbon produced are determined by [Hassler, 1974]:

- the chemical characteristics and the concentration of the oxidising gas
- the temperature at which the activation reaction occurs
- the degree of activation (activation time) and
- the quantity and mineral matter in the precursor carbon

Reactions with steam and carbon dioxide are endothermic and thus can be easily controlled during activation. On the other hand reactions with oxygen are highly exothermic and very difficult to control and thus lead to non-uniform products. Hence manufacturers disregard oxygen as the activating agent as it is seldom practicable.

Hassler [1974] in his publication stresses that while steam may be preferable to carbon dioxide; the optimum conditions for an activated carbon are still directly linked to the activated carbon's ultimate function and to a much greater extent on the history of pyrolysis of the char.

Steam activation takes places place at high temperatures (800-900°C) to provide a rapid rate of oxidation, but temperatures above 1000°C are avoided as they decrease the adsorptive power of the activated carbon. From the studies of Garner *et al* [1980] and Geogova *et al* [1994] on steam activated carbons it was deduced that the surface area and porosity increase with increasing temperature and time, although product yield decreases with time.

Carbon dioxide (CO_2) activation is less energetic than steam, and thus requires a higher temperature. Rand and Marsh [1971] observed that by adding carbon monoxide (CO) to carbon dioxide (CO_2) in the gas stream slows down the rate of gasification and leads to a well developed microporosity of the activated carbon. This increased microporosity is accompanied by an increase in surface area [Jankowska *et al*, 1996; Lu and Chung, 1996].

Steam activation is three times much faster than carbon dioxide (CO_2) activation [Pashchenko et al, 1996]. Tourkow *et al* [1977] have revealed that with increasing degree of activation, steam activated carbons have a higher mesoporisity development compared to carbon dioxide activated carbons. Therefore, physical activation with steam as the activating agent at high temperatures tend to produce an activated carbon having a wide pore size distribution and high surface area within a much shorter time. Thus, activated carbons produced via the steam

activation process would show high adsorption potential for large colour bodies present in unrefined sugar liquor. This assumption is based on their pore size distribution lying mainly in the mesoporous range.

2.3.2.1. Mechanisms of Activation

Activation occurs by the activating agent initially burning off the disorganized carbon that leads to the opening up of blocked pores and subsequently burns the aromatic ring system to widen pores and produce more active sites. This leads to increased surface area and greater porosity with the remaining carbon atoms arranged in configurations having specific affinities. The adsorptive potential of the active carbon can be developed either at the initial period of activation or at the late stages or at a consistent rate throughout the entire period.

Tourkow *et al* [1977] studied the effects of carbon dioxide, steam and oxygen as activating agents on brown coals at 900 ^{O}C. He found that at a low burn-off (low weight loss) all three produced microporous activated carbons but of varying pore size distribution, and the micropore volume was the greatest with oxygen. As the percentage burn-off increased, the varying pore size distributions became more pronounced. Progressive pore development was observed with water vapour until 70% burn-off resulting in a wide pore size distribution such that all pore sizes were present. Furthermore, with steam activation the pore volume increased but surface area was not affected. The micropores contributed to 33 % of pore volume and 63 % to surface area. Even though burn-off increased, the activation with carbon dioxide, maintained the microporosity thus leading to a more uniform pore size distribution with 73% of the micropores contributing to pore volume and 90% to surface area. However, the total pore volume decreased. The effective surface area for carbon dioxide and steam activation was almost the same. For oxygen, activation only occurred in the initial stages and as activation increased the total adsorption potential decreased (low pore volume and surface area) due to the blocking of the micropores as surface oxygen structures were produced at their entrances.

A detailed study on the steam activation of carbonised wood carried out at 950 ^{o}C by Caron (1985) and communicated to Bansal *et al* [1988] demonstrates the effect of varying degrees of activation on the BET (nitrogen) surface area, the benzene index, methylene index and the molasses index of the activated carbons produced (see fig. 2.3). Increasing weight loss resulted in an increase in the activated carbons adsorption capacity for nitrogen, benzene, methylene blue and molasses with the rate of adsorption being faster for the larger molecules.

The formations of the different pore sizes in the final activated carbon produced via steam activation were confirmed by the adsorption of molecules having different molecular dimensions:

Nitrogen: 3 – 4 Å

Benzene: 5 – 6 Å

Methylene Blue: 8 – 9Å

Molasses: 12 – 20Å
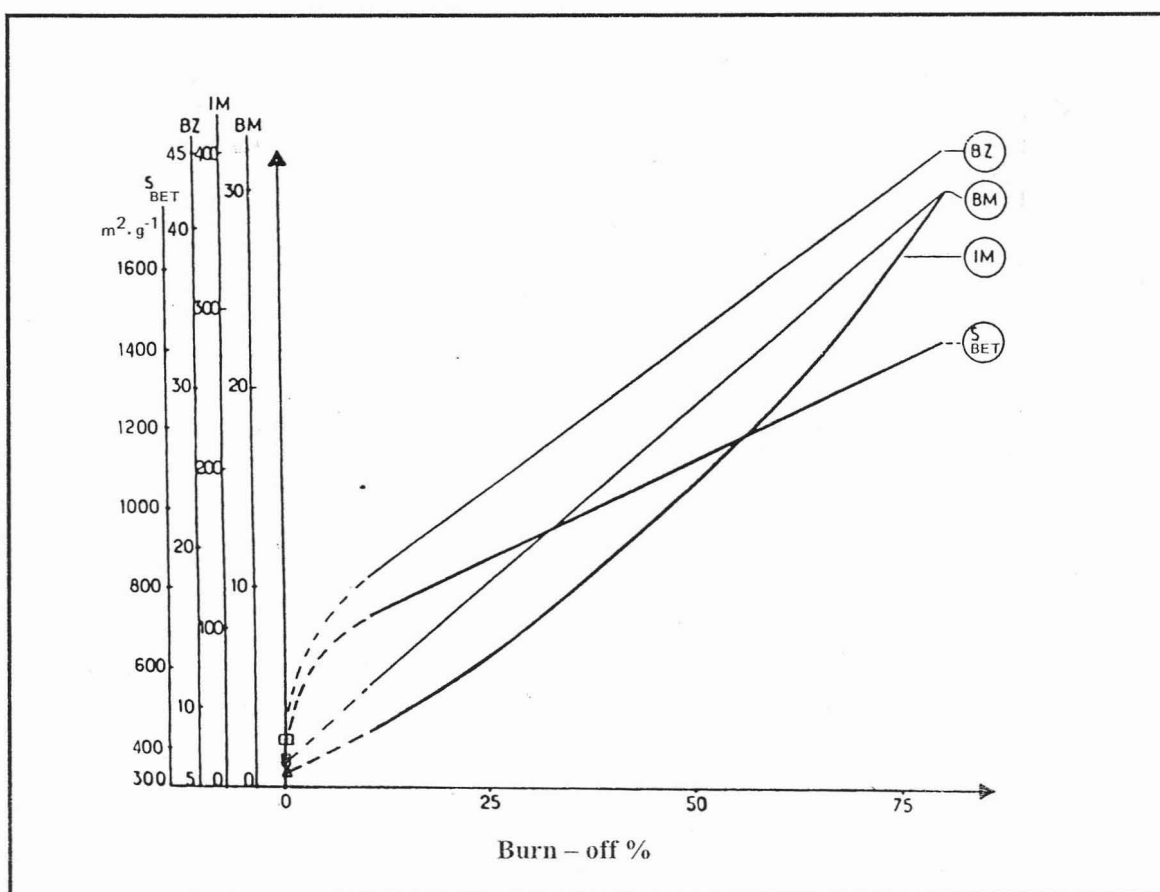
Figure 2.3: Adsorption potential of activated carbon produced from pine wood char activated with steam at 950 °C at different burn-off %. (S$_{BET}$ = surface area, BZ=Benzene index, BM= Methylene Blue index, IM = molasses index) [From Bansal *et al*, 1988]

However, as burn–off increases further there also lies a maximum adsorption capacity for each molecule (see fig 2.4).
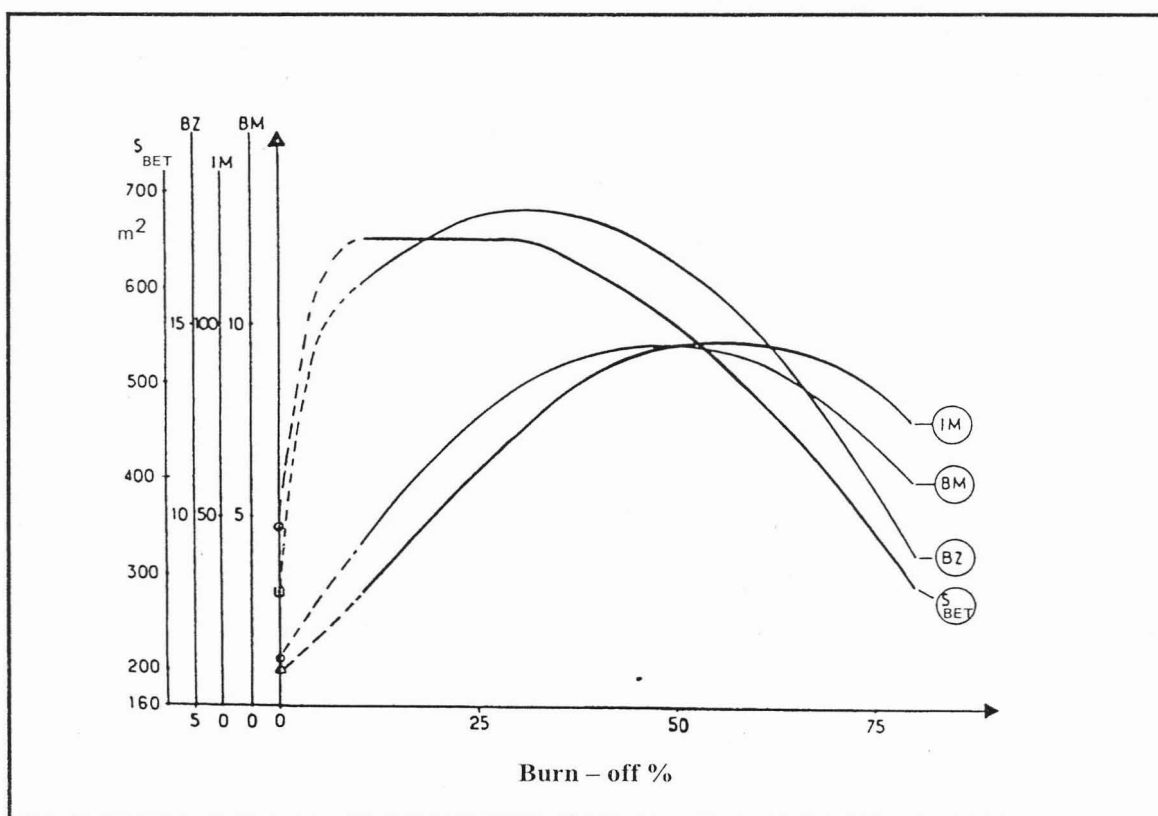
Figure 2.4: Adsorption potential of activated carbon produced from pine wood char activated with steam at 950 °C at different of burn-off % showing optimum conditions, (S_{BET} = surface area, BZ=Benzene index, BM= Methylene Blue index, IM = molasses index) [From Bansal *et al*, 1988].

The above figure (fig 2.4) illustrates that in the initial stages the tarry matter blocking the pores and more accessible single aromatic sheets of the carbon skeleton is burned off producing micropores (see BET surface area and benzene index. As these become limited, the walls of adjacent micropores are burnt giving rise to macropores (see methylene blue number and molasses index).From this study it was concluded that different properties of activated carbon could be produced from the same carbonised material by varying the duration of the activation process.

BAGASSE

In many countries sugar cane is the major raw material for the production of sugar. During sugar processing many by-products are generated [Lutz *et al*, 1998]. In South Africa, the sugar industries crush just over 21 million tons of sugar cane (1999 - 2000 seasonal period) and generate about 5 million tons of bagasse (51 % moisture) as a by-product. Sugar-cane bagasse, also called the cane chaff is the fibrous residue that remains behind after sucrose has been extracted from sugar cane. This waste material is currently:

- burnt as fuel in order to provide energy required by the sugar factory since it is a high energy source.
- processed into pulp for papermaking in the paper industry.
- compressed into furniture material in the furniture industry .
- used as a reactant in the chemical industry to produce furfural ($C_5H_4O_2$) and
- mixed with animal feed.

In spite of being extensively used, quantities of bagasse still remain at the sugar mills and have to be effectively disposed. Large piles of bagasse that remain over long periods lead to fires, fermentation, etc which subsequently impacts on the environment. Since bagasse is a lignocellulosic material having high carbon content, the possibility of it being a potential feedstock in the production of activated carbon has been of great interest to the South African sugar industry. Activated carbon's excellent decolourising capabilities have been well known in the sugar industry from as early as the late 1800's when bone char was used to decolourise raw sugar. Currently, sugar industries in France, Malawi and USA use commercial activated carbons to remove colour from unrefined sugar. At present, the South African sugar industry uses various alternative decolourisation processes to that of the activated carbon process. The main contributing factor is that the use of activated carbons is associated with high operating and capital costs since they have to be imported in South Africa.

The advantages of successfully converting bagasse into activated carbons are that it would:

- add value to a low-value product,
- reduce costs in the decolourisation processes since in-house activated carbon would be used and,
- the spent carbons can be burnt as fuel to generate energy thereby reducing environmental concerns and eliminating costs with respect to regeneration.

No documented research has been found on South Africa bagasse with respect to activated carbon manufacture and this research forms an integral basis on the utilization of SA bagasse in the activated carbon market. However, due to increasing market demands for inexpensive adsorbents and environmental consciousness, researchers have in fact investigated the use of lignocellulosic wastes such as bagasse as alternative feedstocks for the production of activated carbon in other countries [Pendyal et al, 1999]. In their studies sugar cane bagasse has been a successfully converted into activated carbons and much of their investigations are elucidated exclusively in this chapter.

3.1. Generation of Bagasse at a sugar mill in South Africa

The generation of bagasse during the sucrose extraction process at a typical South African sugar mill is illustrated in fig 3.1. Sugar cane after being harvested at the sugar-cane plantations is transported to the mill on trucks. The trucks containing the harvested sugar cane are first weighed on a weighing bridge to determine the amount of cane that is delivered to the mill. The cane is hoisted in bundles and placed on a conveyor. The cane is conveyed to the particle reduction section where the cane is firstly cut into pieces by revolving cane knives thereby exposing the cell tissues and structure to enable efficient juice extraction. The cane is further reduced in size in a shredder. The crushed cane passes through passes through a multicell countercurrent diffuser where the sugar juice is extracted and the fibrous residue is left behind. The crushed cane proceeds through the diffuser by a countercurrent flow of water known as water of imhibtion or maceration. The extracted juice combines with this water to form a dilute concentration of sugar juice. The alternative to diffusion is milling extraction. In this case, the shredded cane moves through a crusher machine consisting of a set of rollers that crushes the cells and tissues and extract the sugar juice. The stream leaving the diffuser contains a high percentage of sugar juice mixed with fine bagasse fibres. The fine bagasse called bagacillo is separated from the juice by a juice screener. The bagacillo is sent back to the diffuser. Bagasse fibres take approximately one hour to pass through the diffuser to the de-watering mills where, bagasse is removed at approximately 51% moisture. The water from the

dewatering mills is recycled to the diffuser and the bagasse is sent to storage. The bagasse is usually stored in piles exposed to the atmosphere at the sugar factory.
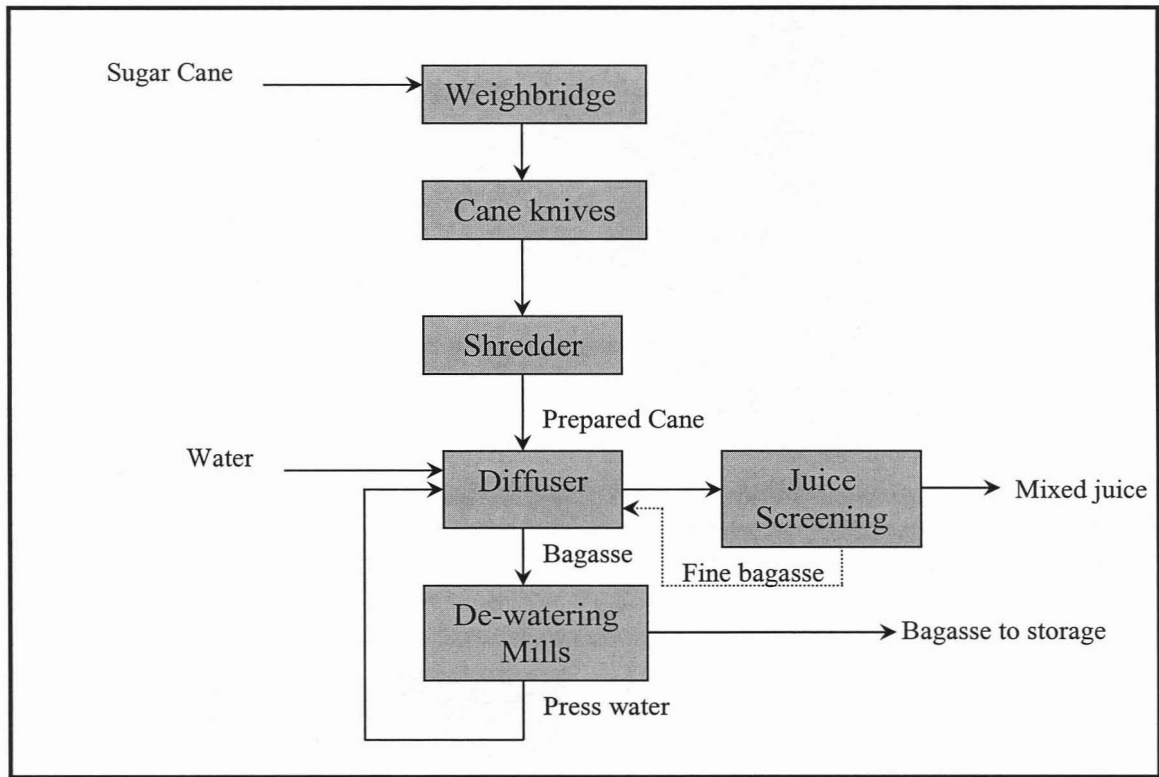
Figure 3.1: Sub-flow sheet of a typical sugar mill in South Africa showing the production of bagasse by-product.

3.2. Properties of Bagasse

Structurally, the cane stalk consists of various types of fibrous tissues that can be classified into true fibres and pith (see fig. 3.2), which have the same chemical composition but different structures. The true fibres are composed of tough, hard-walled, cylindrical cells of the rind and vascular tissue. The true fibres have high length-to-diameter ratios (approximately 70) and possess large coefficients of expansion and contraction upon wetting and drying. This leads to close bonding of the fibers, which enhances its strength and cohesiveness characteristics. The pith comprises of parenchyma cells of irregular size and shape with low length to diameter ratios of 5 and is mainly a carrier of molasses. The pith can adsorb many times its weight of liquid [Patarau, 1969]. These two types of fibres occur in bagasse and its physical appearance can be seen in fig. 3.3.
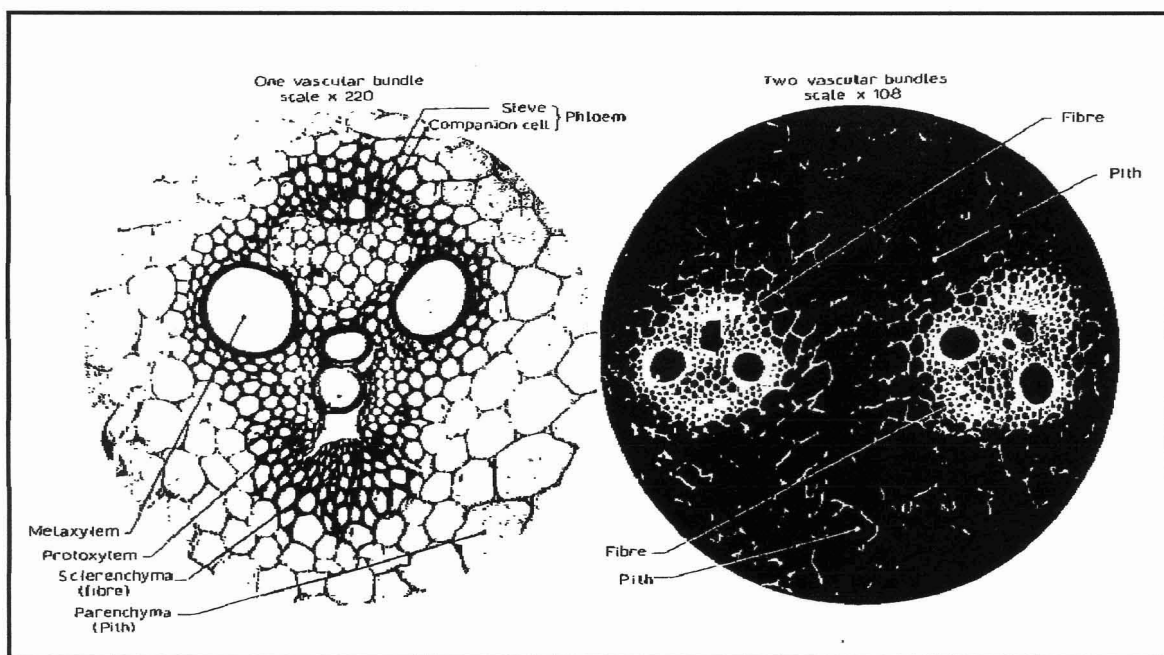
Figure 3.2: Microphotograph of cane section showing the fibrous sections [Patarau, 1969].
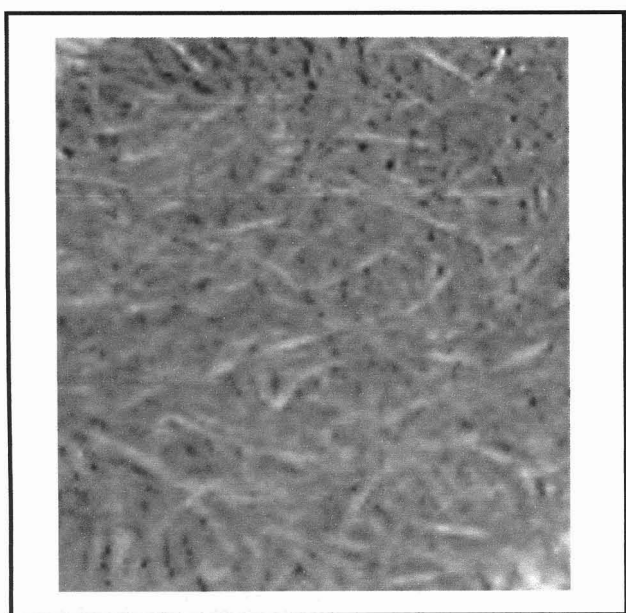
Figure 3.3: Bagasse after passing through the diffuser.

The properties of bagasse vary according to the variety of cane, its maturity, the method of harvesting and finally the efficiency of the milling plant. For example, in South Africa, most sugar cane passes through a diffuser instead of a conventional mill and the bagasse that is generated has different physical and chemical properties to that of, say, Brazil. So one would expect, that the activated carbons produced would also differ due to the raw material properties.

A typical composition of bagasse is as follows:

- Moisture: 46-52 % (av. 50%)
- Fibre: 43-52 % (av. 47.7%) and
- Soluble solids (mostly sugar):   2-6 %   (av. 2.3%)

Bagasse fibres are known to be insoluble in water and have a chemical composition (on a dry basis – db) of:

- cellulose [$(C_6H_{10}O5)_n$]   : 45.3 % (db),
- pentosans ($C_5H_8O_4$)   : 24.1% (db) and
- lignin ($C_{49}H_{52}O_{14}$, possibly) : 22.1% (db).

Bagasse has a high calorific value on average of 19422 kJ/kg of ash free dry bagasse and 7850 kJ/kg moist bagasse [Chen and Chung-Chi, 1993]. Bagasse is a low-density, carbonaceous material with a high volatile content as shown in table 3.1.

Table 3.1: Analysis of bagasse [Patarau, 1969]

Proximate Analysis / (Weight %)		Ultimate Analysis / (Weight %)	
Fixed Carbon	7.0	Carbon	23.7
Volatiles	42.5	Hydrogen	3.0
Moisture	49.0	Oxygen	22.8
Ash	1.5	Moisture	49.0
		Ash	1.5

Shemet *et al*, [1984] report that the ultimate analysis and thermophysical properties of bagasse are similar to those of firewood. Chen and Chung-Chi [1993] performed a comparative study on the characteristics of bagasse and wood and their findings are tabulated below in table 3.2.

The properties of whole and fibre fractions of bagasse compare well with hard and soft wood. However, the pith fraction fall short in the comparison but these fractions can be eliminated from the rest of bagasse or combined with the fibre factions during processing. Both hard and soft wood are excellent precursors for activated carbon (see Chapter2, table 2.1.) and thus, by virtue of its properties and characteristics it is evident that bagasse possesses the desired pre-requisites as a pre-cursor material for the production of activated carbon.

Table 3.2: Comparison of wood and bagasse [Chen and Chung-Chi, 1993]

Characteristic	Hardwood	Softwood	Bagasse		
			Whole	Fibre	Pith
α–cellulose(%)	38-48	40-45	30-39	38-43	26-36
Pentosans(%)	20-25	10-13	24-30	27-32	28-33
Lignin (%)	20-29	26-34	18-22	20-23	18-22
Ash (%)	0.3-1.2	0.2-0.8	1-4	0.6-1.2	1.8-4.6
Average fibre length (mm)	0.7-1.6	2.7-3.6	-	1.0-2.0	0.25-0.4
Average diameter (μ)	20-40	32-43	-	14-28	54-87
Average density (kg/m^3)	550 -800**	400-500**	550 $\pm$ 20*	520 $\pm$ 10*	200*

*   Rasul *et al* [1999]

** Bansal *et al* [1988]

Xia *et al* [1998] concluded via electron microscopy that the surface of bagasse (Brazilian) fibres contain approximately 16 000 pores / unit mm^2 of bagasse surface which vary from $0.7 - 1.5\mu m$ in diameter. This feature has also been observed in South African bagasse during this study (see Chapter 6). Furthermore, this porous nature of the bagasse material enhances its capability as a raw material in activated carbon manufacture since it is believed that these pores would act as channels for gases to escape easily without deforming or collapsing the pores created under processing conditions (pyrolysis and activation).

3.3. Pyrolysis of Bagasse

The pyrolysis process follows raw material preparation in activated carbon manufacture and the history of the pyrolysis step is crucial since this step pre-determines the characteristic of the produced activated carbon. It is in this stage that the fixed carbon skeleton is created and the initial phases of pore development arise, which is further improved during activation. Heating rate, pyrolysis temperature and hold time are the factors, which optimize char yield and develop porosity.

Pyrolytic decomposition studies on lignocellulosic material, for example bagasse, have been studied by using differential thermogravimetric (DTA) and thermogravimetric (TGA) analysis techniques [Nassar *et al*, 1996, Khattab *et al*, 1993, Luo *et al*, 1992] in order determine the transformations and reactions that occur at increasing temperatures. The mechanisms that occur during bagasse pyrolysis are deemed to be difficult to determine due to the complex composition of bagasse and the large number of complex reactions that occur during pyrolysis

[Garcia-Perez, *et al* 2001]. Thermogravimetric analysis is also used to determine the kinetic and thermodynamic parameters such as reaction rate constants, activation energy, entropy change, enthalpy change and Gibbs free energy change for pyrolysis of bagasse [Nassar *et al*, 1996].

3.3.1 Bagasse Pyrolysis Chemistry

The transformations that occur during biomass pyrolysis have been studied at low and high heating rates. For the case of high heating rates, bagasse pyrolysis has been studied especially in conjunction with combustion in suspension-fired and swirl burners [Stubington and Aiman, 1994; Rodriguez *et al*, 1993; Luo and Stanmore, 1994] since during real combustion conditions, not all the fuel source comes in contact with oxygen indicating that anaerobic thermal decomposition (pyrolysis) of the organics occur as well. Rodriguez *et al* [1993] investigated the thermal decomposition of pulverized bagasse in an Od-130 derivatograph heated in helium at high heating rates in order to determine the reaction mechanisms of the process on a thermal basis. They found that the process goes through the following physiochemical stages described in table 3.3.

Table 3.3: Description of the various stages during pyrolysis of bagasse in helium

Temperature Range / (^{O}C)	Description of transformation
25 – 110	Removal of moisture from the particle (drying)
110 – 170	Endothermal decomposition of polysaccharides with simultaneous vaporization of water bound in colloids
170 - 250	Breaking of the weak bonds in oxygen–containing hydroxyl, carboxyl and methoxy groups, thereby liberating CO_2, CO and H_2O. During this stage the reaction is exothermic.
250 - 280	Decomposition of hydrocarbons (hemicellulose and cellulose).
280 - 310	Liberation of hydrocarbons and H_2, accompanied by a decrease in CO and CO_2 yield.
310 - 450	Exothermic decomposition of lignin and of extractable substances. Reaction rate greatest at 350°C. Products are rich in combustible gases (50% CO, 38% CH_4, and liquid tars).
450 - 900	Breaking of C-C chains and endothermal formation of coke residues.

The reactions that occur during the thermal decomposition of polysaccharides are divided into cleavage of glycosidic, C-H, C-O, and C-C bonds, dehyration, decarboxylation, decarbonylation reactions and the formation of C-C, C=C and C-O bonds, and carbonyl and carboxyl groups [Garcia-Perez *et al,* 2001]. Stubington and Aiman [1994] discovered that at extremely high

heating rates from 200-1000 °C/min, the primary products during pyrolysis of bagasse in a nitrogen atmosphere are tar, water and carbon monoxide. At higher peak temperatures (870 °C) secondary reaction of the tars occurs, thereby producing mainly carbon monoxide. They also found that char yield declines with increasing heating rate.

Bilba and Ouensanga [1996] in their research used data from solid FTIR (Fourier Transform Infrared) analysis to study thermal degradation of bagasse at low heating rates (10-30 °C/min). They found that structure modifications took place around 200 °C with a decrease in the O-H, C-O, C=C bonds and an increase in alkyl bonds. This structural change intensified between 300 - 400 °C with a dehydration of carbohydrates from 300 - 320 °C followed by the dehydration of lignin between 340-380 °C. Further increase in temperature (340-380 °C) led to a saturation of aromatic rings, breaking of the C-C bonds present in lignin, liberation of water, CO and CO_2 and finally re-arrangement of the carbohydrates and lignin structures. As temperature progresses (800 °C), a char containing organic acids is left behind. Their study also agrees that at high heating rates hydrogen and hydrocarbon molecules are liberated.

The formation of the char end product is brought about by the decomposition of the lignin fraction in bagasse at higher pyrolysis temperatures [Nassar and Mackay, 1984], whereas the hydrocarbon fractions (cellulose and hemicellulose) are converted to volatile products [Arseneau, 1981] that escape from the solid substrate. Nassar [1999] investigated the thermal analysis kinetics of bagasse in a helium atmosphere at a heating rate of 5 °C/min and found by using DTG and TGA analysis that two main regimes of weight loss exist: decomposition of hemicellulose and the initial stages of cellulose decomposition occur in the lower temperature regime, while the upper temperature regime is associated with late stages of cellulose and lignin decomposition.

Studies have indicated that slight interactions between cellulose, hemicellulose, extractives and lignin during biomass degradation do occur and that biomass pyrolysis behaviour is a combination of these contributing fractions. Thermogravimetric and differential thermogravimetric curves during the thermal decomposition of lignocellulosic material reveal two to three distinct peaks due to hemicellulose, cellulose, and lignin decomposition [Roy *et al*, 1990; Raveendran *et al*, 1996; Caballero *et al*, 1997].

Similar results were discovered by García-Pérez *et al* [2001] who investigated the thermal decomposition of bagasse at various heating rates from 10 to 60 °C/min using a SSC/5200 TG / DTG Seiko microbalance under a nitrogen flow of 150ml/min. They concluded that thermal degradation started at 200 °C and cellulose degradation was almost complete at 373 °C at a

heating rate of 10 °C/min (see fig 3.4.). Two peaks corresponding to hemicellulose (299 °C) and cellulose (351 °C) could be observed quite distinctly with the lignin peak being overlapped by the other two peaks in the derivative thermogravimetric curve (see fig 3.5.). The maximum heating rate increased from 351 °C at 10 °C/min to 385 °C at 60 °C/min (see fig 3.6). They also, found that lignin decomposition reactions occurred at higher temperatures. The charcoal yield was approximately 16% for heating rates from 10 - 40 °C/min.
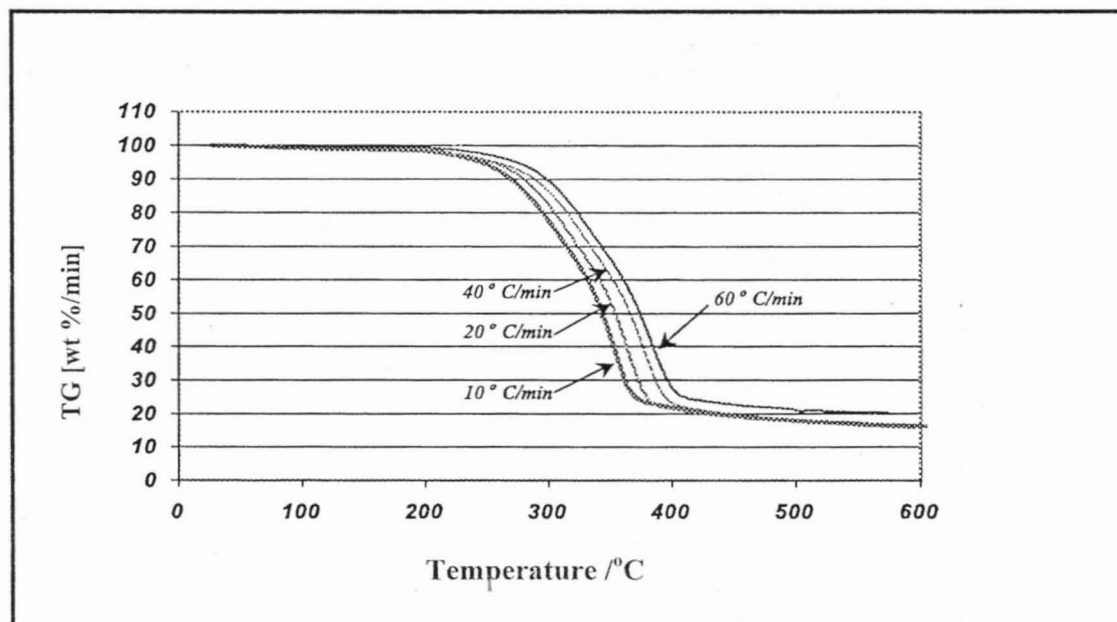
Figure 3.4: TG of sugar-cane bagasse (particle diameter > 0.450mm) at different heating rates [Garcia-Perez _et al_, 2001].
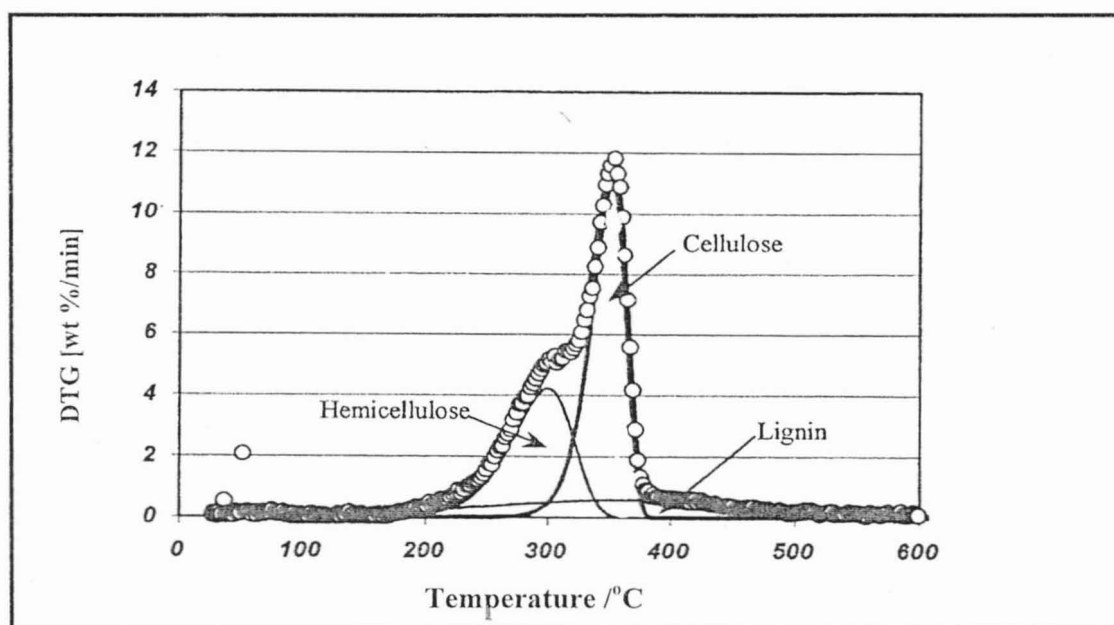
Figure 3.5: DTG of sugar-cane bagasse (particle diameter < 0.450mm) at 10 °C/min heating rate [Garcia-Perez _et al_, 2001].
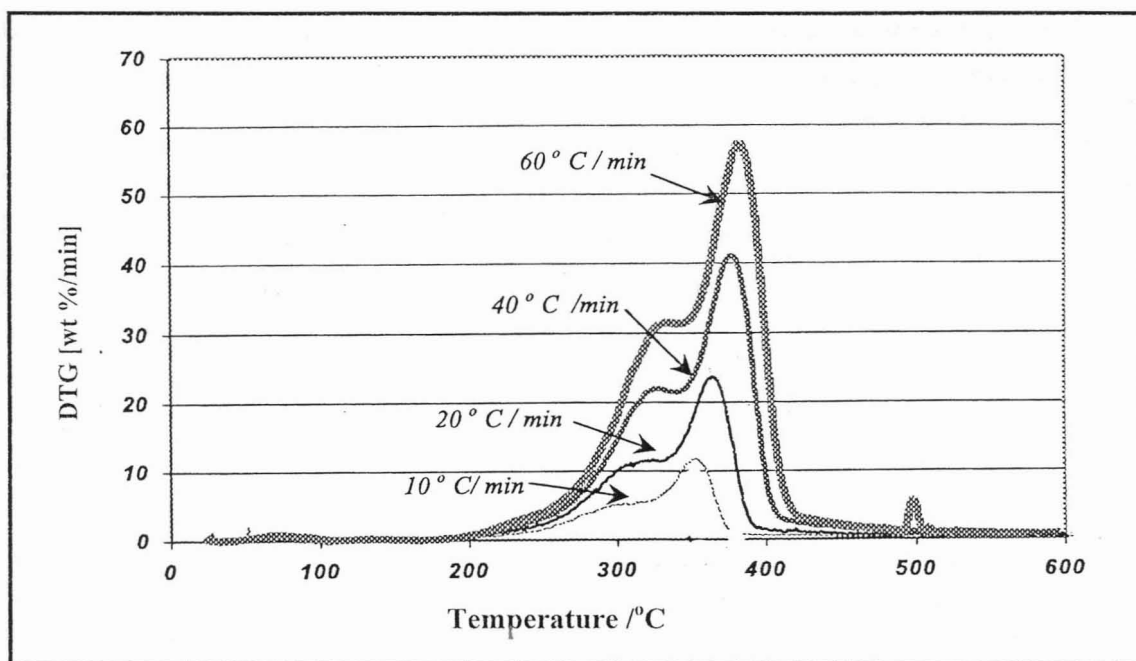
Figure 3.6: DTG of sugar-cane bagasse (particle diameter > 0.450mm) at different heating rates [Garcia-Perez *et al*, 2001]

Thermal degradation of bagasse comprises of two stages: volatilization and carbonization [Nasser *et al*, 1996]. The formation and evaporation of the volatile products are attributed to the cellulose component of bagasse during the volatilization stage [Tang *et al*, 1967]. This was further highlighted by Luo and Stanmore [1994], when studying the effects on particle size and shape during the devolatilisation of bagasse. They found that the cellulose carbon skeleton undergoes more drastic rearrangements compared to the lignin fraction during pyrolysis. This was due to the cellulose having a relatively open structural unit of β-1,4 anhydroglucopyranose whereas lignin is an amorphous compact material involving an aromatic ring.

3.3.1.1. Cellulose Pyrolysis Chemistry & Kinetics

It is was initially emphasized by Antal *et al* [1991] that an understanding of cellulose pyrolysis kinetics is beneficial in order to understand charcoal and activated carbon production. Antal and Varhegyi [1995] proved that when whole biomass undergoes heat treatment in order to remove mineral matter, the pyrolysis kinetics of its cellulose components are similar to those of pure cellulose.

Cellulose pyrolysis can proceed in two directions: one leading to formation of levoglucosan as a relatively stable product and the second yielding glycoaldehyde [Antal and Varhegyi, 1995]. Degradation of the cellulose component during bagasse pyrolysis takes place after the

dehydration stage and occurs by fragmentation through random scission of the macromolecular structure accompanied by the release of volatiles [Shukry *et al*, 1991]. Scission of the glucosidic linkages leads to the formation of a shortened chain, which is terminated by a resonance–stabilized glucosyl cation. This cation stabilizes itself as levoglucosan and a subsequent scission of the glucosidic linkage adjacent to the levoglucosan end group produces levoglucosan, which rapidly escapes from the system due to its volatility. Cellulose pyrolysis is therefore selective towards producing anhydrosugar [Essig *et al*, 1989].

Usually, the char yield is very low during pyrolysis of lignocellulosic material and Antal and Varhegyi [1995] claim that proper control of the pyrolysis chemistry can indeed increase the char yield to 40%, whereas other researchers argue that controlling the temperature-time history of pyrolysis of the raw material influences the char yield. In support of their theory, Antal *et al* [1991] had in fact increased the char yield in his research previously to 47% by controlling the process conditions that influenced the release of vapours from the solid substrate during pyrolysis. Char yield can be increased when vapours are held in contact with the solid substrate. According to Bradbury *et al* [1979], "the residence time of volatiles in the cellulose during pyrolysis reaction largely influences the extent of char formation." Therefore, for pure cellulose decomposition, the released pyrolytic vapours are the only sources of char.

Initially Broidio and Nelson [1975] discovered a competitive reaction model for cellulose pyrolysis (see fig 3.7.), which was later, improved on by Bradbury *et al* [1979].
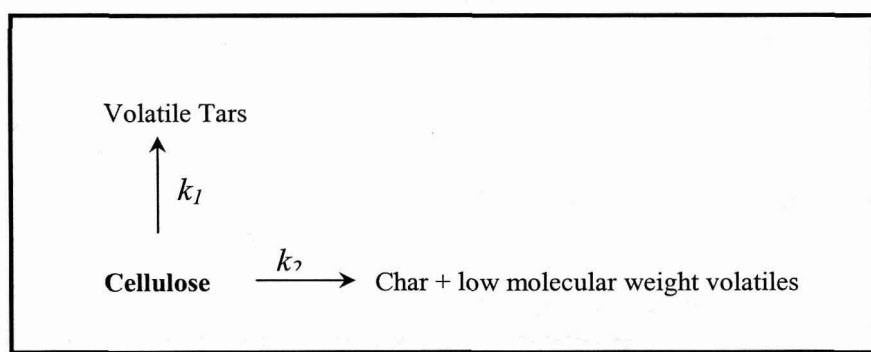
Figure 3.7: Cellulose decomposition [Broidio and Nelson, 1975].

Bradbury *et al* [1979] heated 250mg samples of pure cellulose batch wise at temperatures ranging from 259 to 407 °C in a vacuum, resulting in the cellulose model displayed in fig 3.8. Their studies imply that char formation in cellulose pyrolysis is not a primary step, but occurs because of the repolymerization of the volatile material. This basically means that increasing the vapor-solid interaction would increase the char yield and it is believed that these are the key

reactions that should be considered in the manufacture of charcoal from biomass [Antal and Varhegyi, 1996].
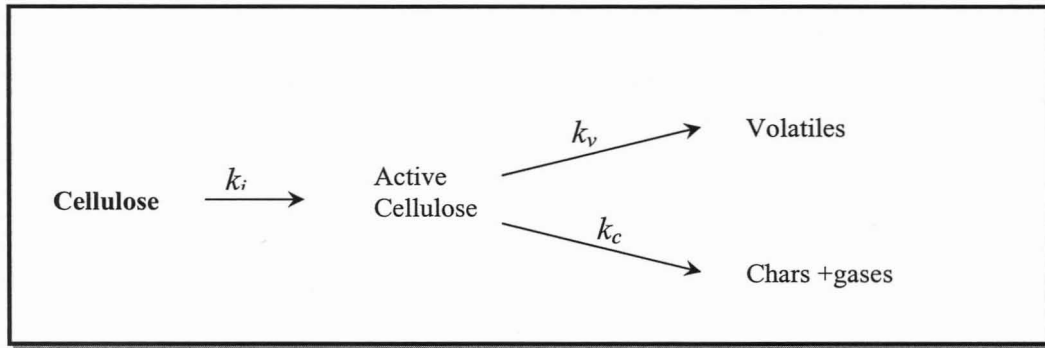
Figure 3.8: Cellulose pyrolysis model [Bradbury *et al*, 1979].

Another distinct feature was that volatilization of levoglucosan with char formation was observed by a strong exothermic reaction. This was iterated by Mok *et al* [1992] who executed tests to increase the char yield in closed containers and found that strong exotherms occur below 350 °C associated with charcoal and hemicellulose. Cellulose pyrolysis was found to be first order reaction with high activation energies of 238 kJ/mol when vapour-solid interactions are minimized and much lower (~130 kJ/mol) when high heating rates apply. However, for pyrolysis of bagasse, the activation energy of its cellulose component was found to be 215 - 226 kJ/mol [Varhegyi *et al*, 1989; Garcia-Perez *et al*, 2001].

3.3.1.2. Bagasse Hemicellulose Pyrolysis

Shafizadeh *et al* [1968] had reported that hemicellulose is less thermally stable than the cellulose and lignin fractions in bagasse and its active degradation begins at a lower temperature. A typical composition of hemicellulose present in bagasse is listed in table 3.4.

Table 3.4: Composition of hemicellulose [Shukry *et al*, 1991]

Component	Composition /(wt %)
Xylose	54.8
Arabinose	18.0
Glucose	21.0
Galactose	6.2

Shukry *et al*, [1991] studied the thermal decomposition of bagasse hemicellulose at a heating rate of 5 °C/min from room temperature to 600 °C/min in the presence of static air. They found

at low temperatures (> 200 °C) endothermic decomposition occurred followed by prominent exothermic reactions at higher temperatures. Between 200 and 320 °C, they found a 60 % weight loss of the hemicellulose, which was subsequently followed, by a smaller weight loss at higher temperatures (> 320 °C). The former case was related to the initial degradation reactions of depolymerization, hydrolysis, oxidation, dehydration and decarboxylation while the latter was suggested to proceed through combustion of the volatile degraded components and the formation of the "char residue".

3.3.1.3. Bagasse Lignin Pyrolysis

Lignins are phenolic polymers containing hydroxyl, carboxyl and carbonyl groups [Lin and Dence, 1992]. Nassar and Mackay [1984] found that lignin thermally degrades to char with no intermediates whereas lignin with hemicellulose and cellulose decomposition proceeds with the intermediate levoglucosan. Even Mok *et al* [1992] found that a strong correlation existed between char yield and lignin content of the feed. Furthermore, Nassar *et al* [1999] found that addition of salts had no effect on lignin decomposition, but did influence the decomposition of hemicellulose and cellulose.

Therefore, during bagasse pyrolysis, it can be deduced that increasing vapour-solid interactions would increase char yield. By employing a slow heating rate, vapour-solid interactions are favoured consequently increasing char yield.

Nassar *et al* [1999] have also related that the effects of bagasse pyrolysis are very much similar to wood. The porous nature of charcoal is developed after 400 °C, whereby active pyrolysis with evolution of volatile flammable products occurs.

3.3.2. Bagasse Pyrolysis Kinetics

Most kinetic studies performed on pyrolysis of bagasse are usually based on the weight loss data obtained by thermogravimetric analysis. According to Tang [1967], a pseudo first order reaction can be assumed for bagasse decomposition.

This can be justified by the following assumptions:

- the internal and external diffusion of mass and heat are relatively fast
- the rate of solid decomposition is proportional to its specific surface
- the ratio of specific surface / non reacted biomass stays constant and
- the yield coefficient defined as the char formed / biomass reacted remains constant [Caballero et al, 1995].

Therefore the reaction rate can be expressed as:

$$-\frac{dC}{dt} = KC \tag{3.1}$$

where: C = concentration of the reactant in moles

       t = time of reaction in minutes and

       K = rate constant in minutes^{-1}

By replacing the concentration by the observed weight w_t, then equation (3.1) changes to:

$$\frac{d(w_o - (w_o - w_t))}{dt} = K(w_o - (w_o - w_t)) = Kw_t \tag{3.2}$$

where: w_o = initial weight of the preheated sample and

       w_t = weight of the sample after time t

Integrating equation 3.2 leads to:

$$\log e^{(w_o - (w_o - w_t))} = \log e^{(w_t)} = Kt + C_c \tag{3.3}$$

where: C_c = an integration constant

At $t = 0$, $w_o - w_t = 0$

Hence, $C_c = -\log e^{w_o}$

And $\log e^{w_o / w_t} = Kt$

If the amount of residue left at the end of heating w_∞ is considered, then:

$$\log\left(\frac{w_o - w_\infty}{w_t - w_\infty}\right) = Kt \tag{3.4}$$

Plotting log $((w_o - w_\infty)/((w_t - w_\infty))$ against time (t) for a first order reaction should give a straight line with slope equal to the reaction rate constant K at the related temperatures. The above set of calculations were used by Nassar *et al* [1996] to determine the reaction rate constants during the volatilization and carbonization stages for thermal decomposition of bagasse in a nitrogen atmosphere. They heated the bagasse sample from room temperature to 800 °C at a heating rate of 5 °C/min. They also used the following set of equations to determine the rate constant based on first order reaction:

The rate constant K can be calculated by:

$$K = -\frac{dC}{dt}\frac{1}{C} \qquad \text{at temperature } T \tag{3.5}$$

By using finite differences instead of differentials, the rate constant K can be calculated by:

$$K = -\frac{\Delta C}{\Delta t}\frac{1}{C_{av}} \tag{3.6}$$

Tables 3.5 and 3.6 tabulate the results obtained by Nassar *et al* [1966] when using the calculation procedure displayed above. They found that the rate constant was greater during the volatilization stage than the carbonization stage. The activation energy during these two stages were determined by using the integrated form of the famous Arrenhuis equation:

$$\ln K = \frac{-E_a}{RT} + \ln K_o \tag{3.7}$$

where: R = gas constant and

E_a = activation energy in kJ/mol

K_o = Arrenhuis rate constant

Table 3.5: Kinetic parameters for devolatilisation stage of bagasse pyrolysis in a nitrogen atmosphere [Nassar et al, 1996]

Time (t) (min)	Temp / (^{O}C)	Residual weight (wt %)	Δw (wt %)	Δt (min)	K (min^{-1} x 10^3)	Log K
45	225	95.0	0.6	5.0	1.263	0.102
50	250	94.4	0.65	2.0	3.440	0.54
52	260	93.7	1.55	3.0	5.510	0.74
55	275	92.2	1.20	2.0	6.510	0.818
57	285	91.0	4.00	2.0	15.380	1.187
60	300	85.0	3.00	2.0	24.760	1.394
62	310	82.0	4.00	2.0	27.270	1.436
64	320	78.0	5.00	2.0	32.050	1.506
66	330	73.0	5.00	2.0	34.260	1.535
68	340	68.0	6.00	2.0	44.117	1.645
70	350	62.0				

Table 3.6: Reaction rate constant for de-carbonization stage of bagasse in a nitrogen atmosphere [Nassar et al, 1996]

Time (t) (min)	Temp / (^{O}C)	Residual weight (wt %)	Δw (wt %)	Δt (min)	K (min^{-1} x 10^3)	Log K
76	380	47	2.0	4.0	10.360	1.026
80	400	45	2.5	4.0	13.880	1.143
84	420	42.5	2.5	4.0	14.700	1.167
88	440	40.0	3.0	4.0	18.750	1.273
92	460	37.0	3.0	4.0	20.270	1.306
96	480	34.0	3.0	4.0	22.050	1.340
100	500	31.0	3.0	4.0	24.190	1.384
104	520	28.0	4.0	4.0	35.714	1.553
108	540	24.0	4.0	4.0	41.600	1.619
112	560	20.0				

However, Garcia et al [2001] et al used thermogravimetric analysis at different heating rates together with the Friedman plot to determine the kinetic parameters with respect to conversion and deduced that the overall activation energy for bagasse pyrolysis was 150-200 kJ/mol (10-40 ^{O}C/min) over a wide range of conversions. Therefore, they were able to conclude that pyrolysis occurs through a cleavage of linkages with similar energy bonds. In their calculations they assumed that the bagasse pyrolysis rate was the sum of its component pyrolysis rates. Hence,

each component, hemicellulose, cellulose and lignin contributed proportionally to the global process. Therefore, for each set of heating rates, the rate constants, activation energy, including the amount of gases released during pyrolysis for each component were obtained by considering first order reaction and their results can be viewed in table 3.7.

Table 3.7: Kinetic parameters from each component used to determine sugar cane bagasse kinetics [Garcia *et al*, 2001]

Heating rate /(^{O}C/min)	Component	E_a / (kJ/mol)	Log K / (min^{-1})	n	Weight fraction of released gases (z_{jo}) / (%)
10	Cellulose	235	19.489	1.0	48
	Hemicellulose	105	9.204	1.0	33.5
	Lignin	26	1.000	1.0	18.5
20	Cellulose	235	19.398	1.0	48
	Hemicellulose	105	9.301	1.0	33.5
	Lignin	26	1.361	1.0	18.5
40	Cellulose	235	19.255	1.0	45
	Hemicellulose	105	9.362	1.0	35.5
	Lignin	26	1.602	1.0	19.5
60	Cellulose	235	19.279	1.0	44.5
	Hemicellulose	105	9.447	1.0	36
	Lignin	26	1.669	1.0	20

Table 3.7 indicates that the high activation energy is associated with cellulose decomposition compared to lignin in sugar cane bagasse. Decomposition of cellulose proceeds at a much faster rate compared to lignin decomposition and this is verified by the higher fraction of gases released from cellulose compared to lignin in sugar cane bagasse. This finding is comparative to that observed by Nassar *et al* [1996] whereby the volatilization stage is associated with cellulose and hemicellulose decomposition while the carbonization stage is related to lignin decomposition. Furthermore, from Garcia-Perez *et al*'s [2001] work presented in the above table, there seems to be a decrease in cellulose pyrolysis rate with a converse effect on hemicellulose and lignin pyrolysis rates as heating rate increases but the total rate constant remains the same.

However, Rodriguez *et al* [1993] calculated the order of the reaction as pyrolysis proceeded instead of assuming first order kinetics, but still used the Arrrenhuis equation to determine activation energy for bagasse pyrolysis at high heating rates. The activation energy required and reaction orders for bagasse pyrolysis together with their released gaseous products at high

heating rates from their study are shown in table 3.8. The activation energy and reaction orders vary during the different stages of bagasse pyrolysis with first order kinetics occurring during pyrolysis at 170-250 °C and 310-380 °C. However, the activation energy at the temperature range falls into the range as obtained by Garciar – Perez *et al* [2001] at high heating rates.

Table 3.8: Bagasse Pyrolysis Kinetics at high heating rates [Rodriguez, *et al*, 1993]

	Temperature Range in °C			
	110 - 170	170 - 250	250 - 310	310 - 380
Reaction order	0.1	1.0	0.4	1.0
E_a /(kJ/mol)	21	14	64	188
Gaseous Products	H_2O	CO, CO_2, H_2O	CO, H_2, CO_2	CO, CH_4

3.3.3. Thermodynamic Properties of Bagasse Pyrolysis

According to the rate theory [Glassstone, 1980] the rate of reaction K can be expressed as:

$$K = \frac{kT}{h} e^{-\Delta G^o / RT} \qquad (3.8)$$

where: h = Plank's constant = 6.6256 x 10^{-34} Js

       R = ideal gas constant = 8.314 J/molK

       T = temperature in Kelvin

       ΔG^o = change in Gibbs free energy J/mol

       k = Boltzmann constant = 1.38408 x 10^{-23} J/K

The change in Gibbs free energy (ΔG^o), is related the change in entropy (ΔS) and enthalpy change (ΔH) of the system, thus equation 3.8 can be rewritten as:

$$K = \frac{kT}{h} e^{\Delta S / R} e^{-\Delta H / RT} \qquad (3.9)$$

where: ΔS = change in entropy (kJ/mol.K)

       ΔH = change in enthalpy (kJ/mol)

According to Smith and van Ness [1987], for a first order reaction, the activation energy, E_a, is related to the change in enthalpy by:

$$E = \Delta H + RT \qquad (3.10)$$

Therefore the reaction rate can also be determined by:

$$K = \frac{kT}{h} e^{\Delta S / R} e^{-(E-RT)/RT}$$

$$K = \frac{kT}{h} e^{\Delta S / R} e^{-E/RT} \qquad (3.11)$$

Using the above calculations, Nassar et al [1996] determined thermodynamic properties for pyrolysis of bagasse, which are displayed in table 3.9.

Table 3.9: Thermodynamic Properties of Bagasse Decomposition in Nitrogen [Nassar *et al*, 1996]

Stage	K / (min^{-1})	Temp (^{O}C)	E_a (kJ/mole)	ΔH (kJ/mole)	ΔS (kJ/mole K)	ΔG^o (kJ/mole)
Volatilization	0.037	315	87.90	83.011	-0.170	183.46
De-carbonization	0.019	470	46.68	40.050	-0.270	237.40

Positive values for Gibbs free energy were obtained as shown in table 3.9 thereby revealing the non-spontaneous nature of the reactions and the free energy of the products is much greater than the reactants.

3.3.4. Char Characteristics and Pyrolysis Process conditions

The chars produced under various pyrolysis conditions have a set of unique characteristics, which are enhanced when they are subjected to activation. Some of these characteristics that have been evaluated by various researchers are discussed in order to get brief idea of type of chars that are produced during pyrolysis.

Luo *et al* [1992] found that char produced by the bagasse pyrolysis step acquired the properties in table 3.10, which were similar to that of low rank coal. The total surface area is approximately half of that of a commercial carbon (usually 1000m^2/g). 80 % of this surface area is contributed by the micropores that have developed due to the pyrolysis mechanisms as

explained above. The macropores and sometimes the mesopores contribute to the external surface area.

Table 3.10: Char properties [Luo *et al*, 1992]

Property	Units	Value
Surface area (BET)	m^2/g	410
External Surface Area*	m^2/g	80
Micropore Area	m^2/g	330
Micropore Volume	cm^3/g	0.15
Micropore Diameter	μm	1 - 5

*Pores > 6μm in diameter

High surface area chars produced from bagasse pyrolysis were also found by Xia *et al* [1998], when they pyrolysed Brazilian bagasse at heating rates from 2 to 10 $^{\circ}$C/min to temperatures ranging from 800 –1000 $^{\circ}$C in a nitrogen atmosphere. They found at the pyrolysis temperature of 900 $^{\circ}$C, the resultant char had an optimum surface area of 532 m^2/g char which was equivalent 101 m^2/g bagasse having a pore volume of 280 cm^3/g. They later show that the char's surface area and pore volume increased during the activation stage (see section 3.4.). Minkova *et al* [2000] found that when bagasse was pyrolysed in a flow of nitrogen, the char's capacity to adsorb iodine was approximately 500 mg/g. Iodine number is related to microporosity and surface area (see Chapter 4) and corroborates what has been found by other researchers.

Petrie and Baldwin [1992] found that fibrous material bound with a binder, extrudated and then pyrolysed produced more porous chars having a higher reactivity. Zandersons *et al* [1999] increased the charcoal yield to 1.4 times by adding sulphuric acid to bagasse prior to carbonization (pyrolysis). However, the bulk density of charcoal was low as 76- 108kg/m^3. Lutz *et al* [1998] converted bagasse to char batch wise under the exclusion of oxygen at 380 $^{\circ}$C for 3 hours yielding 35.4% char. This char was later subjected to partial gasification at 850-900 $^{\circ}$C and yielded high surface area activated carbons. Different process conditions yield different char yields.

3.4. Activated Carbons from Bagasse

Activated carbons can be produced either through physical or chemical methods (see Chapter 2) of activation and sometimes through a combination of both these methods. The aim of the activation step is to increase the porosity and enlarge pore diameters in the resultant chars by the selective removal of the disorganized carbon by the activating agent. The mechanism of activation with different types of activating agents has been discussed early in Chapter 2. Powder and granular activated carbons with unique properties have been successfully produced from sugar cane bagasse by employing various process techniques. Successes will be briefly explained in order to reach a generally consensus on the best processing practices.

3.4.1. Chemical Activation Processes

Activated carbons from bagasse have been produced by chemical activation [Girgis *et al*, 1994 and Tsai *et al*, 2001] with the major focus being on increasing carbon yield and microporosity. Microporosity is linked to surface area available for adsorption of molecules less than 2nm. Xia *et al* [1998] produced activated carbons from bagasse by chemically activating fibrous bagasse with 0.9 zinc chloride ($ZnCl_2$) and heating from room temperature to 600 $^{\circ}$C at an activation hold time of 1 hour in a one-stage process. This method produced a high yield of carbon (36.1 wt %) with the resultant carbons possessing surface areas as large as 1278 m^2/g. The activated carbons ability to adsorb iodine and methylene blue were recorded by the high iodine (1200 mg/g) and methylene blue (171 mg/g) numbers. The total pore volume of the carbon was 0.621 cm^3/g with 50% contributed by micropores. Although the carbon possessed excellent adsorbing characteristics, the activated carbon had to be washed prior to being used in order to remove chemicals and this poses an effluent dilemma.

Lavarack [1997] impregnated different fractions of bagasse (whole, bagacillo, rind and pith) with phosphoric acid, sulphuric acid, zinc chloride and calcium chloride and chemically activated them at pyrolysis temperature of 500 $^{\circ}$C in a nitrogen atmosphere for 3 hours producing powder activated carbons. Again in this process, the carbons prepared chemically were washed to remove the impregnated chemicals. Phosphoric acid carbons gave the best colour removal from brown sugar, but their acid contents contributed to a decrease of pH in the syrup, thereby reducing its potential for sugar decolourisation in the sugar industry. It is worthy to mention that a low pH would cause an irreversible reaction of sucrose to glucose and fructose in sugar syrups, which is unacceptable. Bagacillo and the pith fractions bound with calcium chloride, showed satisfactory results for brown sugar decolourisation.

3.4.2. Physical Activation Processes

Adopting physical activation techniques in producing activated carbons have deemed to produce far superior quality carbons than commercial carbons [Xia et al, 1998]. Xia et al [1998] also tested this theory by producing activated carbons firstly by the two-step physical method and then by employing a one-step physical process with fibrous and compressed bagasse. Both these methods used steam as the activating agent. With respect to hardness of the activated carbon, they found that compressed bagasse subjected to activation with steam at 800 $^{\circ}$C for 1 hour produced activated carbons with a hardness number of 2.5 x 10^{-3} kg/cm^2 and contained 878 m^2/g of surface area with the micropores and mesopores contributing equally to pore volume. Furthermore, they also reveal that the adsorption potential for phenol and acetic acid adsorption was superior to that of a commercial coconut carbon. In keeping with this trend of one-step physical activation of bagasse, Minkova et al [2001] also produced activated carbons from bagasse in the presence of steam in a fixed bed pyrolysis reactor and in a horizontal rotating reactor [Minkova et al, 2001]. They concluded that the water vapour has the ability to penetrate the solid residue and aid in desorption and efficient removal of the volatile products from the solid material. Their optimum processing conditions with respect to iodine adsorption (~ 780 mg/g) were at a temperature of 750 $^{\circ}$C and at a hold time of 2 hours. Minkova et al [2001] also used a mixture of carbon dioxide and steam for activation the resulting carbon had a much lower iodine number of 565 mg/g.

Lutz et al [1998] produced very high surface area (1035 m^2/g) activated carbons by initially converting 200-400 g of Brazilian bagasse to char at a temperature of 380 $^{\circ}$C for 3 hours. About 5-10 g char was then activated with steam / nitrogen mixture at 850 –900 $^{\circ}$C in a rotary furnace for 150 min. This two-step process of physical activation produced activated carbons with the ability to adsorb iodine and methylene blue of 1180 mg/g and 275 mg/g respectively. These adsorption capacities were 2.3 and 4.2 times greater when compared to the commercial Carbotech D47/4 and Norit D10 activated carbons. The carbons contained high micropore and mesopores volumes of 0.5 and 0.2 cm^3/g.

Pendyal et al [1999] produced granular activated carbons by mixing sugar cane bagasse and other biomass materials with various types of binders (coal tar, sugar-cane molasses, sugar beet molasses and corn-syrup) in cane to binder ratios (wt/wt) of 1:0.5 and 1:1 and subsequently pressing them into briquettes. They used the generally two-step physical activation whereby these briquettes were pyrolysed in nitrogen at 700 $^{\circ}$C for 1 hr, crushed, sieved and then activated with 13% CO_2 and 87% nitrogen at 800 $^{\circ}$C for 6 hr. They found that activated carbons from bagasse bound with sugar beet molasses removed approximately 68% of the colour from

molasses whereas bagasse bound with coal tar removed about 55% colour from raw sugar. However, these carbons had low surface areas ranging from 195 to 524 m^2/g with total pore volume of ranging from 0.132 to 0.314 cm^3/g. A closer look at the pore size distribution reveals that bagasse bound with sugar-beet molasses had a lower percentage of mesopores (24.5 %) and macropores (1.3%) compared to bagasse bound with coal (mesopores –31.8%, macropore – 4.5%). The type of pore size distribution present in the activated carbon influences its adsorption potential. They also concluded that the raw material rather than the binder exerted an influence in adsorbing sugar colourants. Pendyl *et al* [1999] in his work indicated that with respect to physical and chemical properties activated carbon from bagasse bound with corn syrup ranked the highest followed by coal tar. However, Ahmedna *et al* [1999] by following the procedures by Pendyal *et al* [1999] produced granular activated carbons from bagasse bound with coal tar and corn syrup with *much higher* bagasse to binder (wt/wt) ratios of 1:1 and 1:2 and activated with CO_2 but at temperatures of 900 °C for 4hr and 20 hr. Again they found that surface area was low (78 –314 m^2/g) and the mesopores and macropore contribution to surface area was 50%. However, bagasse bound with corn syrup showed exceptional adsorption potential to remove colour bodies from sugar (~ 60%) and molasses (~ 90%). Their adsorption potential was linked to their relatively low surface charge (no carboxylic groups). Ahmenda *et al* [2000] again reinforces that bagasse bound with corn syrup produces excellent granular carbons for raw sugar and molasses colour decolourisation.

Therefore, based on the findings by various international researchers on the production of activated carbon from sugar cane bagasse as illustrated above, the following can be concluded:

- Although chemical activation results in the final activated carbon having excellent sugar decolourising potential, the pH of the final activated carbons tend to impact negatively on the sugar solution during the decolourisation process. Thus, for the purpose of manufacturing activated carbons from sugar cane bagasse for sugar decolourisation, chemical activation techniques are undesirable. Furthermore, the high costs associated with the chemical agents and the required washing step does not make this type of activation economical.

- Physical activation with CO_2 requires long activation times (> 3 hours) to produce satisfactory activated carbons from sugar cane bagasse. In terms of cost, efficiency, time and effectiveness, CO_2 activation is not seen to be feasible.

- Granular activated carbons can be produced from sugar cane bagasse, but again the type of activation agent and the binder used influences the properties of the final activated carbon.

- Activating bagasse chars with steam produces excellent powder activated carbons within a much shorter time. Their pore size distribution suggests that these carbons would probably be effective sugar decolourising carbons.

CHARACTERIZATION OF ACTIVATED CARBONS

Each activated carbon has a unique set of physical and chemical characteristics that are dependent on the type of raw material and the processing methods (physical, chemical or a combination) employed in its manufacture [Allen *et al*, 1998]. According to Bansal *et al* [1988], activated carbons are classified by their high adsorption potentials, which can be as high as 0.6-0.8 cm^3/g. The effectiveness of an activated carbon as an adsorbent is accredited to its unique qualities, which include, "large surface area, high degree of surface reactivity, universal adsorption effect and favourable pore size distribution" [Bansal *et al*, 1988]. Hence an activated carbon is usually characterised by the following criteria:

- total surface area
- pore size distribution (pore volume and pore size)
- impact hardness and
- ability to adsorb selected substances such as nitrogen, benzene, carbon tetrachloride from the gaseous phase and iodine, methylene blue, phenol, and molasses from the aqueous phase.

4.1. Adsorption in activated carbons

The method of adsorption of a gas by a solid is usually used to determine information on surface area and porosity. When a porous solid (adsorbent) comes in contact with a gas or vapour (adsorbate), the solid begins to adsorb the gas/vapour onto its surface and then into its pores [Cal, 1995]. Adsorption involves the accumulation of substances at a surface or interface, which occurs by the forces that are exerted by the large surface area of the solids [Suffet and McGuire, 1981]. This occurs by two types of binding forces namely, physical and chemical forces. Physical adsorption results from the action of the short-range attractive van der Waals forces, comprising of London dispersion and classical electrostatic forces that draw the

molecules in their vapour state until they condense into a liquid [Suffet and McGuire, 1981, Dominguez and Hyndshaw, 1976]. Chemisorption is associated with the transfer and sharing of electrons between adsorbate and adsorbent resulting in a chemisorptive bond. The chemical bond is much stronger than van der Waals forces and transmigration of the adsorbate molecules within the interface do not occur [Suffet and McGuire, 1981]. Chemisorption is used to assess the area of active surfaces [Allen *et al*, 1998].

4.1.1. Pore Sizes

Pores are the tortuous micro-chambers that allow for increased surface area in activated carbon. A schematic representation of the microstructure of an activated carbon is displayed in figure 4.1 [Bansal *et al*, 1988].
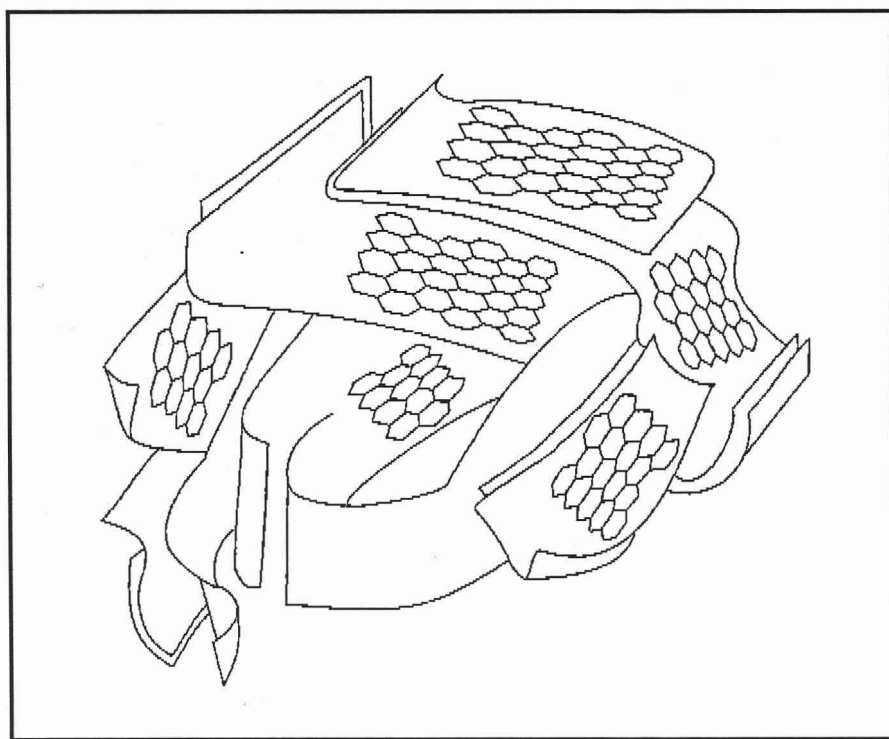
Figure 4.1: Schematic representation of an activated carbon [Bansal *et al*, 1988].

The structure of activated carbon structure comprises principally of carbon atoms that are grouped into stacks of flat, aromatic sheets or planes, randomly cross-linked by aliphatic bridging groups. These sheets are irregularly arranged such that there are free interstices between sheets which creates the porous structure. The width of the sheets is about 5nm. [Baily and Maggs, 1971;Bansal *et al*, 1988; Doying 1965; McEnaney, 1988 and Peters, 1966].

Depending on their preparation activated carbons can possess a distribution of various size and shape pores. They are usually characterized in terms of their width i.e. the diameter of a cylindrical pore or the distance between the walls of slit shaped pores. Dubinin [1960] classified these pores according to their widths (see table 4.1), which has been adopted by the International Union of Pure and Applied Chemistry.

Table 4.1: Pore Classifications [Dubinin, 1960]

Pore Classification	Pore Width
Micropores	< 2nm (20 Å)
Mesopores	Between 2 and 50nm (20 – 500 Å)
Macropores	> 50nm (500 Å)

The physical adsorption of gases and vapours into microporous activated carbon is based on the theory of micropore volume filling developed by Dubinin [1965, 1966, 1975]. Firstly, the gases are adsorbed into the micropores by "volume-filling" due to the greater interaction potential in micropores than larger pores because the pore walls are much closer which enhances adsorption potential [Cal, 1995; Botha, 1992]. "The adsorption then shifts to the meso- and macropores forming gradual multilayers, and exhibiting capillary condensation", [Botha, 1992]. Stoeckli [1990] denotes that the meso- and macropores are mainly used as transport channels although liquid condensation may occur in these pores.

4.1.2. Functional Groups

During the activation of carbons, heteroatoms such as hydrogen and oxygen are incorporated into the carbon structure and are located at the edges of carbon planes and form surface functional groups. These functional groups can influence adsorption as well [Cookson, 1978, Faust and Aly, 1983 and Mattson *et al*, 1969]. Boehm and Voll [1970, 1971] disclose that functional groups and carbon deposits formed during pyrolysis can render certain areas of the microporous network inaccessible. These leads to activated diffusion effects at low adsorption temperatures such that the adsorbate has insufficient energy to penetrate into the micropores,

4.2. Adsorption Isotherms

In a closed system, the adsorption of a gas onto solid can be determined by either measuring the decrease in adsorbate pressure within a known volume or by measuring the gain in adsorbent mass due to the adsorption of the gas molecules. The amount of gas adsorbed (moles/gram) is

related to the partial pressure of the adsorbate at a constant temperature and leads to the construction of an adsorption isotherm. Adsorption isotherms are useful tools in characterising the adsorbent with respect to the adsorbate [Cal, 1995]. Generally nitrogen adsorption at its boiling point of 77 K is used as an adsorbate [Bansal *et al*, 1988; Gregg & Sing, 1982 and Rodriguez-Reinso *et al*, 1989] but other small molecule adsorbates such as Ar (77K), Xe (77K), Kr (77K), CO_2 (195K), alkanes (298K) and O_2 (90K) have also been used. The adsorption isotherms provide an insight of the porous nature of the adsorbent [Allen *et al*, 1998]. Brauner *et al* [1940] classified the adsorption isotherms into 5 types known as the BDDT-classification, which are presented in figure 4.2.
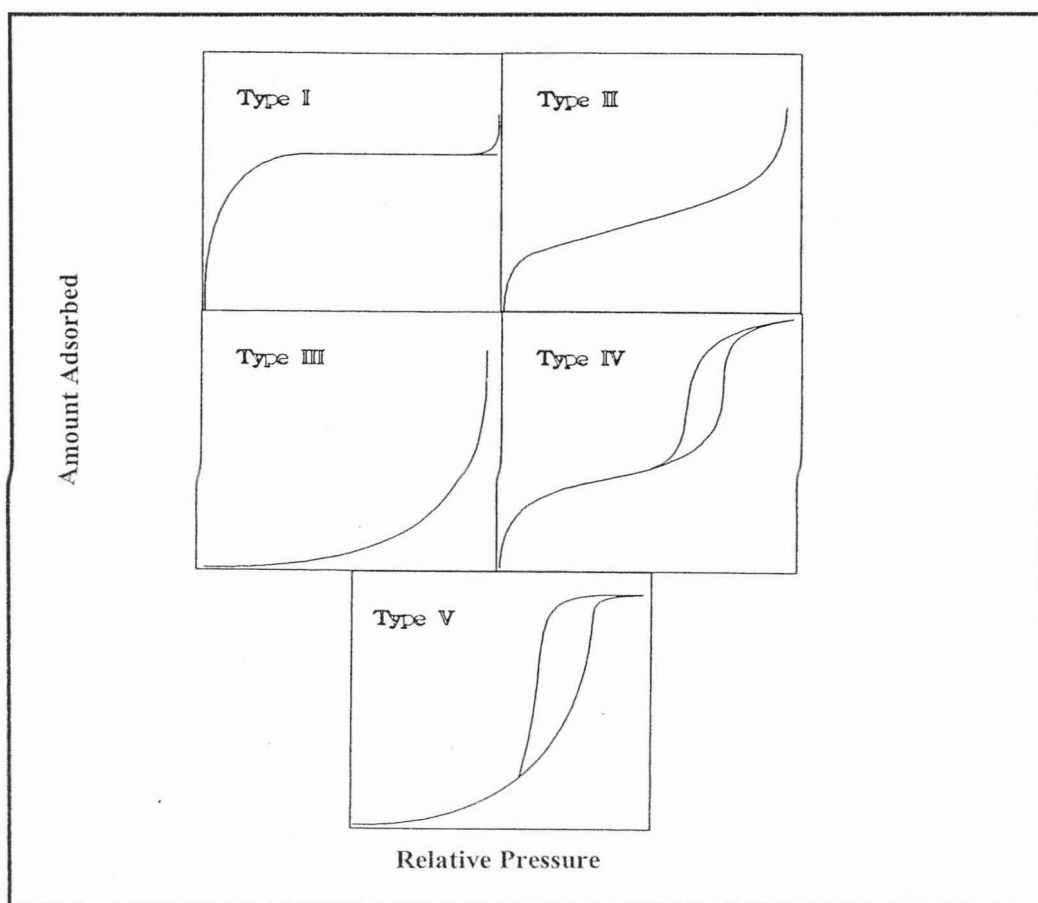
Figure 4.2: The five main types of adsorption isotherms according to the BDDT-classification [Brauner *et al*, 1940]

Type I are reversible isotherms characteristic of microporous solids namely activated carbon and zeolites. The uptake of adsorbate reaches a limiting value as relative pressure (P/P_o) tends to 1, which reveals that adsorption of adsorbate, is dependent on the micropore volume rather than surface area.

Type II isotherms are attributed to non-porous or macroporous solids. These isotherms denote that monolayer-multilayer adsorption takes place.

Type III and V isotherms are related. They are not very common and may originate from the adsorption of either polar or non-polar molecules, with the adsorbent-adsorbate interactions being much weaker than the adsorbate-adsorbate interactions.

Type IV isotherms are recognised by the presence of a hysteresis loop. They are associated frequently with physical adsorption of gases on mesoporous solids. Carbons having both micro and mesopores show adsorption isotherms of this type.

Since, most activated carbons from bagasse fall in the type IV region; more detail on this isotherm is presented.

4.2.1. Type IV Isotherm

A more detailed illustration of the BDDT type IV isotherm is illustrated in figure fig 4.3. As adsorption of a gas proceeds, the initial uptake of adsorbate into the micropores of the solid follows the curve ABC. At about 0.4, relative pressure (P/P_o), the isotherm deviates and moves upward until saturation vapour pressure is reached at point F [Botha, 1992]. Micropores are associated with reversible adsorption [Bansal et al, 1988]. The hysteresis loop (curve FGC) occurs upon desorption and is related to the distribution of mesopores in the solid. The hysteresis loop occurrence was, first explained by Zsigsmondy [1911] in his capillary condensation theory. According to his theory, when pores of unequal diameter are present, the micropores (narrowest) pores fill at the lowest pressures.
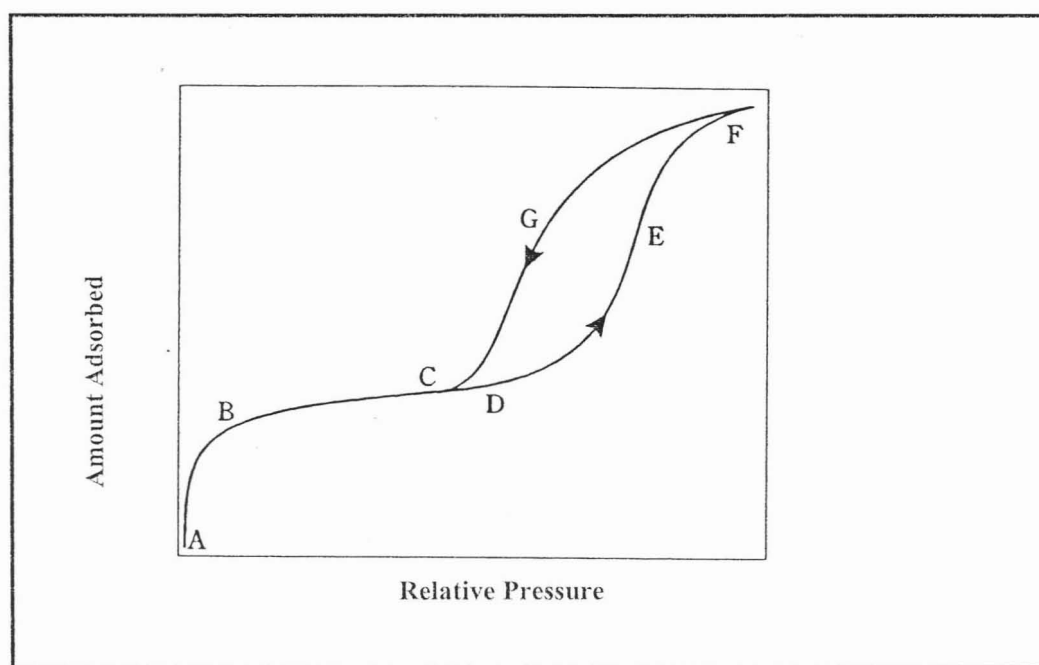
Figure 4.3: Type IV BDDT isotherm [Botha, 1992].

Increasing pressure follows a stepwise filling of larger and larger pores (capillaries) with liquid adsorbate until saturation vapour pressure F is reached. The vapour in the capillaries would condense to a liquid like state forming a meniscus at pressures below those required for normal condensation.   Upon desorption, the mechanism changes to capillary evaporation instead of multilayer formation for adsorption, thereby forming a hysteresis effect. Evaporation in the pore continues until the pore is empty [Botha, 1992].

4.3. Surface Area

4.3.1.   Estimation of Surface Area by the BET model

The BET [Brauner *et al*, 1938] theory is based on the kinetic adsorption model proposed by Langmuir [1916] whereby the surface of the solid is seen as an array of adsorption sites. When the rate at which the molecules of gas arrive at the surface and condense or are adsorbed into unoccupied sites, equals the rate at which molecules evaporate or desorb from occupied sites, equilibrium is achieved. The amount adsorbed at equilibrium is dependent on:

- the average period of when the molecules condenses and its subsequent evaporation,
- the total area of solid, proportion of surface area that attracts molecules and its accessibility,
- pressure of the gas and
- the number of layers adsorbed [Hassler, 1974].

For monolayer adsorption, the Langmuir equilibrium adsorption equation is expressed as [Langmuir, 1916]:

$$\frac{n}{n_m} = \frac{BP}{1+BP} \qquad\qquad (4.1)$$

where: n = moles adsorbate adsorbed on 1g adsorbent

n_m = monolayer capacity (adsorption of one molecular layer of the adsorbate on the adsorbent)

B = an empirical constant and

P = partial pressure of the adsorbate

However, physical adsorption generally involves multilayer adsorption. Multilayer adsorption occurs at pressures below that required by monolayer coverage. Brauner *et al* [1938] proposed

an equation (4.2) based on multiple adsorptive layers in order to determine surface area and monolayer capacity:

$$\frac{n}{n_m} = \frac{c\left(\dfrac{P}{P_o}\right)}{\left(1 - \dfrac{P}{P_o}\right)\left(1 + (c-1)\left(\dfrac{P}{P_o}\right)\right)}$$

(4.2)

where: P_o = saturation vapour pressure of the adsorbate at the temperature of experiment

c = the BET constant expressed as:

$$c = \exp\left(\frac{(H_1 - H_L)}{RT}\right)$$

(4.3)

H_1 = molar adsorption of enthalpy in the first layer

H_L = molar enthalpy for condensation

R = ideal gas law constant

T = temperature in Kelvin [Gregg and Sing, 1982]

Usually adsorption experiments measure volume adsorbed rather than moles adsorbed, therefore, equation 4.2 is then converted to equation 4.4:

$$\frac{V}{V_m} = \frac{c\left(\dfrac{P}{P_o}\right)}{\left(1 - \dfrac{P}{P_o}\right)\left(1 + (c-1)\left(\dfrac{P}{P_o}\right)\right)}$$

(4.4)

where: V = volume adsorbed per gram of adsorbent

V_m = monolayer adsorption capacity in terms of volume

4.3.2. Application of BET to experimental data:

Equation 4.4 can also be written as:

$$\frac{P}{V(P_o - P)} = \frac{1}{V_m c} + \frac{(c-1)}{V_m c}\left(\frac{P}{P_o}\right)$$

(4.5)

By plotting P/P_o versus $1/[V(P_o/P - 1)]$ over the range $0.05 < P/P_o < 0.35$, a straight line is generated with slope $= (c-1)/(V_m c)$ and intercept $= 1/(V_m + c)$ such that the parameters V_m and c can be determined by:

$$V_m = \frac{1}{slope + intercept} \qquad (4.6)$$

and,
$$c = \frac{slope}{intercept} + 1 \qquad (4.7)$$

Using the value for monolayer capacity derived in equation 4.6, the surface area of the adsorbent can be determined by:

$$S_{BET} = \frac{V_m \sigma N_A \rho}{MW} \qquad (4.8)$$

where: S_{BET} = BET surface area of the adsorbent (m^2/g)

σ = average area occupied by the adsorbate molecule (Å^2)

N_A = Avagrado's number = 6.022×10^{23} number/mole

ρ = adsorbate liquid density

MW = molecular weight of the adsorbate

Many sorption analysers measure the amount of gas adsorbed and converts it to volume of gas adsorbed at standard temperature and pressure (at STP - 273K and 1 atm). In this case, the BET surface is calculated as follows:

$$S_{BET} = \frac{V_m \sigma N_A}{V_i} \qquad (4.9)$$

where: V_i = molar volume of the gas at STP = 22.4litres/mol

V_m = cm^3 gas/g adsorbent

The equations above apply to any adsorbate used to obtain surface area with the most common being nitrogen at 77K. The choice of adsorbate used to determine surface area depends on the molecular packing and pore sieving effects. An adsorbate with a relatively large saturation

pressure is considered a good choice since a wide range of relative pressures can be covered at a particular adsorption temperature [Cal, 1995]. Table A-1 in Appendix A contains a list of adsorbate molecules compiled by McClellan and Harnsberger [1967] and Myers and Praustniz [1965].

The BET theory was based on the assumption that all adsorption sites on the solid surface are energetically homogenous, and that the adsorbate-adsorbate reactions are negligible. In fact, in reality it is quite the opposite, since most adsorption surfaces are heterogeneous and adsorbate-adsorbate interactions do occur when the adsorption layer is near complete and the average separation of molecules are small compared to their size [Gregg and Sing, 1982]. Nevertheless, the BET surface area is still widely used and is an important value when dealing with activated carbons.

4.4 Estimation of External surface area, Micropore Volume and Micropore Area.

4.4.1 t –plot Method

The t-plot method, which is based on comparing the adsorption of a porous solid with that of a non-porous solid, has been widely used to determine the micropore volume of porous solids. Mikhail *et al* [1968] demonstrated that these plots provide more detail on the porosity of a solid. The t-plot method is attributed to Lippens and de-Boer [1965]. They discovered that the multilayer adsorption curve for nitrogen at different pressures and constant temperature is identical for wide variety of adsorbents, provided that no capillary condensation occurs. This curve is referred to as the multi-molecular adsorption curve or t-curve. This curve provides a relationship between the statistical thickness of the adsorbed film and the relative pressure (P/P_o). The experimental data points of this curve were found to be in agreement with the isotherm equation of Harkins and Jura presented below. This equation is used in most applications to determine the thickness of the adsorbed gas.

$$th = \left[\frac{13.99}{\log\left(\dfrac{P_o}{P}\right) + 0.034} \right]^{0.5} \tag{4.10}$$

where: th = statistical thickness in Å

Lippens and Boer suggested plotting the volume of nitrogen adsorbed at different relative pressures (P/P_o) versus statistical thickness determined from equation 4.10. If the multilayer adsorption is applicable over the entire pressure range, a straight line passing through the origin with slope equal to the surface area for a non-porous solid is generated. However, for a porous solid with a pore size distribution, the smaller pores are filled with adsorbate molecules as pressure increases. These pores become saturated and cannot accommodate more adsorbate resulting in a decrease in the slope of the curve as adsorption progresses further. De Boer *et al* [1965] found that the surface areas still available can be related to the slope of the t-plot at a considered P/P_o point. For most materials the linear portion of the t-plot is when the statistical thickness t is between 3.5 and 6 Å. The external surface area (S_{ext}) is related to slope of the t-plot by:

$$S_{ext} = 15.47(V/th) \qquad (4.11)$$

The contribution to the external surface area in activated carbons is due to the meso- and macropores and a typical value is between 10 and 200 m^2/g [Bansal *et al*, 1988]. Extrapolation of the linear portion of the t-plot to the y-axis, of which the intercept corresponds to the pores that have been filled with nitrogen and this is then used to evaluate the micropore volume with the use of a density correction factor for nitrogen when using nitrogen as the adsorbate.

Together with external surface area (equation 4.11) and the BET surface area (equation 4.9), the micropore surface (S_{micro}) area can be determined by:

$$S_{micro} = S_{BET} - S_{ext} \qquad (4.12)$$

The statistical thickness *th* cannot be used to determine the mesopore sizes since capillary condensation takes place at a certain pressure.

4.5. Estimation of Mesoporosity and Macroporosity

4.5.1 Mercury Porosimetry

Mercury porosimetry has been extensively used to determine macroporosity and almost the entire range of mesoporosity [Bansal *et al*, 1988] in porous solids. Smetana [Ritter and Drake, 1945] when studying the porous nature of wood in 1842, first suggested using mercury penetration methods to determine the pore size distribution. Later, Washburn [1921] and Ritter and Drake [1945] proposed a method to determine the pore sizes. According to Washburn

[1921], mercury is a non-wetting liquid having a contact angle θ near 140 $^{\circ}$ and when subjected under pressure (P), it fills the cylindrical pores of radii $r > r_p$ determined by:

$$r_p = -2\left(\frac{\gamma}{P}\right)\cos\theta \qquad\qquad (4.13)$$

where: θ = contact angle between the solid and mercury

       γ = surface tension of the liquid adsorbate

       P = pressure applied

       r_p = pore radius

The Pressure P is the difference between the pressure of mercury in the liquid and gas phase ($P = P_{Hg} - P_g$). At any applied pressure, P_i, a certain amount of mercury (V_i) penetrates the pores having a radius $r \geq r_{pi}$, called the cumulative pore volume. A plot of cumulative pore volume (V_p) versus log r_p gives a pore sized distribution graph. For activated carbons from agricultural by-products, a bimodal distribution of pore sizes is typical. From a plot of V_p versus r_p, the cumulative surface area (S_{cum}) of the pores filled by mercury can be determined. This value is less than S_{ext} due to mercury porosimetry being limited to 3.5 nm at 2000 atm. The limit of mesoporosity is 2 nm; therefore, mercury porosimetry does not cover the range of 2 –3.5 nm, which contributes significantly to external surface area.

A plot of log S_{cum} versus log (r_p) is a straight line in the region of 4-15nm from which total area of mesopores ($r_p > 2$nm) can be extrapolated. Values obtained this way have agreed with values from immersion calorimetry techniques and benzene adsorption [Bansal et al, 1988].

Ritter and Drake [Allen et al, 1998] have revealed that during desorption with a mercury pressure volume relationship, a proportion of mercury stays behind in the pores thereby displaying a hysteresis effect. Therefore, surface areas determined from mercury porosimetry may be inaccurate.

4.5.2 BJH Adsorption and Desorption model [Barret et al, 1951]

Almost all models make use of the fact that the pressure at which capillary condensation occurs in a particular pore is related to the size of the pore. Barret et al [1951] proposed a set of methods to determine the pore size of meso and macro-pores based on the Kelvin equation. The

Kelvin equation is only applicable in the larger pore size ranges and breaks down when the molecular texture of the fluid influences adsorption.

The fundamental Kelvin equation (4.14), relates the relative pressure with pore size based on the assumption that perfect wetting occurs such that the contact angle is zero:

$$\ln\left(\frac{P_d}{P_o}\right) = \frac{-2\gamma V_m}{RTr_k} \tag{4.14}$$

where: P_d = pressure at which a cylindrical pore of radius r_k is desorbed

V_m = molar volume

P_o = saturation pressure of the liquid adsorbate at temperature T

For split shaped mesopores, the Kelvin radius, r_k, is replaced by the width L_k of the slits. Adsorption occurs naturally on the walls of the mesopores. After, desorption a layer of thickness t_l is left behind and has to be also taken into consideration, therefore the dimensions of mesopores are:

$$r_p = r_k + t_l\left(\frac{P}{P_o}\right) \tag{4.15}$$

and

$$L_p = L_k + 2t_l\left(\frac{P}{P_o}\right) \tag{4.16}$$

Bansal *et al* [1988] provides an explanation of the above concept with the aid of figure 4.4.
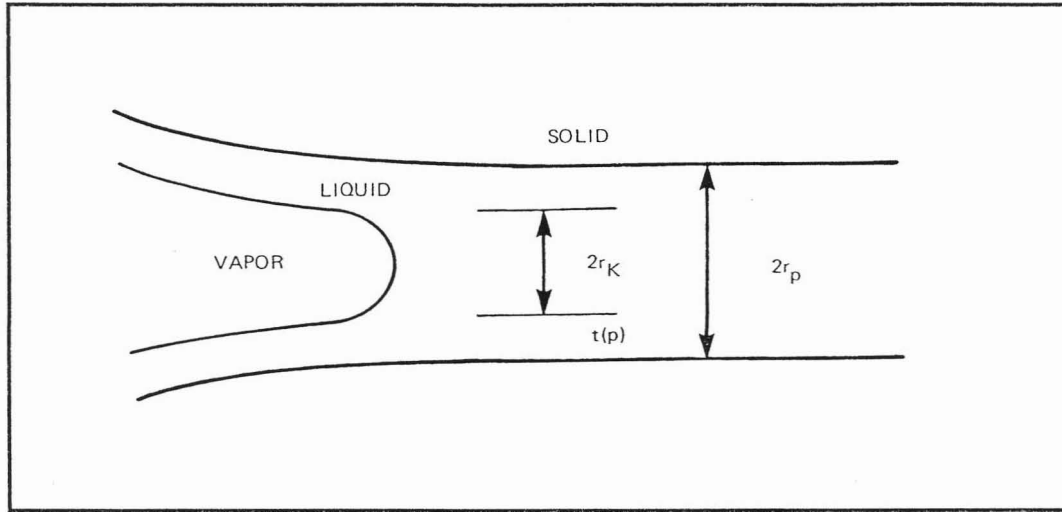
Figure 4.4: Relation between the Kelvin radius r_k and true radius, r_p of a cylindrical mesopores, $t\,(p)$ – statistical thickness [Bansal, _et al_, 1988].

When desorption occurs only the central core with cylinder of diameter 2 r_k (or slice of width L_k) will be desorbed and a multilayer of thickness of $t_l(P/P_o)$ remains on the pore wall. This thickness function corresponds to the natural adsorption isotherm of the same solid whereby the average thickness is:

$$t_l\left(\frac{P}{P_o}\right) = \sigma n_a\left(T; \frac{P}{P_0}\right) n_m \tag{4.17}$$

On the basis of experiments carried out in various open spaces, equation 4.18 has been expressed for nitrogen at 77K:

$$t_l\left(\frac{P}{P_o}\right) = 0.35\left[\frac{-5}{\ln(\frac{P}{P_o})}\right]^{0.33} \tag{4.18}$$

The above equation has found to be a good approximation in equation 4.19, which, indicates that the total volume adsorbed by an adsorbent (in this case activated carbon) is a contribution from the filling of micropores and adsorption on the external surface area..

$$V\left(T; \frac{P}{P_o}\right) = V_{micro}\left(T; \frac{P}{P_o}\right) + S_{ext} t_l\left(\frac{P}{P_o}\right) \tag{4.19}$$

The Kelvin radius, for nitrogen desorption at 78K, becomes:

$$r_k = \frac{0.940}{\ln\left(\dfrac{P_o}{P}\right)} \qquad (4.20)$$

since: γ = 8.72 mN/m for nitrogen at 78 K

V_m = 34.68 cm^3/mol of pure liquid

Equations 4.18, 4.20 and 4.15 or 4.16 are then used yield information on the mesopores size distribution using nitrogen adsorption. Adsorption in mesopores is related to surface area rather than pore volume [Bansal *et al*, 1988]. Mesopore surface area and pore volume have been determined by for both adsorption and desorption using the plotting techniques related in section 4.5.1 on mercury porosity.

The pore size distribution can be determined by the relationship between cumulative pore volume (V_{cum}) versus pore radius (r_p). The pore size distribution is usually defined as:

$$f(r_p) = \frac{dV_{cum}}{dr_p} \qquad (4.21)$$

$$f(r_p) = \frac{dV_{cum}}{d(\log r_p)} \qquad (4.22)$$

4.6. Calculation of average Pore Sizes (Mean pore radius)

Different pores have walls and the types of surfaces associated with them i.e. the microporous surface area (internal area) which is represented by the walls of slits and the second is the non-microporous or external surface area which includes the walls of meso- and macropores.

The mean pore radius can be determined from the pore size distribution by the condition of equal catalytic surfaces for a cylindrical pore by:

$$2\pi \overline{r_p} L = 2\pi \int_0^\infty r_p f(r_p) dr_p \qquad (4.23)$$

where the total pore length (L) is:

$$L = \int_0^\infty f(r_p)dr_p \qquad (4.24)$$

Thus, the mean pore radius is found by:

$$\bar{r}_p = \frac{\int_0^\infty r_p f(r_p)dr_p}{\int_0^\infty f(r_p)dr_p} \qquad (4.25)$$

When the pore size distribution is not known, the mean pore radius is determined by:

$$\bar{r}_p = \frac{Volume}{SurfaceArea} \qquad (4.26)$$

Therefore for a mesoporous cylindrical pore, the average pore diameter can be determined by:

$$D_{pore} = 2\bar{r}_p = 4\left(\frac{\pi r^2 L}{2\pi r L}\right) = 4x\frac{V_{pore}}{S_{pore}} \qquad (4.27)$$

and for a split shaped micropore, the diameter is:

$$L_{pore} = 2x\frac{V_{pore}}{S_{pore}} \qquad (4.28)$$

4.7. Topography

The porous nature of an activated carbon's exterior can be pointed out by topographical studies. It has been mentioned on several occasions that the external pores (meso – and macropore) of an activated carbon normally are the transport pores allowing the passage of the adsorbing species into the internal microporous structure of the carbon. Scanning electron microscope (SEM) techniques can be used to identify these transport pores on the surface. SEM's provide a

three-dimensional picture of the surface structure and, are very effective and accurate method of surface investigations [Allen *et al*, 1998]. Stoeckli *et al* [1989] have also used transmission electron microscopy (TEM) to confirm results in adsorption experiments. But in this study, SEM techniques were adopted.

4.8. Adsorption from Solutions by Activated Carbon

4.8.1   Freundlich Isotherm

Bansal *et al* [1988] relate that it is rather difficult to assess the whether nature of adsorption of solution is monomolecular or multimolecular since this is usually determined by:

- the porosity and chemical nature of the adsorbent
- the nature of components in solution
- the concentration of the solution and
- the mutual solubility of the components

Freundlich and Heller in 1939 [Treybal, 1980] investigated the adsorption of solutions on activated carbons in their early studies. They developed an empirical correlation for adsorption isotherms for which there is a linear correlation between the adsorption capacity and the adsorbate concentration shown by:

$$\frac{X}{M} = K_a C^{1/n_c}$$
(4.29)

where: X = the mass of solute adsorbed

      M = mass of adsorbent

      K_a = adsorption capacity of adsorbent

      n_c = effect of concentration on adsorption capacity

      C = equilibrium concentration of the adsorbate in the bulk phase

The valid concentration range that applies to the Freudlich equation depends on the adsorbate-adsorbent combination. By plotting *X/M* versus *C* on a log-log axis will generate a straight line with slope = *1/n_c* and intercept =*K_a*. The limitation of the Freudlich plot is that each isotherm is unique for every adsorbate-adsorbent combination.

4.8.2. Iodine Adsorption

Iodine adsorption test method is used to determine the iodine number (mg iodine adsorbed/ g activated carbon) for an activated carbon. Iodine is a small molecule and this test is a measure of the number of pores greater then 10 Å [Bansal *et al*, 1988]. Basically, the iodine number is a relative indicator of microporosity in an activated carbon. For activated carbons having a large surface area (> 900 m^2/g), the iodine is comparable to the BET surface area value, but for very low surface area carbons, this one-one correlation of surface area is not applicable.

4.8.3. Methylene Blue

Methylene Blue is a soluble azine dye with a low charge density that is rapidly adsorbed by the meso- and macropores of an activated carbon. Adsorption of methylene provides an estimation of the surface area contribution by pores in this size range and also is an indicator of the activated carbon's ability to adsorb molecules of the methylene blue size and smaller. The adsorption test of methylene blue gives rise to the methylene blue number defined as the mass of methylene blue adsorbed per gram of activated carbon.

4.8.4. Molasses Number

The molasses number in contrast to the iodine number represents the amount of large pores in an activated carbon. It is an indicator of the decolourising capacity of the activated carbon. The molasses number is based on a single point comparison and is calculated from the ratio of the optical densities of the molasses solution treated with a standard active carbon and the one with the activated carbon in question. This test is limited to the concentration of the molasses solution used and is dependent on the standard activated carbon.

4.9. Adsorption of colour bodies from sugar

Activated carbons in the sugar industry are mainly used to remove colouring matter from sugar syrups thereby improving the appearance of sugar and its processing properties. Active carbons help in removing surface-active agents and colloidal substances thus raising their surface tension and decreasing viscosity. This leads to higher rates of sugar crystallization and improved separation of syrups from crystals during centrifugation [Bansal,*et al*, 1988].

A typical activated carbons pore size distribution is shown in fig 4.5. Comparatively to a gas carbon, a sugar carbon contains more meso-macropores that are responsible for the removal of large colour bodies. Pores greater than 30 Å and larger are active in decolourisation. Treumper [1968] indicates that pores make up diffusion barriers for the colour bodies. According to Dominguez and Hyndshaw [1976], a granular or powder activated carbon should generally have the same surface area, pore structure and surface complex when produced from the same parent raw material and when either applied to sugar decolourisation both would produce the same effect [Treumper, 1968].
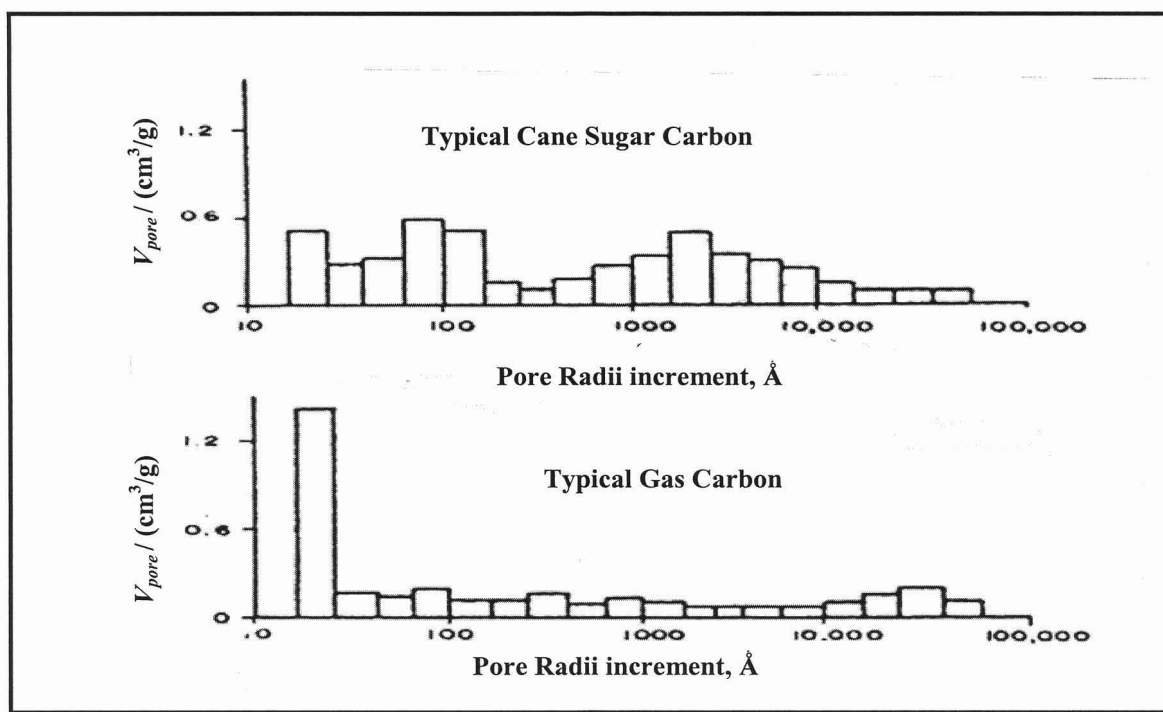
Figure 4.5: Pore Size Distribution of a typical sugar carbon [Treumper, 1968].

4.9.1. Factors affecting sugar decolourisation

The most important criteria in sugar decolourisation is pH of the activated carbon. Low pH activated carbons tend cause the irreversible reaction of converting sucrose to fructose and glucose [Mead and Chen, 1977]. These sugars do not form solid crystals and in fact stay in the in the liquid phase. Even an alkaline carbon would not be favourable since during sugar decolourisation colour development could occur by the alteration of the molecular structure of the sugar impurities [Bernadin, 1985]. A carbon having a pH of 7 is deemed to be more appropriate for sugar decolourization. A high ash content of activated carbon is also unsuitable for decolourisation as it could interfere with carbon utilization through competitive adsorption and blockage of pores [Marshall, 1999].

4.9.2. Activated Carbon Application

Powder activated carbon is used on a batch operation, whereby the carbon dosage is determined by the desired purity. The process involves adding the activated carbon to the sugar melt, dispersing it and keeping it in contact with the liquor for a predetermined length of time before being separated from the melt by separation. On the other hand granular carbons are continuous processes whereby the unwanted impurities are in intimate contact with the activated carbon's surface as the liquor passes through the packed column of granular carbon. There are many disadvantages associated with granular activated carbons, which include:

- its ability to catalyse a reaction resulting in the formation of an acid which consequently lowers the pH of the solution.
- its response to regeneration, since during regeneration, approximately 5% of the activated carbon is lost and even its porous characteristics are reduced.

EXPERIMENTAL

5.1. Process

5.1.1 Choice of Process

Keeping in context that the final use of the activated carbon from South African sugar-cane bagasse would be to decolorize raw sugar liquor, the two-step physical method of activation, i.e. pyrolysis followed by activation with steam was adopted. Chemical activation was seen negatively as a result of it being associated with the generation of large amounts of effluent due to the subsequent washing of the produced activated carbon in order to remove the chemical activating agent. In view of the fact that sugar is a food product, the risk of chemical contamination during decolourisation with chemically activated carbons may lead to higher costs by possibly adding a further step of purification in trying to meet specifications of sugar quality.

Steam was chosen as the activating agent because many sugar mills produce excess steam, which is readily available. Studies performed with using carbon dioxide as activated agent indicated that low surface area activated carbons were produced from bagasse and that the activation time was much longer in order to reach a certain burn-off percentage [Pendyal *et al*, 1999]. It has been alleged that steam is more reactive than carbon dioxide [Rodriguez-Reinoso and Molina-Sabio, 1992] and confirmation was received by Gergova *et al*, [1992] when they found that the reaction rate is three times faster than carbon dioxide at 800 ^{O}C thereby lowering activation time. The water molecule has a smaller dimension than carbon dioxide leading to a much faster diffusion into the porous structure created during pyrolysis and hence a faster reaction rate.

Finally, the option of using the physical method was also based on making a low-cost adsorbent seeing as the spent activated carbon will be burnt as a fuel source in the boilers instead of being regenerated.

Fig 5.1 illustrates the specific processing options that have been generated to produce activated carbon from South African sugar cane bagasse. A more generalized set of process options has been presented by Bansal *et al* [1988].
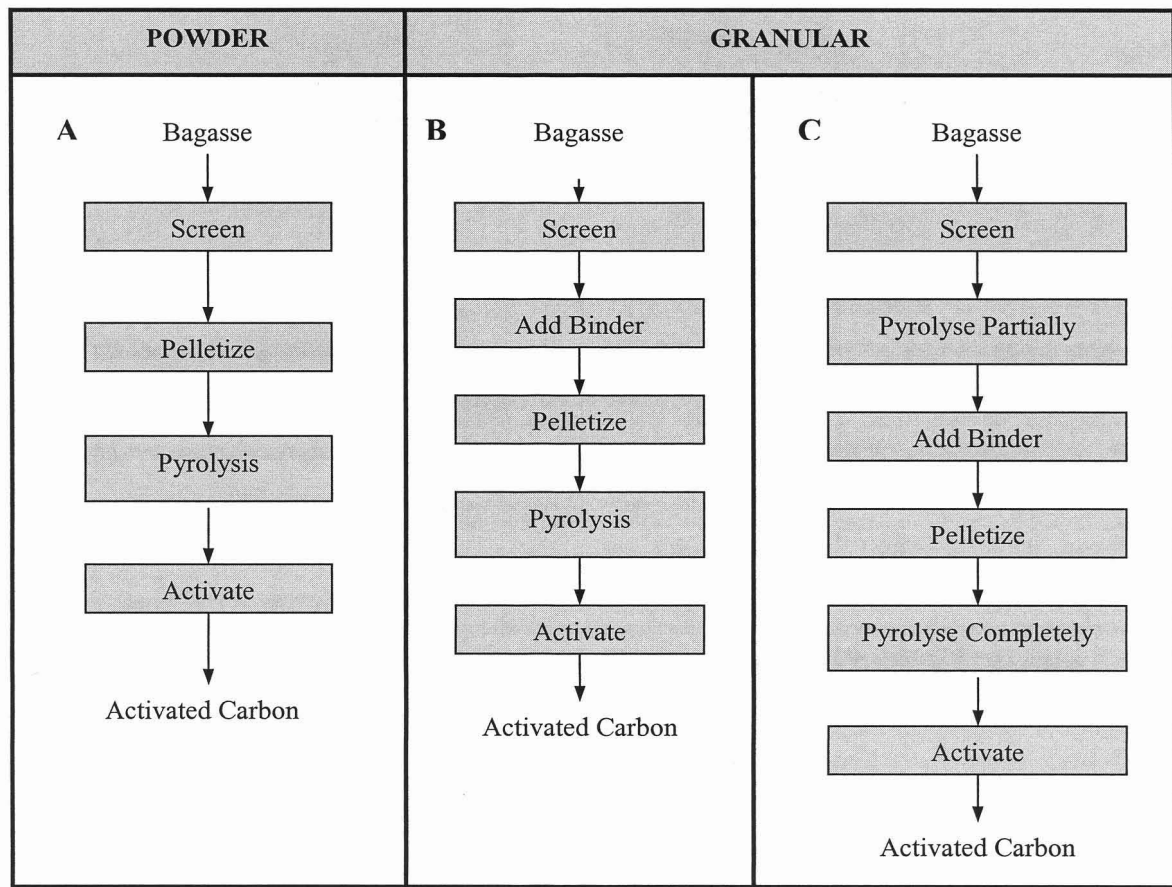
Figure 5.1: Processing options generated for producing activated carbon from sugar-cane bagasse.

5.1.2. Activated carbon manufacturing process from sugar cane bagasse

From fig. 5.1, option C indicates that much longer activation times are required compared to A and B by the pyrolysis process being split into two and the chances of developed pores becoming filled with the binder material is much greater. These pores can become available during activation, but the chances of a microporous activated carbon being produced is much greater compared to the desired mesoporous carbon. Options A and B reveal, that a

microporous carbon produced during the pyrolysis can be further developed into meso-macroporous carbons during activation. Hence, with respect to time, cost and desired properties of the final activated carbon, processes A and B were chosen from fig 5.1. A generalized block flow diagram of the established activated carbon processes from bagasse is presented in figure 5.2.
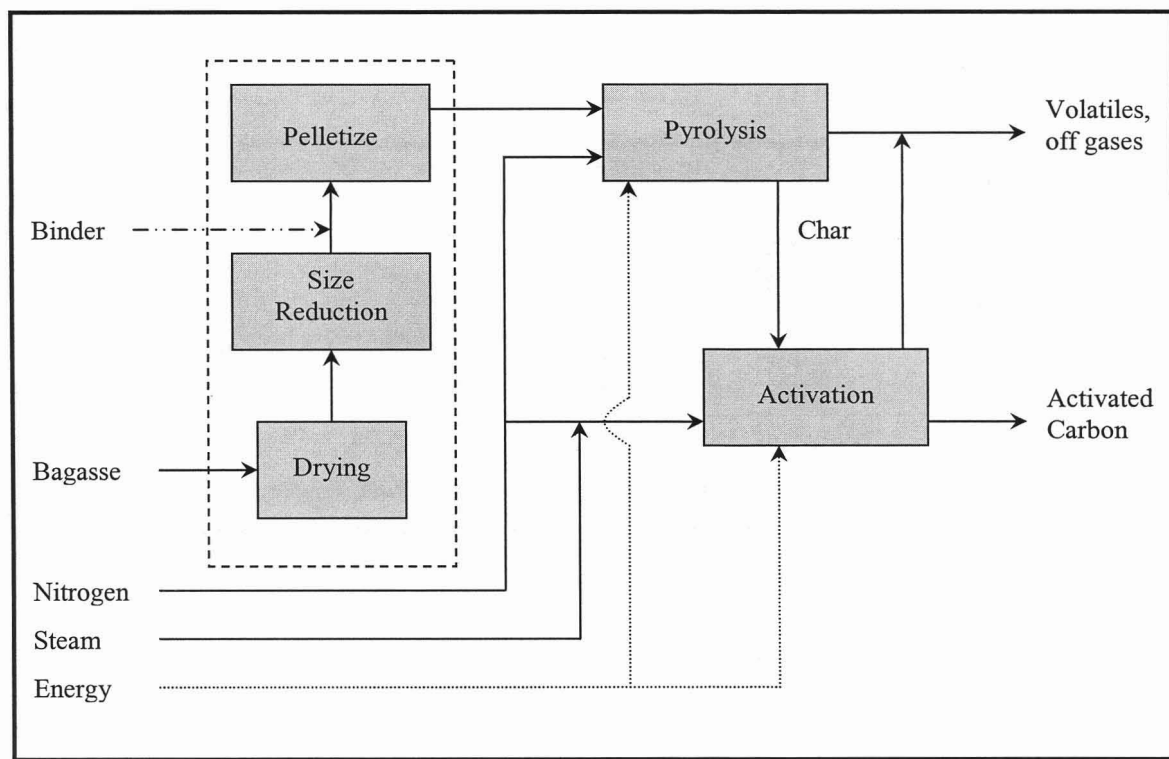
Figure 5.2: Block Flow Diagram of Activated carbon production from S.A. Bagasse.
         ---- Raw material Preparation

5.2. Raw Material Preparation

Received bagasse was initially hand-sieved in order to determine the particle size distribution of the bagasse fibres. Manual sieving was employed since bagasse fibres tend to mat due the shape factor of high length to diameter ratios. The particle size distribution of raw bagasse is presented in fig 5.3. The majority of the fibres have diameters less than 710μm.

Bagasse is a low-density material with a small mass occupying a large volume and it has been anticipated that if processed directly, low yields of activated carbon would be obtained. In order to increase char yield; it was decided to compress bagasse fibres into pellets. Compressed bagasse will enhance vapour-solid interactions during pyrolysis, which will subsequently

increase char yield. This decision was also based on Xia *et al*'s [1998] work, who found that high surface area activated carbons can be produced from lumped bagasse.
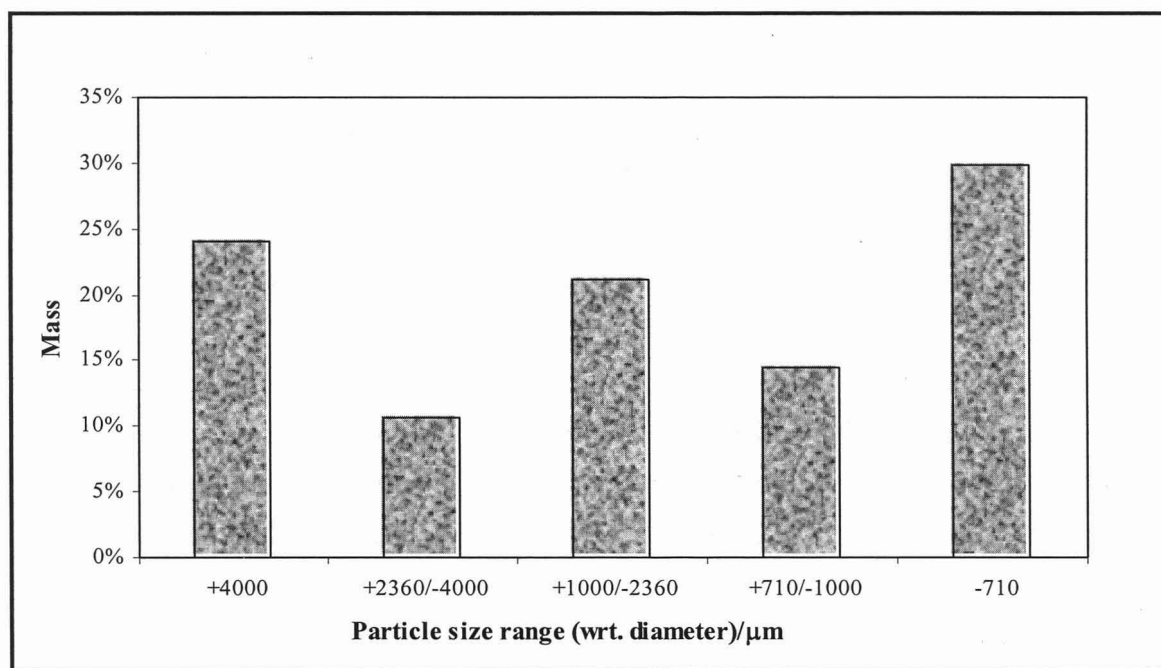
Figure 5.3: Particle Size Distribution of South African sugar received from Sezela mill.

Initially, as received bagasse was formed into pellets, but these did not form compact pellets. Therefore, a size reduction stage was introduced prior to pelletization.

The received bagasse was initially dried to constant weight in an oven set at 110 $^{\circ}$C. The dried bagasse was then crushed in a "Kenwood food processor" for 15 minutes and sieved, giving rise to a bagasse particle size distribution presented in table 5.1. A plot of cumulative mass % of bagasse versus average particle size revealed that the average bagasse particle size after crushing was 420μm.

Table 5.1: Size distribution of crushed sugar cane bagasse

Size Range / μm	Average diameter /μm	Cumulative mass %
+1000	1189.2	18
+710 / -1000	842.6	26
+500 / -710	595.8	38
+355 / -500	421.3	54
+250 / -355	297.9	69
+ 180 / -250	212.1	79
-180	151.4	100

Approximately 20 g of crushed bagasse comprising of the above size distribution were fed into a die and piston (see fig 5.4) and compressed into cylindrical pellets in a hydraulic press (see fig 5.5) at a rate of 0.333cm/s by applying a force of 110 kN. The resulting pellets were 30 mm in diameter and between 35-38mm in length having a bulk density of 700-900kg/m^3. The pellets were extremely compact and did not lose shape. The pellets resistance to shatter when dropped from a height of approximately 1.3m to the ground provided a good indication of its compactness. The pellets were housed in a dessicator prior to use since some void spaces still existed in the pellet and if exposed to the atmosphere for lengthy periods, adsorption would occur, thereby causing the pellets to loose their compactness and expand.

In the production of granular activated carbons, two types of binders were readily obtainable at the sugar mill, one being molasses and the other being sucrose. Molasses has high ash content and studies performed with bagasse bound with molasses as the binder produced satisfactory activated carbons but having even higher ash contents. However, Evans *et al* [1999] produced very high surface area (1500 m^2/g) activated carbons from sucrose. Based on his findings, the option of using household grade sugar crystals were chosen as a binder with bagasse instead. The sugar crystals were mixed with crushed bagasse prior to pelletizing. Pellets formed with the binder displayed similar characteristics as portrayed for bagasse with no binders.
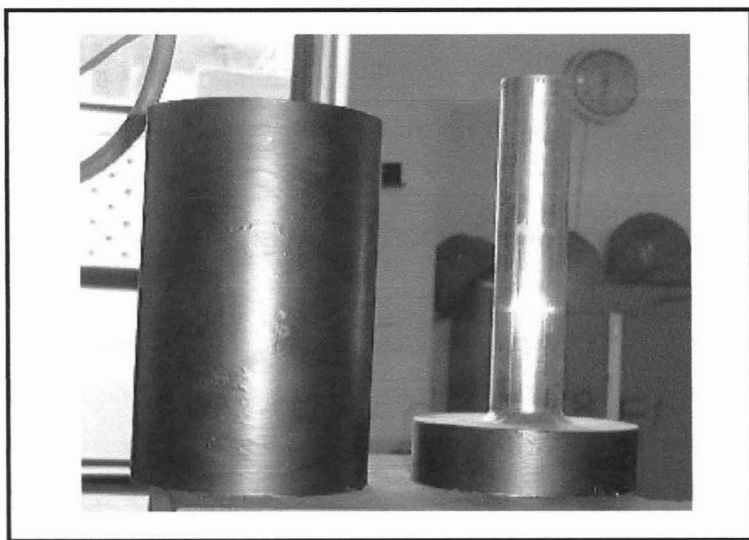
Figure 5.4: Photo of die and piston used to form cylindrical bagasse pellets
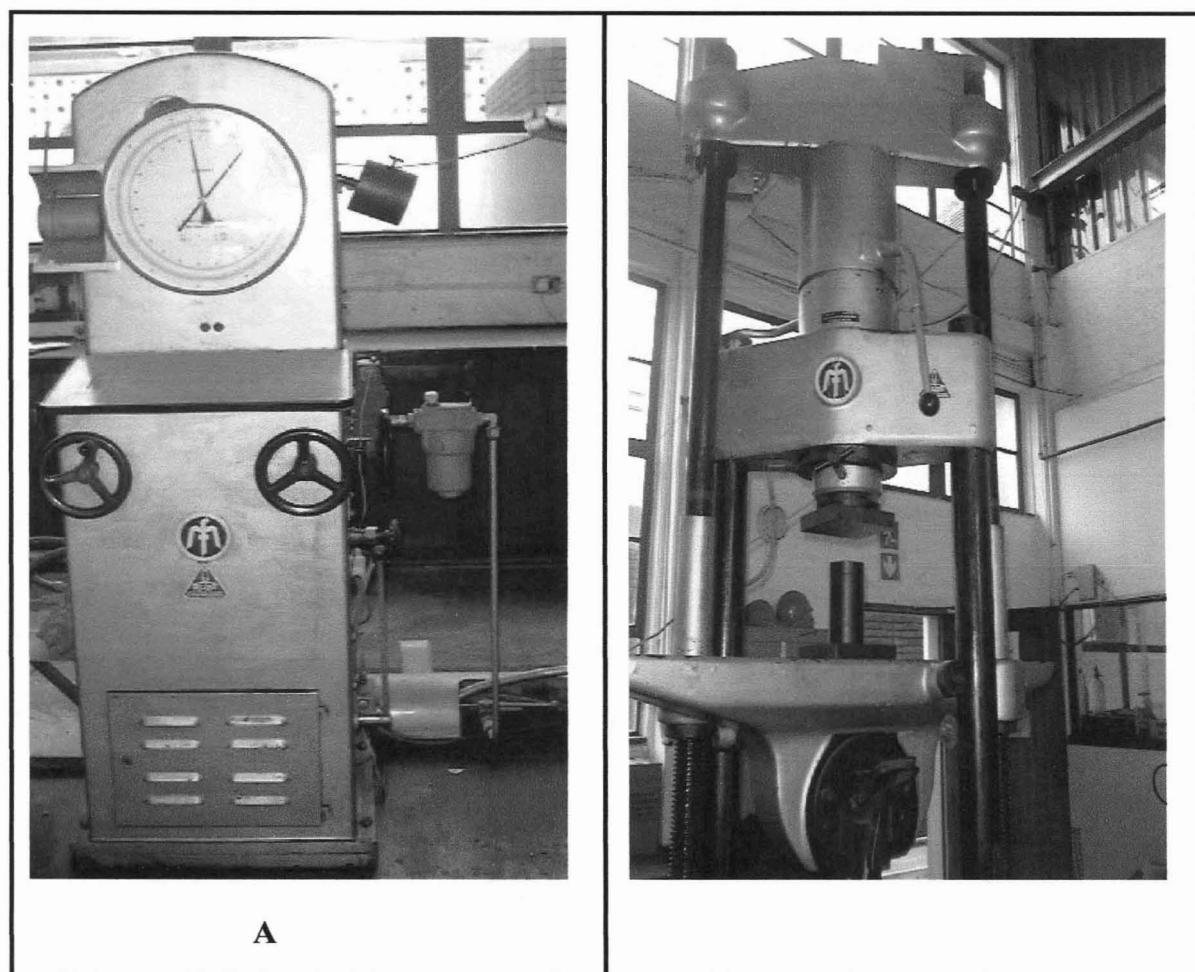
Figure 5.5: Photo of the hydraulic press used to compress bagasse into pellets. A – Control panel; B – Hydraulic press with die and piston set –up.

5.3. Pyrolysis and Activation Process Flow Diagram

After raw material preparation, the bagasse pellets were firstly pyrolysed under a nitrogen atmosphere and the resultant chars were subjected to partial gasification with steam. A process flow diagram of the pyrolysis and activation sections is presented in figure 5.6. The basic control and instrumentation information are also presented in figure 5.6. Process units for pyrolysis of lignocellulosic material and bagasse used by other researchers consist mainly of four components; a pyrolysis furnace, a gas treatment and supply system, an electrical system to record temperature-time history and a products collection system [Stubington and Aiman, 1994; Conti *et al*, 1994, Encinar *et al*, 1997].
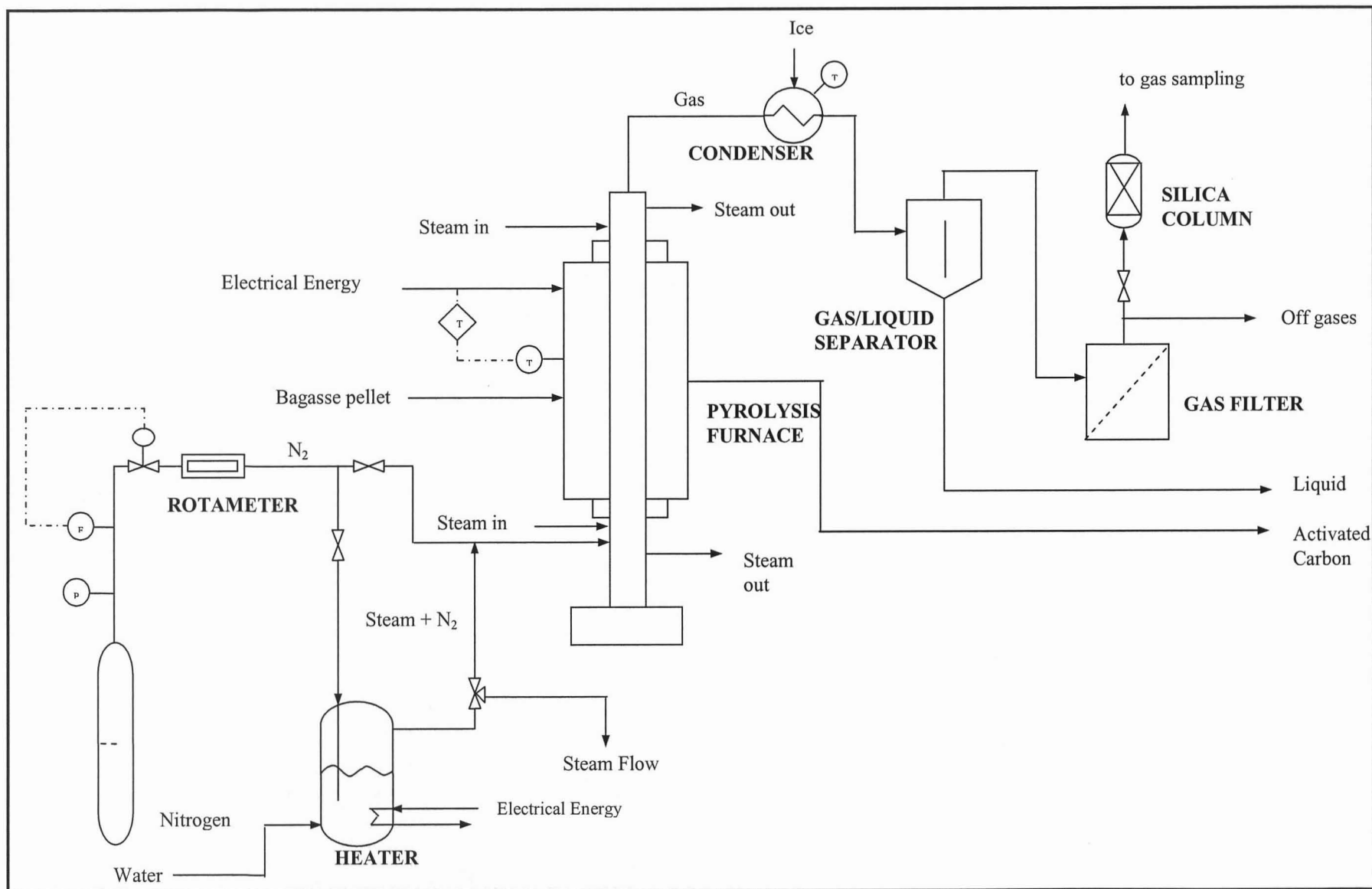
Figure 5.6: Process flow diagram of the activated carbon process from South African sugar cane bagasse.

The process flow diagram illustrated in fig 5.6 also includes the following major equipment:

- steam supply unit
- pyrolysis furnace
- downstream units: condenser, gas-liquid separator, gas filter system and gas sampling unit

5.4. Equipment

5.4.1. Pyrolysis Furnace

An existing thermobalance had been modified such that it depicted a vertical pyrolysis furnace. A diagram of the pyrolysis furnace is shown below in fig. 5.7.
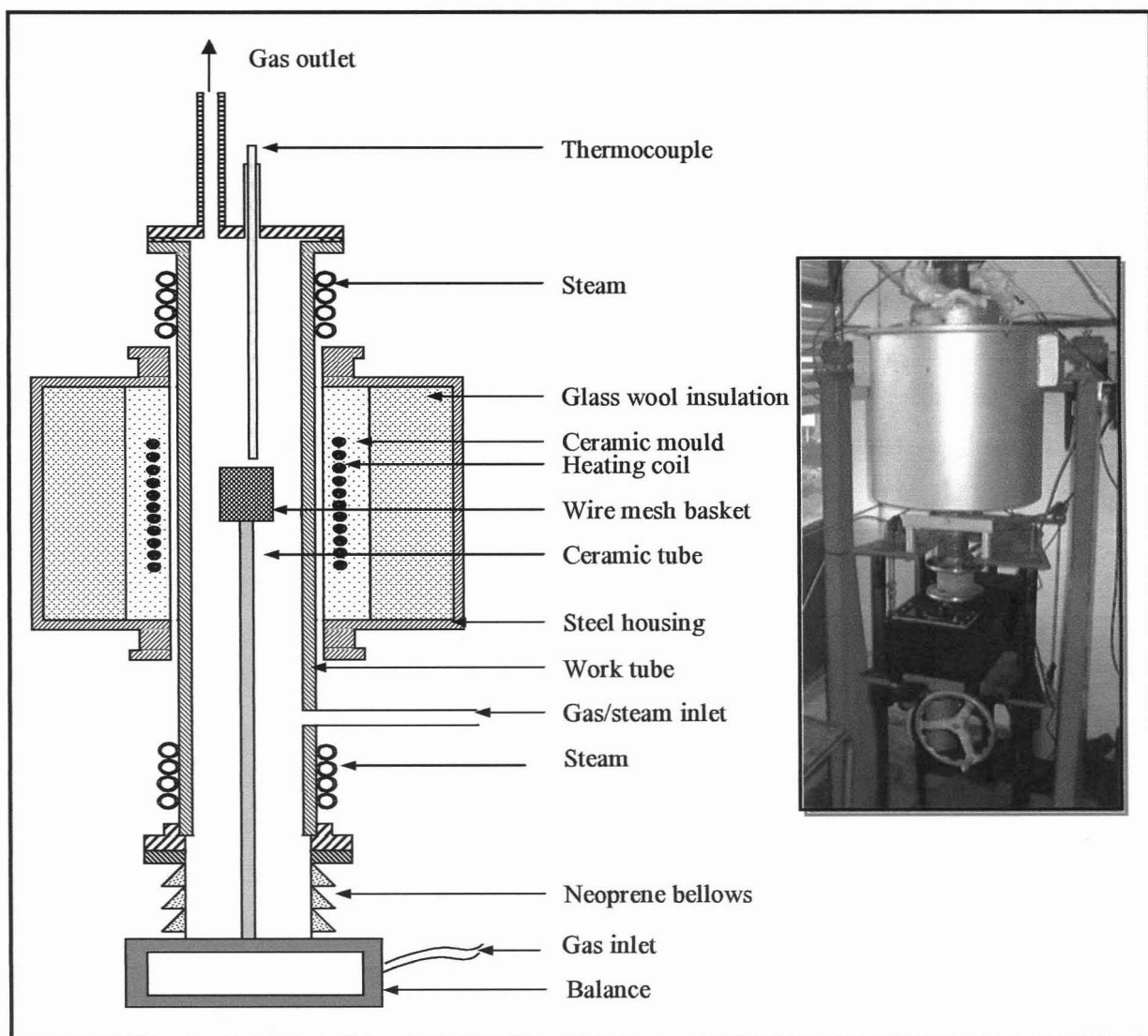
Figure 5.7: Diagram and photo of the pyrolysis furnace.

The pyrolysis furnace comprises of:

- An electronic Mettler, top–pan mass balance encased in a metal box that has a see through panel made of Perspex for a mass readout. Provision had been made for a flow rate of gas to pass through the balance housing thereby ensuring that it is in the correct temperature range for proper operation.

- A 410 μm wire mesh, cylindrical, basket sample holder (see fig 5.8) designed and constructed such it allows for the rapid diffusion of gases into and out of the sample. The sample holder also contains a wire mesh lid, such that the entire sample is encased in the basket, which allows for increased vapour-solid interaction during pyrolysis. The wire mesh basket is attached to a ceramic tube, which connects it to the mass balance. The sample holder with support rod is allowed to move freely into and out of the hot zone of the reaction chamber. This represents a fixed bed reactor configuration. Minkova *et al* [2000] in their studies have indicated that a rotary furnace is used to generate more gaseous product whereas, a fixed bed reactor for the production of char. Their results of low surface area activated carbons in a rotary reactor prompted the decision to choose a fixed bed reactor system.

- A 55mm (i.d) stainless cylindrical pipe called the reaction chamber (work tube). Three layers of insulation, namely air, ceramic and glass wool, surround the upper section of the work tube. This section is referred to as the thermal section of the unit. A 4kW-heating coil is embedded in the ceramic mould such it provides heat required to heat up the unit and for the reaction. The coil is embedded in order to avoid resistance from the metal tube if the heating coils and metal tube come in contact, which results in power breakage. The allowance for a space of air insulation between the tube and the ceramic is mainly for the purposes of heat transfer during cooling.

- An R-type thermocouple encased in a ceramic rod, which is placed in the hot zone of the work tube. The thermocouple sits just above the sample because placing the thermocouple in the sample would lead to recording of incorrect mass readings. The thermocouple is linked to a PID Eurotherm temperature controller that controls the amount heat inputted by the heating coils by the signals received from the thermocouple. The controller is designed to reach 1200 °C.

- Neoprene bellows that allows flexibility in raising or lowering the sample when the unit is closed. The neoprene bellows are bolted between the balance housing and the lower end of the reaction chamber which also links them both.

- A set of coils above and below the thermal section which allows either steam or cooling water to flow through during heating and cooling stages of the process.

During operation, the upper section of the unit is again thermally insulated with a layer of glass wool insulation as an extra precaution.

Both the temperature and mass units are linked through the RS232 ports to a computer, which logs both the mass and temperature in one-second intervals. The interface program for recording mass and temperature was written in visual basic and can be viewed in Appendix B-1.
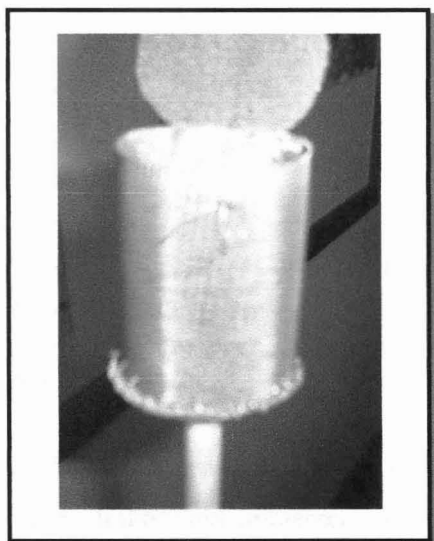
Figure 5.8: Photo of the wire mesh Sample holder with lid.

5.4.2. Steam Supply

The steam supply in Xia *et al*'s [1998] studies on producing activated carbon from bagasse was done by pouring water at the entrance of the reactor. Although simple, this method was seen to be difficult to control However, Lutz *et al* [1998] during their experiments of activation of bagasse chars used a mixture of steam and nitrogen. The steam was supplied by bubbling nitrogen gas through a water bath at 92 °C in order to obtain a steam to nitrogen ratio of 1:1 that enters the reactor. Their experimental set-up is shown below in fig 5.9
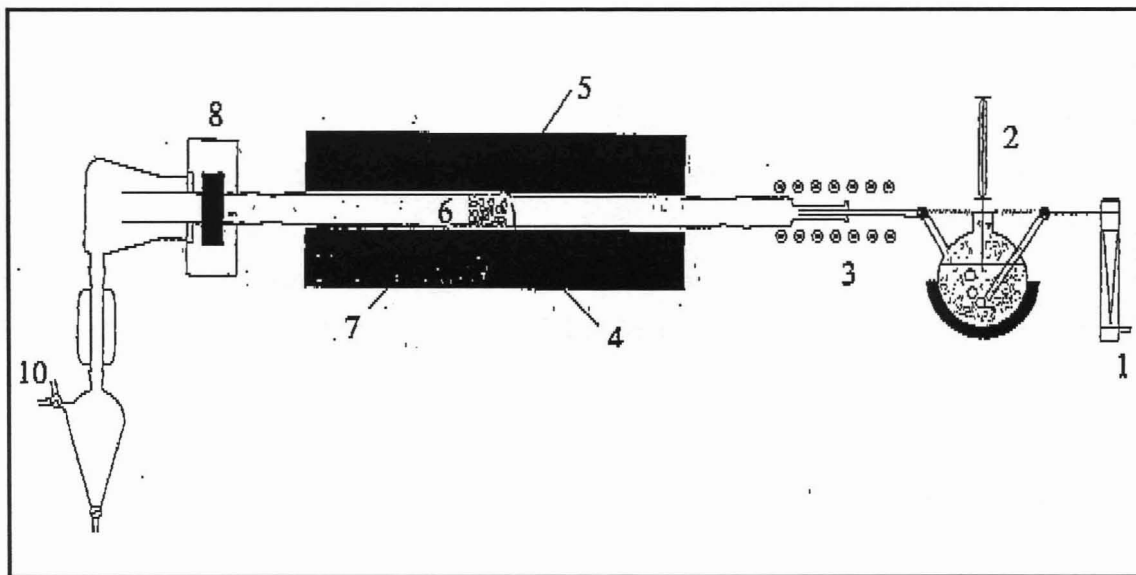
Figure 5.9: Experimental set-up for bagasse char activation by Lutz *et al* [1998] 1 – Gas inlet, 2 - water bath, 3 – heating belt, 4 – sample, 5 – oven, 6 – quartz tube, 7 – controller, 8 – drive motor, 9 – condenser, 10 – exhaust gas.

Following their work, a system of dreschel bottles with sintered glass fittings were filled with water, linked and immersed in a water bath. Nitrogen gas was bubbled through these sets of dreschel bottle such that a steam and nitrogen mixture exited the system and entered the reactor. The water bath has a temperature controller and heating element and the temperature was set around 92 °C. The amount of steam supplied was regulated by controlling the nitrogen flowrate. The steam flowrate was measured by allowing the steam/nitrogen gas to flow through a vessel immersed in an ice bath for a specific time. The amount of water condensed was weighed and the steam flow rate recorded at set nitrogen gas flow rates.

5.4.3. Downstream Units

Gases exiting the reactor during pyrolysis also include tars and condensable vapours. After exiting the reactor the gases are usually condensed and passed through a tar trap before being sampled or vented (see fig 5.9.). Initially a U-tube filled with glass wool and immersed in an ice bath was used to remove condensable gases and tarry matter. This concept was based on earlier work by Hajaligol *et al* [1982] in their experimental set-up to determine the kinetics of cellulose pyrolysis. However, during the commissioning stage this system broke down since the tube blocked leading to a pressure runaway in the Pyrolysis furnace. However, this was solved by replacing the system with three separate units in the gas treatment section. These are discussed below.

5.4.3.1. Condenser

The condenser type used for cooling the exiting reactor gases was a double-pipe heat exchanger. A diagram of the condenser type is displayed in fig.5.10. Crushed ice was used as the heat transfer medium to condense the condensable gases inside the tube between 0 and 5 °C. The shell side containing the ice was open to the atmosphere and temperature was regulated on the shell side with the aid of a thermometer and manual addition of ice. The equipment includes a valve that allows for fluid on the shell side to be drained.
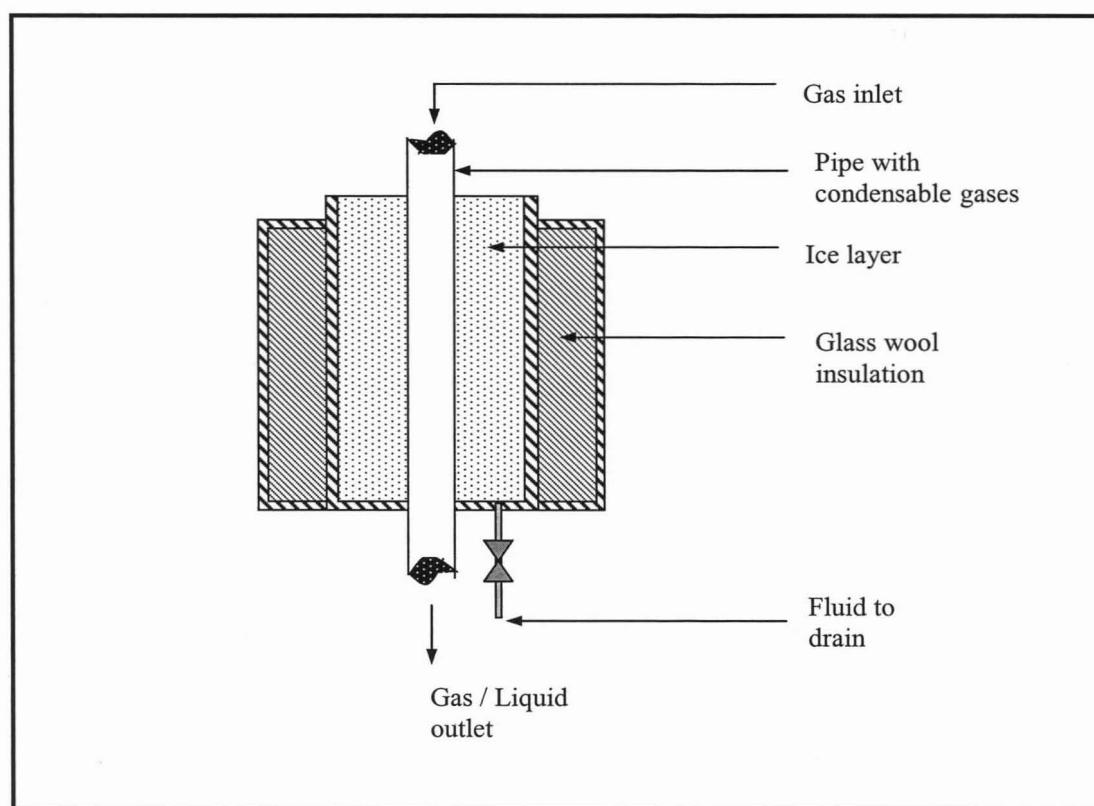
Figure 5.10: Schematic diagram of the condenser

5.4.3.2. Gas-Liquid Separator

The gas-liquid medium exiting the condenser flows into a gas-liquid separator. A separating funnel was modified with a side arm that allows the gas to exit the separator (see fig 5.11). As the fluid flows into the separator, the liquid flows and settles in the vessel due to gravity, whereas, the gaseous stream separates and flows through the side arm. The side arm contains a splashguard that ensures that no liquid is carried with the exiting gas stream. The lower section

of the vessel that contains the liquid/gas interface is kept at a low temperature by being placed in an ice bath.
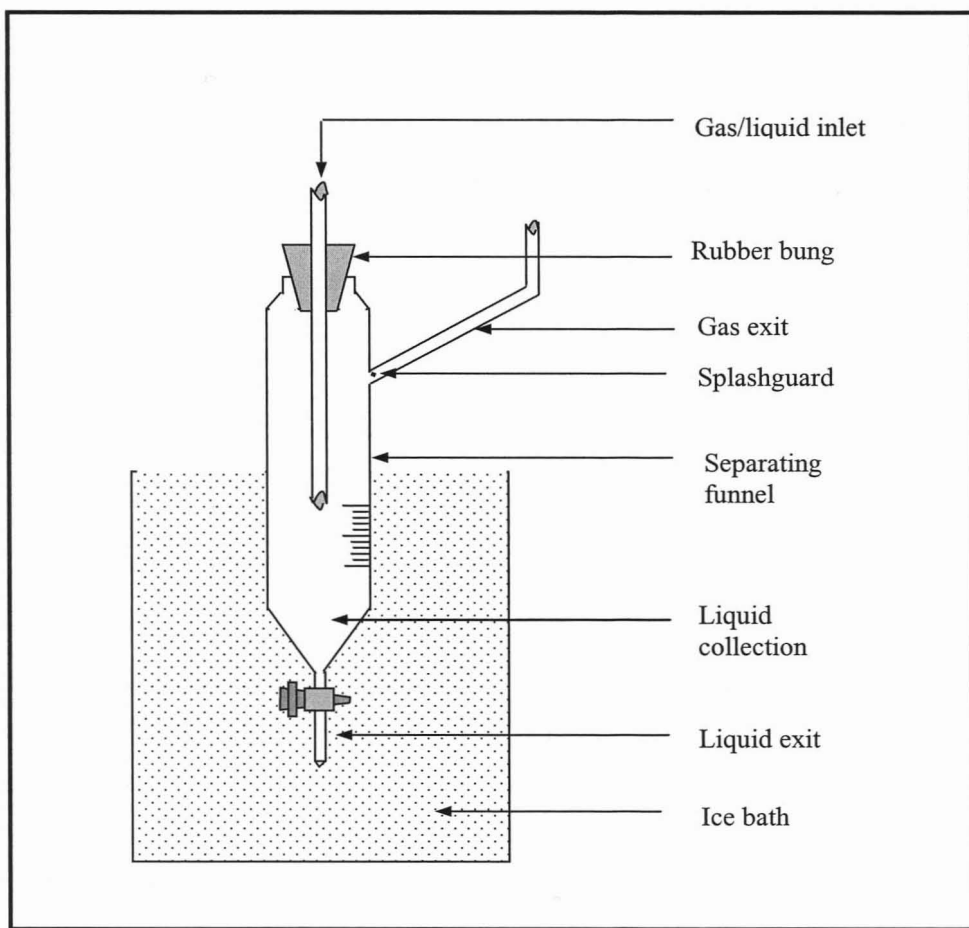
Figure 5.11: Schematic Diagram of the Gas-Liquid Separator.

At the end of the run, the liquid that collects in the vessel is drained and its mass is weighed.

5.4.3.3. Gas Filter

The light gases exiting the separator unit, is further treated in the gas filtering system. This system is a Pyrex vessel that contains glass wool that sits on a wire mesh. The glass wool traps the last traces of tarry matter so that virtually clean gases flow to the gas analyzers, or vented to the atmosphere. A diagram of this set-up is illustrated in fig 5.12. Many researchers have used glass wool as a means of cleaning the gas streams (Antal and Varhegi, 1995).
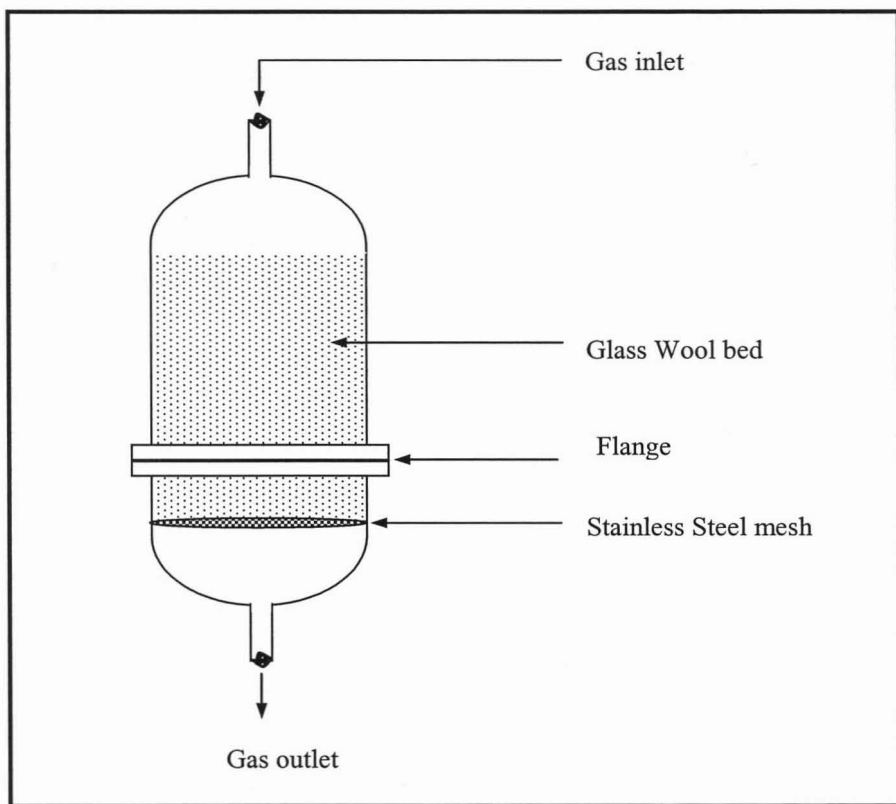
Figure 5.12: Diagram of the Gas Cleaning unit

The mass of the glass wool is weighed prior to being inserted in the unit and after completion of experimental run in order to attain the amount of tarry matter that is left behind.

After passing through the gas filter, the exiting gases were either sampled or vented.

A diagram of the experimental set displaying the equipment mentioned above is presented in fig. 5.13. To get a more realistic idea of the equipment set-up, a photo was taken and can be seen in fig 5.14.
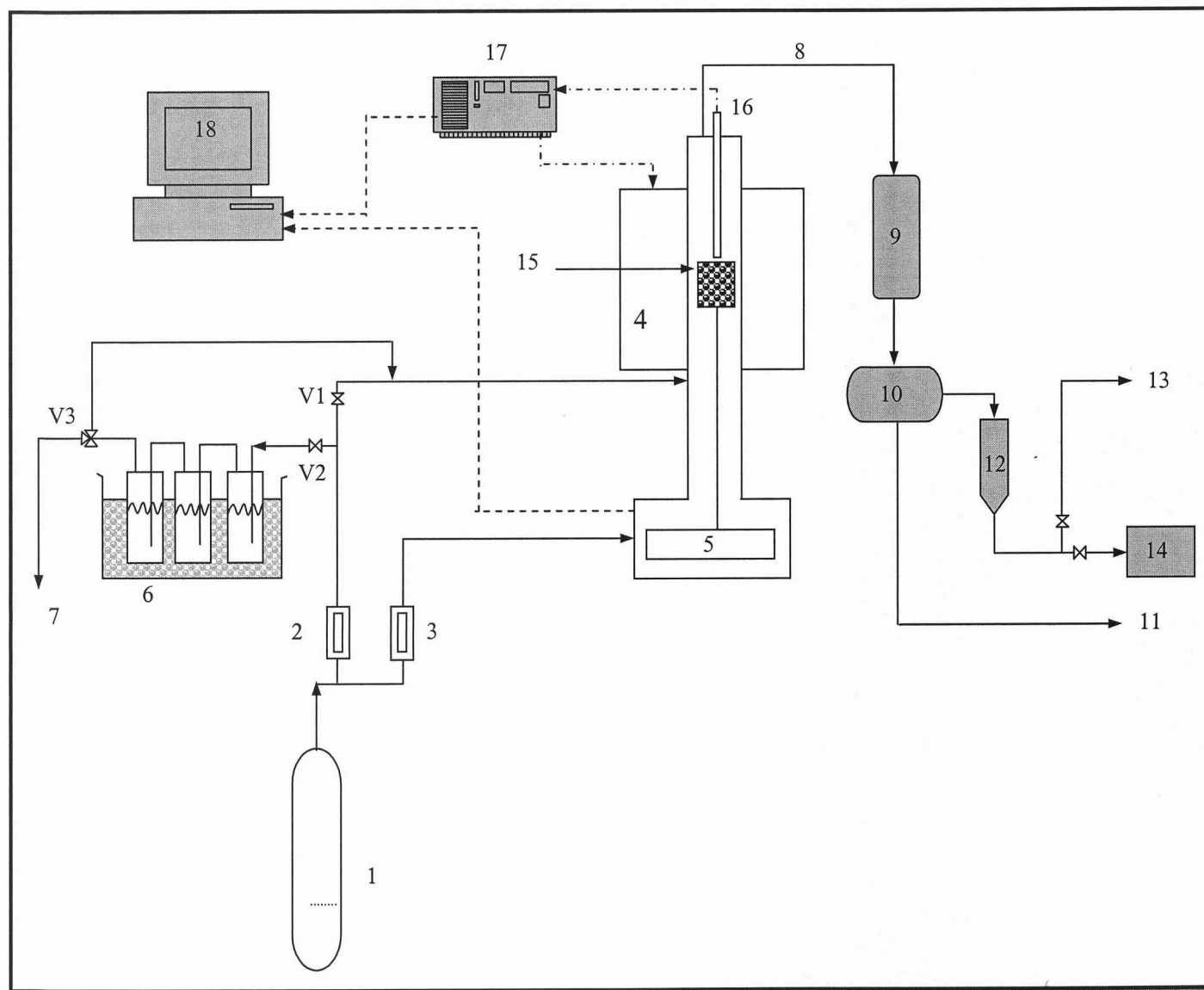
Figure 5.13: Schematic diagram of the equipment set-up.

1 - Nitrogen gas,

2 & 3 - rotameters,

4 – pyrolysis furnace,

5 - mass balance,

 6 – steam / nitrogen set-up,

7 - steam sampling valve,

8 - exit gases,

9 - condenser,

10 - separator,

11 - liquid,

12 - gas filter system,

13 - gases to vent,

14 - gases to gas analyzer,

15 - wire mesh basket,

16 -thermocouple,

17 - Eurotherm Temp controller,

18 – Computer
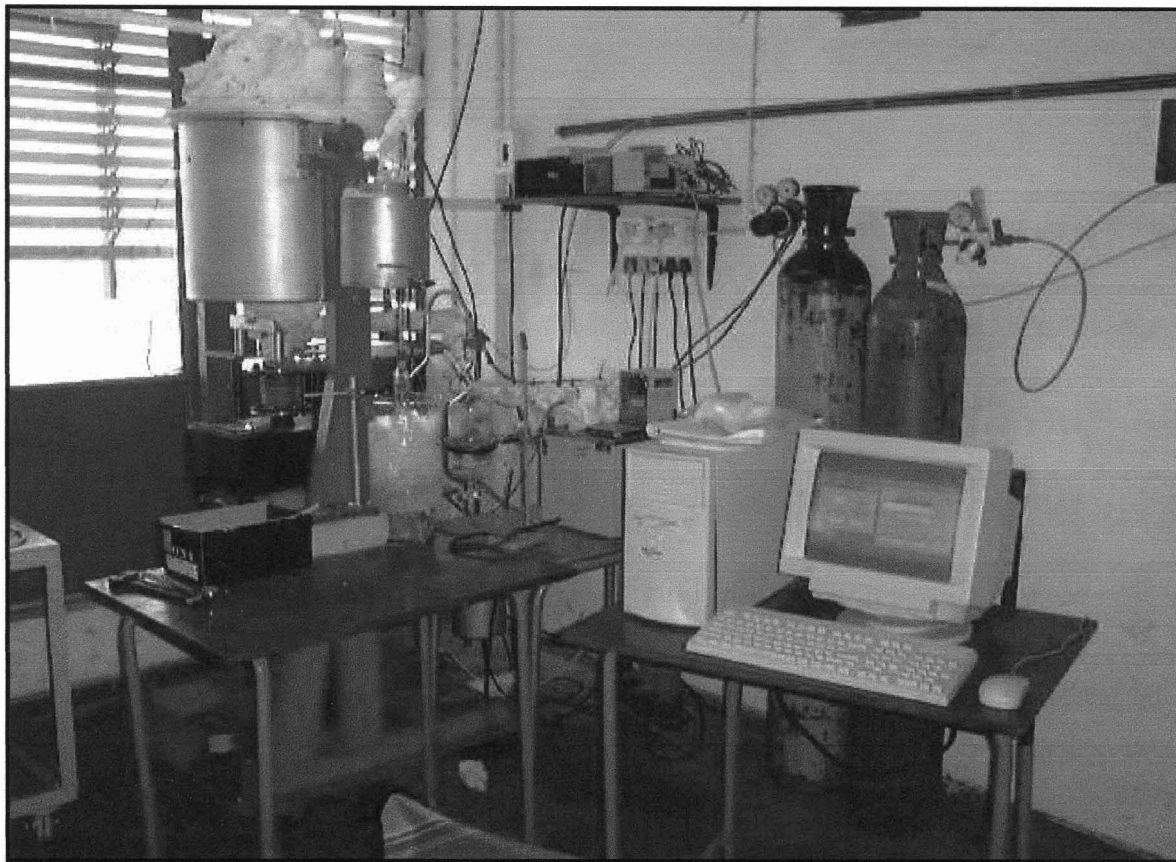
Figure 5.14: Photo of the Equipment Set-up.

5.5. Pyrolysis of Bagasse

After raw material preparation, bagasse pellets were inserted into the wire mesh basket holder. This was then placed inside the hot zone of work tube of the pyrolysis furnace. The mass of bagasse (approximately 20g) was recorded. Nitrogen gas was introduced to the balance housing via rotameters 3 and through rotameters 2 with valve the V1 being opened and valves V2 and V3 closed. The total flow rate of nitrogen flowing through the work tube was 235ml/min during pyrolysis. The nitrogen flow rate was chosen such that gases that exit will escape easily and also such that no buoyancy effects will be experienced by the sample during pyrolysis. After purging with nitrogen, the temperature controller was switched on to the desired set point temperature at a heating rate of 10 °C/min. Heating rate of 10 °C/min was chosen, since from various studies, a low heating would bring about a greater char yield and also ensure that deformation of pores created during pyrolysis is avoided. The temperature was determined by the thermocouple (8) that sits approximately 4 mm above the sample. The sample was kept at the set point for a specific hold time. Pyrolysis was carried out at atmospheric pressure.

The gases exiting the reactor during pyrolysis were cooled by being passed through the condenser. The gas/liquid stream was separated and the exiting gas from the separating unit was further cleaned before being sent to the gas analyzer or vented. The entire system is set –up under a fume hood and the gases were vented through the extraction unit.

After pyrolysis time had elapsed, the sample is lowered such that it does not sit in the hot zone of the furnace. Heating is shut-off and the sample is allowed to cool under a nitrogen atmosphere to room temperature. The char samples were subsequently characterized and the optimum pyrolysis process conditions were determined.

5.6. Activation of bagasse chars

The same equipment used for pyrolysis was also used for activation. After the chars were produced at the optimum temperature and hold time, they were then subjected to partial gasification with steam, which took place in the same pyrolysis furnace. The steam entered the reactor by bubbling nitrogen gas through a set of dreschel bottles filled with water that were kept at a constant temperature of 92 ^{O}C. The temperature in the pyrolysis furnace was set to the desired set point. Valve V1 was closed while V2 and V3 were open. The nitrogen gas bubbles through the dreschel bottle set-up, picking up water vapour as it flows and this nitrogen/steam stream flows and enters the furnace. The lines from the steam supply unit to the reactor entrance are heated with nichrome heating wire and insulated with glass wool in order to prevent steam from condensing in the lines.

The steam/nitrogen mixture flows through the reaction chamber and reacts with the bagasse chars in the wire mesh sample holder. The reaction gaseous products and un-reacted steam exits the reactor and follows the same path as in pyrolysis.

The partial pressure of steam in the reaction chamber was varied and controlled by controlling the nitrogen flow rate by adjusting rotameter2. The activation step proceeded for varying temperatures and activation times. The mass and temperature was also logged during this step.

The burn off % was determined by [Pendyal *et al*, 1999]:

$$Burn - off = \left[\frac{w_{ba} - w_{aa}}{w_{ba}} \right] x100 \qquad (5.1)$$

and the activated carbon yield was determined by:

$$Yield = \left[\frac{w_{aa}}{w_{rm}}\right] x100 \qquad (5.2)$$

where: w_{ba} =   dry weight before activation

w_{aa} =   dry weight after activation

w_{rm} =   dry weight of raw material after activation

At the end of activation, the sample was again moved away from the hot zone, by lowering the bottom section of the unit. The sample was cooled to room temperature with nitrogen before being removed. The samples were analyzed following the characterization criteria listed in chapter 4 to obtain the best activation process conditions.

Both pyrolysis and activation takes place on a semi batch scale.

5.6.1 Activation Experiments

According to Hassler [1974], the properties of the final activated carbon are affected by the concentration of the oxidizing gas, the activation temperature, activating time and the mineral matter present in the precursor carbon. Thus, to obtain the best activation process conditions that would yield high surface area activated carbons consisting of a combination of micro, meso and macropores, required for adsorption of colour bodies from raw sugar, activation experiments were conducted isothermally at varying steam partial pressures, activation temperatures and activation times. The effect of chars prepared at a final pyrolysis temperature of 680 $^{\circ}$C and different pyrolysis exposure times on the final activated carbons were also investigated at varying activation times. Tables 5.2 to 5.5 summarize the activation experiments that were carried out.

Table 5.2: Pyrolysis and Activating Conditions for the production of powder activated carbons at varying steam partial pressures from sugar-cane bagasse

| Sample | Binder | Pyrolysis | | | Activation | | |
		Heating Rate / °C/min)	Temperature / (°C)	Hold Time /(hr)	Steam / Nitrogen ratio	Temperature / (°C)	Time /(hr)
J	None	10	680	1	1.0 : 0.6	800	4
L	None	10	680	1	0.5 : 0.5	800	4
G	None	10	680	1	0.4 : 1.0	800	4

Table 5.3: Pyrolysis and Activation Conditions of Activated Carbons produced from Sugar-cane bagasse at different pyrolysis and activation hold-times

| Sample | Binder | Pyrolysis | | | Activation | | |
		Heating Rate / °C/min)	Temperature / (°C)	Hold Time /(hr)	Steam / Nitrogen ratio	Temperature / (°C)	Time /(hr)
A	None	10	680	1	0.56 : 044	800	1
B	None	10	680	1	0.56 : 0.44	800	3
C	None	10	680	1	0.56 : 0.44	800	4
D	None	10	680	2	0.56 : 0.44	800	1
E	None	10	680	2	0.56 : 0.44	800	3
F	None	10	680	2	0.56: 0.44	800	4

Table 5.4: Pyrolysis and Activation conditions used to produce powder activated carbons at different activation temperatures

| Sample | Binder | Pyrolysis | | | Activation | | |
		Heating Rate / °C/min)	Temperature / (°C)	Hold Time /(hr)	Steam / Nitrogen ratio	Temperature / (°C)	Time /(hr)
I	None	10	680	1	1 : 06	900	2
J	None	10	680	1	1 : 0.6	800	4
K	None	10	680	1	1 : 0.6	700	4

Table 5.5: Processing conditions used to prepare powder and granular activated carbons from sugar-cane bagasse.

| Sample | Binder | Binder/ Bagasse ratio | Pyrolysis | | | Activation | | |
			Heating Rate / (^{O}C/min)	Temp / (^{O}C)	Hold Time /(hr)	Steam / Nitrogen ratio	Temp /(^{O}C)	Time /(hr)
I	None	0	10	680	1	1 : 06	900	2
O	None	0	10	680	1	1 : 0.6	900	2
P	Sugar	0.5:1.0	10	680	1	1 : 0.6	900	2.5

The resulting activated carbons were consequently characterized by the methods discussed in chapters 4 and section 5.7 to determine the effect of activation and pyrolysis process conditions on their properties.

5.7. Gas and Liquid Adsorption

5.7.1. Gas Adsorption

Bagasse chars and activated carbons were submitted to nitrogen adsorption at 77K using an ASAP 2010 Surface Area Analyzer to determine, their surface area, pore areas, pore volumes and average pore size. This equipment contains a pressure transducer that detects the changes in pressure and an analyzer, which determines the number of adsorbed gas molecules from the changes in pressure, temperature of the gas and the volume of the container. This unit is connected to a computer which controls the analysis, collects data, stores the sample and operating conditions on a file and generates reports and is based on Windows software [Particle and Surface Sciences, Pty Ltd). The Nitrogen gas adsorption testing was performed at the University of Potchefstroom.

5.7.2. Iodine Numbers

The iodine adsorption test method is based upon a three-point adsorption isotherm. A standard iodine solution (0.100 +- 0.001N) was treated with varying weights of activated carbon under specific conditions (time and temperature). The carbon treated solution was filtered, and the filtrate (residual solution) concentration determined. The concentration of the residual iodine solution was determined by titrating with a known concentration of sodium thiosulphate solution (0.100 N). The amount of iodine adsorbed per gram carbon was measured for each dosage and plotted as a Freudlich adsorption isotherm. The iodine number was determined from

the isotherm plot as the mg iodine adsorbed per gram of carbon at the residual iodine concentration of 0.02N.

The procedure used was an ASTM standard test method to determine the iodine number of activated carbon and is clearly described in more detail in ASTM D4607 –86.

5.7.3. Methylene Blue Number

This test was performed on dried pulverised carbon. 25 cm^3 of Methylene blue solution was added to 100mg of activated carbon samples. This mixture was shaken in a linear shaker at medium speed for 25 minutes. The samples were filtered through a Whatman No.2 filter paper with the first 5cm^3 being discarded. 10 cm3 of the residual methylene blue solution were diluted with acetic acid solution and their absorbance was measured at 620nm in a 1cm cell in a spectrophotometer. A calibration graph of absorbance, at a wavelength of 620nm, versus concentration was plotted for the methylene blue solution prior to running the test with activated carbon. This plot was used to determine the concentration of the final methylene blue solution.

The methylene number was obtained by:

$$MBno. = \left[\frac{(I-F)}{M_c}\right] x \left(\frac{V_s}{1000}\right) \tag{5.3}$$

where: $MBno.$ = methylene blue number (mg/g)

I = initial methylene blue concentration (mg/l)

F = final sample methylene blue concentration (mg/l) from graph x dilution

V_s = volume of contacting stock solution (acetic acid) (litres)

Various methods have been used to determine the methylene blue number and one of the many was developed and used by Aktasorb Systems (Pty) Ltd and has been used in this study.

5.7.4. Molasses Number

0.46g of pulverized activated carbon and a standard activated carbon were treated with 50 ml of blackstrap molasses solution. The standard activated carbon used was Chemviron CaneCal (coal parent material, patented activation, granular) carbon. The samples were boiled for 30seconds

and then filtered through a prepared Whatman No 3 filter paper suspension. The initial 20 ml of filtrate solution was discarded. The absorbance of the rest of the filtrate was measured in a spectrophotometer at 425nm wavelength.

The molasses number was calculated as:

$$Molasses - no. = \frac{M_t x A_s}{A}$$ (5.4)

where: M_t = molasses number of standard activated carbon (usually 400)

      A_s = absorbance of filtrate from the standard activated carbon

      A = absorbance of the filtrate of the test activated carbon.

The procedure followed was a tried and tested method written by Pawlowski [1971].

5.7.5. Adsorption of Colour Bodies from Sugar

These tests were carried out at the Sugar Milling Research Institute (SMRI) on a batch scale. Varying dosages of pulverised activated carbon samples were added to 66 Brix sugar liquor. The sugar liquor-activated carbon slurry mixture was stirred for 24 hr at a contant temperature of 80 $^\circ$C. A blank containing only the 66 Brix sugar liquor was subjected to the same treatment. A photo of the equipment that was used is displayed in fig 5.15.
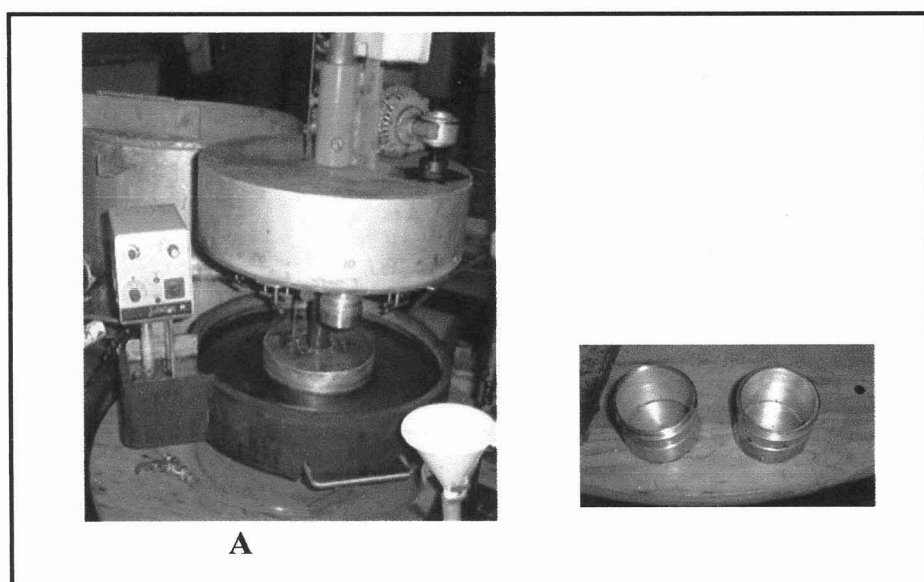
Figure 5.15: Photo of the equipment used to perform the sugar decolourisation tests, A – unit, B – sample holders.

The samples were then filtered to remove the suspended carbon particles, adjusted to a pH of 7.00 and the colour was measured at 420nm using a UV-VIS spectrophotometer. Standard Norit PN2 (peat parent material, steam activated, powder) activated carbon was also subjected to the same experimental treatment.

The percent colour removed was determined by:

$$\%colour - removed = \left[\frac{C_b - C_s}{C_b} \right] x100 \qquad (5.5)$$

where: C_b = colour of blank

C_s = colour of sample

An isotherm of percent colour removed versus g activated carbon/100g Brix brown liquor was plotted for all carbons tested.

5.8. Ash and Moisture tests

Portions of received bagasse were weighed and inserted into a drying oven set at 110 ^{o}C until constant weight was reached. The weight of the sample prior to and after drying was recorded and the moisture determined.

Dried bagasse samples were inserted into a preheated muffle furnace set at 850 ^{o}C. After 10 minutes, the door of the muffle furnace was kept open to allow oxygen from the atmosphere to react. After one hour, the samples were removed and placed in a dessicator to cool. The weight of the ashed samples was measured and the ash content determined from the difference in weight.

Similiarly, the ash content of the carbons were measured by placing dried carbon samples in the muffle furnace set at 850 ^{o}C. This was left in the furnace for one hour and cooled in a dessicator. The ash content was measured by the difference in weight.

5.9. Scanning Electron Micrographs

Scanning electron microscopes creates magnified images by using electrons instead of light by a light microscope.

Samples of bagasse and carbons were initially attached to aluminium stubs. These samples were then dried and sputter coated with gold in a Polaron sputter coater. This was done in order to make the samples electrically conductive. These samples (specimens) were then placed inside the microscope's vacuum column through an air tight door. After air was pumped out of the column, a beam of high energy electrons were emitted by an electron gun at the top of the column. This beam travelled downwards through a series of magnetic lenses designed to focus the electrons to a particular spot. Near the bottom of the column, a set of scanning coils moved the focused beam back and forth across the specimen, row by row. As the electron beam hit each spot on the sample, secondary electrons were knocked loose from its surface. A detector counted these electrons and sent the signals to an amplifier. The final image was built up on a monitor screen from the number of electrons emitted from each spot on the sample.

RESULTS AND DISCUSSION

6.1. Raw Material

6.1.1. Bagasse Analysis

Ash and moisture tests were performed on the sugar cane bagasse received from the dewatering mills. These tests indicated that the sugar cane bagasse contained 48 % (average) moisture. Ash testing revealed that received bagasse contained 1.9% ash (average). These results are in agreement to those recorded in literature [Patarau, 1969]. An approximate elemental analysis of untreated sugar cane bagasse samples were determined by scanning electron microscopy on a moisture free basis and is tabulated in table 6.1.

Table 6.1: Approximate analysis of raw sugar-cane bagasse

Element	% Moisture free (Excluding hydrogen)
Carbon	17.89
Oxygen	75.60
Aluminum	1.47
Silica	2.67
Phosphorous	0.75
Sulfur	0.07
Potassium	0.04
Calcium	0.58
Iron	0.40

Unfortunately, the scanning electron microscope was not able to detect the hydrogen elements present in the raw bagasse. However, from the analysis in table 6.1, the elements contributing to ash content were detected with silica being the major component. The calcium fraction found in

bagasse is as a result of lime being added during sucrose extraction process to alter the pH of the sugar juice.

6.1.2. SEM study on raw sugar-cane bagasse

Dry, untreated sugar cane bagasse samples were subjected to topographical characterization using scanning electron microscopy. As foretold in the literature, bagasse has a large number of pores on its surface [Xia *et al*, 1998] and similar findings were observed in fig 6.1.
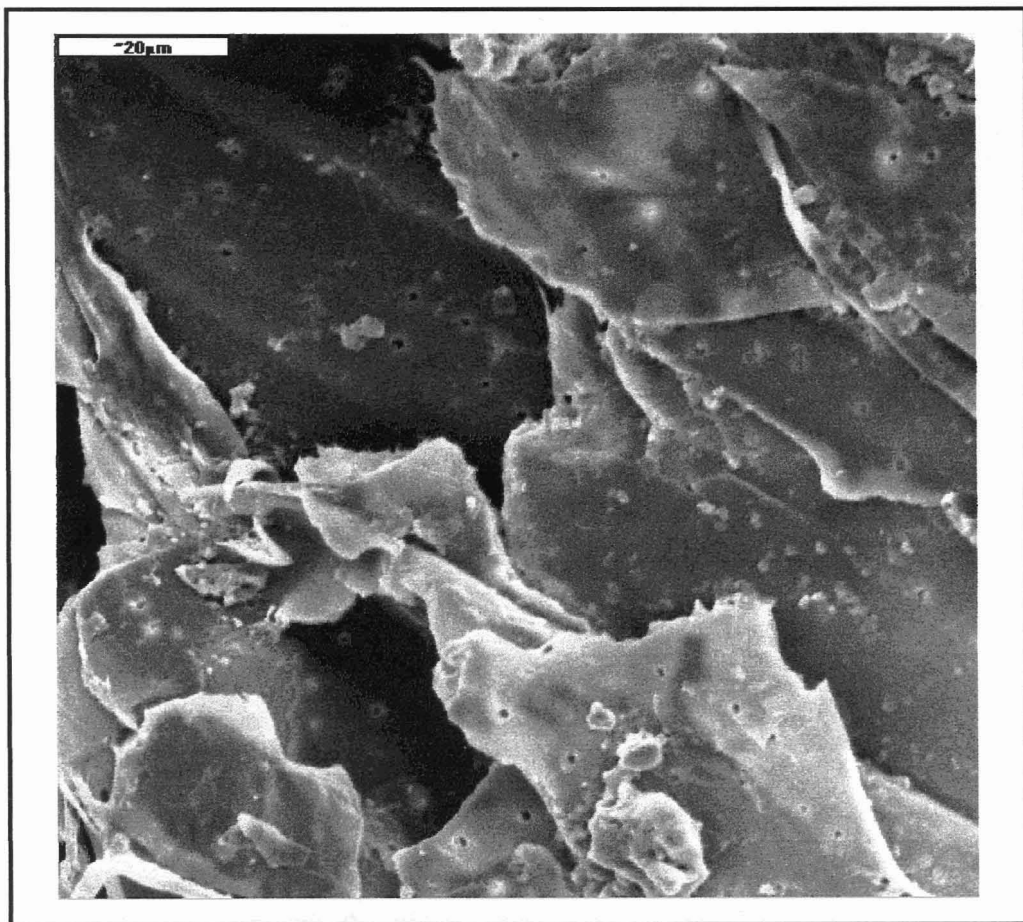
Figure 6.1: Scanning electron micrograph of raw sugar-cane bagasse showing pores on its surface.

An investigation was carried out to determine the source of this porous characteristic of bagasse by comparing sugar cane bagasse fibres with samples of fresh sugar cane stalks. Scanning electron micrographs were taken of different sections of the fresh sugar cane.
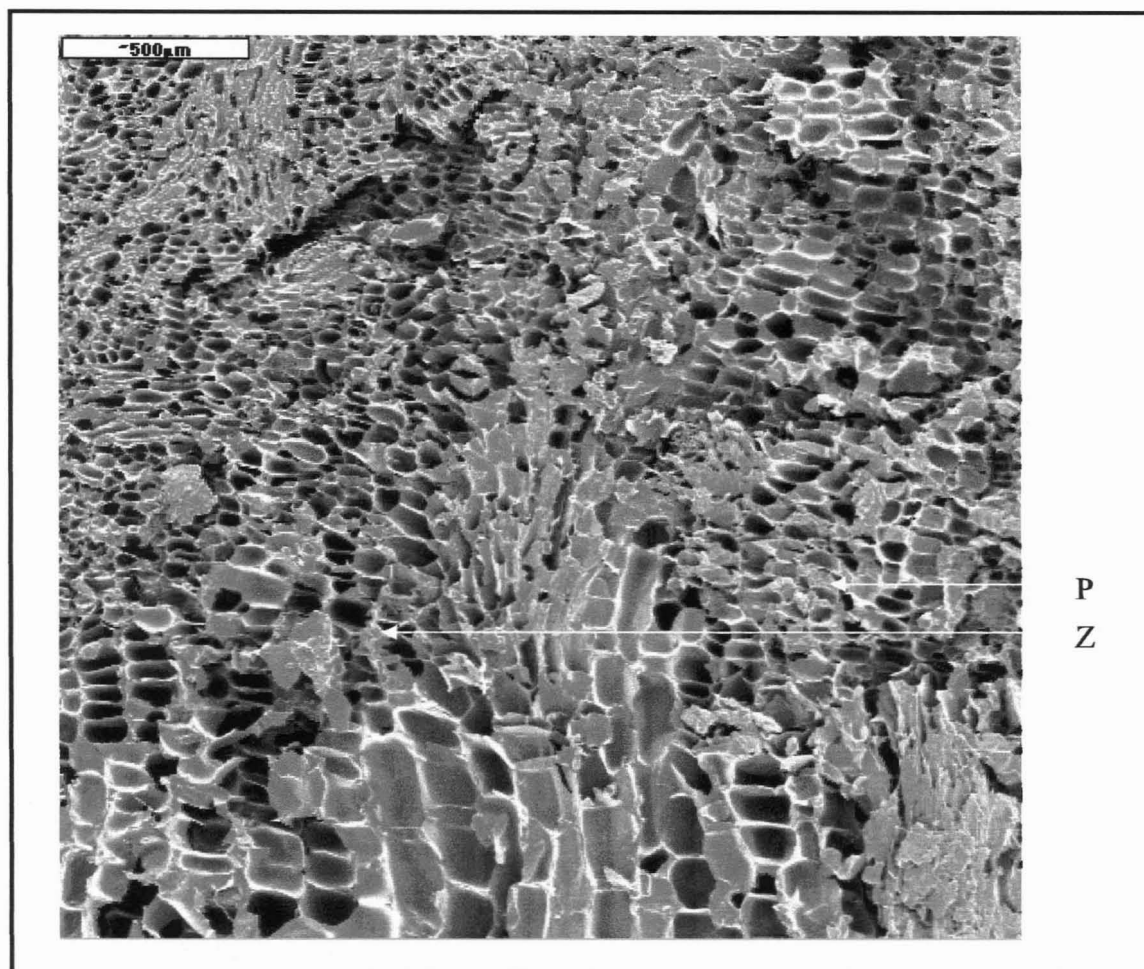
Figure 6.2: SEM of a cross-section through the node of fresh sugar cane showing P-Parenchyma and Z – xylem.

A scanning electron micrograph of a cross-sectional view through the node of fresh sugar cane in fig 6.2 shows secondary xylem (Z) and parenchymal cells (P). Secondary xylem is composed of two types of cells called tracheids and vessels. The trachieds are cylindrical, thick walled cells while their vessel segments are generally wider, shorter and thin walled. The trachieds transport water through the plant. These cells do not have living protoplasts [Porter and Ledbetter 1970] and this is evident in figure 6.2. The primary walls and middle lamella of adjacent tracheids are indistinguishable in the figure 6.2 due to the low magnification of the micrograph. However, along their sidewalls, adjacent trachieds do establish connections via pits which are channels allowing for the passage of food and nutrients. A longitudinal view of the sugar cane stalk was looked at via the scanning electron microscope and is presented in figures 6.3 to 6.5.
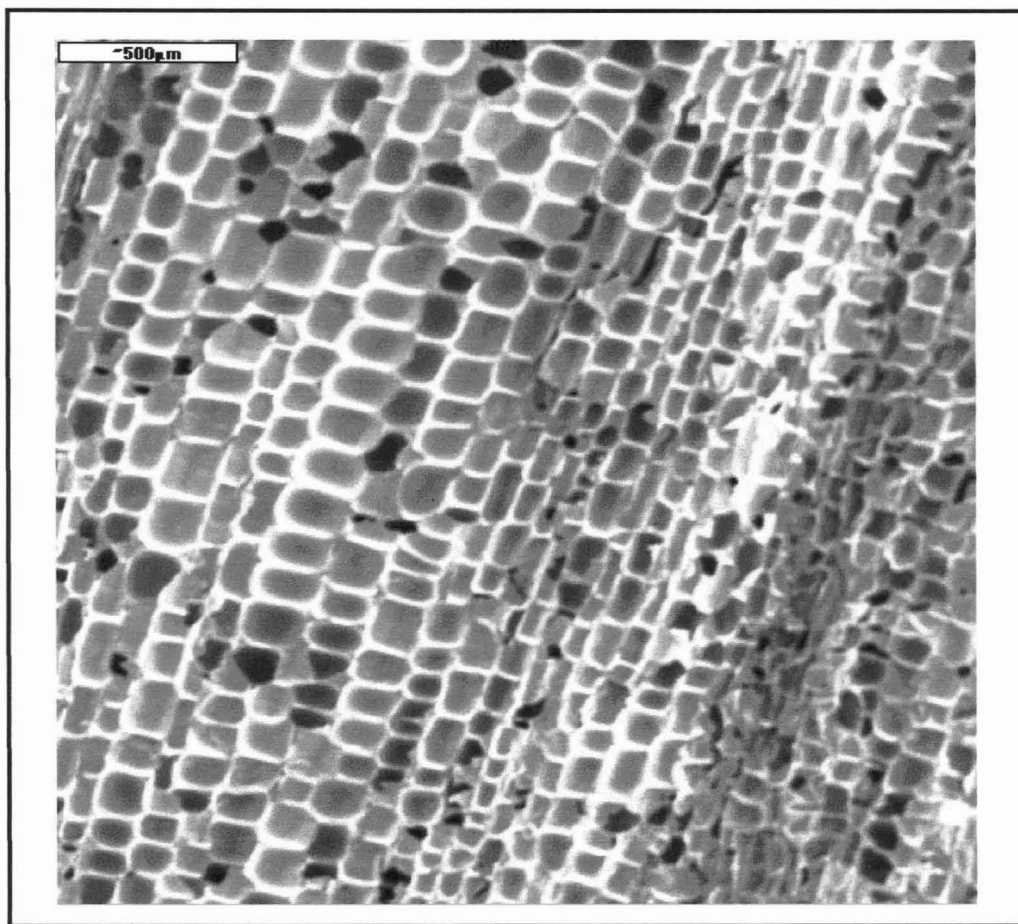
Figure 6.3: SEM of a longitudinal section through the node of a sugar cane stalk.

Figure 6.3 displays the intact parenchymal cells of the cane stalk, which consist of short, cell groups of square or rhomboid shaped cells. A noticeable feature is the cell wall linking cells together. Zooming in at a higher magnification, provided a much more detailed view of the cells and cell wall structure, and is presented in figure 6.4.
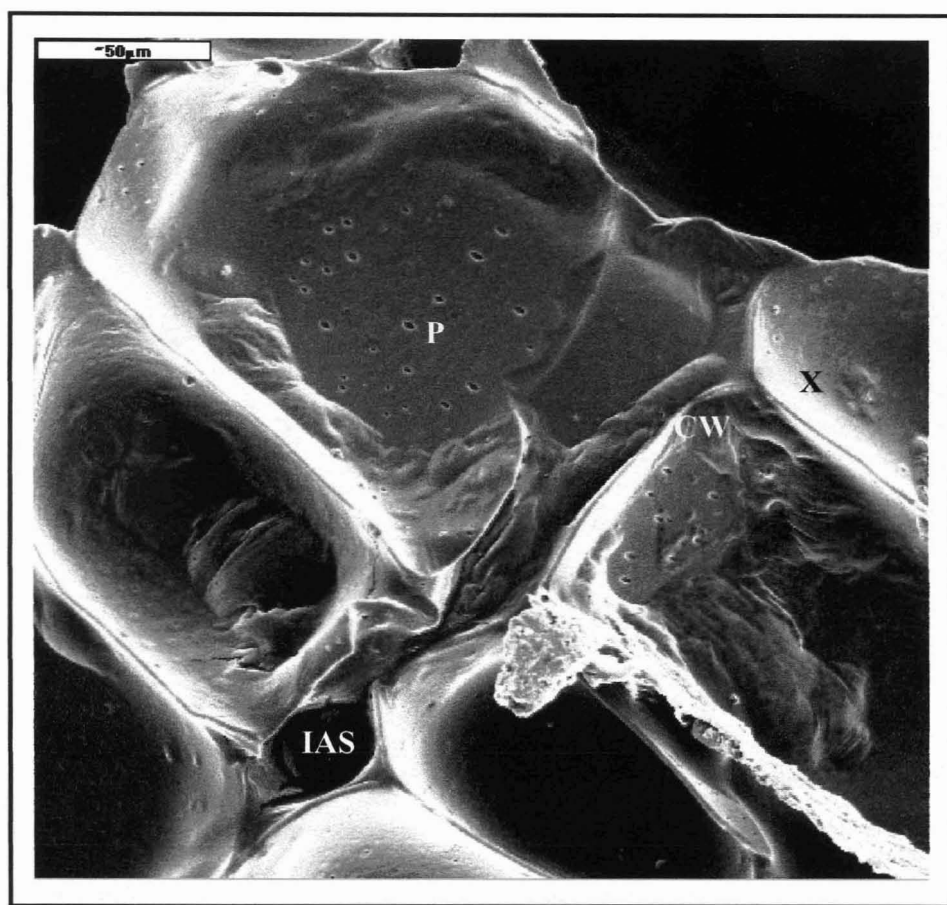
Figure 6.4: SEM of a longitudinal section of fresh sugar cane showing: CW – cell wall, X – parenchyma cells, P –pores, IAS – intercellular air spaces.

The longitudinal section of fresh cane shown in fig 6.4 at higher magnification under the scanning electron microscope, again confirms the intact parenchymal tissue. Clearly visible is the cell wall (CW) and the most noticeable feature is the pores (P) in the cell tissue and walls. A lighter colour rim around the pore mouth of each cell is observed and according to Delavier and Shokrani, [1970] this presents a "ring bulge" which indicates that, the rim of pores has a higher level than the cell wall. The distribution of the pores seems to be relatively uniform and also a part of the cell wall. These observations indicate that the porous nature of bagasse is an inherent feature of the cane stalk and has not been created during the sugar extraction process. These pores act as transport channels through which living matter is exchanged and transported through the cells [Delavier and Shokrani, 1970]. At an even higher magnification in fig 6.5, a much more detailed view of the pores on the cell wall can be seen enabling the evaluation of the pore sizes.
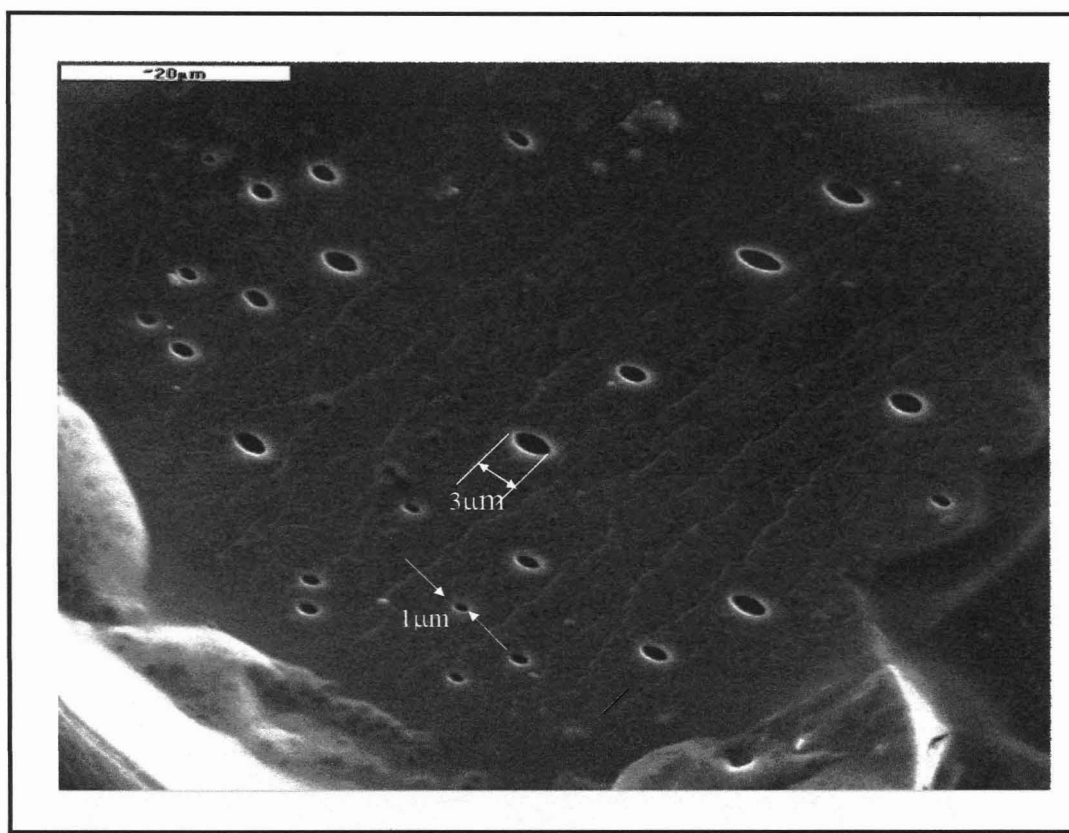
Figure 6.5: SEM of a longitudinal section of fresh cane at a higher magnification.

The pore sizes vary from less than 1 μm to around 3 μm in size. These pore sizes also seem to be around the maximum values determined by Delavier and Shokrani [1970] who found that the pore sizes were between 0.3 to 1.0μm. However, it must be pointed out that the type of cane differs for each country and it may perhaps be that larger pore sizes are found in South African bagasse. Furthermore, the variation in pore sizes could also be due to the variety of cane and the difference in processing i.e. diffuser versus milling process.

Pressed cane leads to the generation of bagasse fibres which show the same type of porous nature as observed on fresh cane. Figures 6.6 to 6.7 are scanning electron micrographs of sugar-cane bagasse fibres. From figure 6.6, it can be seen that pores are enlarged and more oval in shape. The pores on the fibre surfaces are not uniformly distributed. This difference between the pore size and shapes of original and pressed cane can be due to the cell contents such as sucrose, hemicellulose and pectins (at higher temperatures), etc, being squeezed through these openings [Delavier and Shokrani, 1974]. The diameter of a sucrose molecule is 0.44nm, which would be the smallest pore diameter that allows sucrose to pass through [Delavier and Shokrani, 1974].
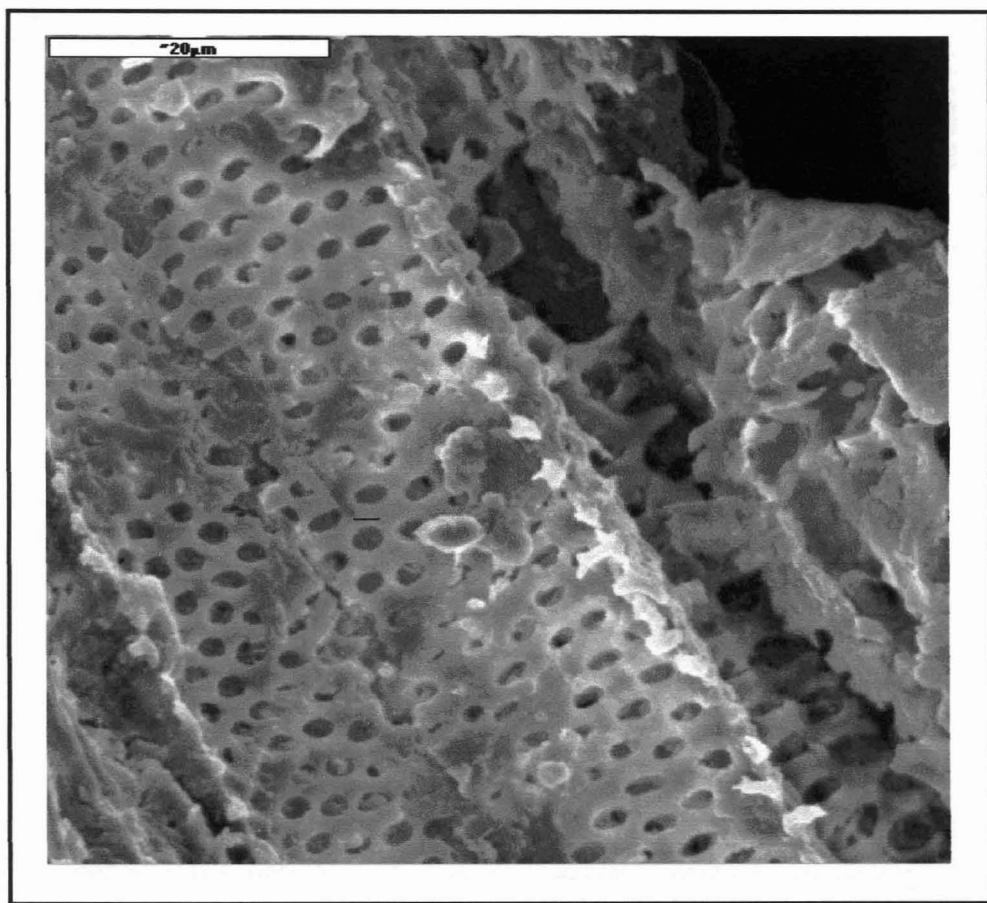
Figure 6.6: SEM of bagasse fibers showing an array of pores on its surface – phloem tissue.

According to Frey-Wyssling, these pores could also be plasmodesmata since they show no cytoplasm [Frey-Wyssling, 1958]. Plasmodesmata allows for direct communication between adjacent cells [Delavier and Shokrani, 1974].

The cluster of pores seen in fig 6.7, are associated with the sieve areas (sieve plate) which provide a connection between vascular elements (phloem tissue). These sieve tubes are closely related to the parenchymal cells. The tubes are involved with the transportation of organic nutrients from the sites of photosynthesis and storage to regions of growth. The organic nutrient can have as high as 30 % sucrose concentration [Porter and Ledbetter, 1970]. The lighter rim around the pores is more pronounced in pressed cane. Plasmodesmata are also a common feature in the primary walls of these cells and sieve elements. Plasmodesmata actually provide for the intercellular movements of large and small molecules and for the transport of particles as large as viruses from cell to cell [Porter and Ledbetter, 1970].
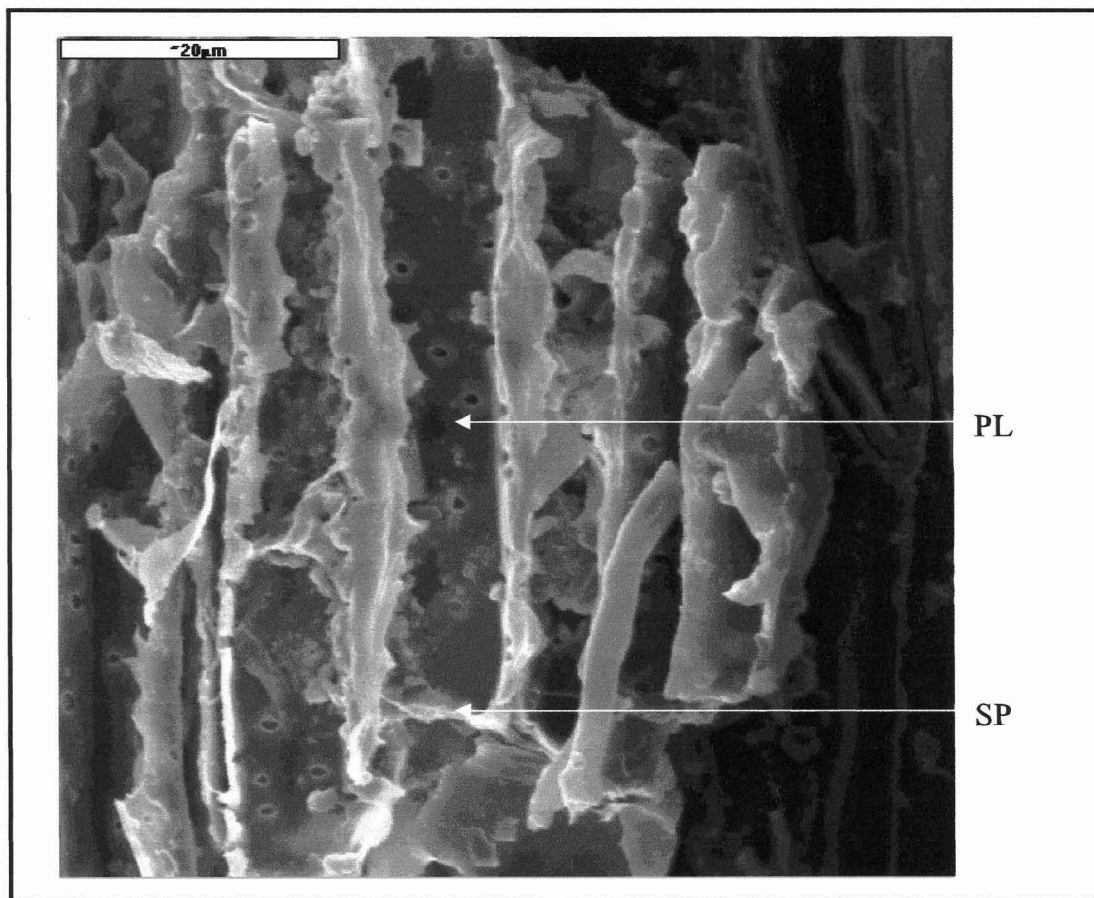
Figure 6.7: SEM of pressed bagasse showing SP - sieve plates and PL – Plasmodesmata.

From the above study, it can be concluded that the porous feature seen on the surface of bagasse fibres are in fact characteristics passed on from their parent material. These pores are part of the cell wall and are dedicated to the transport of species from cell to cell along the cane stalk. The pores found on bagasse are larger and more oval in shape as a result of the forced extraction of the sugar cane juice (sucrose) from the cells.

6.2. Bagasse Pyrolysis

According to Bansal *et al* [1988], the heating rate, the final pyrolysis temperature and the hold time at the final temperature are important parameters that influence the surface area, pore size distribution and pore volume of the final activated carbon produced from the resultant pyrolysis chars. Experiments were carried out in order to establish the best pyrolysis process conditions that produce chars having a positive impact in producing high surface area activated carbons. Bagasse pellets were pyrolysed at a constant heating rate of 10 °C/min to different final pyrolysis temperatures and hold times in a nitrogen atmosphere.

6.2.1. Thermogravimetric simulation of the pyrolysis process

The pyrolysis behaviour of bagasse pellets heated to different final pyrolysis temperatures were simulated by thermogravimetric experiments. The bagasse pellets were heated at a rate of 10 ^{O}C/min up to final temperatures ranging from 500 ^{o}C to 900 ^{o}C. Once this final temperature was reached, the sample was held at this temperature for one hour. The recording of mass and temperature during all experiments in one-second intervals enabled thermograms to be generated and are given in fig 6.8.
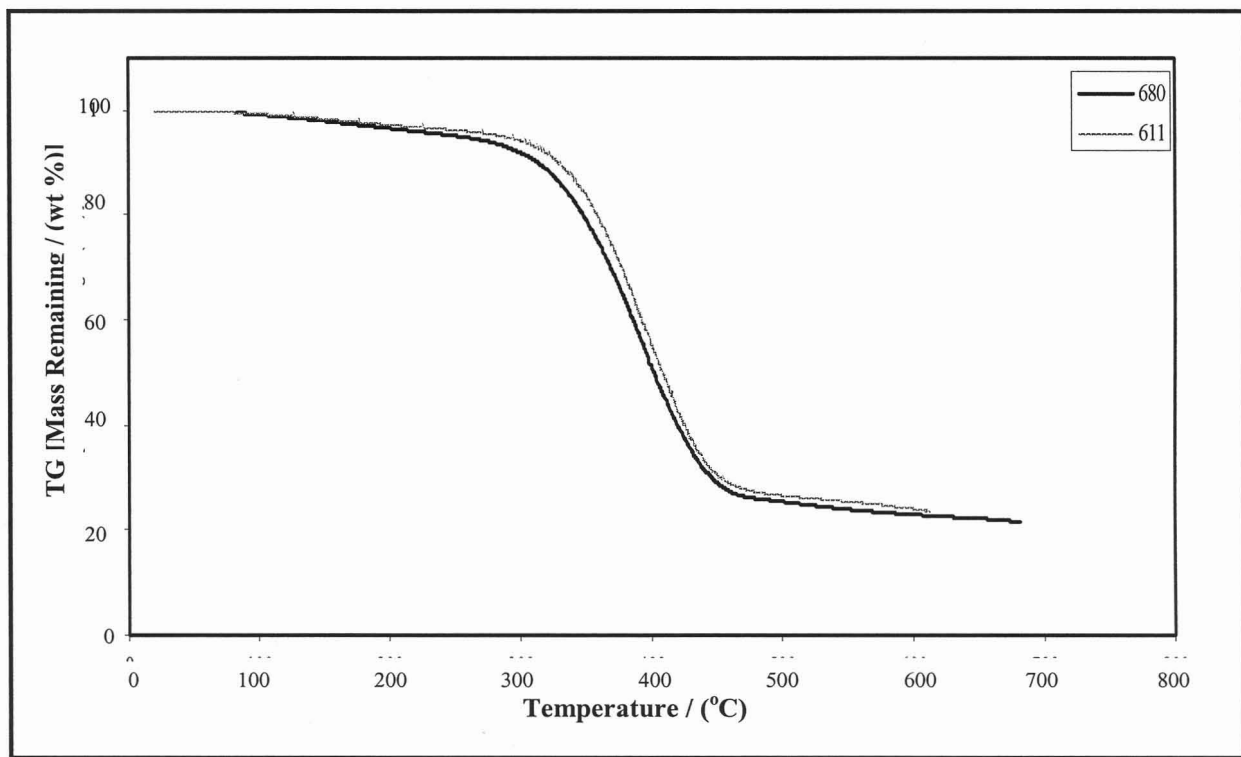
Figure 6.8: Thermograms of bagasse pellets at a heating rate of 10°C/min during pyrolysis process.

Two thermograms are shown here, one for experiments at a final pyrolysis temperature of 680 ^{o}C and the other for 611 ^{o}C. Both thermograms are similar which confirms the equipment and the established process's ability to produce repeatable results. The above thermograms show that a small mass loss of 4% occurs from room temperature to 200 ^{o}C. This initial weight loss is attributed to the release of inherent water vapour and endothermic decomposition of polysaccharides. The release of water vapour was verified by water collecting in the gas-liquid separating vessel during this stage. Rapid thermal degradation of South African bagasse begins around 280 ^{o}C and ends around 450 ^{o}C. This is due to the release of volatile matter from the

bagasse samples. At temperatures greater than 450 °C, smaller decreases in mass loss are observed. The final mass of char remaining was 23.56 % at 611 °C. Increasing the pyrolysis temperature to 680 °C, yielded 21.48 % char from bagasse. The shape of the thermograms is comparable to those observed by Garcia *et al* [2001]. The yield is much higher than 16.0% obtained by Garcia *et al* [2001]. A differential thermogram was plotted in fig 6.9 in order to obtain more details of bagasse pyrolysis.
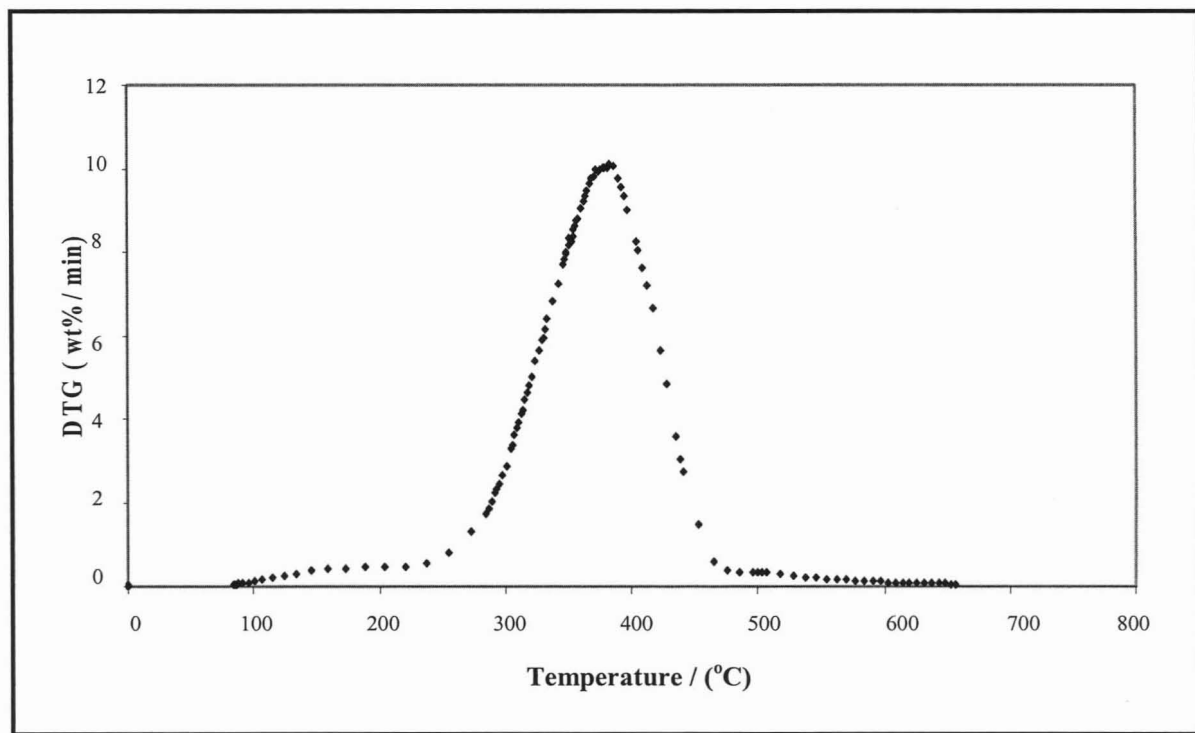
Figure 6.9: Differential Thermogram (DTG) of South African sugar cane bagasse pellets at a heating rate of 10 °C/min.

Only a single peak at 384 °C is observed in the DTG curve for pyrolysis of South African bagasse pellets. This corresponds to a cellulose peak according to the work presented by Antal and Varhegyi [1995]. However, pyrolysis of sugar cane bagasse occurs by the combined degradation of hemicellulose, cellulose and lignin. The hemicellulose peak is usually observed around 300 °C [Garcia *et al*, 2001]. But, in this case, the hemicellulose peak cannot be distinguished in fig 6.9 and is perhaps merged into one broad peak. Decomposition of lignin does occur, but its peak cannot be seen which is in agreement to Evans and Milne [1987] who have pointed out that lignin decomposition occurs slowly over a broad range of temperatures and is overlapped by the cellulose peak. This featureless, broad, single peak for pyrolysis of bagasse is representative of samples that have not been pretreated [Antal and Varhegyi, 1995]. Another possibility for the difference in the DTG curves presented in fig 6.9 and that reported by Garcia *et al* [2001] is that these are compact bagasse pellets whereas most pyrolysis studies are carried out on de-ashed and loose bagasse fibres. Lumping bagasse fibres together increases

the vapour-solid interactions during pyrolysis such that the vapour product formed during hemicellulose and cellulose decomposition is converted into char instead of escaping. It is perhaps possible that enhancing vapour-solid interactions would lead to a single peak as seen in the DTG curve in fig 6.9. Similar DTG curves were found in this study for all bagasse pellet samples that were pyrolysed. It is also evident that vapour-solid interactions were enhanced since the char yields were high.

The mass remaining for each set of experimental runs at the final pyrolysis temperatures and soak time of 1 hour were plotted and is shown below in fig 6.10.
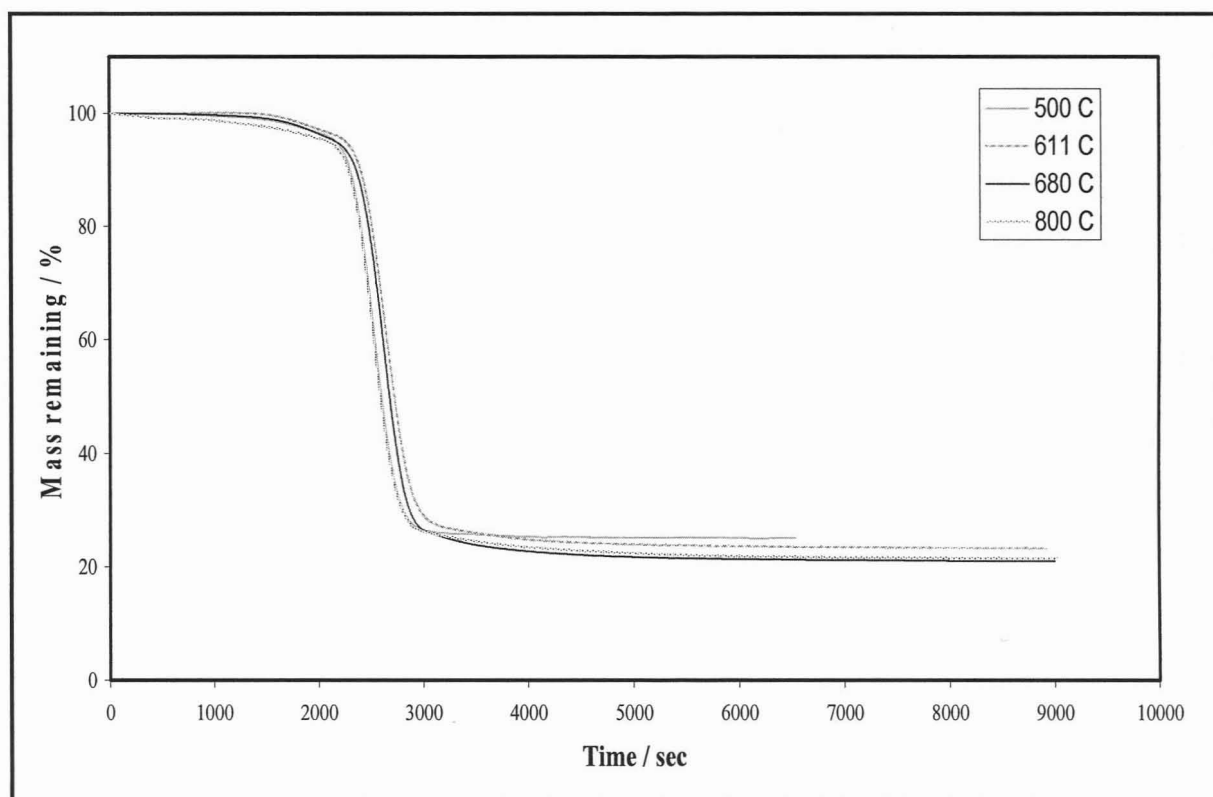
Figure 6.10: Bagasse char yields at different final pyrolysis temperatures at an initial heating rate of 10 °C/min.

Again the equipment's and the established process's abilities to reproduce results remarkable well is illustrated clearly in fig 6.10. This is confirmed by the general trend of rapid mass loss between 2000 and 3000 seconds observed in all experimental runs. The final percentage of char remaining decreases with increasing temperature from 25 % at 500 °C to 21% at 800 °C.

6.2.2. Bagasse Pyrolysis Kinetic Parameters

The kinetic parameters such as rate constant, activation energy and the thermodynamic properties such as entropy change, enthalpy change and Gibbs free energy were calculated for the pyrolysis of bagasse in a nitrogen atmosphere at a heating rate of 10 $^{\circ}$C to a final pyrolysis temperature of 680 $^{\circ}$C. In relation to Nassar *et al*'s [1996] work, bagasse pyrolysis was found to occur through two stages namely volatilization and decarbonization. By assuming that both these stages are first order reactions and following the calculation procedure outlined in Chapter 3, section 3.3.2, and using the mass loss curves in fig 6.10, figures 6.11 and 6.12 were produced in order to determine the rate constants for both these stages.

The y-axis is labelled $\log [(w_o - w_\infty)/(w_t - w_\infty)]$ and the x-axis is labelled **Time / (min)**. The fitted equation is $y = 0.4099x - 16.875$, $R^2 = 0.9904$.
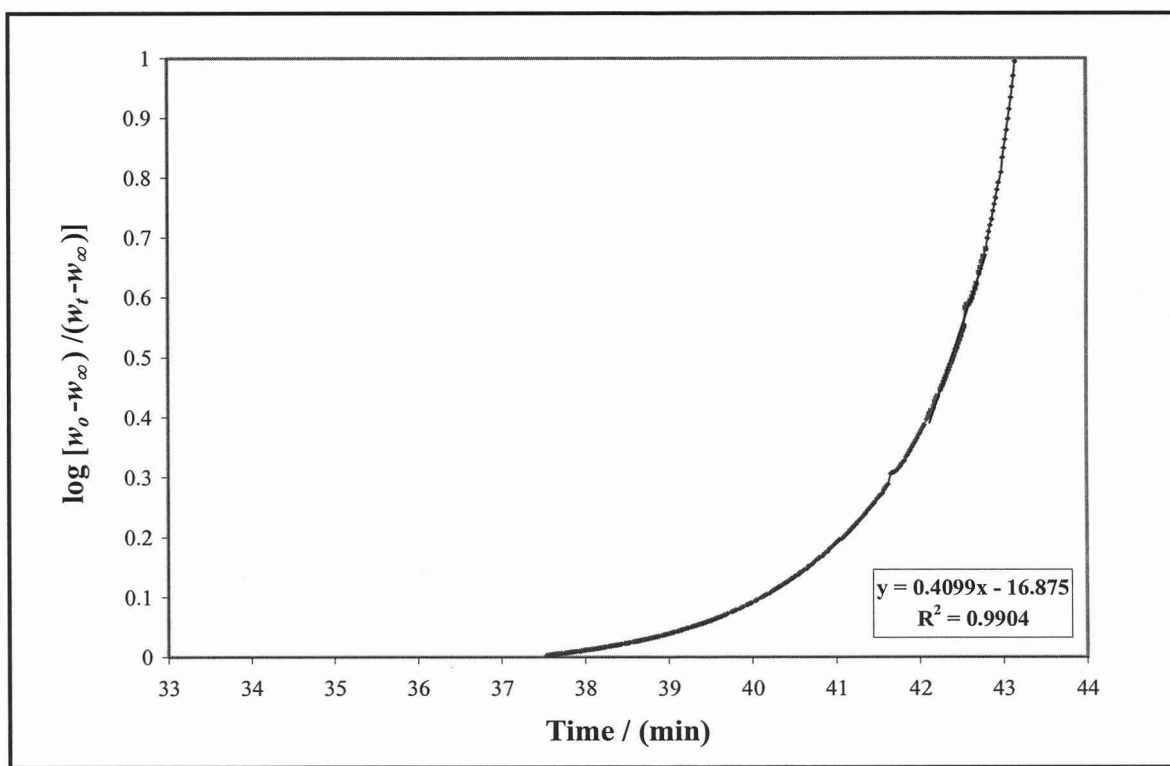
Figure 6.11: Plot used to determine the rate constant for the volatilization stage of bagasse pyrolysis.

From fig 6.9 and 6.10, the maximum weight loss occurs around at 384 $^{\circ}$C and the mass remaining at this point, 62%, was considered to be w_∞ for the volatilization stage. A slight curvature is observed in the beginning of the volatilization graph in fig 6.11, which is attributed to the initiation of the reactions. This plot is comparable to those obtained by Nassar *et al* [1996] who used the same method to determine the rate constants. They also found a slight curve at the start of the plot. However, a straight line is obtained after the initial curve.

Neglecting the initial section of the graph, the rate constant determined from straight line of the graph is 0.4099/min for the volatilization stage during bagasse pyrolysis.
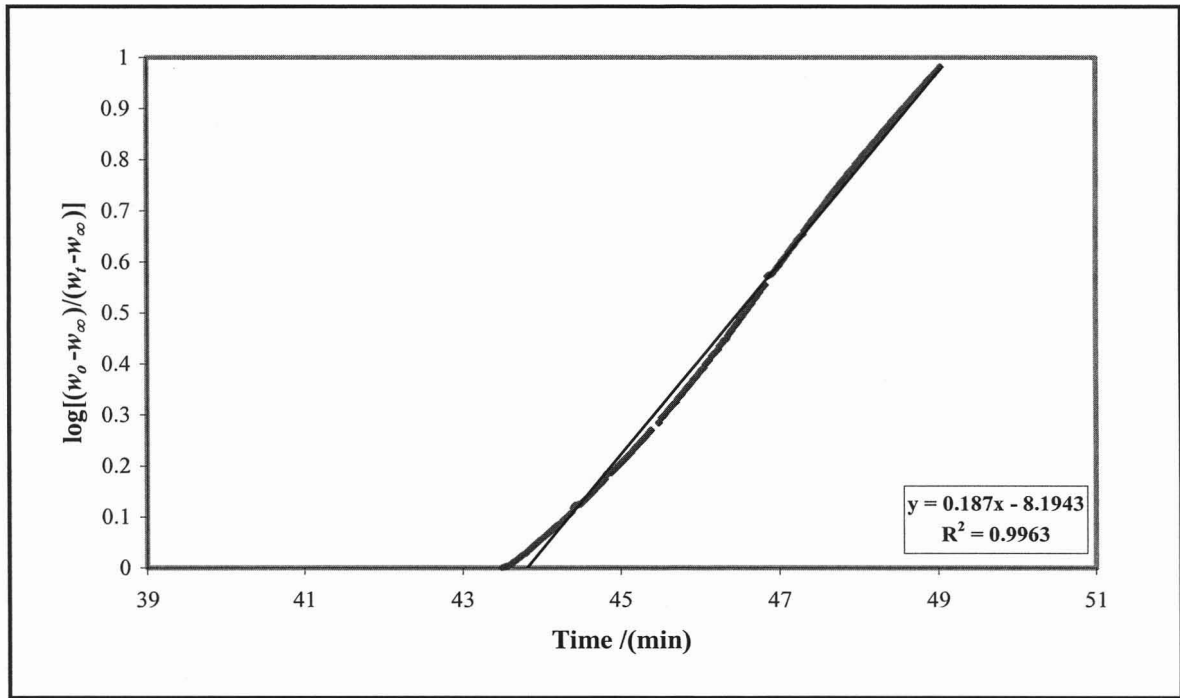
Figure 6.12: Plot to used to determine the rate constant for the decarbonization stage of bagasse pyrolysis

For the decarbonization stage, 23.5 % remaining mass was used as w_∞ A straight-line plot was generated giving rise to the decarbonization rate constant of 0.187 /min for the temperature range from 384 to 588 °C. This straight line coincides with the initial assumption of a first order reaction. The rate constant is much lower for decarbonization than volatilization. Similar findings were observed by Nassar *et al* [1996].

The rate constant at temperature T was determined by the equations obeying first order kinetics (see chapter 3, section 3.3.2). The Arrenhuis plot of ln (K) versus $1/T$ (see fig 6.13) was generated for volatilization and decarbonization stages in order to determine the activation energies.
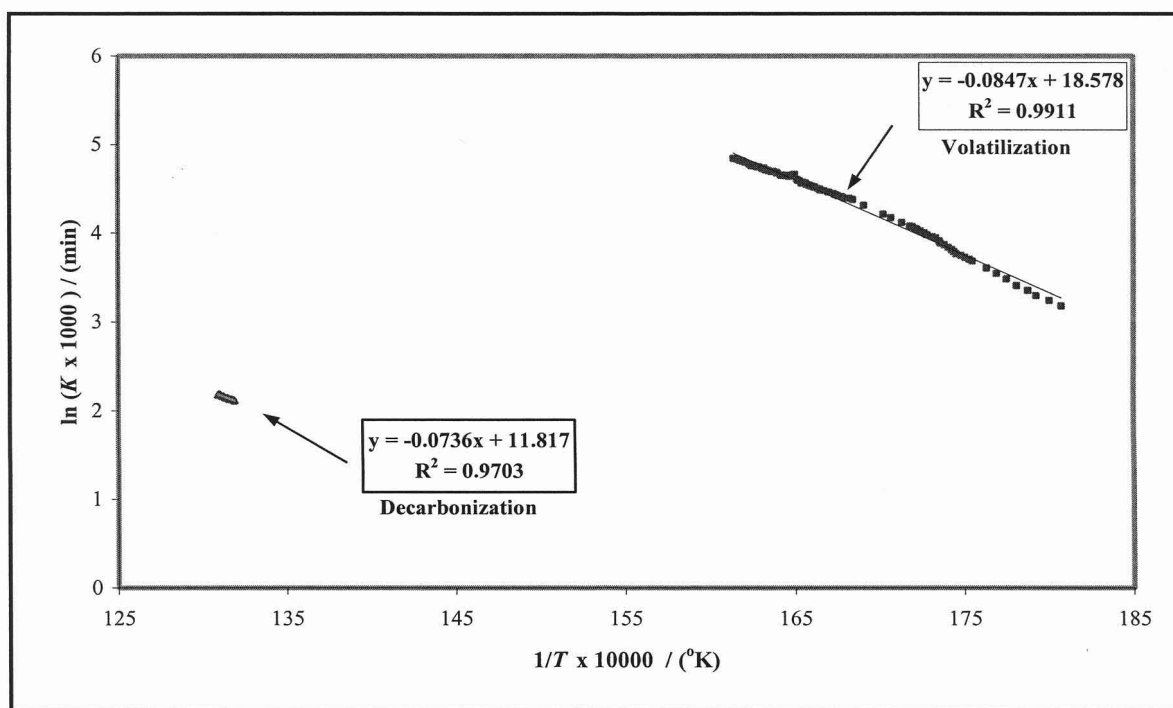
Figure 6.13: Arrenhuis plot for the pyrolysis of S.A sugar cane bagasse.

The activation energies determined from the Arrenhuis plot are tabulated in table 6.2. The plot for the decarbonization stage is not as distinguishable as that for volatilization. This could be as a consequence of the degradation peaks not being distinguishable in the DTG curves in fig 6.9. Furthermore, it must be taken into account that the aim of bagasse pyrolysis was to increase char yield and develop porosities instead of completing gasifying sugar cane bagasse into liquid and gaseous products. Using the rate constants, the thermodynamic properties; change in enthalpy, entropy and Gibbs free energy for each stage were also calculated and tabulated in table 6.2.

Table 6.2: Thermodynamic Properties of S.A bagasse pyrolysis in a nitrogen atmosphere

Stage	K / (min^{-1})	Temp (^{o}C)	E_a (kJ/mole)	ΔH (kJ/mole)	ΔS (kJ/mole ^{o}K)	ΔG^{o} (kJ/mole)
Volatilization	0.0797	320	70.42	65.48	-0.195	181.19
De-carbonization	0.0089	490	61.19	54.84	-0.254	248.52

The rate constants in table 6.2 represent the average rate constant at the chosen temperature range. Positive values for Gibbs free energy are found indicating the non-spontaneous nature of the reactions. This also points out that the free energy of the products is higher than for the reactants (bagasse). With respect to the results presented by Nassar et al [1996], who pyrolysed

bagasse at a heating rate of 5 °C/min, the values obtained in this study for activation energy in the decarbonization stage is approximately 15 kJ/mole higher, but in contrast the volatilization activation energy is approximately 17 kJ/mole lower. The net effect is about 2 kJ/mole lower in comparison. At twice the heating rate the rate constants are approximately two times greater. However, all other thermodynamic properties, change in Gibbs free energy, change in entropy and change in enthalpy are very close to those obtained by Nassar *et al*, [1996] which are tabulated in table 3.9 in chapter 3.

6.2.3. Determination of Pyrolysis Temperature

Bagasse was pyrolysed to final temperatures ranging from 500 to 900 °C at a heating rate of 10 °C /min and held at the final pyrolysis temperature for one hour. The resulting bagasse chars were subsequently characterized in terms of iodine and methylene blue numbers to identify the best pyrolysis temperature that would yield activated carbons with the desired properties. These two characterization methods were used because these characterization techniques are generally accepted methods and are much easier, cheaper and quicker to apply when gaining information on microporosity and mesoporosity of the carbon. The iodine molecule is representative of pores less than 20 Å and its adsorption is indicative of the microporosity of the carbon and methylene blue is related to the mesoporosity of the carbon.

The iodine adsorption isotherms for carbons produced at different pyrolysis temperatures were plotted and is presented in fig 6.14. All carbons were treated with 0.1 N iodine solutions. Each set of carbons that were produced has a unique isotherm associated with it. The mass of carbons used to obtain a residual iodine solution of 0.03N is similar for carbons produced at the final pyrolysis temperatures of 800, 680 and 611 °C. Carbons produced at 500 and 900 °C have very low affinities for iodine because large quantities of carbon are used to reduce the iodine concentration from 0.1 N to 0.03 N as shown by their isotherms in fig 6.14.
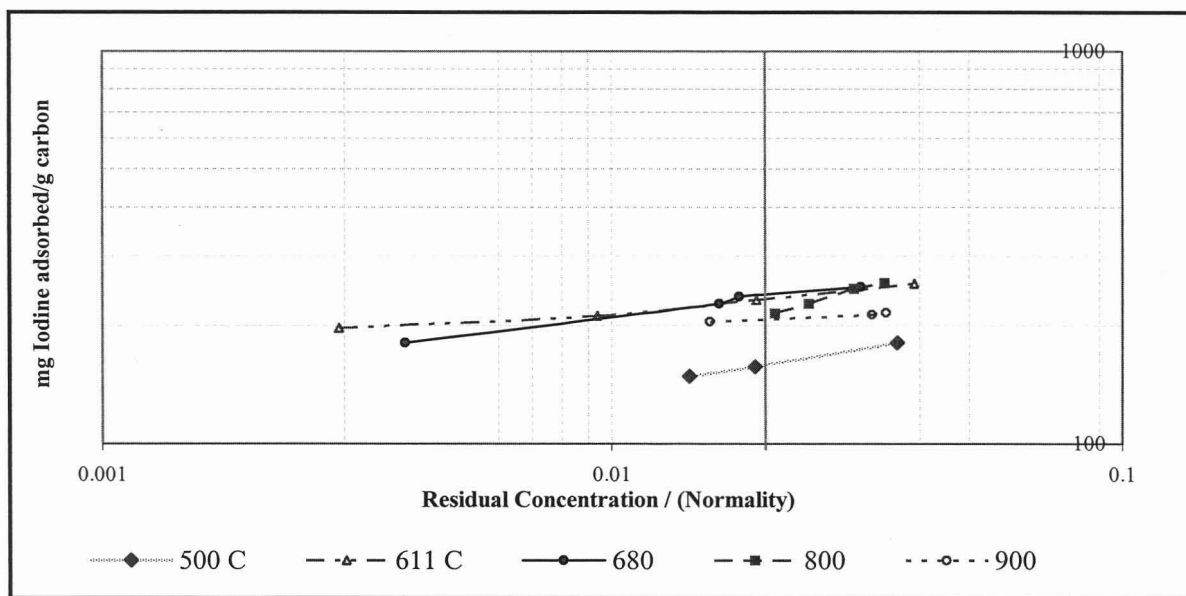
Figure 6.14: Iodine isotherms of carbons produced from bagasse at different pyrolysis temperatures at a heating rate of 10 °C/min and a hold time of 1 hour

The Freudlich parameters for each carbon were determined from the isotherm plots in figure 6.14 and are tabulated in table 6.3. Carbon produced at final pyrolysis temperature of 800 °C, has the greatest adsorption capacity (k) with the effect of concentration (n) being small on adsorption capacity.

Table 6.3: Freundlich isotherm parameters for bagasse carbons

Carbon produced at Temperature / °C	n_c	K_a
500	4.8	360.4
611	10.0	347.3
680	6.1	448.2
800	2.7	904.5
900	15.4	267.6

Carbon at 900 °C has the lowest adsorption capacity and the effects of concentration on adsorption capacity are large. A balance between concentration and adsorption capacity would indicate a more stable carbon, which corresponds to carbons produced at 680 °C.

The iodine number was determined as the mg iodine adsorbed / g carbon at the residual concentration of 0.02 N from the isotherm plot portrayed in fig 6.14. A plot of iodine number and methylene number versus final pyrolysis temperature was produced and is presented in fig 6.15.
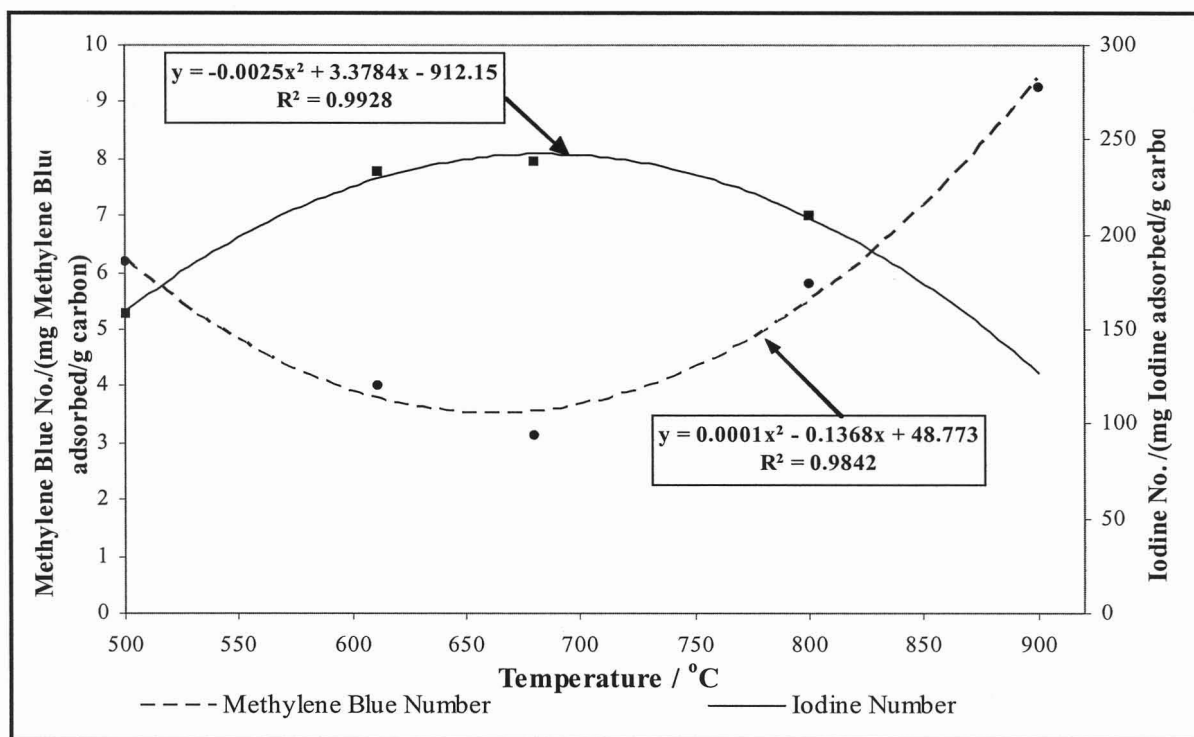
Figure 6.15: Methylene Blue and Iodine characterization of bagasse chars at produced at a heating rate of 10 °C/min and different pyrolysis temperatures at a hold time of 1 hour.

Fig 6.15 indicates that as the final pyrolysis temperature increases from 500 to 900 °C, an increase in iodine number occurs until 680 °C and then decreases at higher temperatures. The opposite effect is observed with respect to methylene blue number at increasing final pyrolysis temperatures. Chars produced at 680 °C possessed the highest iodine number (240 mg/g carbon) and the lowest methylene blue number (3.13 mg/g carbon). A carbon having a high iodine number indicates a char consisting of a large quantity of micropores. Upon activation of microporous chars, surface areas increases and the meso-macropores are also created by pore widening of micropores. However, high methylene blue numbers indicate high amounts of mesopores and upon activation these pore sizes will be further increased leading to macropores which act as channels for adsorbates to reach adsorption sites instead of taking part in adsorption. This results in a decrease in surface area available for adsorption. Thus, the desired pyrolysis temperature of 680 °C was seen as the optimum pyrolysis temperature in terms of producing activated carbons from sugar cane bagasse. The optimum pyrolysis temperature obtained for this case is comparable to those used by many researchers who have produced

bagasse chars at pyrolysis temperatures ranging from 700-800 ^{O}C [Pendy *et al*, 1999; Minkova *et al*, 2000; Xia *et al*, 1998].

Furthermore, from the results presented in fig 6.15, a second order polynomial correlation exists between final pyrolysis temperature and methylene blue and iodine numbers. If for instance, an estimate of the pore structure of a carbon produced between final pyrolysis temperatures of 500 to 900 ^{o}C at the specific hold time of 1 hour and heating rate of 10 ^{o}C/min needs to be known, the above correlations for methylene blue number and iodine number can be used a relative indicators of meso and microporosity.

Pyrolysis hold time has also been identified as an influencing factor on the properties of the activated carbon produced during activated. The impact of exposure times at the final pyrolysis temperature on the surface area, pore volume and pore size distribution is discussed in section 6.3.2.

6.2.4. Characterization of Bagasse Chars

The best bagasse carbons produced at the final pyrolysis temperature 680 ^{O}C and hold time of one hour were further characterized by adsorption of nitrogen at 77K. A typical isotherm for the sorption of Nitrogen onto the bagasse carbon is displayed in fig 6.16.
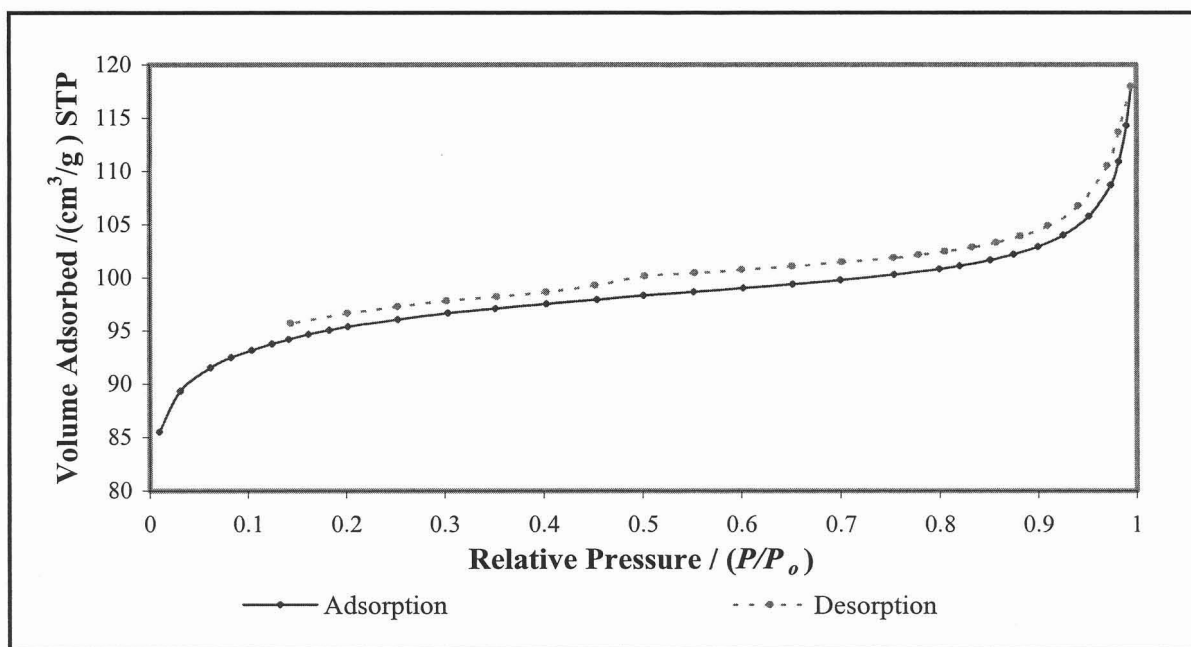
Figure 6.16: Nitrogen sorption isotherms at 77 K for chars prepared from bagasse at a heating rate of 10 ^{o}C /min to a pyrolysis temperature of 680 ^{o}C and hold time of 1 hour

By visual inspection, the shape of the isotherm corresponds to Type I in the BDDT classification [Brauner *et al*, 1940] indicating that the carbon is predominately microporous. This was foreseen in the methylene blue and iodine adsorption tests. As the relative pressure approaches 1.0, the upswing in the curve reveals that the adsorption of nitrogen in the gaseous phase has shifted to capillary condensation with pores being filled with liquid adsorbate. Open–loop hysteresis occurs at low relative pressures indicating that activated diffusion of nitrogen through the narrow openings in the microporous network occur, because of the aperture size being similar to that of a nitrogen molecule. The steep fall and closure of the desorption isotherm at a relative pressure of ~ 0.45 can be seen. According to Schoefield [1948], the relative pressure at which closure occurs is due to the tensile strengths of the adsorbate whereby the adsorbate undergoes a phase transition from liquid-like to a gaseous-like state.

The surface area, pore volume and pore size distribution of the bagasse char were determined by the volume of nitrogen adsorbed or desorbed at 77K at different relative pressures. These characteristics of the resultant bagasse chars are tabulated in table 6.4. The total, external, and micropore surface areas and micropore volumes listed in table 6.4 were evaluated by using the slopes and intercepts from linear plots which can be found in fig C-1 to C-3 in Appendix C-1.1 and C-1.2.

Table 6.4: Characteristics of bagasse char produced at a heating rate of 10 ^{O}C/min to the final pyrolysis temperature of 680 ^{O}C and hold time of 1 hour

Parameter	Units	Value	Method Used
Total Surface Area	m^2/g	331.46	Single point
Total Surface Area	m^2/g	320.03	BET
Total Surface Area	m^2/g	423.50	Langmuir
Micropore Surface Area	m^2/g	271.79	t-plot
External Surface Area	m^2/g	48.24	t-plot
Cumulative Surface Area	m^2/g	28.47	BJH Adsorption[1]
Cumulative Surface Area	m^2/g	26.74	BJH Desorption[1]
Total Pore Volume[2]	cm^3/g	0.1682	Single point
Micropore Volume	cm^3/g	0.1263	t-plot
Cumulative Pore Volume	cm^3/g	0.0482	BJH Adsorption[1]
Cumulative Pore Volume	cm^3/g	0.0453	BJH Desorption[1]
Ave Micropore Diameter	Å	21.074	Single point / BET
Ave Meso-Diameter	Å	67.67	BJH Adsorption[1]
Ave Meso-Diameter	Å	67.80	BJH Desorption[1]

-   [1] between 17.0 and 3000.0 Å diameter

-   [2] pore volume of pores less than 816.1Å diameter and $P/P_o = 0.0976$

Table 6.3 points out that the bagasse carbons have high surface area with micropore contribution being 84 % (of BET surface area). The surface area created for adsorption corresponds to approximately one third of a commercial activated carbon (Norit PN2 – 1000 m^2/g). The graphs used to evaluate the cumulative surface area by the BJH method for pores in the range of 17 - 3000 Å shown above in table 6.3, can be found in fig C-4 to C-6 in Appendix C-1.3. Pores in this size range contribute to 9 % of the total surface area. The micropore contribution to total pore volume amounts to 75% with rest being from the mesopores which further classifies South African bagasse chars from optimum pyrolysis conditions as microporous carbons. Slightly higher values for cumulative surface area and pore volume are depicted during adsorption than desorption when using the BJH methods. However, the average pore size is slightly greater during desorption as it takes into account the layer of thickness that is left behind on the walls of the pores. The pore size distribution of the bagasse carbon in terms of dV_{cum}/dD and dV / d($logD$) versus pore diameter between 17 and 3000 Å are given in fig 6.17 and 6.18.

Both figures 6.17 and 6.18 show maxima's below 20 Å corroborating that the highest pore volume contribution is from the micropores. A second smaller maximum is observed in the desorption curves in the pore range of 30-40 Å revealing that the initial development of mesopore begins but the contribution is extremely low.
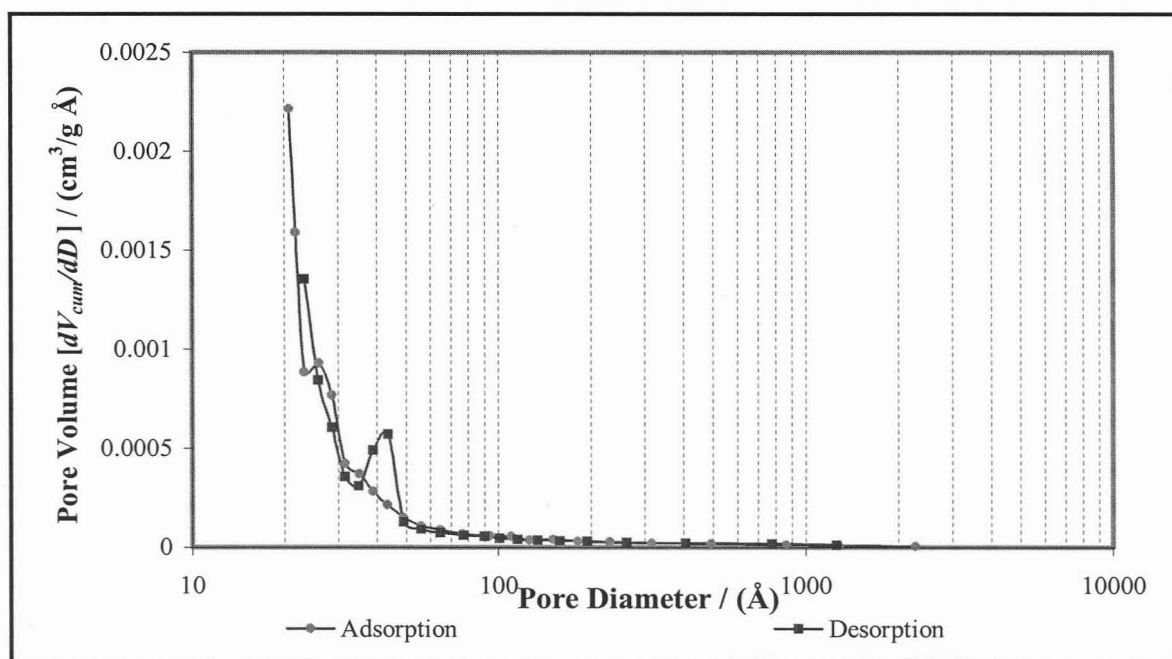
Figure 6.17: Pore size Distribution (dV_{cum}/dD versus pore diameter) of bagasse chars produced at a heating rate of 10 ^{o}C/min to a final pyrolysis temperature of 680 ^{o}C and hold time of 1 hour.
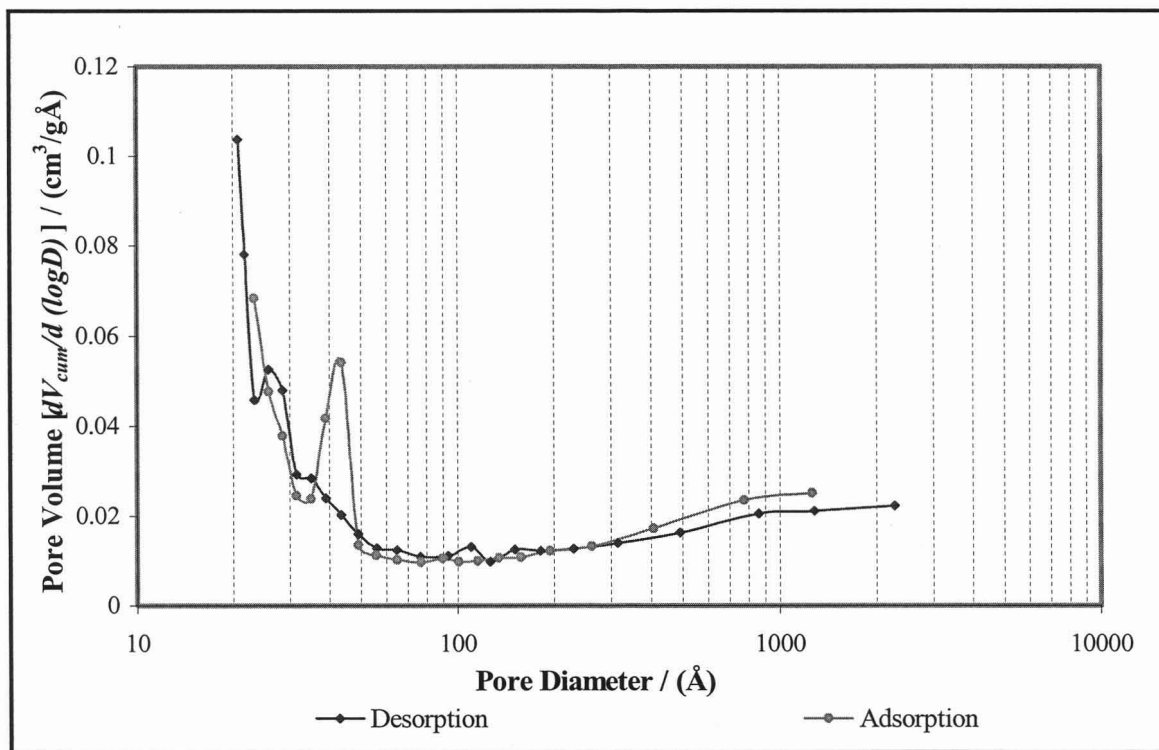
Figure 6.18: Pore size Distribution (*dV_cum/d(logD)*) versus pore diameter of bagasse chars produced at a heating rate of 10 °C/min to a final pyrolysis temperature of 680 °C and hold time of 1 hour.

The pore size distribution in terms of cumulative pore volume versus pore diameter has also been plotted and is added in fig C-7 in Appendix C-1.1.3. The pore area distribution plots are also included in Appendix C-1.1.3 (see fig C 4-6) and can be viewed if required.

6.2.5 Topographical Study

Scanning electron microscopy was used to determine the elemental analysis of the bagasse char on a dry basis and is tabulated in table 6.5.

Table 6.5: Elemental Analysis of Bagasse char produced at a heating rate of 10 °C/min to a final pyrolysis temperature of 680 °C and hold time of 1 hour

Element	% (dry basis excluding Hydrogen)
Carbon	22.36
Nitrogen	30.69
Oxygen	30.52
Ash	2.91

Comparison of the elemental analysis of bagasse char to that of sugar–cane bagasse raw material reveals that a decrease in oxygen content, increase in carbon and ash % results after bagasse has been pyrolysed. These differences are attributed to the removal of volatiles and development of the carbon skeleton.

An SEM of the bagasse char is shown in fig 6.19. The scanning electron micrograph in this figure verifies the rudimentary pore structure of the bagasse char that was by created by pyrolysis. A large number of randomly distributed and oval shaped pores are shown on the surface of the bagasse chars. In comparison to raw bagasse, these pores are larger and the collapsing of walls between adjacent pores can be seen which give rise to meso and macropores.
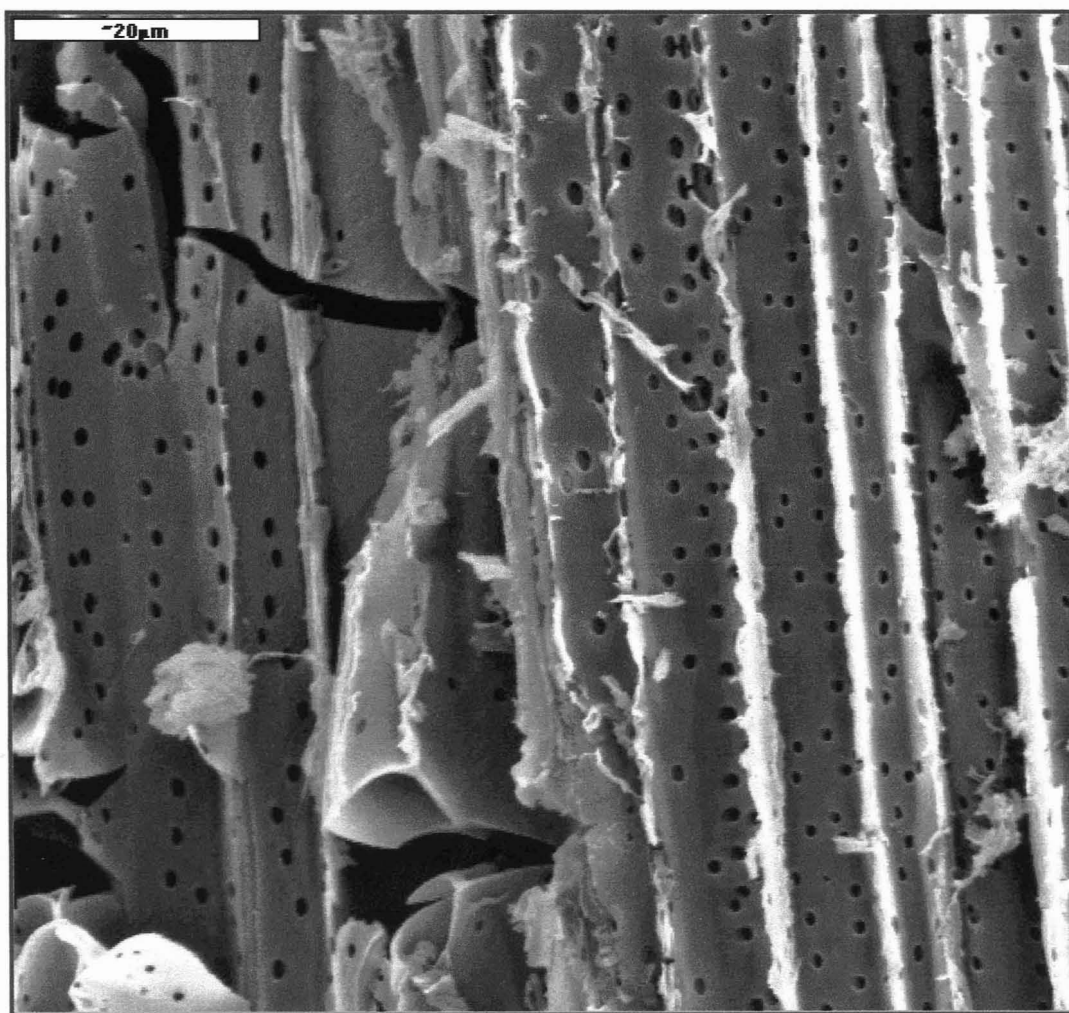
Figure 6.19: Scanning electron micrograph of bagasse chars producing at a heating rate of 10 °C/min to a final pyrolysis temperature of 680 °C and hold time of 1 hour.

## 6.3 Activation of Bagasse chars

The bagasse chars that were produced at a heating rate of 10 °C/min to a final pyrolysis temperature of 680 °C, for a specific hold time were subsequently subjected to partial gasification with steam as the activating agent during the activation stage. The results from the activation experiments that were carried out at different steam partial pressures, activation times, activation temperatures and the effect of pyrolysis conditions on the final activated carbon are presented and discussed in this section.

6.3.1. Effect of Steam Partial Pressure on the Activated Carbons

Three types of final activated carbons were produced from the activation experiments on bagasse chars that were carried out at different steam partial pressures at an activating temperature of 800 °C for an activation time of 4 hours (see table 5.2 in chapter 5) in order to establish the steam partial pressure that gives rise to activated carbons having the desired properties for sugar decolourisation.

The amount of steam being passed through the system at the different nitrogen flows was determined by methods explained in chapter 5, section 5.6. A direct proportional relationship between the steam/nitrogen ratio and steam partial pressure exists. The steam concentration was converted to steam to nitrogen ratios by using the flow rates and densities of both components.

The percentage burn-off reached for each set of conditions at the varying steam/nitrogen ratios are expressed in table 6.6.

Table 6.6: Extent of activation at varying steam partial pressures

Sample	Steam / Nitrogen ratio	Burn-off / (%)
J	1.0 : 0.6	30.0
L	0.5 : 0.5	26.0
G	0.4 : 1.0	24.5

As the steam / nitrogen ratio increases in the reactor, indicating increasing steam partial pressure, so too does the burn-off percentage increase. A higher burn-off percentage in gasification reactions is associated with high surface area and porosity. Increasing burn-off percentage results in a decreasing yield of product as well. A higher burn-off percentage

resulted in activated carbon J and implies that the surface area and porosity is much higher than carbons L and G.

Fig 6.20 shows the nitrogen adsorption isotherms obtained at 77K for the powder activated carbons J, L and G that were prepared from bagasse chars activated at different steam partial pressures. The nitrogen adsorption isotherms displayed in fig 6.20 are representative of Type IV isotherms in the BDDT classification [Brunauer *et al*, 1940] related to activated carbons having both micro and mesopores. As the steam/nitrogen ratio increases from G to J, the increase in adsorbed volume becomes more gradual indicating that the pores are widened and the pore size distribution becomes wider. The development of mesoporosity is clearly revealed by the increase in slope of the isotherms at higher relative pressures and the pronounced hysteresis loop effect that occurs during desorption for activated carbons J and L produced at higher steam partial pressures. The increase in uptake of nitrogen at low relative pressures reflects an increase in microporosity as steam partial pressure increases. Therefore, the extent of adsorption increases with an increase in steam concentration which is shown by the increase in micro and mesoporosity in the adsorption isotherms.
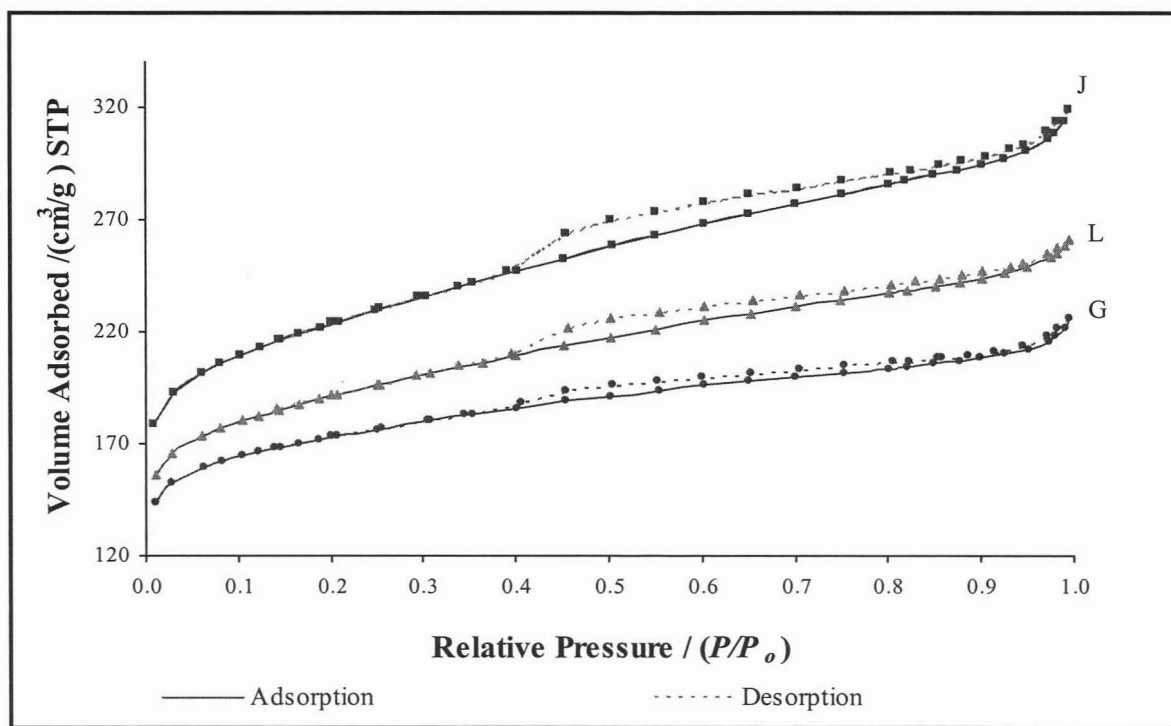
Figure 6.20: Nitrogen Adsorption isotherms at 77 K for activated carbons produced from bagasse chars activated for 4 hours at 800 ^{O}C at varying steam partial pressures (steam/nitrogen ratios), (■) J – 1:06, (▲) L -0.5:0.5 & (●) G – 0.4:1.

The physical values for activated carbons J, L and G were determined from the nitrogen adsorption isotherm plots and are given in table 6.7. The total, external and micropore surface areas, and micropore volumes for each activated carbon listed in table 6.7 were calculated from the slopes and intercepts of the straight line BET, Langmuir and t-plots in fig C-8 to C-10 in Appendix C-2.1.1 and C-2.1.2. Liquid adsorption tests with methylene blue and iodine as the adsorbates were also carried to verify the adsorption capacity and porosity of the activated carbons which are identified by their methylene blue and iodine numbers included in table 6.7.

Table 6.7: Characteristics of the powder activated carbons produced from sugar-cane at varying steam partial pressures.

Parameter	Units	Sample			Method Used
		J	L	G	
Total Surface Area	m^2/g	773.41	661.35	598.16	Single point
Total Surface Area	m^2/g	760.95	649.56	584.33	BET
Total Surface Area	m^2/g	1026.34	873.44	785.66	Langmuir
Micropore Surface Area	m^2/g	445.16	398.84	387.09	t-plot
External Surface Area	m^2/g	315.80	250.72	197.24	t-plot
Micro- Area / Total Area	%	59	61	66	
Cumulative Surface Area	m^2/g	253.40	196.54	142.92	BJH Adsorption[1]
Cumulative Surface Area	m^2/g	280.14	215.7	157.14	BJH Desorption[1]
Total Pore Volume	cm^3/g	0.4729	0.3913	0.3339	Single point
Micropore Volume	cm^3/g	0.2075	0.1858	0.1808	t-plot
V_{micro}/ V_{total}	%	44	47	54	
Cumulative Pore Volume	cm^3/g	0.2624	0.1970	0.0147	BJH Adsorption[1]
Cumulative Pore Volume	cm^3/g	0.2730	0.2042	0.0152	BJH Desorption[1]
Ave Micropore Diameter	Å	24.86	24.09	22.86	Single point / BET
Ave Meso-Diameter	Å	41.42	40.09	41.12	BJH Adsorption[1]
Ave Meso-Diameter	Å	38.98	37.85	38.74	BJH Desorption[1]
Methylene Blue No	mg MB / g	162.13	127.03	126.27	Aktasorb Systems
Iodine No.	mg I_2 / g	824.16	786.2	780.05	ASTM method

-     [1] between 17.0 and 3000.0 Å diameter

Increasing steam partial pressure, results in an increase in total surface area and pore volume, micro and mesopore surface area and volume. However, with an increasing steam partial pressure a decrease in the micropore surface area and pore volume contributions occur with a subsequent increase in the fraction of mesopores. Higher steam partial pressure results in an increase in burn-off % which leads to the opening up of blocked pores to form more micropores and pore widening creating mesopores resulting in the increase in meso-macropore volumes.

From the liquid adsorption tests, increasing steam partial pressures increases the adsorptive capacity and porosity which is confirmed by the increase in methylene blue and iodine numbers. The pore size distributions of the activated carbons J, G and L determined by the BJH adsorption and desorption techniques are presented in figures 6.21 to 6.24. Fig 6.21 and 6.22 illustrates the pore size distributions in terms of the average pore volume contributed by a certain diameter range, whereas fig 6.23 and 6.24 illustrates the pore area contribution by on the average pore diameter range. The illustration of pore size distribution shown below has been evaluated by using equations 4.21.
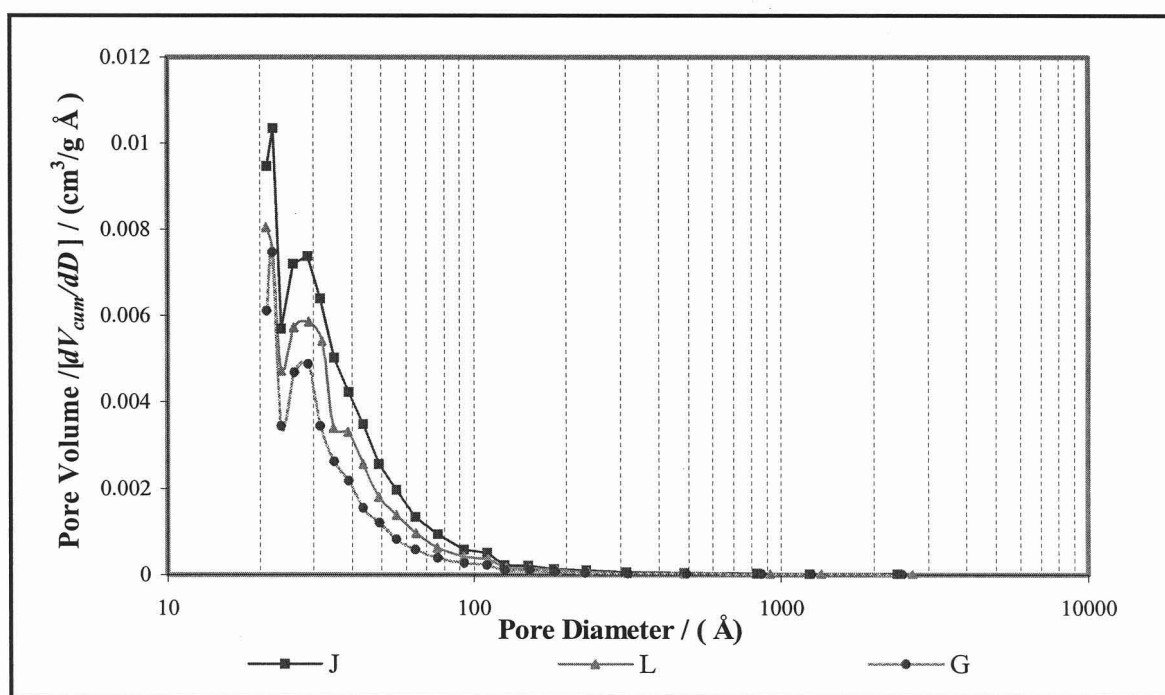
Figure 6.21: Pore size distribution (dV_{cum} /dD versus pore diameter) determined by BJH adsorption for activated carbons produced at varying partial pressures (steam/nitrogen ratios), J – 1:06, L -0.5:0.5 & G – 0.4:1.
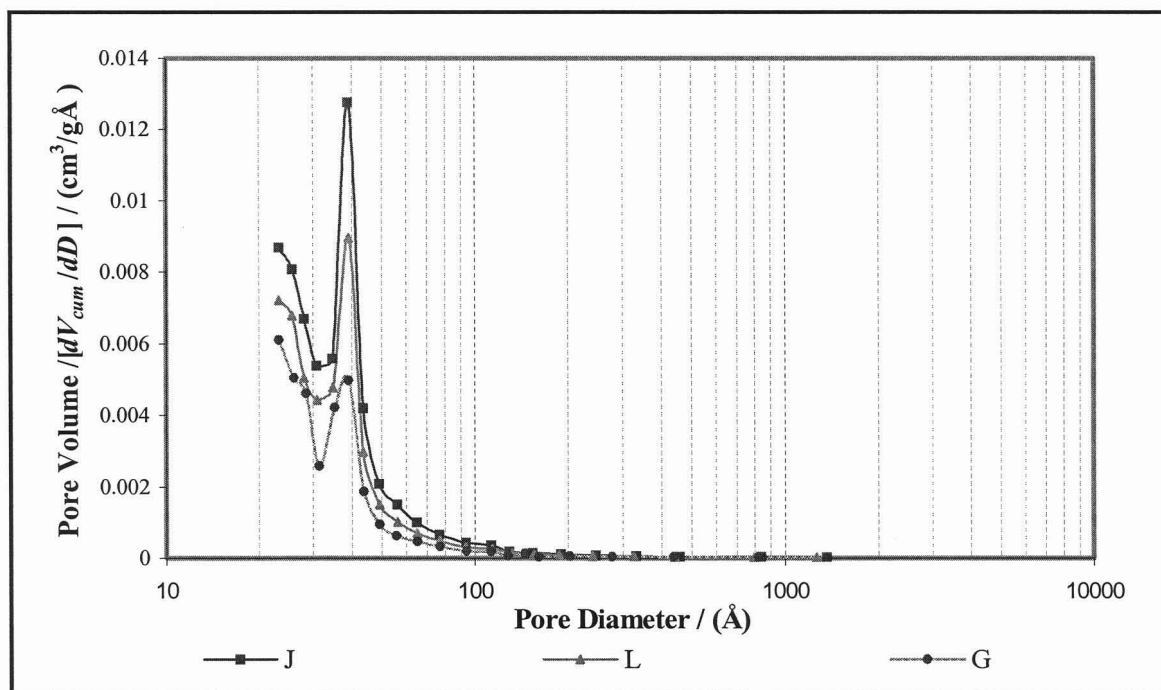
Figure 6.22: Pore Volume distribution (dV_{cum}/dD versus pore diameter) determined by BJH desorption for activated carbons produced at varying partial pressures (steam/nitrogen ratios), J – 1:06, L -0.5:0.5 & G – 0.4:1.
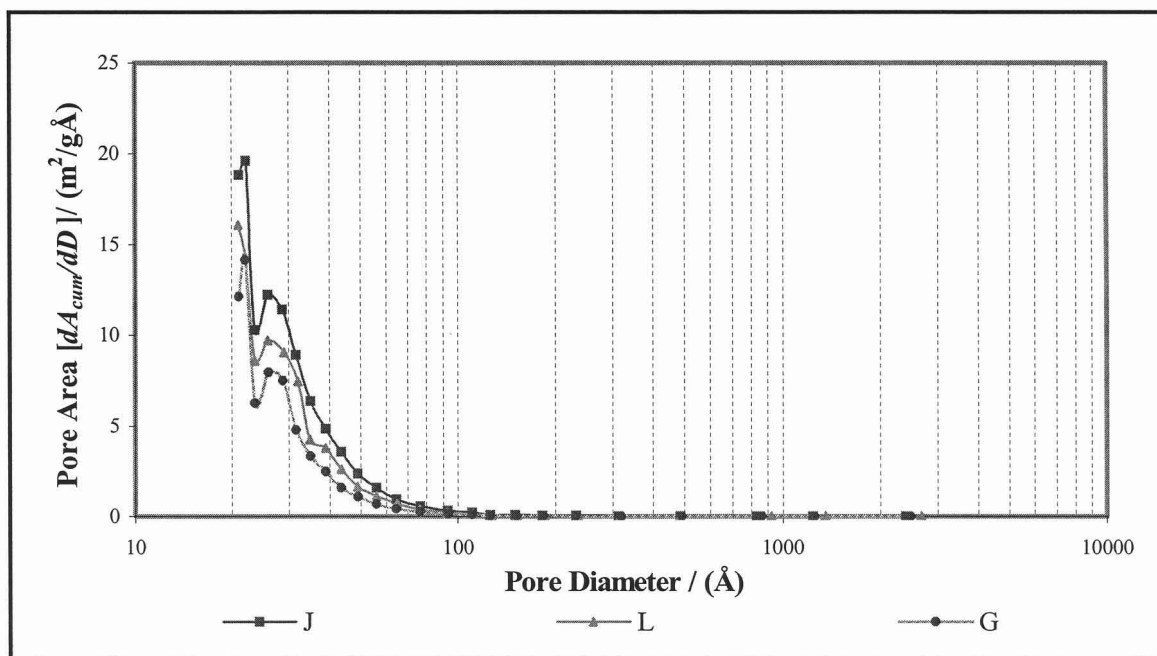
Figure 6.23: Pore Area distribution (dA_{cum}/dD versus pore diameter) determined by BJH adsorption for activated carbons produced at varying partial pressures (steam/nitrogen ratios), J – 1:06, L -0.5:0.5 & G – 0.4:1.
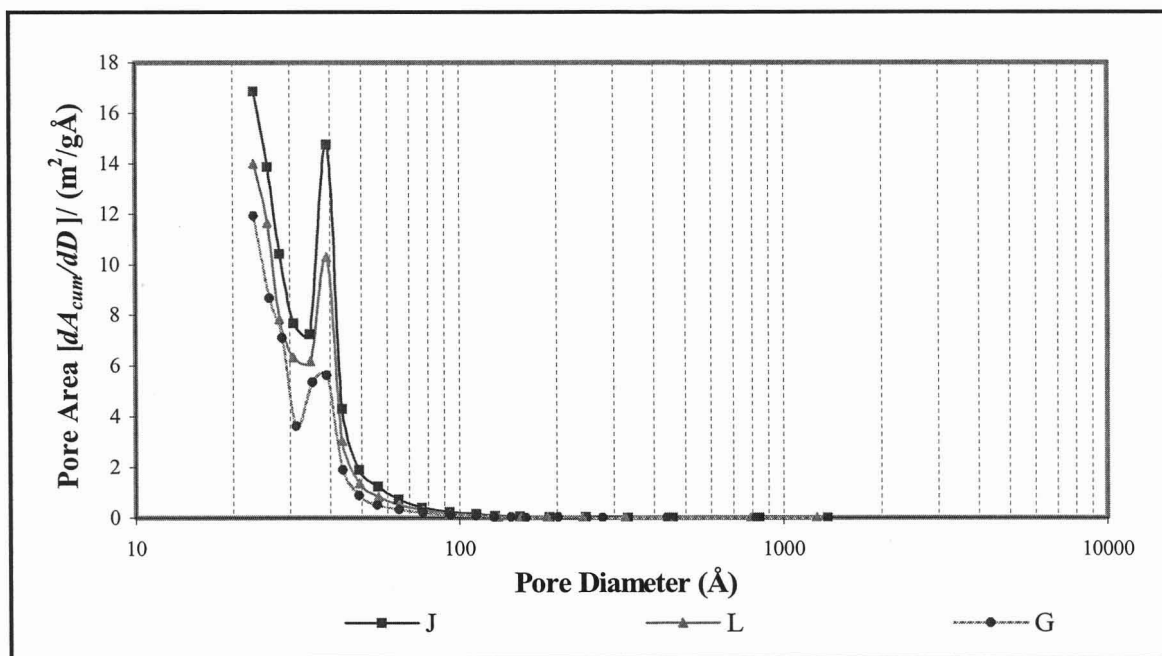
Figure 6.24: Pore Area distribution (dA_{cum}/dD versus pore diameter) determined by BJH desorption for activated carbons produced at varying partial pressures (steam/nitrogen ratios), J – 1:06, L -0.5:0.5 & G – 0.4:1.

From the pore size distribution curves of volume and area it can be seen that upon adsorption, a maxima lies around 22 Å (fig 6.22 and 6.23) for carbon J and for desorption which includes the layer left behind on the pore walls, the prominent peak is around 40 Å (fig 6.23 and 6.24). The pore size distribution for activated carbons L and G includes maxima below 20 Å but also includes smaller peaks in the mesopore region at 40Å. However in both adsorption curves smaller peaks at 30 Å are observed and are indicative of incipient mesoporosity. The pore volumes and areas in the specific pore size ranges increase with increasing steam partial pressures. This effect can be attributed to the increasing burn-off % as partial pressure increases which lead to a greater amount of mesopores being converted. However, the pore size distribution (area and volume) trends are the same for all the activated carbons produced at the activating temperature of 800 °C for a reaction time of 4 hours with carbon J having highest pore volume and area distributions among meso and micropores. More graphical plots of pore area and volume distribution for these activated carbons are included in fig C-11 to C-18 in Appendix C-2.1.3.

Based on these set of experiments, the steam to nitrogen ratio of 1:0.6 was subsequently employed in further experiments that were performed to obtain activated carbons with higher adsorption capacities for large molecules.

6.3.2. Effect of Pyrolysis and Activation Hold times on Activated carbons

The history of the pyrolysis process with respect to temperature and the exposure period during the final pyrolysis temperature has been known to effect to the quality of the activated carbon produced. The effects of pyrolysis hold-times, 1 and 2 hours on the activated carbons produced from sugar-cane bagasse were investigated (see chapter5, table 5.7). Concurrently, the effect of the activation time on the quality of the activated carbons produced from bagasse chars prepared at different pyrolysis exposure times were also explored (see chapter 5, table 5.7).

The burn-off percentages reached from these experiments are presented in table 6.8. Increasing the activation time resulted in an increase in burn-off percentage of carbons produced at pyrolysis exposure times of 1 and 2 hours. However, the burn-off percentage was much higher from chars that were prepared at a pyrolysis exposure time of one hour compared to those prepared at 2 hours. Chars produced from a pyrolysis exposure time of 2 hours and then activated for 3 and 4 hours reach almost the same burn-off % indicating very little difference in their pore structures and that further increase in activation time will probable impact negatively on the activated carbon. Chars prepared from a pyrolysis exposure time of 1 hour and activated for 4 hours leads to the greatest percentage burn-off, which implies that activated carbon, C, has a greater surface area and possibly a more pronounced pore size distribution.

Table 6.8: Extent of activation for different pyrolysis exposure times and activation times

Sample	Pyrolysis Hold time /(hr)	Activation Hold Time /(hr)	Burn-off (%)
A	1	1	9.9
B	1	3	21.5
C	1	4	26.0
D	2	1	8.7
E	2	3	18.3
F	2	4	18.6

The nitrogen adsorption isotherms at 77 K for these activated carbons are given in fig 6.25.

Activated carbons A and D pyrolysed at different exposure times, but activated for the same amount of time closely resemble Type I isotherms in the BDDT classification [Brunauer, *et al*, 1940] showing that these activated carbons predominately consist of micropores. A slight slope in their isotherms at higher relative pressures reveals the initial development of mesopores. The uptake of nitrogen is much greater for activated carbon A compared to B. Activated carbons B,

E and F isotherms lie very closely to each other on the isotherm plot and exhibit Type IV isotherms in the BDDT classification [Brunauer *et al*, 1940] having large hysteresis loops. Even though carbon F was exposed for a longer pyrolysis exposure time but activated for a much longer time than B and E, the carbon seems to show more microporosity than mesoporosity development. This is attributed to the burn-off percentages being similar to the other carbons. The adsorption isotherm for carbon C displays a Type IV isotherm consisting of both micro and mesopores. The increased uptake of nitrogen at low relative pressures compared to carbons A, B, C, D and E reveal a much higher amount of micropores and the increase in the slope of the isotherm also reinforces the fact that this carbon contains much more mesopores.
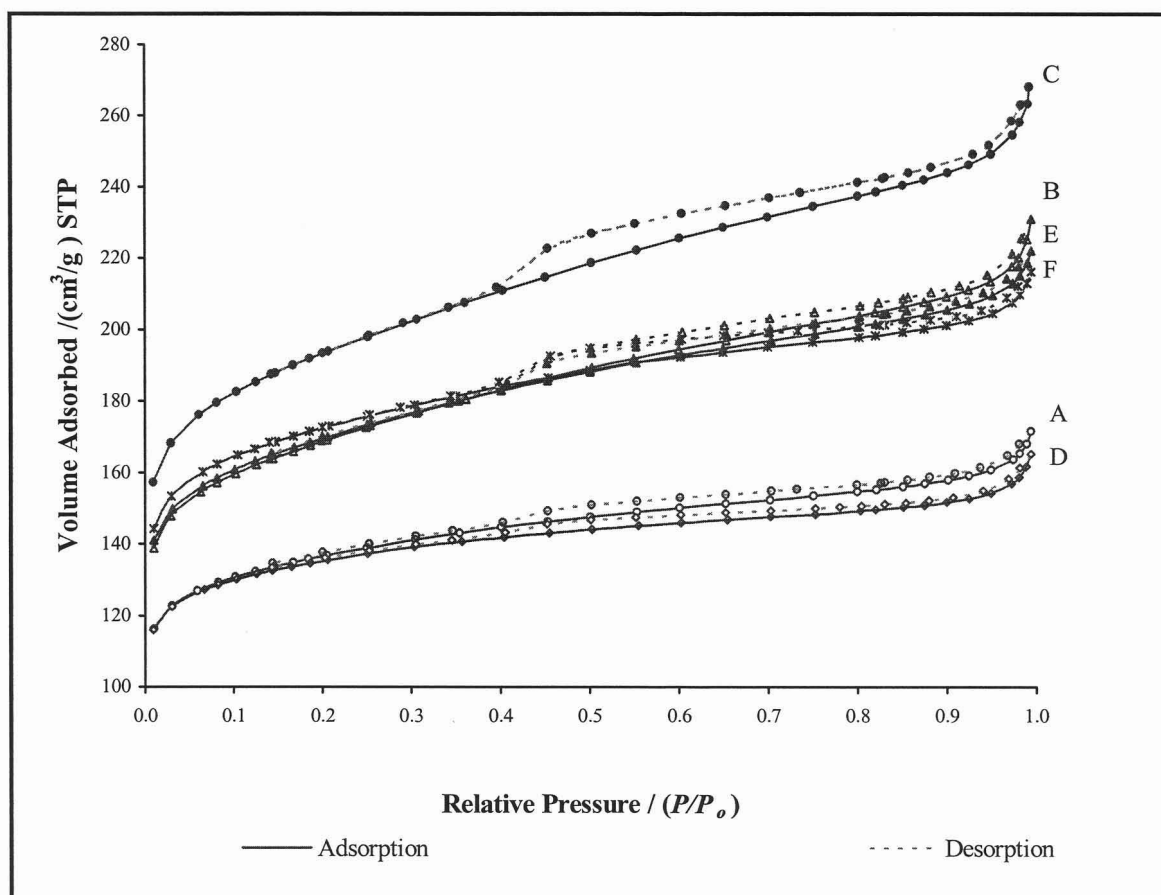
Figure 6.25: Nitrogen Adsorption isotherms at 77 K for activated carbons produced from bagasse at different pyrolysis and activation hold-times. (o)A -pyrolysis time 1hr, activation time 1hr, (△)B - pyrolysis time 1hr, activation time 3hr, (•)C - pyrolysis time 1hr, activation time 4hr, (◇)D -pyrolysis time 2hr, activation time 1hr, (▲)E - pyrolysis time 1hr, activation time 3hr, (✳)F -pyrolysis time 1hr, activation time 1hr

The pronounced hysteresis loop in activated carbon C is also attributed to well-developed porosities. Pyrolysis exposure times of 1 hour for a constant activation time, has a positive impact on the activated carbon produced compared to exposure time of 2hours. The extent of

adsorption increases with increasing activation time as shown by the increase in micro and mesoporosity in the isotherm plots in fig 6.25.

The characteristics of these activated carbons are tabulated in table 6.9. The graphical plots used in evaluating the BET, Langmuir and t-plots presented in table 6.9 are included in fig C-19 to C-21 in Appendix C-2.2.1 and C-2.2.2.

Table 6.9: Characteristics of the powder activated carbons produced from sugar-cane bagasse for a combination of pyrolysis exposure times and activation times

Parameter	Units	Sample					
		A	B	C	D	E	F
Single Point Surface Area	m^2/g	473.59	584.73	669.41	468.17	587.53	596.63
BET Surface Area	m^2/g	462.36	572.45	656.94	454.38	573.98	581.77
Langmuir Surface Area	m^2/g	615.95	768.93	881.51	609.26	771.42	781.29
Micropore Surface Area	m^2/g	329.89	366.40	412.89	337.87	377.52	390.85
External Surface Area	m^2/g	132.48	206.05	244.05	116.52	196.46	190.92
Micropore Area/ Total Area	%	71	64	63	74	67	67
BJH Cumulative Surface Area[1]	m^2/g	89.15	155.70	187.49	75.08	143.99	123.46
BJH Cumulative Surface Area[1]	m^2/g	93.87	170.81	210.07	77.72	156.05	140.87
Mesopore Area/ Total Area	%	20	29	32	17	25	24
Total Pore Volume	cm^3/g	0.2531	0.3367	0.3939	0.2426	0.3295	0.3211
Micropore Volume	cm^3/g	0.1533	0.1708	0.1921	0.1581	0.1763	0.1837
BJH Cumulative Pore Volume[1]	cm^3/g	0.0946	0.1668	0.2005	0.0806	0.1463	0.1234
BJH Cumulative Pore Volume[1]	cm^3/g	0.0945	0.1728	0.2098	0.0802	0.1506	0.1305
V_{meso}/V_{total}	%	37	51	53	33	46	40
Ave Pore Diameter (by BET)	Å	21.89	23.53	23.99	21.36	22.96	22.08
BJH Ave Meso-Diameter[1]	Å	42.45	42.85	42.77	42.92	40.63	39.98
BJH Ave Meso-Diameter[1]	Å	40.44	40.46	39.95	41.29	38.61	37.06
Methylene Blue No	mg MB / g	47.50	96.22	139.71	43.77	96.05	113.37
Iodine No.	mg I_2 / g	596.47	602.98	720.11	587.47	619.03	676.45

-    [1] between 17.0 and 3000.0 Å diameter

Table 6.10 shows that increasing the activation time from 1 to 4 hours at a constant activation temperature results in an increase in surface area and pore volumes for activated carbons (A, B and C) prepared from chars produced at a pyrolysis exposure time of 1 hour. The micropore contribution decreases with a subsequent increase in mesopore contribution due to the widening of micropores to form mesopores. Activating chars prepared at a pyrolysis exposure time of 2 hours at increasing activation times result in an increase in total surface area and micropore

volume of the final activated carbons (E, F and G) However, as the activation time increases from 1 to 3 hours for chars prepared at a pyrolysis exposure time of 2 hours, an increase in external surface area and mesopore volume occurs and further increase in activation time to 4 hours results in a decrease in these properties. This indicates that the maximum activation time has been reached and chars pyrolysed for an exposure time of 2 hours give rise to microporous activated carbons with very little mesopores. Activated carbons prepared by this method fall short in fulfilling the role of sugar carbons.

As the activation time increases, greater burn-off percentages occur as shown in table 6.8, which brings about the increased mesoporosity (reduced microporosity), higher pore volumes and surface areas and larger pore diameters as seen in table 6.9. Furthermore, increasing activation time, also results in greater adsorption capacity and porosity which is evident by the increase in methylene blue and iodine numbers. Comparison of the pyrolysis exposure times revealed that the activated carbons prepared at the pyrolysis exposure time of one hour resulted in much higher methylene and iodine numbers.

From the characteristics listed in table 6.9, carbon C activated for 4 hours and prepared from bagasse chars exposed at the final pyrolysis temperature of one hour have the best properties and could be possible sugar carbons.

The pore size distributions (area and volume) for activated carbons A, B, C, D, E and F are plotted in fig 6.26 to 6.29.

Figure 6.26: Pore volume distribution (dV_{cum}/dD) determined by BJH adsorption for activated carbons produced at different pyrolysis exposure times and varying activation times, A -pyrolysis time 1hr, activation time 1hr, B - pyrolysis time 1hr, activation time 3hr, C - pyrolysis time 1hr, activation time 4hr, D -pyrolysis time 2hr, activation time 1hr, E - pyrolysis time 1hr, activation time 3hr, F -pyrolysis time 1hr, activation time 1hr.
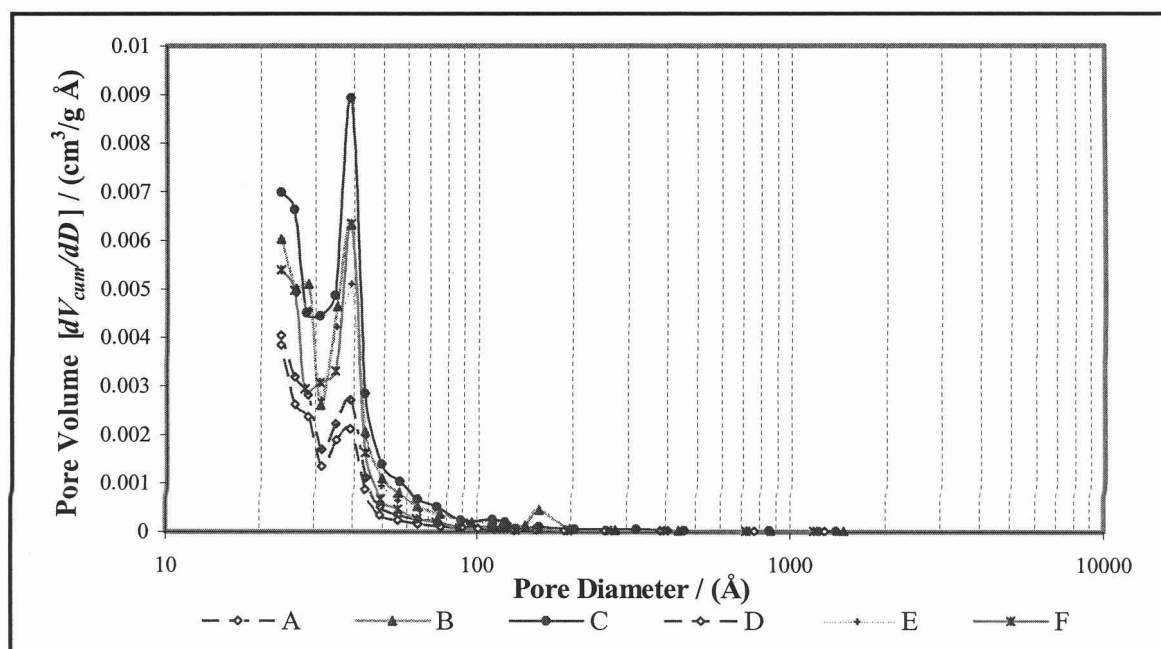
Figure 6.27: Pore volume distribution (dV_{cum}/dD) determined by BJH desorption for activated carbons produced at different pyrolysis exposure times and varying activation times, A -pyrolysis time 1hr, activation time 1hr, B - pyrolysis time 1hr, activation time 3hr, C - pyrolysis time 1hr, activation time 4hr, D -pyrolysis time 2hr, activation time 1hr, E - pyrolysis time 1hr, activation time 3hr, F -pyrolysis time 1hr, activation time 1hr.
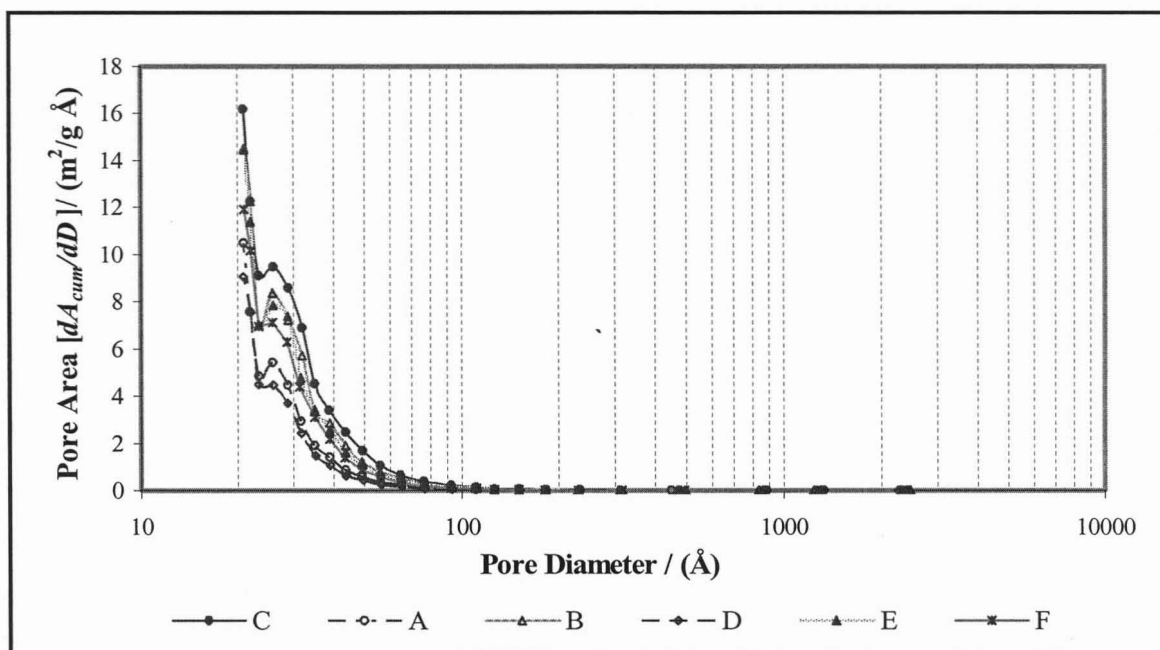
Figure 6.28: Pore area distribution (dA_{cum} /dD) determined by BJH adsorption for activated carbons produced at different pyrolysis exposure times and varying activation times, A -pyrolysis time 1hr, activation time 1hr, B - pyrolysis time 1hr, activation time 3hr, C - pyrolysis time 1hr, activation time 4hr, D -pyrolysis time 2hr, activation time 1hr, E - pyrolysis time 1hr, activation time 3hr, F -pyrolysis time 1hr, activation time 1hr.
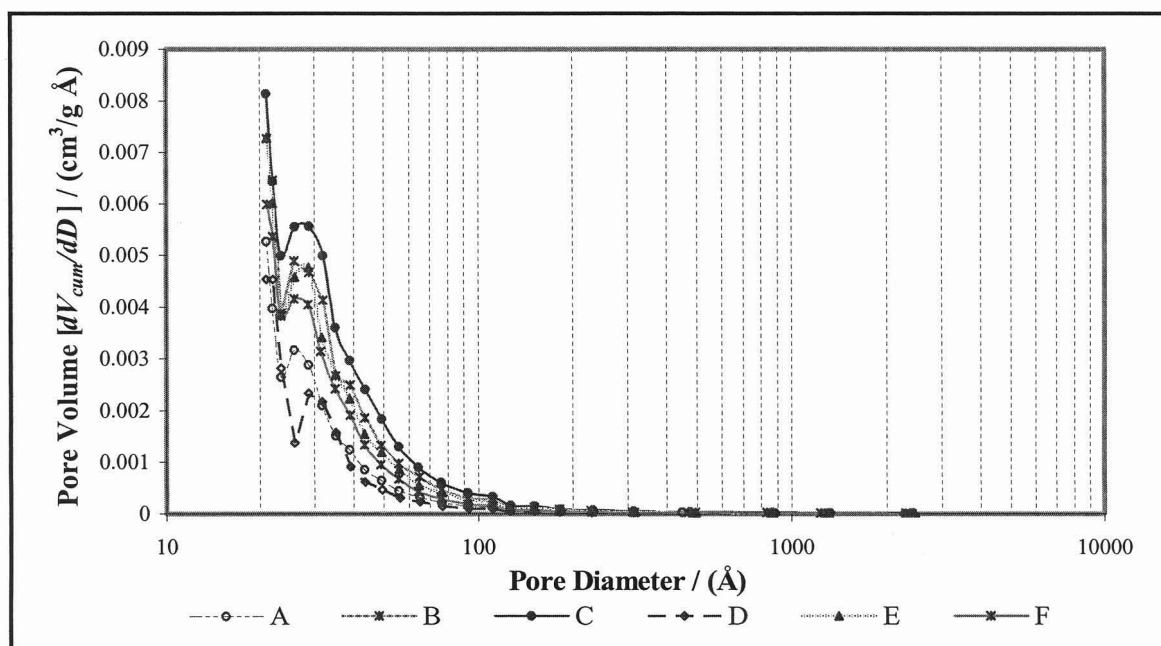

Figure 6.29: Pore area distribution (dA_{cum} /dD) determined by BJH desorption for activated carbons produced at different pyrolysis exposure times and varying activation times, A -pyrolysis time 1hr, activation time 1hr, B - pyrolysis time 1hr, activation time 3hr, C - pyrolysis time 1hr, activation time 4hr, D -pyrolysis time 2hr, activation time 1hr, E - pyrolysis time 1hr, activation time 3hr, F -pyrolysis time 1hr, activation time 1hr.
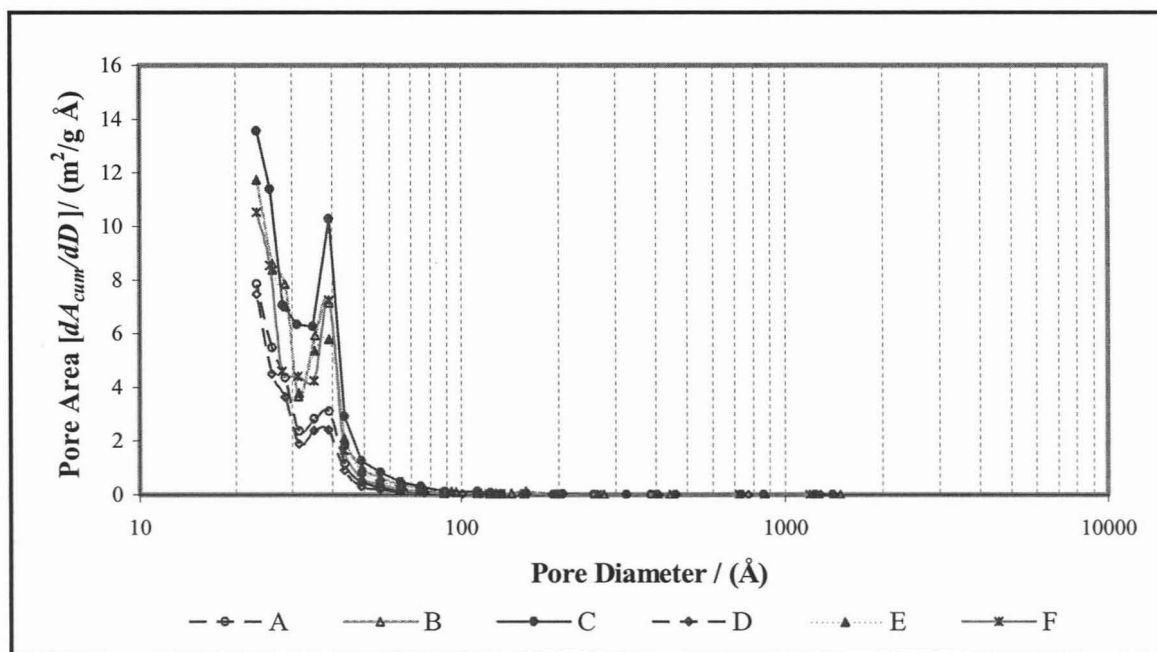
The pore size distribution curves displayed by the BJH adsorption in fig 6.26 and 6.28 indicate that that maximum contribution to total pore volume and area are from pores having diameters around 20 and 30 Å. The BJH desorption curves show that the maximum contribution in the mesopore range results from pores of 40Å in diameter since this method takes into account the layer of thickness left behind on the walls. All plots show similar trends in pore size distribution for carbons A to F.

The pore size distribution of activated carbon C has the highest pore volume and area and the mesopore development is much greater, which further emphasizes the possibility of this carbons capability of adsorbing colour bodies from raw sugar. Thus, chars prepared at a pyrolysis exposure time of one hour and then activated for a longer time produce high surface area carbons with well developed mesoporosites.

The pore volume and area distribution can be plotted in different ways and these are included in figures C-22 to C-29 in Appendix C-2.2.3.

6.3.3. Effect of Activation Temperature

The effect of activating temperature on the properties of bagasse activated carbons was investigated by partially gasifying bagasse chars prepared at the pyrolysis exposure time of 1 hour at 680 ^{O}C, with the a mixture of steam/nitrogen in the ratio of 1:06 and activated at temperatures for an activation time of 4 hours. The experimental process conditions that were used can be seen in table 5.8 in Chapter 5.

The burn-off percentages reached for the different sets of activation temperatures are recorded in table 6.10. For chars activated at 900 ^{O}C, (I), a burn-off percentage of 50% was reached within 2 hours whereas by the end of 4 hours chars activated at lower temperatures (700 and 800 ^{O}C) reached lower burn-off percentages. A mixture of micro and mesopores are usually formed at a burn-off % around 50 – 75 %. The higher the temperature, the faster the reaction rate which leads to a greater activation extent in a shorter space of time.

Table 6.10: Effect of activation temperature on the extent of activation

| Sample | Activation | | Burn-off (%) |
	Hold Time /(hr)	Temperature /(^{O}C)	
I	2	900	50.0
J	4	800	30.0
K	4	700	6.35

The pyrolysis furnace was equipped such that the mass and temperature were also recorded in one second intervals during the activation. A typical mass and temperature profile generated at the activation temperature of 900 ^{O}C generated activated carbon I, is included in figure 6.30. The curves plotted also include the pyrolysis history and the heating up to the final activation temperature.

Fig 6.30 reveals excellent temperature control in the reactor which was provided by the Eurotherm PID controller. The partial gasification reaction at a constant steam/nitrogen ratio of 1:0.6 proceeded initially at a constant rate of 0.2 / min and then decreased to 0.11 /min. This change in rate could be attributed to the burning off the disorganized carbons resulting in increasing microporosity in the initial stages and the diffusion of steam into these micropores, consequently increasing pore sizes by burning of the aromatic ring system which leads to the formation of mesopores. From figure 6.30, it can be seen that the final yield with a 50 % burn-off occurring at the end of 2 hour activation time was 10%. The mass and temperature profiles also provide an indication of the stability of the activation process.
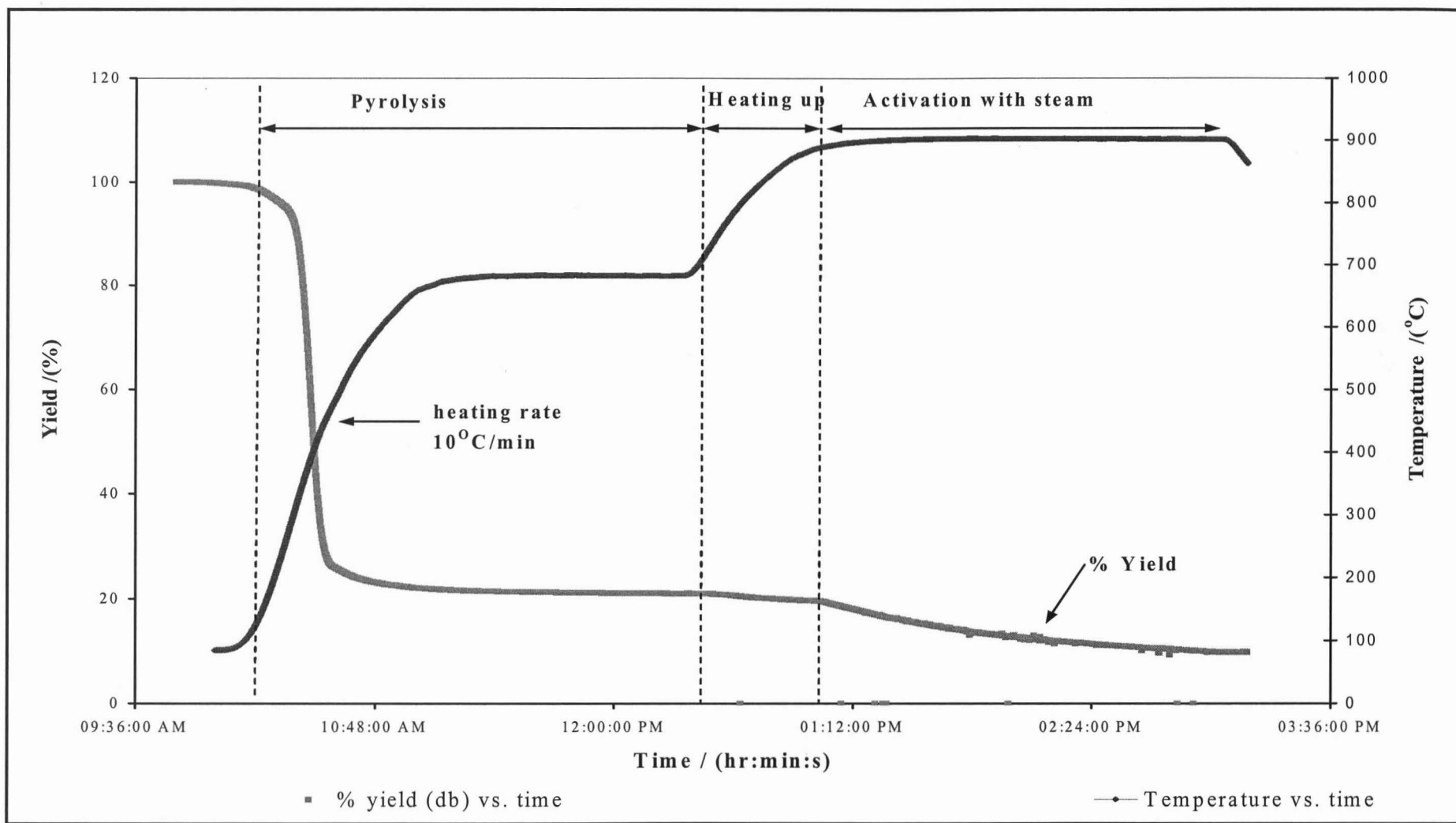
Figure 6.30: Mass and Temperature Profiles for activated carbons produced at 900 °C and 2 hour with steam as the activating agent [Devnarain *et al*, 2002].

The characteristics of the surface area and pore development in activated carbons I, J and K produced at different activation temperatures were evaluated by nitrogen adsorption at 77 K. The nitrogen adsorption isotherms for carbons I, J and K are given in fig 6.31.
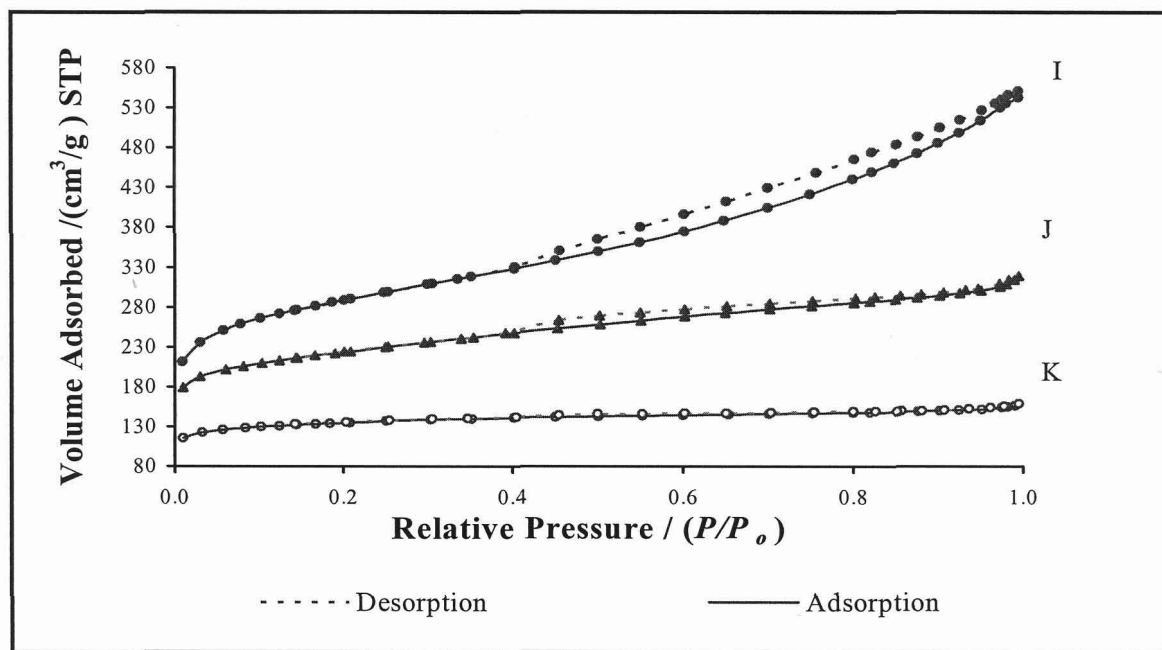
Figure 6.31: Nitrogen adsorption isotherms of carbons produced at different activation temperatures with steam as the activating agent, (●)I – 900 °C, 2hr, (▲)J – 800 °C, 4hr & (o)K – 700 °C, 4hr.

Activated carbon K activated at 700 °C resembles a Type I isotherm in the BDDT classification [Brunauer *et al*, 1940]. This carbon appears to consist mainly of micropores. The reversible adsorption and desorption trend of Type I isotherms is evident in this particular activated carbon. Carbon I produced at 900 °C closely resembles a Type IV isotherm in the BDDT classification consisting of both micro and mesopores. The microporous feature is depicted by the reversible sorption shown by the nitrogen isotherm. At higher relative pressures a rapid increase in the slope of the isotherm and the pronounced hysteresis loop common to well developed, mesoporous adsorbents are observed for activated carbon I. According to Gregg and Sing [1982] the pore widening of microporous apertures is shown by the reduction in low pressure hysteresis which shown is evident in activated I and J. Activated carbon, J, produced at the temperature of 800 °C also resembles a Type IV isotherm having micro and mesopores present but porosities are much lower than that shown for I. The uptake of nitrogen is much greater in carbon I than the other two activated carbons prepared at lower temperatures indicating greater surface area and higher porosities are produced by the increase in extent of activation brought about increasing temperature.

The properties of activated carbons I, J and K are quantified and compared in table 6.11. By applying the procedures discussed in chapter 4, graphical plots (included in figures C-30 to C-40 in Appendix C-2.3) were used to obtain the surface areas and pore areas and volumes listed in table 6.11.

Table 6.11: Characteristics of the powder activated carbons produced from sugar-cane at different activation temperatures

Parameter	Units	Sample			Method Used
		I	J	K	
Total Surface Area	m^2/g	1000.08	773.41	466.43	Single point
Total Surface Area	m^2/g	995.38	760.95	455.27	BET
Total Surface Area	m^2/g	1345.39	1026.34	606.29	Langmuir
Micropore Surface Area	m^2/g	479.19	445.16	338.52	t-plot
External Surface Area	m^2/g	516.19	315.80	116.75	t-plot
Cumulative Surface Area	m^2/g	462.65	253.40	71.47	BJH Adsorption[1]
Cumulative Surface Area	m^2/g	517.37	280.14	73.21	BJH Desorption[1]
Total Pore Volume[2]	cm^3/g	0.8199	0.4729	0.2379	Single point
Micropore Volume	cm^3/g	0.2207	0.2075	0.1574	t-plot
V_{micro}/V_{total}	%	28	43	66	
Cumulative Pore Volume	cm^3/g	0.6049	0.2624	0.0692	BJH Adsorption[1]
Cumulative Pore Volume	cm^3/g	0.6419	0.2730	0.0683	BJH Desorption[1]
V_{meso}/V_{total}	%	78	58	29	
Ave Micropore Diameter	Å	32.95	24.86	20.90	Single point / BET
Ave Meso-Diameter	Å	52.30	41.42	38.72	BJH Adsorption[1]
Ave Meso-Diameter	Å	49.62	38.98	38.31	BJH Desorption[1]
Methylene Blue No	mg MB / g	256	162.	37	Aktasorb Systems
Iodine No.	mg I_2 / g	992	824	538	ASTM method
Ash	%	28	12	9	

- [1] between 17.0 and 3000.0 Å diameter

The total surface area and pore volumes increase with increasing activation temperature. As temperature increases, the micropore volume decreases with a subsequent increase in mesopore volume. Activated carbon J has an equal distribution in pore volume between micro and mesopores indicating high adsorption potential for molecules of both sizes. The distribution of pore volume by mesopores are about twice that of the micropores in activated carbon I, pointing out that the structure of this carbon can be classified as a mesoporous carbon. Its affinity for mesoporous molecules is demonstrated by its high methylene blue number. The iodine number

for this carbon can be considered to have a one to one correlation with BET surface area. Although a mesoporous activated carbon, carbon I does in fact have a larger amount of micropores and is confirmed by the high iodine number. Therefore adsorption of molecules in the micro and mesopore range is high.

Comparing carbon K produced at 700 °C to that of carbon I reveals that at higher activation temperature the surface area is twice that of the lower temperature. Carbon K can be classified as a microporous carbon and can be considered as unacceptable sugar decolourising carbons.

As activation temperature increases, an increase in burn-off occurs and the final activated carbon ash % increases as shown in table 6.11 which corresponds to discussions by Bansal *et al* [1988].

At this stage bagasse chars activated at 900 °C for 2 hours seem to possess the desirable properties required for sugar decolourisation as depicted by their characteristics in table 6.13 and is confirmed with decolourisation tests in the subsequent sections of this chapter.

The pore size distribution in terms of pore volume and area for activated carbons, I, J and K are shown in figures 6.32 to 6.35.

Figure 6.32: Pore volume distribution (dV_{cum} /dD) determined by BJH adsorption for activated carbons produced at different activation temperatures with steam as the activating agent, I – 900 ^{O}C, 2hr, J – 800 ^{O}C, 4hr & K – 700 ^{O}C, 4hr.
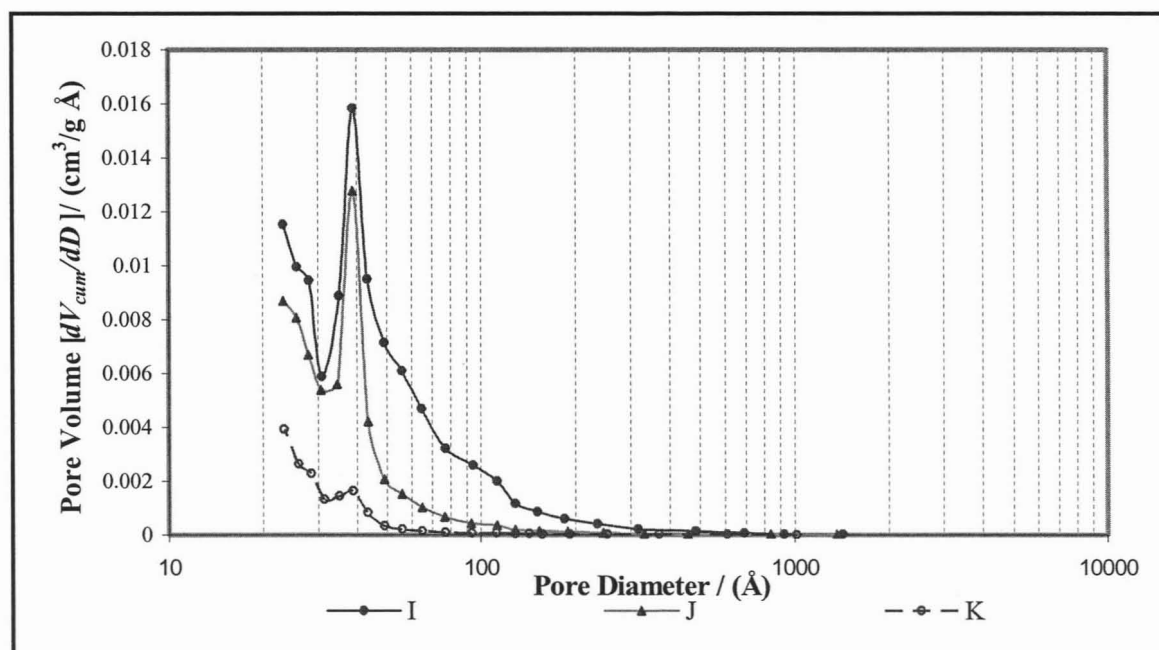
Figure 6.33: Pore volume distribution (dV_{cum} /dD) determined by BJH desorption for activated carbons produced at different activation temperatures with steam as the activating agent, I – 900 ^{O}C, 2hr, J – 800 ^{O}C, 4hr & K – 700 ^{O}C, 4hr.

Figure 6.34: Pore area distribution (dA_{cum} /dD) determined by BJH adsorption for activated carbons produced at different activation temperatures with steam as the activating agent, I – 900 ^{O}C, 2hr, J – 800 ^{O}C, 4hr & K – 700 ^{O}C, 4hr.
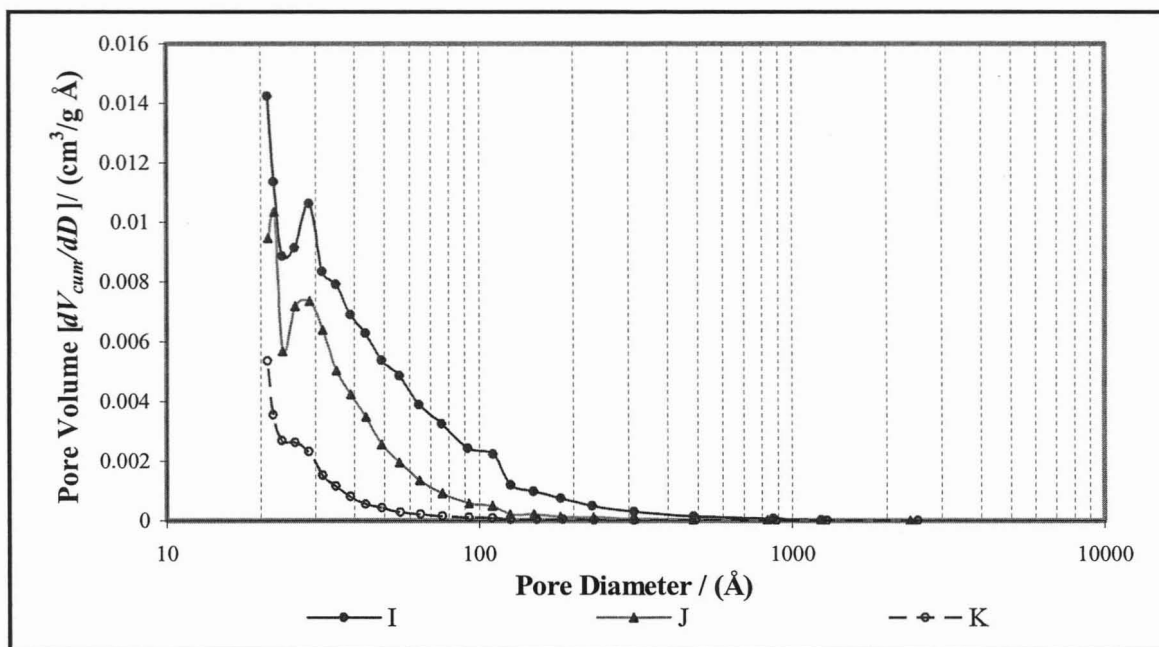

Figure 6.35: Pore Area distribution (dA_{cum} /dD) determined by BJH desorption for activated carbons produced at different activation temperatures with steam as the activating agent, I – 900 ^{O}C, 2hr, J – 800 ^{O}C, 4hr & K – 700 ^{O}C, 4hr.
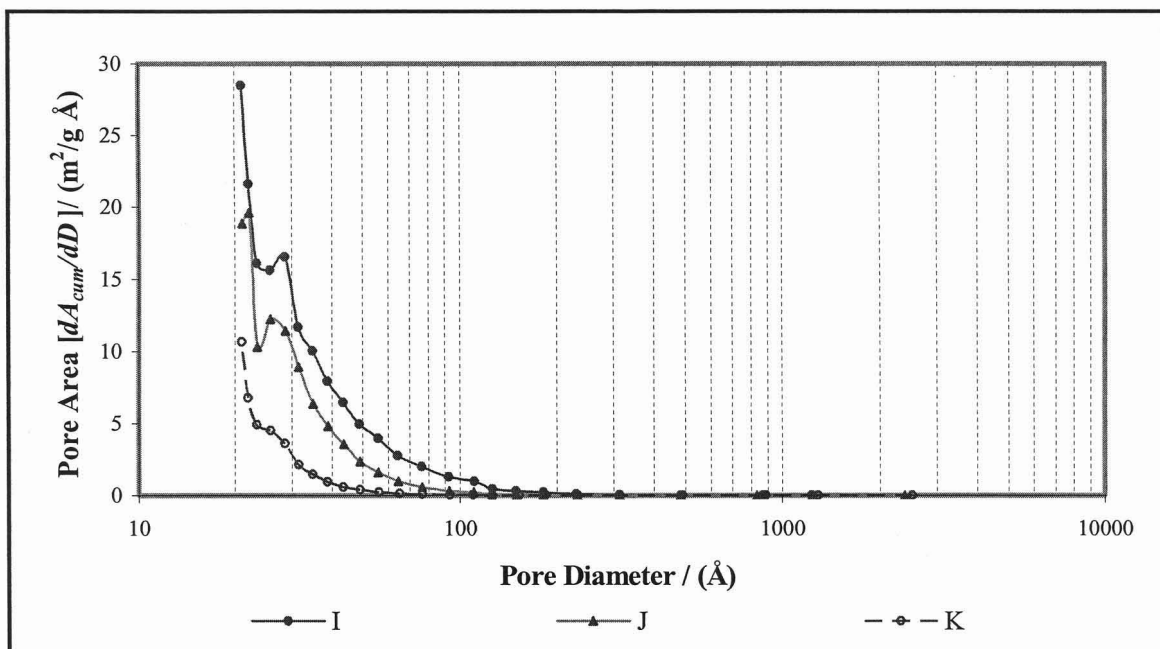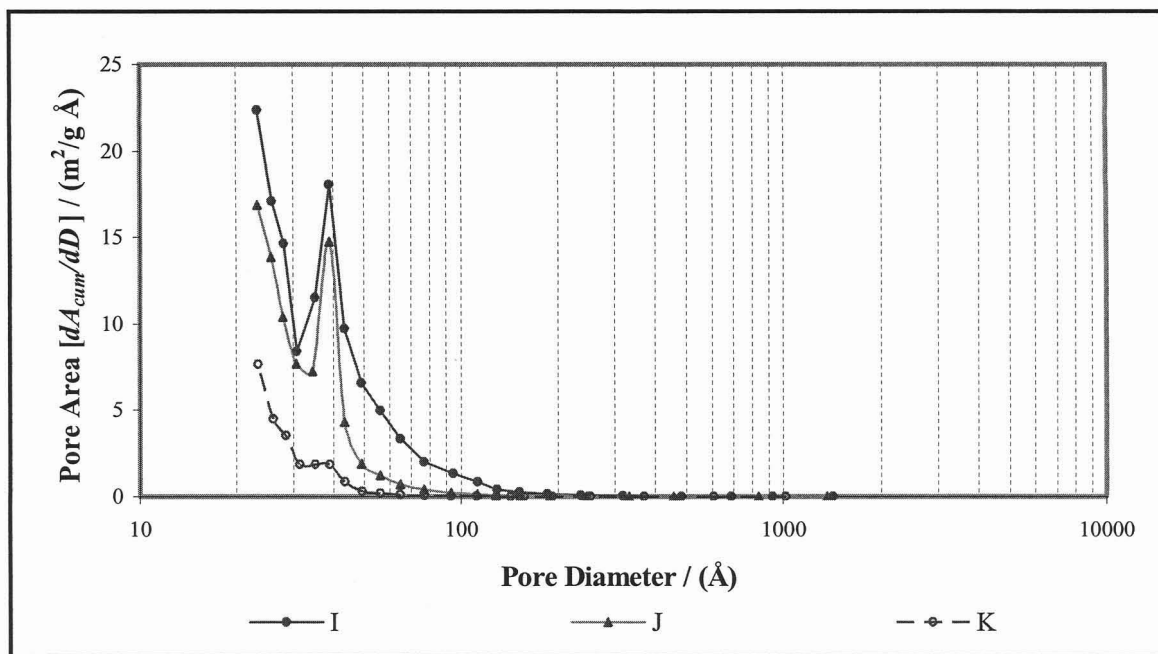
For the adsorption case maximum peaks are observed in the micropore range of 20 Å and smaller peaks around 30Å. Figures 6.33 and 6.35 reveal that activated carbon I has greater pore

volume and area contribution by pores in the ranging from 30 to 100Å. This same effect is shown by all activated carbons in the distribution plots in fig 6.33 and 6.35. However, the maximum peak at 40Å shows the highest contribution of pore volume and area occurring from the mesopore region in the desorption distribution plots. The trend in the pore size distribution plot is the same for all activated carbons I, J and K, but activated carbon I has the highest pore volume and area, and a much wider pore range. The size distribution of activated carbon, I, is comparable to that of a typical sugar cane carbon pore size distribution presented in chapter 5.

6.3.4 Comparison of South African Bagasse Activated Carbons with Commercial Carbons

Granular activated carbons were also produced by using refined sugar as a binder. The processing methods were similar to those produced for powder activated carbons but the activation time was increased to 2.5 hours in order to obtain the same burn-off %. Table 5.9 in chapter 5 provides information on the final processing conditions that were used to prepare powder activated carbons and granular activated carbons from sugar-cane bagasse based on the results of experiments investigated above. Table 6.12 includes the extent of activation for these activated carbons.

Table 6.12: Extent of activation achieved during preparation of powder and granular activated carbons from sugar-cane bagasse.

Sample	Binder	Binder/Bagasse ratio	Activation Time /(hr)	Burn Off / (%)
I	None	0	2	50
O	None	0	2	50
P	Sugar	0.5:1.0	2.5	50

A longer time was required to obtain the same burn-off % with bagasse bound with refined sugar than without a binder. This could be attributed to the reaction with dense and large particle chars produced from pyrolysis, thereby limiting the diffusion of steam into the micropores of the carbon skeleton.

Activated carbons were also prepared from high ash sugar-cane bagasse (O) and their effect on the final activated carbon was also investigated. A comparison between low and high ash powder bagasse activated carbons, granular bagasse activated carbons and a granular standard Chemviron Cane Cal (coal parent material, patented activation) carbon were performed. The nitrogen adsorption isotherms for these carbons are presented in fig 6.36.
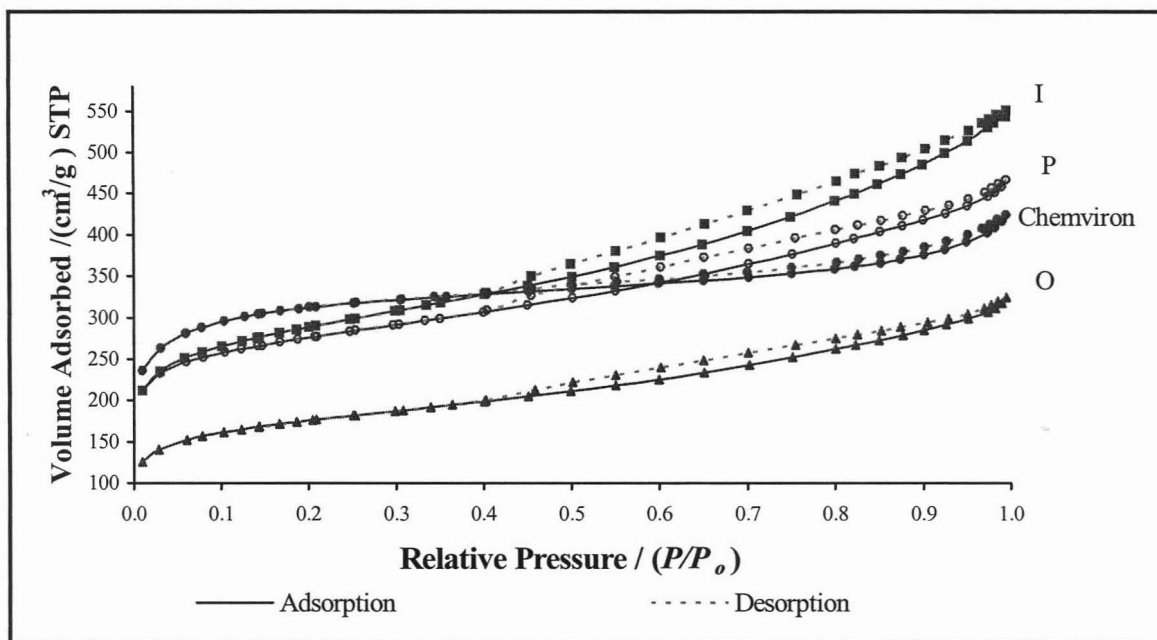
Figure 6.36: Nitrogen adsorption isotherms of bagasse activated carbons; (▲) O – 56% ash, powder, (o) P – granular sugar/bagasse, (■) I – 28% ash, powder and a standard granular Chemviron CaneCal carbon (●),

Bagasse carbons all resemble type IV isotherms in the BDDT classification [Brunauer *et al*, 1940]. Increasing slopes and the pronounced desorption hysteresis loops indicate that these carbons have high mesoporosity. The low uptake of nitrogen at low relative pressures for carbon (O) suggests activated diffusion occurs. All carbons display reversible sorption isotherms at low relative pressures. The standard Chemviron Canecal carbon also seems to resemble a Type IV isotherm but it's desorption hysteresis loop is not as pronounced as those presented by the bagasse carbons. The highest adsorption of nitrogen occurs with activated carbon I which is a low ash bagasse carbon. However, the initial uptake of nitrogen at low relative pressures is less than the Chemviron carbon. High ash bagasse activated carbon O isotherms suggest that the micro and mesoporosity is far less than that observed for the other carbons. Activated carbons I and P adsorption isotherms suggests that these carbons have greater mesoporosity but lower microposity compared to the standard Chemviron Canecal.

The characteristics of these carbons are quantified in table 6.13. The BET, Langmuir, t-plots and the pore area and volume plots used to calculate the values presented in table 6.15 can be seen in fig C-41 to C-51 in Appendix C-5.

Table 6.13: Comparison of powder and granular bagasse activated carbons and a standard Chemviron Canecal carbon [Devnarain *et al*, 2002]

Parameter	Units	Sample				Method Used
		I	O	P	Chemviron CaneCal	
Total Surface Area	m^2/g	1000.08	607.81	954.78	1077.60	Single point
Total Surface Area	m^2/g	995.38	606.22	942.34	1063.62	BET
Total Surface Area	m^2/g	1345.39	823.49	1273.46	1429.42	Langmuir
Micropore Surface Area	m^2/g	479.19	281.83	529.54	733.80	t-plot
Micro Area/ Total Area	%	48	47	56	69	
External Surface Area	m^2/g	516.19	324.38	412.79	329.82	t-plot
Cumulative Surface Area	m^2/g	462.65	274.10	357.73	204.35	BJH Adsorption[1]
Cumulative Surface Area	m^2/g	517.37	307.62	404.27	223.68	BJH Desorption[1]
Total Pore Volume	cm^3/g	0.8199	0.4747	0.6900	0.6200	Single point
Micropore Volume	cm^3/g	0.2207	0.1295	0.2462	0.3343	t-plot
V_{micro}/V_{total}	%	27	27	36	54	
Cumulative Pore Volume	cm^3/g	0.6049	0.3551	0.4579	0.2674	BJH Adsorption[1]
Cumulative Pore Volume	cm^3/g	0.6419	0.3698	0.4780	0.2752	BJH Desorption[1]
V_{meso}/V_{total}		78	78	69	44	
Ave Micropore Diameter	Å	32.95	31.32	29.29	23.41	Single point / BET
Ave Meso-Diameter	Å	52.30	51.83	51.20	52.29	BJH Adsorption[1]
Ave Meso-Diameter	Å	49.62	48.08	47.30	49.21	BJH Desorption[1]
Methylene Blue No	mg MB / g	256	174	250	242	Aktasorb Systems
Iodine No.	mg I_2 / g	992	671	1096	1000	ASTM method
Molasses No.		701	327	607	230	
Ash	%	28	56	14	13	

-   [1] between 17.0 and 3000.0 Å diameter

The standard Chemviron Canecal possessed the greatest surface area which is attributed the highest concentration of micropores in its structure. Irrespective of their ash contents, powder bagasse activated carbons (I and O) prepared by the same process method have the same percentage of micropore and mesopore area and volumes. However, in terms of quantities the high ash bagasse values are much lower. This can be attributed to the ash content in the sample that blocks pores and them inaccessible thus rendering lower values. The possibility of adding a

de-ashing step prior to pyrolysis may be necessary when ash levels become too high. The granular bagasse activated carbon (P) is also a very high surface area carbon with well developed porosities but contain slightly lower percentage of mesopores. The highest methylene blue numbers are found for the low ash prepared activated carbons (I) revealing its potential to adsorb molecules in the same size range as the methylene blue molecule. The granular sugar/bagasse carbons (P) have the greatest iodine number and display its ability to adsorb smaller molecules. The prepared powder and granular bagasse carbons exhibit higher molasses number than the standard carbon. This value indicates the bagasse carbons contain larger amount of meso and macropores and are therby able to adsorb large colour bodies present in molasses solution. This has been reflected in the increased values for BJH surface area and pore volumes in table 6.13. The higher ash carbon gave similar molasses value to the standard carbon. The molasses number is an initial indicator of the carbon's ability to decolourise raw sugar.

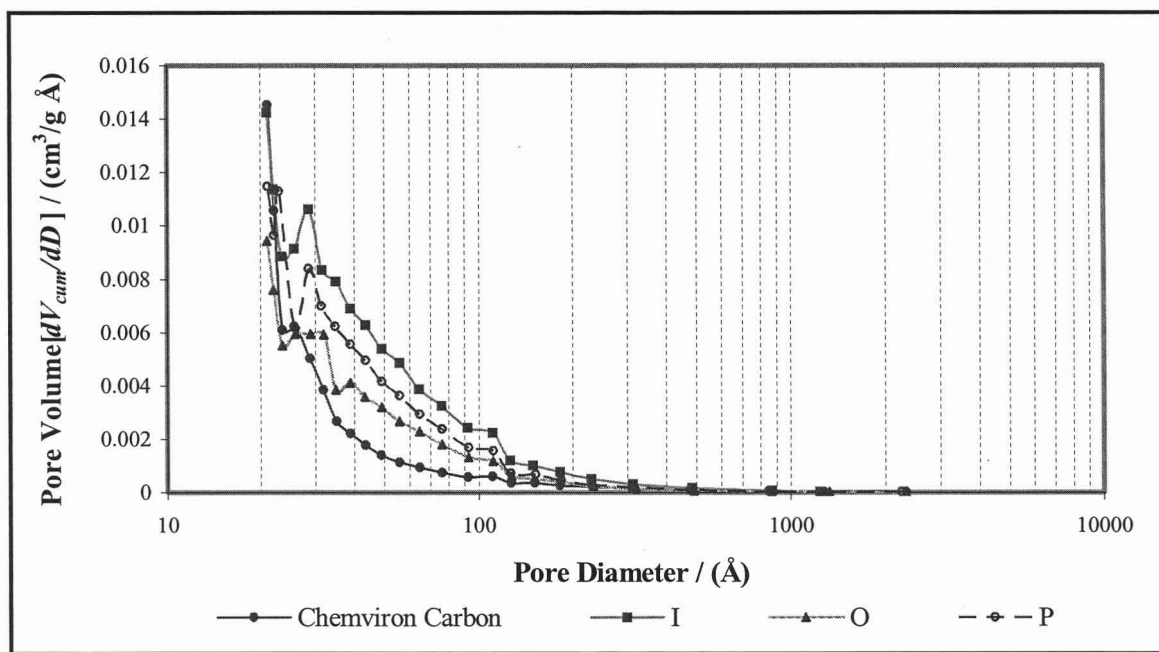The pore size distributions of these carbons in terms of pore area and volume are compared in fig 6.37 to 6.40.

Figure 6.37: Pore volume distribution (dV_{cum}/dD) determined by BJH adsorption of bagasse activated carbons; (▲) O – 56% ash, powder, (○) P – granular sugar/bagasse, (■) I – 28% ash, powder and a standard granular Chemviron CaneCal carbon(●).
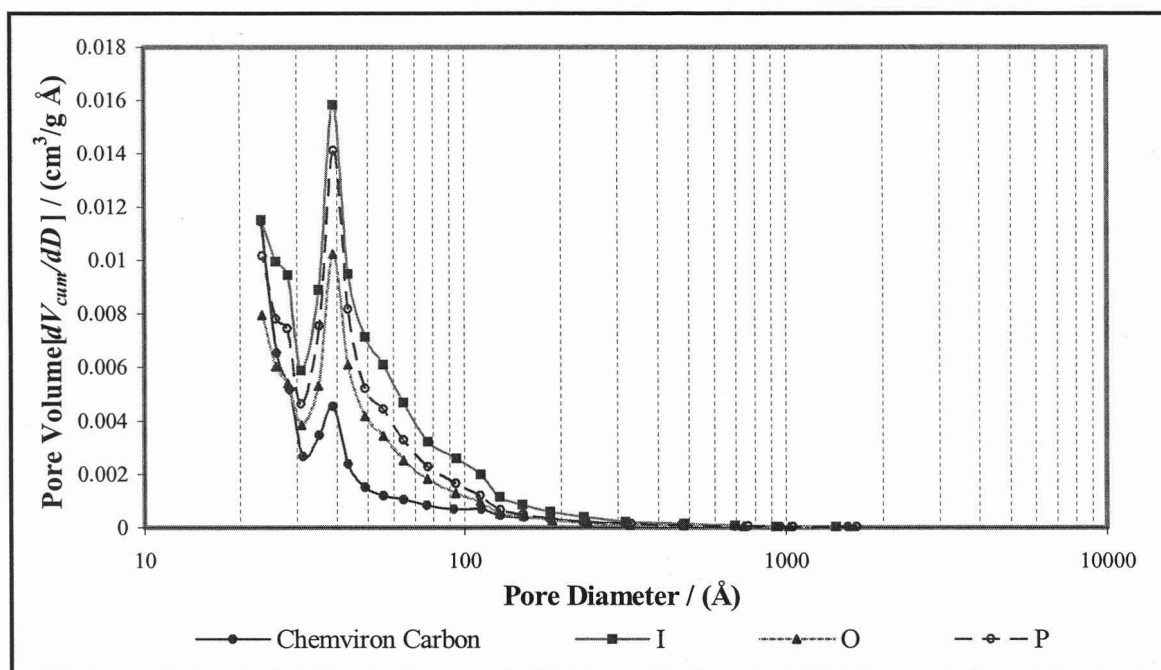
Figure 6.38: Pore volume distribution (dV_{cum}/dD) determined by BJH desorption of bagasse activated carbons; (▲) O – 56% ash, powder,(○) P – granular sugar/bagasse, (■) I – 28% ash, powder and a standard granular Chemviron CaneCal carbon(●).

Figure 6.39: Pore area distribution (dA_{cum}/dD) determined by BJH adsorption of bagasse activated carbons; (▲) O – 56% ash, powder, (○) P – granular sugar/bagasse, (■) I – 28% ash, powder and a standard granular Chemviron CaneCal carbon (●).

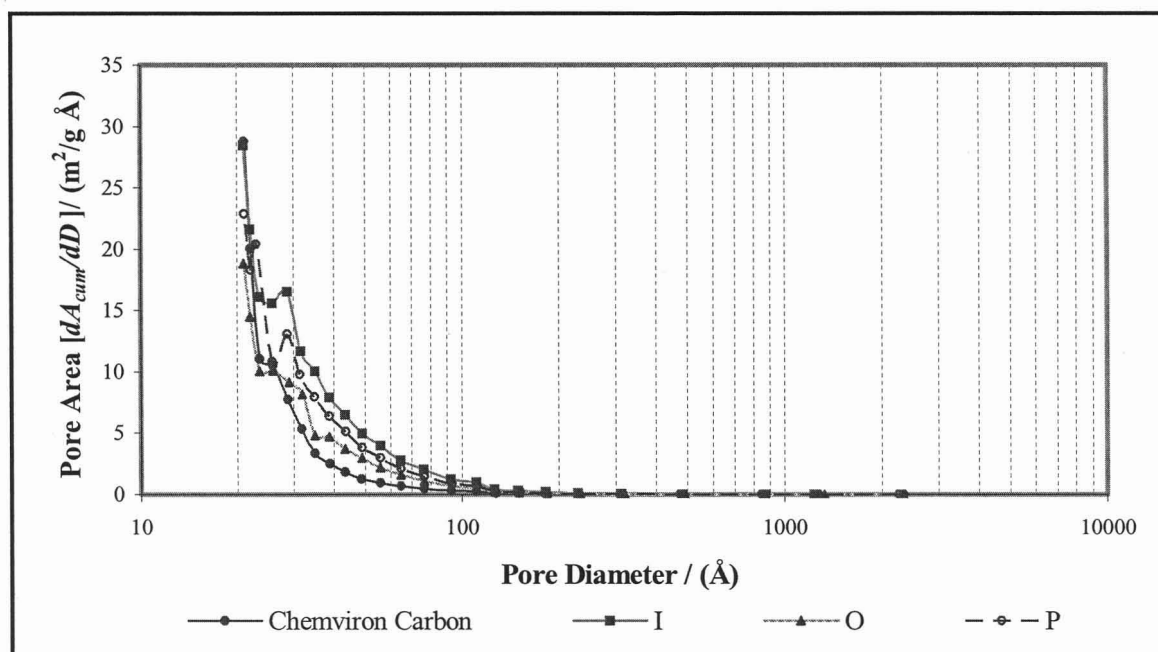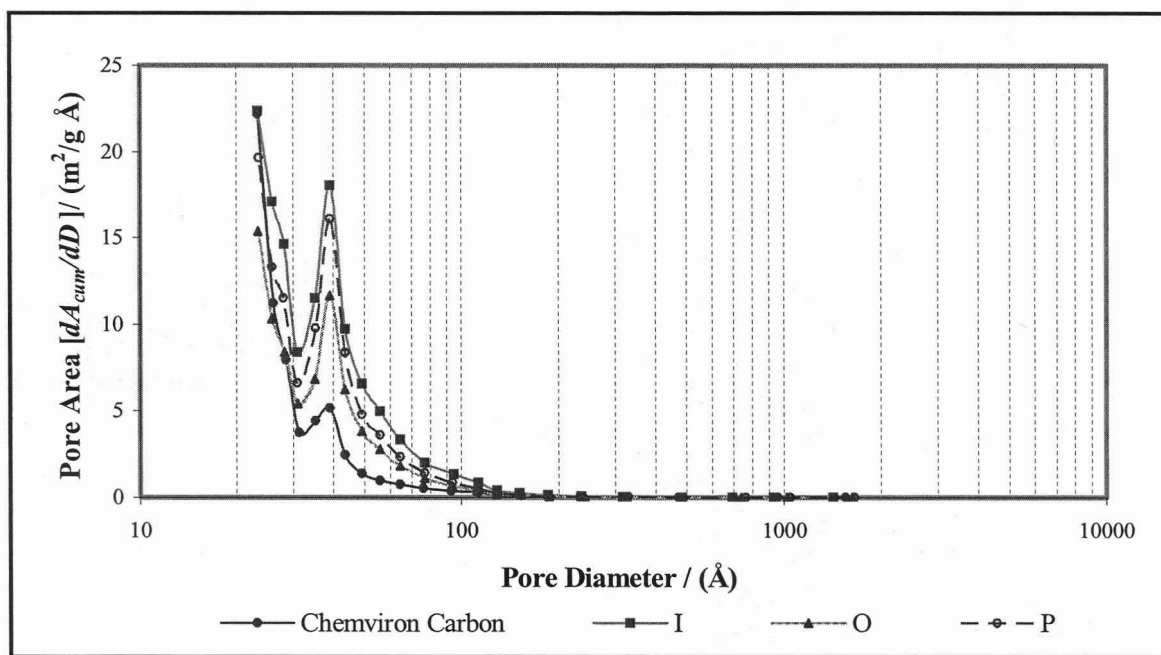**Figure 6.40: Pore area distribution (*dA_cum* /dD) determined by BJH desorption of bagasse activated carbons; (▲) O – 56% ash, powder,(○) P – granular sugar/bagasse, (■) I – 28% ash, powder and a standard granular Chemviron CaneCal carbon(●).**

The pore size distributions by the BJH adsorption methods (fig 6.37 and 6.39) reveal that the highest pore volume and area contribution are from pores of size 23 and 30Å. However, their desorption pore size distributions (fig 3.8 and 3.40) indicate that pore of 40Å in diameter contribution to pore volume and area is highest. The pore size distribution curves follow the same trend, but activated carbon I, has the largest pore size distribution with meso and macropores contributing largely to pore volume and external surface area. These pore size distribution curves further emphasizes the ability of the prepared powder and granular activated carbons to adsorb large colour bodies present raw sugar solutions. The bagasse activated carbon's porous structure in displayed in the above figures proves to be much more superior than the standard Chemviron Canecal carbon.

Scanning electron micrographs were also taken for the prepared low ash powder and granular bagasse activated carbons I and P, and the Chemviron carbon which are presented in figures 6.41 to 6.43.
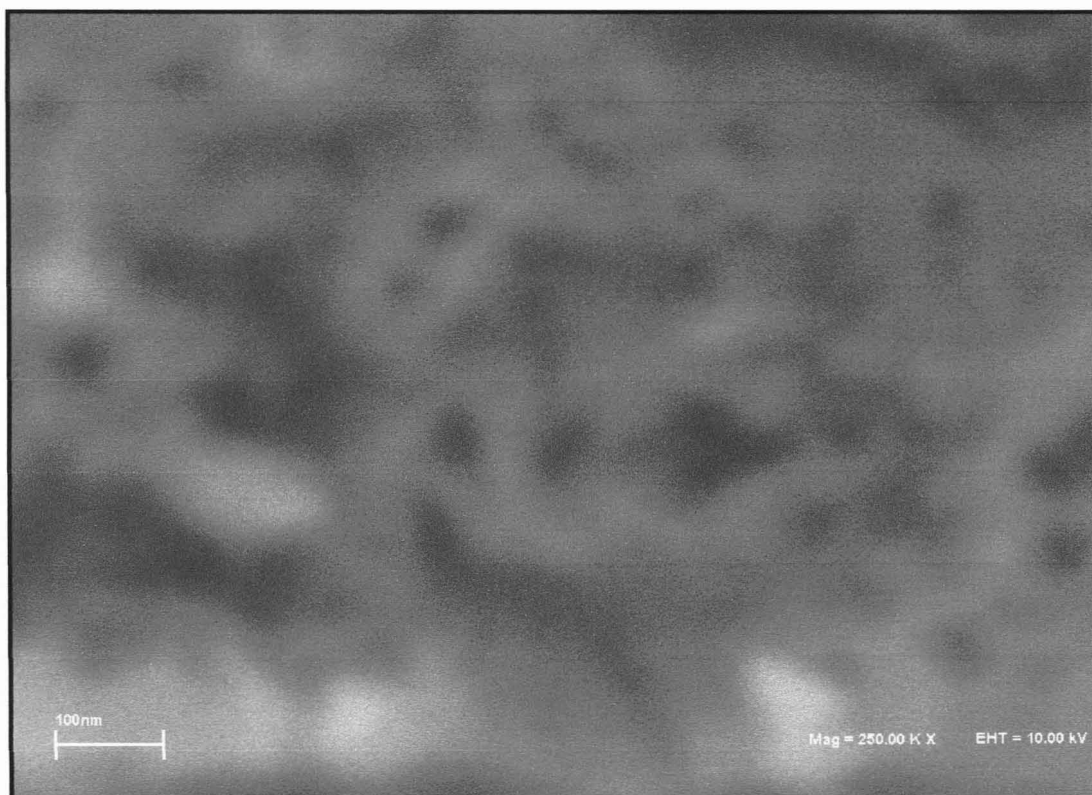
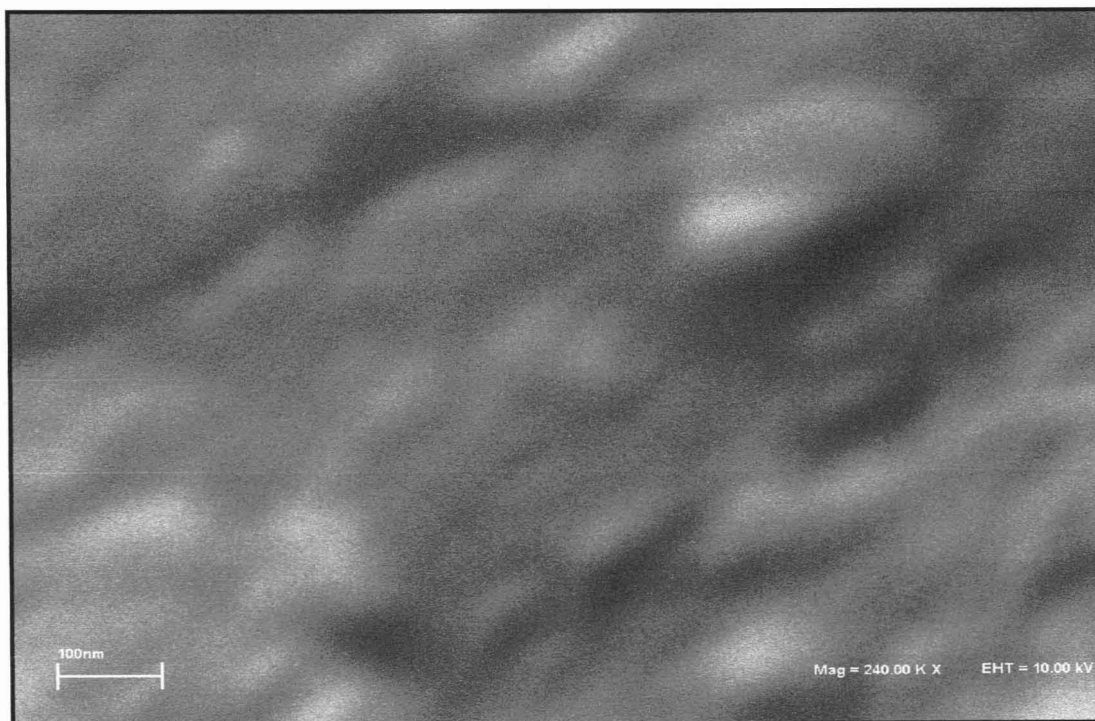**Figure 6.41: Scanning electron micrograph of low ash powder bagasse activated carbon, I.**

Figure 6.42: Scanning electron micrograph of granular sugar/ bagasse activated carbon, P.

Figure 6.43: Scanning electron micrograph of commercial Chemviron CaneCal activated carbon.

High surface area and porosity can be seen in all scanning electron micrographs. Macroporous openings are observed for prepared low ash activated carbons indicating their ability to capture large molecules as proved by their molasses test. These pores also act as transport pores directing smaller molecules to be adsorbed into their internal micro and mesopore structure. These electron micrographs provide evidence of the porous nature of the prepared activated carbon's exterior.

6.4 Decolourisation of sugar solutions

The potential of the prepared powder and granular powder activated carbons from sugar cane bagasse and reference carbons, to decolourise raw sugar were tested on a batch scale. The procedure followed is described in chapter 5.

The activated carbons have a very high decolourising potential as shown by their isotherms in figure 6.44.
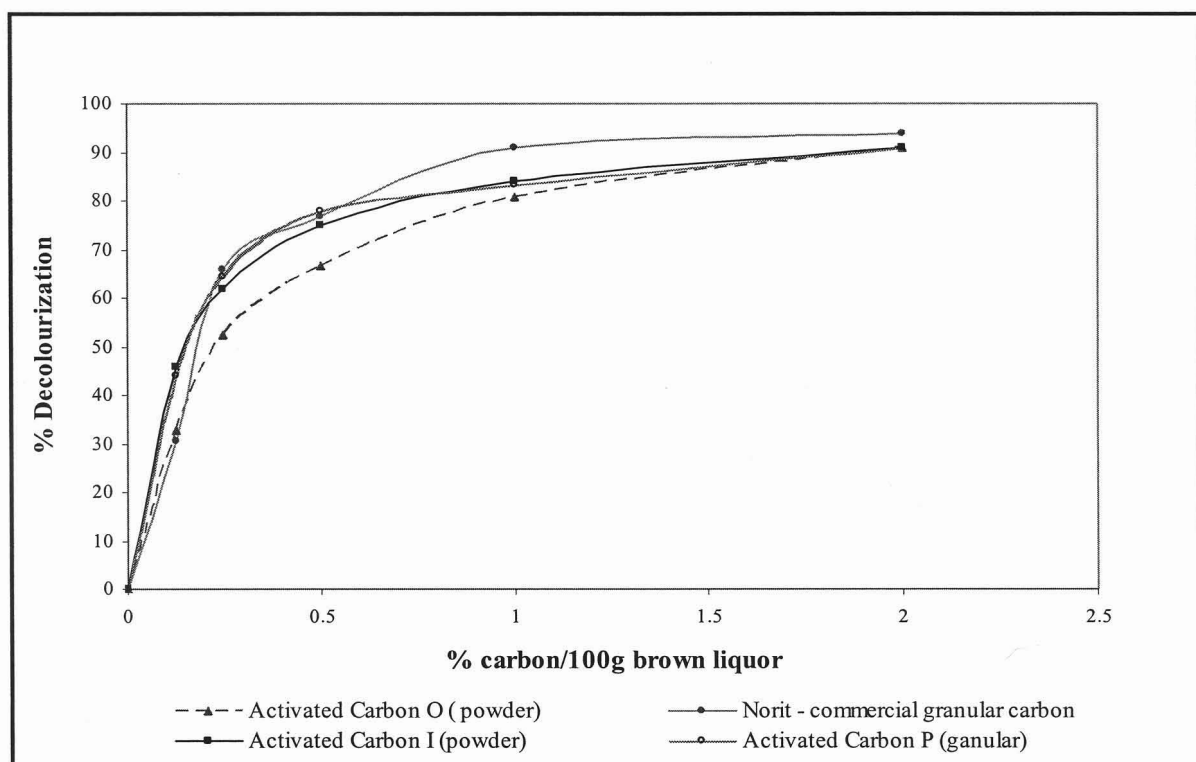
Figure 6.44: Decolourisation isotherms of prepared powder and granular South African bagasse carbons, (▲) O – 56% ash, powder,(○) P – granular sugar/bagasse, (■) I – 28% ash, powder and commercial Norit PN2 carbon (●) [Devnarain, *et al*, 2002].

The commercial carbons (Chemviron CaneCal and powder Norit PN2) were tested in parallel with the prepared carbons, but problems were experienced with the Chemviron CaneCal carbon and are not presented. Both the low ash powder and granular activated carbons are excellent sugar decolourisers and compare extremely well with the commercial Norit PN2 carbon. Even the high ash bagasse carbon's decolourising potential is high. Approximately 80% colour removal was achieved by using 0.5g carbon /100 Brix brown liquor coinciding with the value obtained for the commercial Norit PN2 carbon. Tests were also carried out by using activated carbons in acidic and basic brown sugar solutions to determine the effect on decolourisation by the carbons. Figures 6.45 and 6.46 show the decolourisation potential of all activated carbons contacted in acidic and basic solutions.
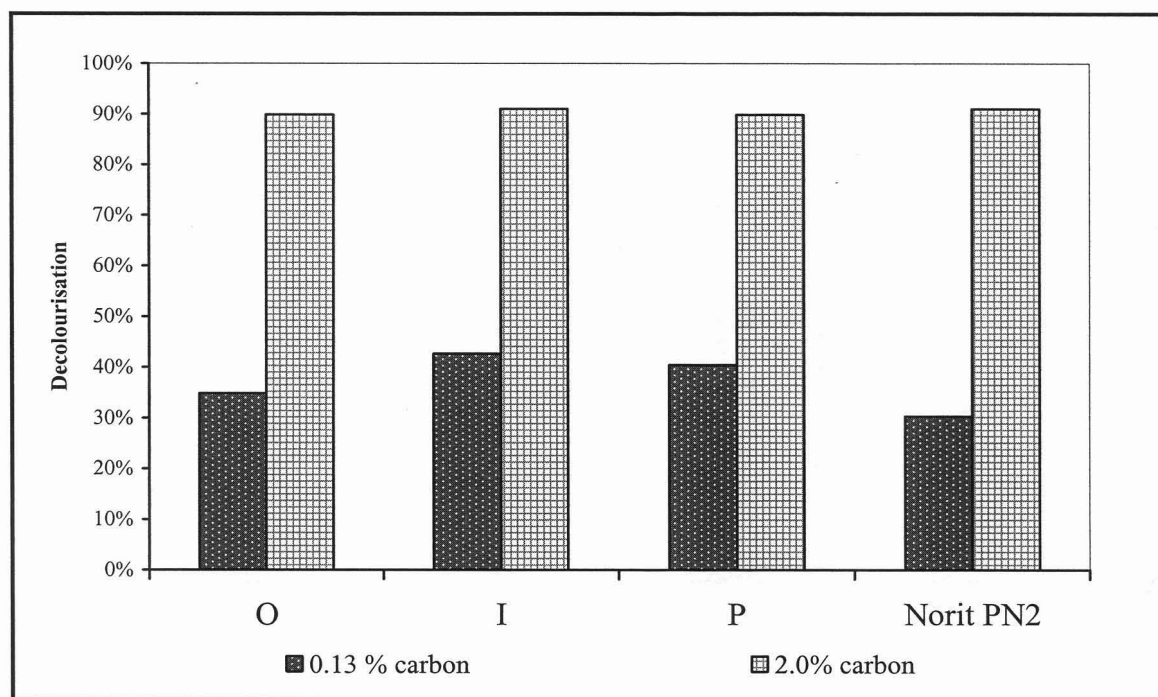
Figure 6.45: Brown Liquor decolourisation at pH 2 with prepared powder and granular South African bagasse carbons, O – 56% ash, powder, P – granular sugar/bagasse, I – 28% ash, powder and commercial Norit PN2 carbon .

Acidic solutions treated with 0.13% activated carbons removed approximately 40-50% colour with the low ash bagasse carbon and granular carbon showing the greatest decolourising percentage of 50%. Acidic solutions treated with 2 % carbon removed 80% colour from the brown liquor for all carbons. Again the prepared carbons are comparable with the commercial carbon.
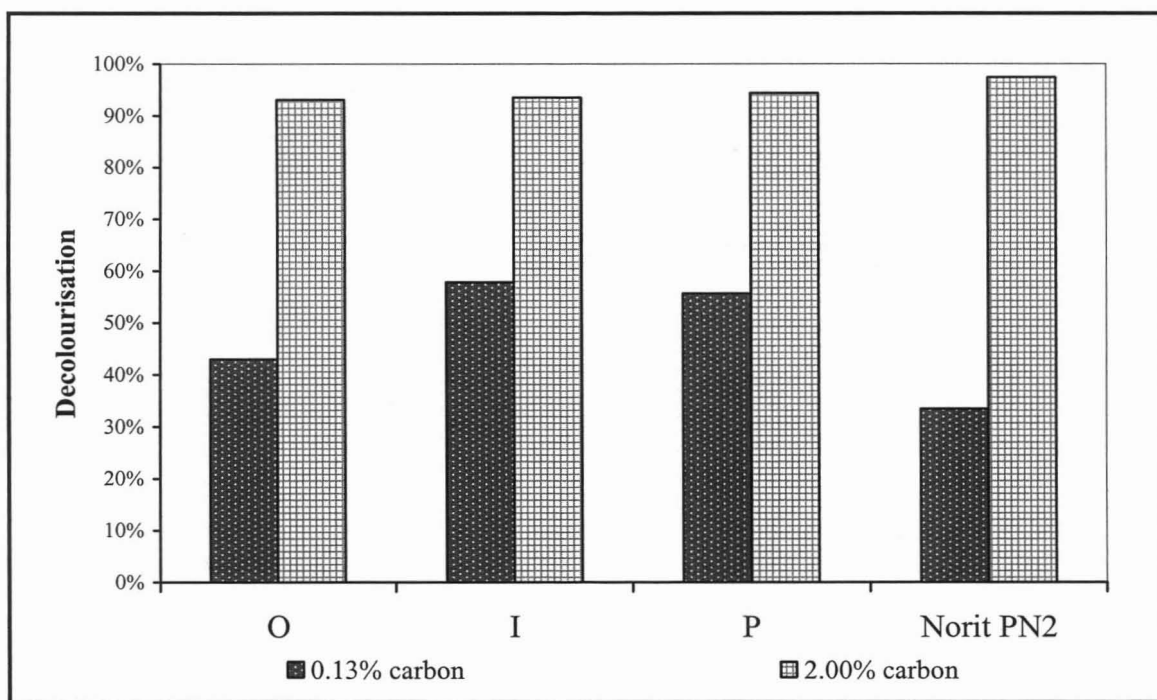
Figure 6.46: Brown Liquor decolourisation at pH 9 with prepared powder and granular South African bagasse carbons, O – 56% ash, powder, P – granular sugar/bagasse, I – 28% ash, powder and commercial Norit PN2 carbon .

0.13% activated carbon in contact with basic sugar liquors brought about 60% colour removal for low ash powder and granular activated carbons compared to the lower removals of 40 and 30% by the high ash powder bagasse carbon and commercial Norit PN2 carbon. Increasing the carbon percentage to 2%, brought about a 93% colour removal for the bagasse prepared carbons and a 95% removal for the commercial carbon. These tests again show that the bagasse activated carbons are excellent sugar decolourisers.

The sugar decolourisation tests above prove that the activated carbons prepared from sugar-cane bagasse have the ability to replace existing commercial carbons [Devnarain *et al*, 2002].

CONCLUSION & RECOMMENDATIONS

7.1 Conclusion

This research has shown that South African sugar cane bagasse can be successfully converted into unique activated carbons having excellent sugar decolorizing capacity. The quality of the final activated carbon produced from sugar-cane bagasse is dependent on the nature of the raw material used, the method and processing conditions such as heating rate, temperature, exposure time and activating medium.

The employment of the two step physical processing method comprising of bagasse pellets pyrolysed under a nitrogen atmosphere and their resulting chars being subjected to partial and controlled gasification with steam as the activating agent enabled high surface area carbons with well developed porosities to be produced from sugar cane bagasse raw material.

By using compressed bagasse fibres in the form of pellets and employing a low heating rate of 10 ^{O}C/min to the final pyrolysis temperature, enhanced the vapour-solid interactions during pyrolysis bringing about high char yields. Thermal degradation of bagasse fibres at a heating rate of 10 ^{O}C/min under a nitrogen atmosphere proceeds by a first order reaction generating char, gaseous and liquid products. Based on the fact that microporous chars will allow further development of surface area and conversion of micropores to mesopores, the optimum pyrolysis processing conditions were found to be a heating rate of 10 ^{O}C/min to the final pyrolysis temperature of 680 ^{O}C and exposure time of one hour. The optimum pyrolysis conditions generated chars having high microporosity and very little meso-macroporosity. Increasing the exposure time at the optimum pyrolysis temperature results in chars reaching a maximum burn-off % during activation with steam at 800 ^{O}C, such that the final activated consists of mainly micropores, thus not meeting the specifications of a sugar decolorizing carbon.

Increasing the steam partial pressure, activation temperature and activation time during the activation step increases the burn-off %, which consequently results in higher surface areas, pore volumes and an enhanced pore size distribution of micro, meso and macropores to be produced. A combination of high steam partial pressures and temperatures results in the gasification reaction proceeding at a faster rate, giving rise to the most well developed mesoporous activated carbons from bagasse having high adsorption capacity for large colour bodies present in molasses.

High ash bagasse raw material results in the final activated carbons having high ash contents that tend to block the pores making the internal surface inaccessible thereby reducing surface area and pore volume available for adsorption. However, the ratio of micro and mesopore volumes to the total pore volume available remains the same for both high and low ash bagasse activated carbons manufactured under the same processing conditions.

Furthermore, South African sugar cane bagasse fibers also contain a vast amount of randomly distributed oval shaped pores of varying sizes on its surface, which is a characteristic passed on by its parent material. The high value of activated carbons produced from bagasse can also be attributed to these pores, since they act as passageways for easy diffusion of gases into and out of the particle without deforming or collapsing pores created during processing.

Both powder and granular activated carbons can be produced from sugar cane bagasse fibres by the established process with latter being mixed with refined sugar prior to pyrolysis and activating for a slightly longer time of approximately half an hour. Both low ash powder and granular activated carbons from bagasse display high adsorption potentials for large colour bodies present in molasses and brown liquor and have the ability to replace commercial sugar decolourising activated carbons. The option of producing both types of activated carbons allows flexibility of the sugar industry to choose between batch or continuous adsorption systems during sugar decolourisation.

7.2. Recommendations

This study has already established the fact that invaluable activated carbons from sugar cane bagasse are produced and their ability as high sugar decolourisers creates an opportunity for the sugar industry to produce and utilize bagasse activated carbons in their process. However, more work needs to be carried out in order to take this process into commercial production and the following actions are recommended:

- In order to consider the option of using spent bagasse activated carbons as part of the fuel source, a comparative study on the calorific values of spent bagasse activated carbons and raw sugar bagasse fibres need be performed together with a study on the impact on the performance of the burners.

- An establishment of the optimum activated conditions needs to be carried out.

- Options of increasing the yield of the activated carbon product while maintaining the desired specifications needs to be considered and this lies mostly in improving char yield during pyrolysis and the type of reactor used.

- Scale-up to pilot plant using the established processing method and conditions has to be done to make more viable conclusions

- An economic study to determine the feasibility of making in-house activated carbons from bagasse

- Opportunity of using them in other industries needs to be carried out by determining its adsorption potentials for other gas and liquid substances.

REFERENCES

Ahmadpour, A. and Do, D.D. (1998). Preparation of Active Carbons from coal by Chemical and Physical activation, *Carbon,* Vol. 34 (4), 471-479.

Ahmedna, M., Johns, M.M., Clarke, S.J., Marshall, W.E. and Rao, R.M. (1997). Potential of agricultural by-product-based activated carbons for use in raw sugar decolourisation. *Journal of the Science of Food Agriculture*, Vol. 75, 117-124.

Ahmedna, M., Marshall, W.E. and Rao, R.M. (2000a). Production of Granular Activated Carbons from Select Agricultural By-products and Evaluation of their Physical, Chemical and Adsorption Properties. *Bioresource Technology*, Vol. 71, 113-123.

Ahmedna, M., Marshall, W.E. and Rao, R.M. (2000b). Surface Properties of Granular Activated Carbons from Agricultural By-products and their Effects on Raw Sugar Decolourisation. *Bioresource Technology*, Vol. 71, 103-112.

Allen, S. J., Whitten, L., McKay, G. (1998). The Production and Characterization of Activated Carbons: A Review. *Developments in Chemical Engineering and Mineral Process*, Vol. 6(5), 231-261.

American Society for Testing and Materials. (1984).*Annual Book of ASTM Standards*, D4607 –86. Philadephia, 1984.

Antal, M.J., DeAlmeida, C., Mok, W.S-L. and Sinha, S. (1991). A New Technology for Manufacturing Charcoal from Biomass. In the *Proceedings of the IGT Conference on Energy from Biomass and Wastes XV*, Washington, DC, Institute of Gas Technology: Chicago.

Antal, M.J.and Varhegyi,G. (1995). Cellulose Pyrolysis Kinetics: The Current State of Knowledge. *Industrial Engineering & Chemistry Research*, Vol. 34, 703-717.

Arseneau, DF (1981). Competitive reactions in the thermal decomposition of cellulose. *Canadian Journal of Chemistry*, Vol. 49 (4), 632-38.

Baily, A. and Maggs, F.A.P. (1971). *British Patent*, 1310101.

Bansal, RC, Donnet, J-B and Stoekli, F (1988). *Active Carbon*, Marcel Dekker, New York, 1988.

Barret, E.P., Joyner, L.C. and Halenda, P.H. (1951). The Determination of Pore Volume and Area Distributions in Porous Substances I: Computations from nitrogen isotherms. *Journal of American Chemical Society*, Vol. 73. 373.

Bernadin, F.E., Jr. (1985). Experimental Design and Testing of Adsorption and Adsorbates. Edited by Sleijko, F.L. in *Adsorption Technology*: A step-by step Approach to Process Evaluation and Application. *Chemical Industries*, Vol. 19, Chapter 1, Marcel Dekker In., New York, 37-90.

Bernado, EC, Egashira, R and Kawaski, J (1997). Decolourisation of molasses waste water using activated carbon prepared from cane bagasse. *Carbon*, Vol. 35 (9), 1217-1221.

Bilba, K. and Ouensanga, A. (1996). Fourier Transform Spectroscopic Study of Thermal Degradation of Sugar Cane Bagasse. *Journal of Analytical and Applied Pyrolysis*, Vol. 38, 61-73.

Boehm, H.P. and Voll, M. (1970). *Carbon,* Vol. 7, 227.

Boehm, H.P. and Voll, M. (1971). *Carbon,* Vol. 8, 481.

Botha, F.D. (1992). Characterization of the Structure and Adsorption Capacity of Activated Carbons Produced from South African Coals. *Ph.D Thesis*, University of Bath, July 1992.

Bradbury, A.G.W., Sakai, Y. and Shafizadeh, F. (1979). A Kinetic Model for Pyrolysis of Cellulose. *Journal of Appied. Polymer Scence*, Vol. 23, 3271-3280.

Broidio, A. and Nelson, M.A., (1975). Char Yield on Pyrolysis of Cellulose. *Combustion Flame*, Vol. 24, 263-268.

Brunauer, S.H., Emmet, P.H., and Teller, E. (1938). Adsorption of Gases in Multimolecular Layers. *Journal of American Chemical Society*, Vol. 60, 309-322.

Brunauer S.H., Emmet, P.H. and Teller, E. (1940). Classification of isotherm shapes. *Journal of Chemical Society*, Vol. (62), 1723-1735.

Buczek, B., Biniak, S. and Swiatkoski, A. (1999). Oxygen Distribution within Oxidised Carbon. *Fuel*, Vol. 78, 1443-1448.

Busy, A, (1822), *Journal of Pharmaceutical Science Accesorrires*, Vol.8, 257.

Caballero, J.A., Font, R., Marcilla, A. and Conesa, J.A. (1995). New Kinetic Model for Thermal Decomposition of Heterogeneous Materials. *Industrial Engineering Chemical Research*, Vol. 34, 806-812.

Cal, M.P. (1995). *Characterization of Gas Phase Adsorption Capacity of Untreated and Chemically Treated Activated Carbon Cloths*, PhD Thesis, University of Illinois, Urbana Champaign, 1995.

Caron (1985), Private Communications with Bansal et al (1988)

Chen, J.C.P. and Chung-chi, C. (1993). *Cane Sugar Handbook: A Manual for Cane Sugar Manufacturers and their Chemists*. 12th Ed., Wiley, New York, 1993.

Cookson, J.T. (1978). In *Carbon Adsorption Handbook*, edited by Cherimisinoff, P.N. and Ellerbusch, F., Ann Arbor Science Inc., Michigan, 1978.

Conti, S,G. and Boufala, J. (1994). Bio-oils from Arid Land Plants: Flash Pyrolysis of Euphorbia Characias Bagasse. *Biomass and Bioenergy*, Vol. 7 (1-6), 291-296.

Delavier, H.J. and Shokrani, R. (1970). Microstructure of Sugar Cane Tissue for Solid-Liquid Extraction. *Manufacturing Processing*, Vol. 1, 1475-1484.

Devnarain, P.B., Arnold, D.R. and Davis, S.B. (2002). Production of Activated Carbon from South African Sugar Cane Bagasse, In the *Proceedings of South African Sugar Technology Assosciation*, Vol. 76, 477-489.

Dietz, V. R. (1944). Bibliography of Solid Adsorbents. *Unit States Cane Sugar Refiners and Bone Char Manufacturers and National Bureau of Standards*, Washington D.C., History of Adsorbent Carbon, P ix ff, Abstracts of Reviews, Histories and general Discussions, 689-696.

Dominguez, A.R. and Hyndshaw, A.Y. (1976), Activated Carbon for Refining Sugar, *Process*, Vol. XVI, 2645-2656.

Doying, E.G. (1965). *U.S. Patent*, 3256206.

Drozhalina, ND, Bulgakova, NA, Zhukov, VK, and Raiskaya, MF (1984). Porous structure of adsorbents made by a mixture of peat and brown coal. *Khim. Tverd Topl*, Vol. 4, 82-86.

Dubinin, M.M. (1960). The Potential Theory of Adsorption of Gases and Vapors for Adsorbents with Energetically Non-uniform Surfaces. *Chemical Reviews,* Vol. 60, 235-241.

Dubinin, M.M. (1965). *Zh. Fizs. Khimi.*, 1305.

Dubinin, M.M. (1966). In *Chemistry and Physics of Carbon*, edited by Walker Jr., P.L., Vol. 2, 51-120., Marcel Dekker Inc., New York.

Dubinin, M.M. (1975). Physical Adsorption of Gases and Vapors in Micropores. In *Progress in Surface and Membrane Science,* edited by Cadenhand D.A., Vol. 9, 1-70., Academic Press, New York.

Dubnin, M.M. and Zaverina, E.D. (1949). *Dokl. Akad. Nauk. SSSR*, Vol. 65, 295.

Encinar, J. M., Beltran, F.J., Ramiro, A. and Gonzalez, J.F. (1997). Catalyzed Pyrolysis of Grape and Olive Bagasse. Influence of Catalyst type and Chemical treatment. *Industrial Engineering & Chemistry Research*, Vol. 36, 4176-4183.

Essig, M.G., Richards, G.N.and Schenk, E.M. (1989). Mechanisms of Formation of the Major Volatile Products from the Pyrolysis of Cellulose. *Cellulose and Wood Technology*, Schuerch, Cd, Ed., J. Wiley & Sons, New York, 1989.

Evans, R.J. and Milne, T.A. (1987a). Molecular Characterization of the Pyrolysis of Biomass. 1: Fundamentals. *Energy Fuels*, Vol. 1, 123-137.

Evans, R.J. and Milne, T.A. (1987b). Molecular Characterization of the Pyrolysis of Biomass. 2. Application. *Energy Fuels*, Vol. 1, 311-319.

Evans, M.J.B., E. Haliop, and J.A.F. MacDonald. (1999). The Production of Chemically-Activated Carbon. *Carbon,* Vol. 37, 269-274.

Faust, S.D. and Aly, O.M.(1983). In *Chemistry of Water Treatment*, Butterworth & Company, Woburn, Massachusetts.

Frey-Wyssling, A. (1958). *Die Pflanzliche Zellwand*. Springer-Verlang, Berlin, Goettingen, Heidelberg, Vol. 75, 1958.

Garcia-Perez, M., Chaala, A., Yang, J. and Roy, C. (2001). Co-pyrolysis of Sugar Cane Bagasse with Petroleum Residue, Part I: Thermogravimetric analysis. *Fuel*, Vol. 80, 1245-1258.

Gergova, K., Galushko, A., Petrov, N. and Minkova, V. (1992). Investigation of the Porous Structure of Activated Carbons prepared by Pyrolysis of Agricultural By-products in a Stream of Water Vapour. *Carbon*, Vol. 30(5), 721-727.

Gergova, K, Petrov, N and Eser, S (1994). Adsorption properties and microstructure of activated carbons produced from by-products by steam pyrolysis. *Carbon*, Vol. 32 (4), 693-702.

Girgis, B.S., and Ishak, M.F. (1999). Activated Carbon from Cotton Stalks by Impregnation with Phosphoric Acid. *Materials Letters*, Vol. 39 (2), p 107-114.

Glasstone, S. (1980*). Textbook of Physical Chemistry*, 2nd Ed., Macmillan Co., India, 1980.

Gregg, S.J. and Sing, K.S.W. (1982). *Adsorption, Surface Area and Porosity*. 2nd ed., Academic Press, London, 1982.

Hajaligol, M.R., Howard, J.B., Longwell, J.P., and Peters, W.A. (1982). Product Compositions and Kinetics for Rapid Pyrolysis of Cellulose. *Industrial Engineering Chemical Process Design &. Development*, Vol. 11, 457-465.

Hassler J. W., (1974), *Purification with Activated Carbon*, USA, Chemical Publishing Company, Inc. New York.

Harkins, W.D. and Jura, G.J. *Journal of Chemistry & Physics*, Vol. 11, 431.

Higa, M, Miyashiro, S and Teruya, K (1989). The use of prefectural resources for wastewater treatment agent. *Okinawaken Kogyoshikensho Gyomuhokoku*, Vol. 17, 51-59.

Hu, Z., Vansant, E.F., Vigmeron, S., and Hermia, J. (1996). Tailoring the Porosity of Activated Carbons by Chemical Activation. In *The Proceedings of The European of Carbon Conference 'Carbon 96'*, Newcastle, UK, Vol. 2, 469-470, July.

Hunter, J. (1865). *Journal of Chemical Society*, Vol. 18, 285.

Jankowska, A (1996). Porosity Development in Polish Anthracite: Influence of Activating Agent. *The Proceedings of the European Carbon Conference 'Carbon 96'*, Newcastle, UK, Vol. (2), July, 600-601.

Johns, M.M., Marshall, W.E. and Toles, C.A. (1998). Agricultural By-products as Granular Activated Carbons for adsorbing Metals and Organics. *Journal of Chemical Technology and Biotechnology*, Vol. 71, 131-140.

Khattab, M.A., Hosny, A.Y., Nassar, M.M. and El-Geundi, M. (1993). Thermal Studies of Some Dye-Adsorbent Material. *Energy Sources*, Vol. 15, 505-512.

Laine, J. and A. Calafat. (1991). Factors affecting the preparation of activated carbons from coconut shells catalized by potassium. *Carbon,* Vol. 29, 949-953.

Langmuir, I. (1916). *Journal of American Chemical. Society*, Vol. 38, 2221.

Lavarack, B.P. (1997). Chemically Activated Carbons from Sugar-cane Bagasse Fractions. *Hungarian Journal of Industrial Chemistry*, Vol. 25, 157-160.

Dence, C. W and Lin, Lin, S. Y. (1992). The determination of lignin. In Methods in Lignin Chemistry; Eds.; Springer-Verlag, Heidelberg, 33-61.

Lippens, B.C, and de Boer, J.H. (1965). Studies on Pore Systems in Catalysts: V. *Journal of Catalysis*, Vol.4, 319-323.

Lowitz, B. (1786). *Crell's Chem. Ann. I*, 211-218.

Lu, W. and Chung, D.D.L. (1996). Mesoporous Activated Carbon Filaments. In the *Proceedings of the European Carbon Conference 'Carbon 96'*, Newcastle, UK, 1, July, 26-27.

Lua, A.C. and Gua, J. (1999) Chars Pyrolyzed from oil palm wastes for activated carbon preparation. *Journal of Environmental Engineering*, American Society of Civil Engineers, Vol. 125(1), 72-76.

Luo, M. and Stanmore, B. (1992). The Combustion characteristics of char from pulverized bagasse. *Fuel*, Vol. 71, September, 1074-1076.

Luo, M. and Stanmore, B.R. (1994). Modelling Combustion in a Bagasse-fired Furnace 1: Formulation and Testing of the Model. *Journal of the Institute of Energy*, Vol. 67, 128-135, September.

Lutz, H., Esuoso, K., Kutubuddin, M. and Bayer, E. (1998). Low temperature conversion of sugar-cane by-products. *Biomass and Bioenergy*, Vol. 115 (2), 155-162.

MacKay, D.M. and Roberts, P.V. (1982a). The influence of pyrolysis conditions on yield and microporosity of lignocellulosic chars. *Carbon*, Vol. 20 (2), 95-104.

MacKay, D.M. and Roberts, P.V. (1982b). The dependence of char and carbon on lignocellulosic composition. *Carbon*, Vol. 20 (2), 87-94.

Mattson, J.S. and Mark H.B. (1971). *Activated Carbon*, Marcel Dekker, New York, 1971.

Mattson, J.S., Mark, H.B. (Jr.), Malbin, M.P., Weber, W.J. and Crittenden, J.C. (1969). *Journal of Colloid Interface Science*, Vol. 31(1), 116.

Marshall, W.E., Ahmedna, M., Rao, R.M. and Johns, M.M. (1999). Granular Activated Carbons from Sugar Cane Bagasse. *International Conference on Value Added Products for the Sugar Industry*, Anderson Sugar Institute, Louisanna, April, 1-10.

McClellan, A.L. and Harnsberger, H.F. (1967). Cross-sectional Areas of Molecules Adsorbed on Solid Surfaces. *Journal of Colloid and Interface Science*, Vol. 23, 577-599.

McEnaney, B. (1988). Review Article: Adsorption and Structure in Microporous Carbons. *Carbon*, Vol. 26, 267.

Mead, G.P. and Chen J.C.P. (1977). *Cane Sugar Handbook*. John Wiley & Sons, New York, 1977.

Mikhail, R.S. Brunauer, S. and Bodor, E.E. (1968). *Journal of Colloid Interface Science*, Vol. 26, 45.

Minkova, V., Marinov, S.P., Zanzi, R., Bjornbom, E., Budinova, T., Stefanova, M. and Lakov, L. (2000). Thermochemical Treatment of Biomass in a Flow of Steam or in a Mixture of Steam and Carbon Dioxide. *Fuel Processing Technology*, Vol. 62, 45-52.

Minkova, V., Razvigorova, M., Bjornbom, E., Zanzi, R., Budinova, T. and Petrov, N. (2001). Effect of Water Vapour and Biomass Nature on the Yield and Quality of the Pyrolysis Products from Biomass. *Fuel Processing Technology*, Vol. 70, 53-61.

Mok, W.S., Antal, M.J., Szabo, P., Varhegyi, G. and Zelei, B. (1992). Formation of Charcoal from Biomass in a Sealed Reactor. *Industrial Engineering & Chemistry Research*, Vol. 31, 1162-1166.

Morgan ,J.J. and Fink C.E. (1946). Binders and base materials for active carbon, *Indian Engineering Chemistry*, Vol.38 (2), 219-288.

Myers, A.L. and Praustnitz, J.M. (1965). Thermodynamics of Mixed Gas Adsorption. *AIChE Journal*, Vol. 11(1), 121-127.

Nassar, M.M. and Mackay, G.D.M. (1984). Mechanism of thermal decomposition of lignin. *Wood Fiber Science*, Vol.16, 441-453.

Nassar, M.M., Ashour, E.A. and Wahid, S.S. (1996). Thermal Characteristics of Bagasse. *Journal of Applied Polymer Science*, Vol.68, 885-890.

Nassar, M.M. (1999). Thermal Analysis Kinetics of Bagasse and Rice Straw. *Energy Sources*, Vol. 21, 131-137.

Otowa, T, Nojima, Y, ad Itoh, M (1996). Activation Mechanism, surface properties and adsorption characteristics of KOH activated high surface area carbon. *Fundamentals of Adsorption,*and In the *Proceedings of the Fifth International Conference on Fundamentals of Adsorption*, Kluwer Academic Publishers, 709-716.

Pashenkco, LV, Khazipov, VA, Shendrik, TG and Galushko, LYA (1996). The Reception of adsorbents from carbon containing waste. *Proceedings of the European Carbon Conference 'Carbon 96'*, Newcastle, UK, Vol. (2), July, 433-433.

Paturau, J.M. (1989). *By-products of the Cane Sugar Industry*. 3rd Edition, Elsevier, Amsterdam. The Netherlands, 1989.

Pawlowski, B.S. (1971), Determination of the Molasses Number of Activated Carbon, *Control Lab Test Methods*, Carbon.

Pendyal, B., Johns, M.M., Marshall, W.E., Ahmenda, M. and Rao, R.M. (1999a). The effect of binders and agricultural by-products on physical and chemical properties of granular activated carbons. *Bioresource Technology*, Vol. 68, 247-254.

Pendyal, B., Johns, M.M., Marshall, W.E., Ahmenda, M. and Rao, R.M. (1999b). Removal of Sugar colourants by Granular Activated Carbons made from Binders and Agricultural By-products. *Bioresource Technology*, Vol. 68, 45-51.

Peters, E.M. (1966). *U.S.Patent*, 3235323.

Petrie, J.G. and Baldwin, S. (1922). Devolatilisation of Pelletised and Briquetted Wastes. *Journal of the Institute of Energy*, Vol. 65, 185-191, December.

Pollard, S.J.T., Fowler, G.D., Sollars, C.G. and Perry, R. (1992). Low cost adsorbents for waste and water treatment: a review. *Science of the Total Environment*, Vol. 116, 31-52.

Porter, K.R. and Ledbetter, M.C. (1970). *Introduction to the Fine Structure of Plant Cells.* Springer-Verlag, Berlin, Heidelberg, New York, 1970.

Rand, B. and Marsh, H. (1971). *Carbon*, Vol. 9, 79

Raveendran, K., Ganesh, A. and Khilar, K. (1996). *Fuel*, Vol. 75, 987.

Ritter, H.L. and Drake, L.C. (1945). *Ind. Chem. Analyt*. Ed., Vol. 17, 782.

Rodriguez-Reinoso, R.F. and Solano, A.L. (1989). Microporous Structure of Activated Carbons as revealed by Adsorption Methods. Edited by Thrower, P.A., In *Chemistry and Physics of Carbon*, Chapter 1, Vol. 21, Marcel Dekker, New York, 1989.

Rodriguez-Reinoso, R.F.and Molina-Sabio, M. (1992). Activated carbons from lignocellulosic material by chemical and/or physical activation: an overview. *Carbon*, Vol. 30 (7), 1111-1118.

Rodriguez, A.D., Roquet, P. and Khristich, V.A. (1993). Combustion of Pulverised Biomass (Bagasse) in a New Rotary Burner. *Heat Transfer Research*, Vol. 25 (1), 73-81.

Roy, C., Pakdel, H. and Brouillard, D. (1990), *Journal of Applied. Polymer* Science, Vol. 41, 337.

Shafizadeh, F. (1968). Pyrolysis and Combustion of Cellulosic Materials. *Adv, Carbohydrate. Chemistry*, Vol. 23, 419-474.

Schoefield, R.K. (1948). *Disc. Faraday Soc.*, Vol. 3, 103.

Shukry, N., Ishak, F. and Sefain, Z. (1991). DTA Study of Thermal Degradation of Bagasse and Rice Straw Hemicelluloses. *Journal of Thermal Analysis*, Vol. 37, 915-926.

Smisek, M and Cerny, S (1970). *Active Carbons–manufacture and properties and applications.* Elsevier Ltd., 1970.

Smith, J.M. and van Ness, H.C. (1987). *Introduction to Chemical Engineering Thermodynamics*, 3rd Ed., McGraw Hill, 1987.

Stenhouse J, (1856). *British Patent*, 1395

Stenhouse J, (1872) *Chem News*, Vol. 3, 78.

Stoeckli, H.F. (1990). Microporous carbons and their characterization: The present state of the art. *Carbon*, Vol. 28(1), 1-6.

Stubington, J.F. and Aiman, S. (1994). Pyrolysis Kinetics of Bagasse at High Heating rates. *Energy Fuels*, Vol. 8, 194-203.

Suffet, I.H. and McGuire, M.J. (1981). *Activated Carbon Adsorption*, Vol. I, II, Ann Arbor Science Pub., Ann Arbor, Mich., 1981.

Tang, W.K. (1967). Effect of Inorganic Salts on Pyrolysis of Wood. *U.S. Forest Service Research Paper FPL*, Vol.71.

Teker, M, Saltabas, O and Imamoglu, M (1997). Adsorption of cobalt by activated carbon from rice hulls. *Journal of Environmental Sciences and Health A*, Vol. 32 (8), 2077-2086.

Teng, C-L., and F.S. Wang. (1999). Intermittent continuous method for recovering refined activated carbon from waste tires and the like and the device therefor. *US Patent*, 5,976,484.

Tourkow, K., Siemieniewska, T., Czeckowski, F. and Gankowska, A. (1977). *Fuel*, Vol. 56, 121.

Treumper, J.T. (1968). The Porosity of Activated Carbon and its Relation to Cane Sugar Refining. *Proc. Cane Sugar Refining Research*, 24-34.

Treybal, R.E. (1980). *Mass Transfer Operations*, 3rd ed., McGraw Hill, New York, 581-582, 1980.

Tsai, S.C. (1982). In *Fundamentals of Coal Beneficiation and Utilization*, edited by Anderson, L.L., Elsevier Scientific Pub. Co., Amsterdam.

Tsai, W. T., Chang, C. Y., Lin, M. C., Chien, S. F., Sun H. F., and Hsieh M. F. Adsorption of acid dye onto activated carbons prepared from agricultural waste bagasse by $ZnCl_2$ activation, *Chemosphere*, Vol. 45 (1), 51-58.

Varhegyi, G., Anatl, M.J., Szekely, T. and Szabo, P. (1989). Kinetics of the Thermal Decomposition of Cellulose, Hemicellulose, and Sugar Cane Bagasse. *Energy Fuels*, Vol. 3, 329-335.

Washburn, E.W. (1921). The dynamics of capillary flow. *Proc. Nat. Acad. Sci.*, USA, Vol. 7, 115.

Xia, J, Kiyoshi, N, Kagawa, S and Wakao, N (1998). Production of activated carbon from bagasse (waste) of sugarcane grown in Brazil. *Journal of Chemical Engineering of Japan*, Vol. 13, 987-990.

Youssef, AM and Mostafa, MR (1992). Removal of copper ions by modified activated carbons. *Indian Journal Technology*, Vol. 30 (8), 413-416.

Zandersons, J.Gravitis,J., Kokorevics, A. Zhurinsh, A. Bikovens, O. Tardenaka, A.and Spince B..(1999). Studies of the Brazilian Sugarcane Bagasse Carbonisation Process and Products properties, *Biomass and Bioenergy*, 1999, Vol.17 (3), 210-219.

Zulkarnain, Z., Hussein, M.Z. and Muhammad, B. (1993). Preparation and Characterizatin of Activated Carbon from Mangrove Wood (Rhizophora apiculata). *Pertanika Journal of Scence. & Technology*, Vol. 1(2), 169-177.

Zsigsmondy, A. (1911). Journal of *Anorgic Chemistry*, Vol. 71, 356.

MOLECULAR DIMENSIONS

Table A-1: Cross-sectional Areas of adsorbate molecules [Cal, 1995]

Adsorbate molecule	Cross-sectional Area $^{1}\sigma$ (Å^2)	Molecular Dimensions ^{2} (Lennard-Jones) (Å)
Water (H_2O)	12.5	2.64
Nitrogen (N_2)	16.2	3.80
Acetone (C_3H_6O)	16.7	4.60
Carbon Dioxide (CO_2)	22.0	3.94
Benzene (C_6H_6)	43.0	5.35 (3.7 Å x 7.0 Å)

[1] – McClellan and Harnsberger [1967]

[2] - Myers and Praustnitz [1965]

DATA LOGGING PROGRAM

B – 1. Mass - Temperature Logging Computer Program
VISUAL BASIC, VERSION 5.00

Object = "{648A5603-2C6E-101B-82B6-000000000014}#1.1#0"; "MSCOMM32.OCX"

```
Begin VB.Form massfrm
        Caption        =  "Mass log"
        ClientHeight   =  3945
        ClientLeft     =  60
        ClientTop      =  345
        ClientWidth    =  3960
        LinkTopic      =  "Form1"
        ScaleHeight    =  3945
        ScaleWidth     =  3960
        StartUpPosition =  3  'Windows Default


Begin VB.TextBox Text3
        Height         =  375
        Left           =  2280
        TabIndex       =  10
        Top            =  2640
        Width          =  1095
        End


Begin VB.CommandButton Command2
        Caption        =  "Send to temp      controller"
```

DATA LOGGING PROGRAM

B – 1. Mass - Temperature Logging Computer Program
VISUAL BASIC, VERSION 5.00

Object = "{648A5603-2C6E-101B-82B6-000000000014}#1.1#0"; "MSCOMM32.OCX"

```
Begin VB.Form massfrm
        Caption         =   "Mass log"
        ClientHeight    =   3945
        ClientLeft      =   60
        ClientTop       =   345
        ClientWidth     =   3960
        LinkTopic       =   "Form1"
        ScaleHeight     =   3945
        ScaleWidth      =   3960
        StartUpPosition =   3  'Windows Default


Begin VB.TextBox Text3
        Height          =   375
        Left            =   2280
        TabIndex        =   10
        Top             =   2640
        Width           =   1095
        End


Begin VB.CommandButton Command2
        Caption         =   "Send to temp       controller"
```

```
        Height          =   495
        Left            =   720
        TabIndex        =   9
        Top             =   3360
        Width           =   1215
        End


Begin VB.TextBox Text2
        Height          =   375
        Left            =   720
        TabIndex        =   8
        Top             =   2640
        Width           =   1095
        End


Begin VB.CommandButton Command1
        Caption         =   "   Send Command"
        Height          =   375
        Left            =   2280
        TabIndex        =   7
        Top             =   480
        Width           =   1095
        End


Begin VB.TextBox Text1
        Height          =   375
        Left            =   720
        TabIndex        =   6
        Top             =   480
        Width           =   1095
        End


Begin VB.CommandButton getmass
        Caption         =   "get mass"
        Height          =   375
        Left            =   720
        TabIndex        =   5
```

```
        Height          =   495
        Left            =   720
        TabIndex        =   9
        Top             =   3360
        Width           =   1215
        End


Begin VB.TextBox Text2
        Height          =   375
        Left            =   720
        TabIndex        =   8
        Top             =   2640
        Width           =   1095
        End


Begin VB.CommandButton Command1
        Caption         =   "  Send Command"
        Height          =   375
        Left            =   2280
        TabIndex        =   7
        Top             =   480
        Width           =   1095
        End


Begin VB.TextBox Text1
        Height          =   375
        Left            =   720
        TabIndex        =   6
        Top             =   480
        Width           =   1095
        End


Begin VB.CommandButton getmass
        Caption         =   "get mass"
        Height          =   375
        Left            =   720
        TabIndex        =   5
```

```
        Top           =  1200
        Width         =  1095
    End
Begin VB.TextBox timetxt
        Height        =  375
        Left          =  720
        TabIndex      =  3
        Top           =  1800
        Width         =  1095
    End


    Begin VB.CommandButton zero
        Caption       =  "Zero Tare"
        Height        =  375
        Left          =  2280
        TabIndex      =  2
        Top           =  1200
        Width         =  1095
    End


    Begin VB.Timer Timer1
        Interval      =  1000
        Left          =  600
        Top           =  0
    End


    Begin MSCommLib.MSComm MSComm1
        Left          =  0
        Top           =  0
        _ExtentX      =  1005
        _ExtentY      =  1005
        _Version      =  327680
        DTREnable     =  -1  'True
        InputLen      =  20
        RTSEnable     =  -1  'True
    End
```

Begin VB.TextBox masstxt

    Height   = 375

    Left   = 2280

    TabIndex   = 0

    Top   = 1800

    Width   = 855

    End

Begin MSCommLib.MSComm MSComm2

    Left   = 0

    Top   = 2640

    _ExtentX   = 1005

    _ExtentY   = 1005

    _Version   = 327680

    CommPort   = 2

    DTREnable   = -1 'True

    InputLen   = 20

    RTSEnable   = -1 'True

    End

Begin VB.Label Label4

    Caption   = "recvd temp"

    Height   = 255

    Left   = 2400

    TabIndex   = 12

    Top   = 3120

    Width   = 855

    End

Begin VB.Label Label2

    Caption   = "send"

    Height   = 255

    Left   = 1080

    TabIndex   = 11

    Top   = 3120

    Width   = 495

    End

Begin VB.Label Label3

Caption = "Time"

Height = 255

Left = 960

TabIndex = 4

Top = 2280

Width = 735

End

Begin VB.Label Label1

Caption = "Mass"

Height = 255

Left = 2520

TabIndex = 1

Top = 2280

Width = 495

End

End

Attribute VB_Name = "massfrm"

Attribute VB_GlobalNameSpace = False

Attribute VB_Creatable = False

Attribute VB_PredeclaredId = True

Attribute VB_Exposed = False

Private Sub Command1_Click()

 send (Text1.Text)

End Sub

Private Sub Command2_Click()

On Error GoTo eror

' MSComm2.Output = Trim(Text2.Text) & CRC(Trim(Text2.Text)) 'outputs to temperature controller

Dim temp As String

"**

temp = Chr$(2) & Chr$(7) & Chr$(65) & Chr$(18)

"**

```
   MSComm2.Output = temp '& CRC(temp)  'outputs to temperature controller


eror:
End Sub


Private Sub Form_Load()

   ' Open the communications port.
   On Error Resume Next
   MSComm1.PortOpen = True


   If Err Then
      MsgBox "CommPort: not available. Change the CommPort property to another port." &
Err
      Exit Sub
   End If


   ' Flush the input buffer.
   MSComm1.InBufferCount = 0


Open "C:\mass\mass.dat" For Output As #1
   ' Open the communications port.
   On Error Resume Next
   MSComm2.PortOpen = True


   If Err Then
      MsgBox "CommPort: not available. Change the CommPort property to another port." &
Err
      Exit Sub
   End If


   ' Flush the input buffer.
   MSComm2.InBufferCount = 0
End Sub


Private Sub send(this As String)
On Error GoTo eror
```

```
 MSComm1.Output = this & Chr$(13) & Chr$(10) 'outputs to massmeter
eror:
End Sub


Private Sub getmass_Click()
 send ("SIR")
End Sub


Private Sub MSComm2_OnComm()


'If MSComm2.PortOpen = True Then
 Text3.Text = MSComm2.Input
'End If
     ' Flush the input buffer.
 MSComm2.InBufferCount = 0


End Sub


Private Sub Timer1_Timer()


If MSComm1.PortOpen = True Then


masstxt.Text = MSComm1.Input
If masstxt.Text <> "" Then
 If (Asc(masstxt.Text) > Asc("0")) Then
  masstxt.Text = Mid(MSComm1.Input, 6)
   timetxt.Text = Time
     ' Flush the input buffer.
    MSComm1.InBufferCount = 0
   Write #1, timetxt.Text & "," & (Val(masstxt.Text))
 End If
End If
End If
End Sub


Private Sub zero_Click()
 send ("TI")
```

```
send ("Z")
End Sub


Private Function CRC(message$) As Long
crc16& = 65535
 For c% = 1 To Len(message$)
   crc16& = crc16& Xor Asc(Mid$(message$, c%, 1))
   For Bit% = 1 To 8
    If (crc16& Mod 2) Then
     crc16& = (crc16& / 2) Xor 40961
    Else
     crc16& = crc16& / 2
    End If
   Next Bit%
 Next c%


 crch% = crc16& / 256
 crcl% = crc16& Mod 256


 message$ = message$ + Chr$(crcl%) + Chr$(crch%)
CRC = crc16&


 Text3.Text = Str(crcl%) & Str(crch%)
End Function
```

****

By Nelson Naidoo & P.B. Devnarain, University of Natal, 2001

****

CHARACTERIZATION

C-1 Characterization of Bagasse Chars

C-1.1 Final Pyrolysis Temperature of 680 ^{O}C

C-1.1.1.Total Surface Area
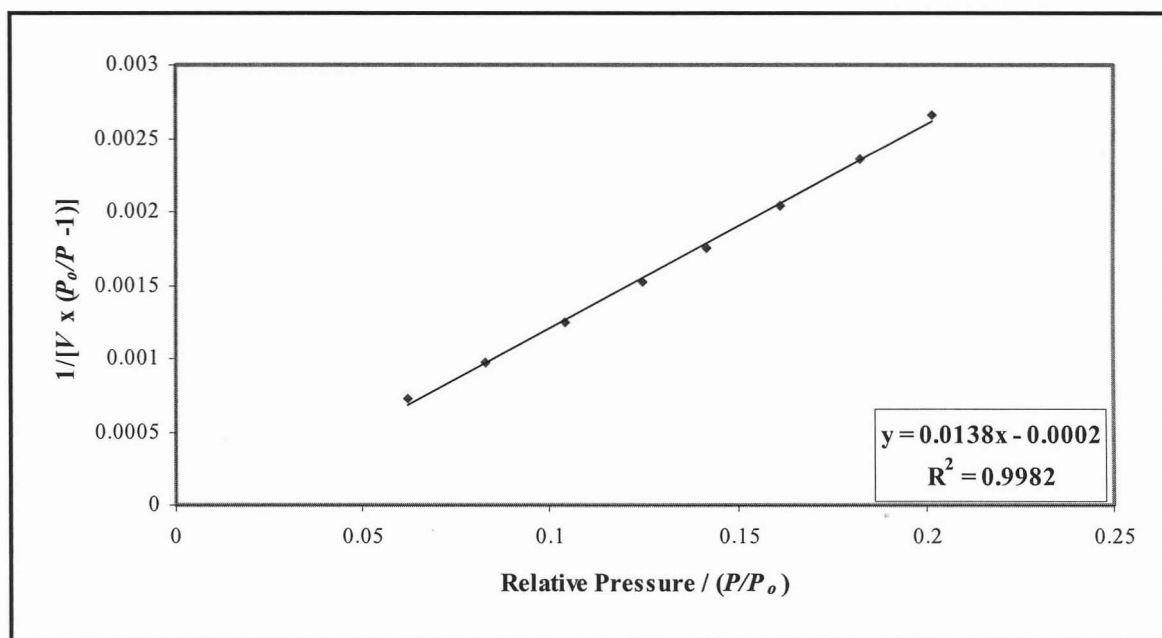
Figure C-1: BET surface area plot for bagasse chars produced under a nitrogen atmosphere at a heating rate of 10 ^{O}C/min to a final pyrolysis temperature of 680 ^{O}C and hold time of 1 hour.
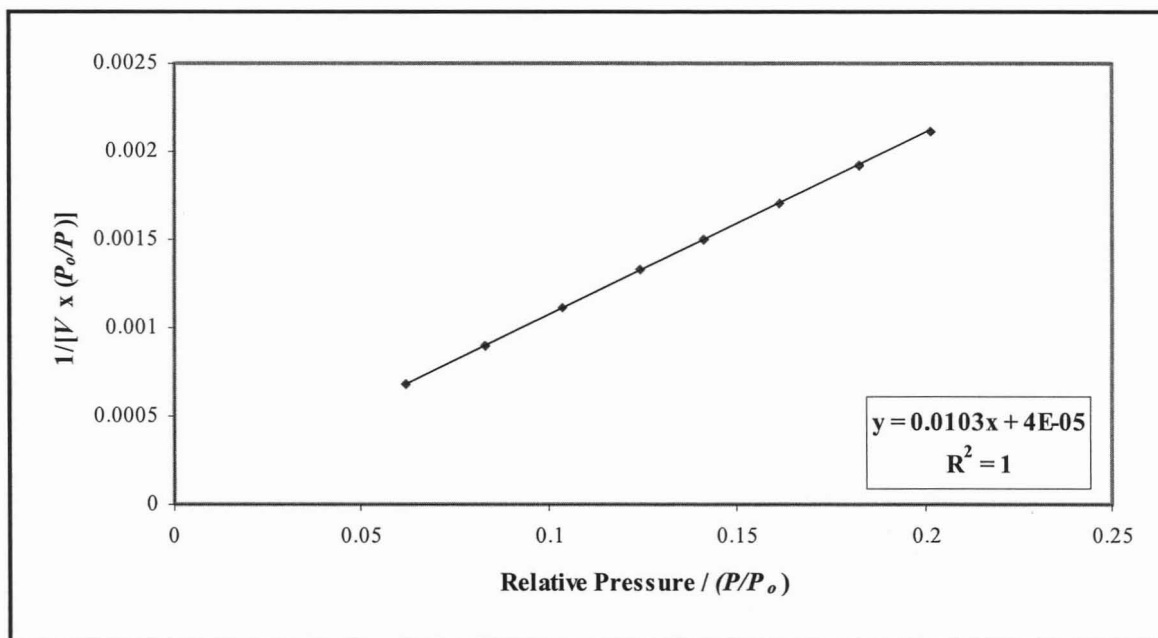
Figure C-2: Langmuir surface area plot for bagasse chars produced under a nitrogen atmosphere at a heating rate of 10 ^{O}C/min to a final pyrolysis temperature of 680 ^{O}C and hold time of 1 hour.

C-1.1.2. External Surface Area, Micropore Area and Micropore Volume
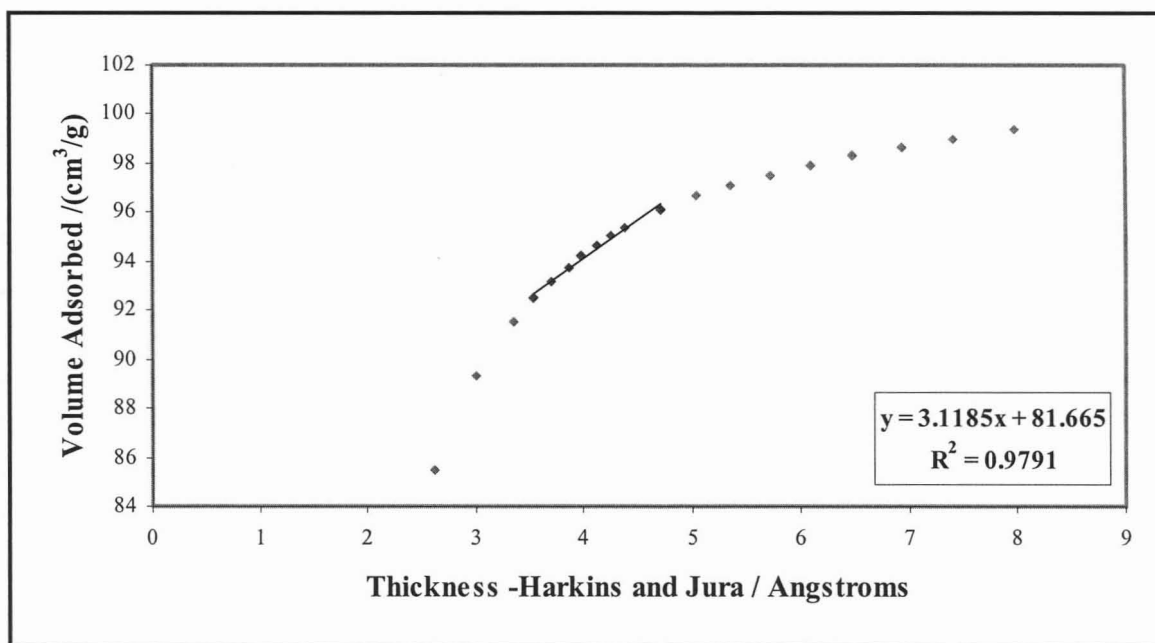
Figure C-3: t-plot to determine external surface area and micropore volume for bagasse chars produced under a nitrogen atmosphere at a heating rate of 10 ^{O}C/min to a final pyrolysis temperature of 680 ^{O}C and hold time of 1 hour.

C-1.1.3 Meso-macropore size distributions
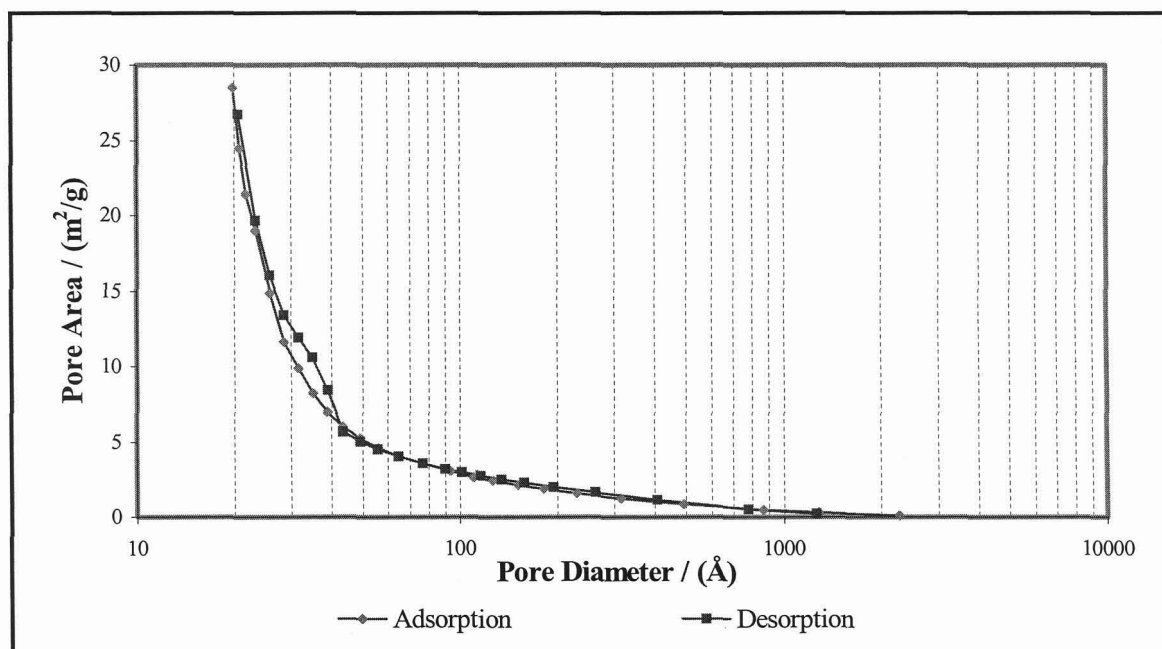
Figure C-4: BJH adsorption and desorption plots of cumulative pore area versus pore diameter for bagasse chars produced under a nitrogen atmosphere at a heating rate of 10 ^{O}C/min to a final pyrolysis temperature of 680 ^{O}C and hold time of 1 hour.
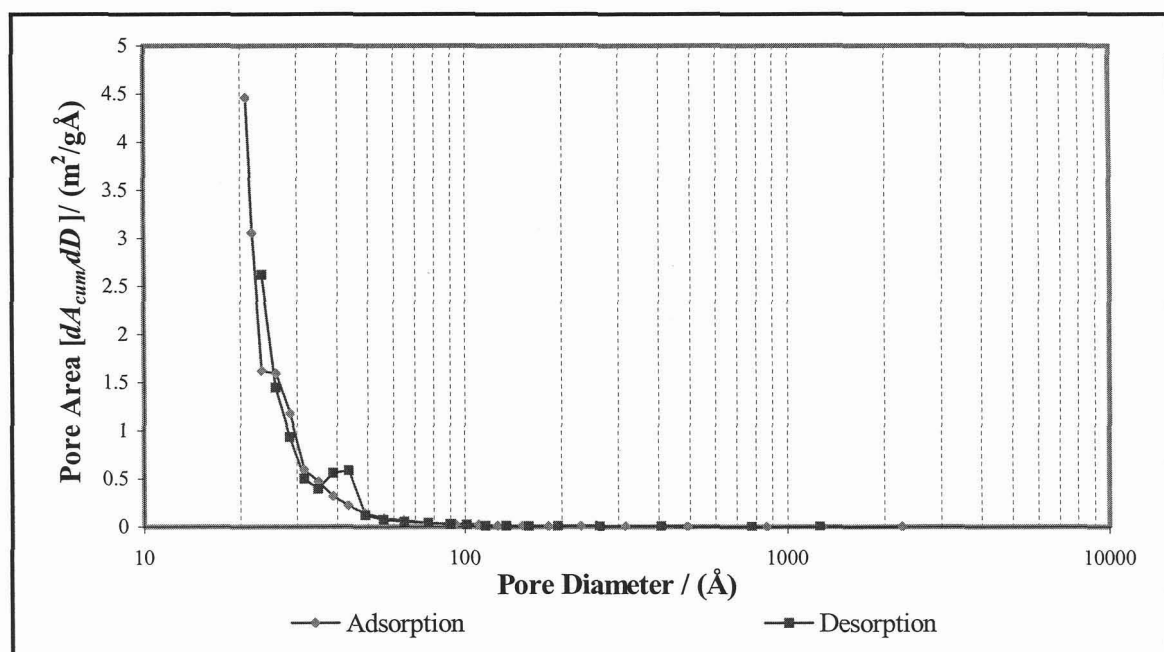
Figure C-5: BJH adsorption and desorption plots of pore area (dA_{cum}/dD) versus pore diameter curves for bagasse chars produced under a nitrogen atmosphere at a heating rate of 10 ^{O}C/min to a final pyrolysis temperature of 680 ^{O}C and hold time of 1 hour.
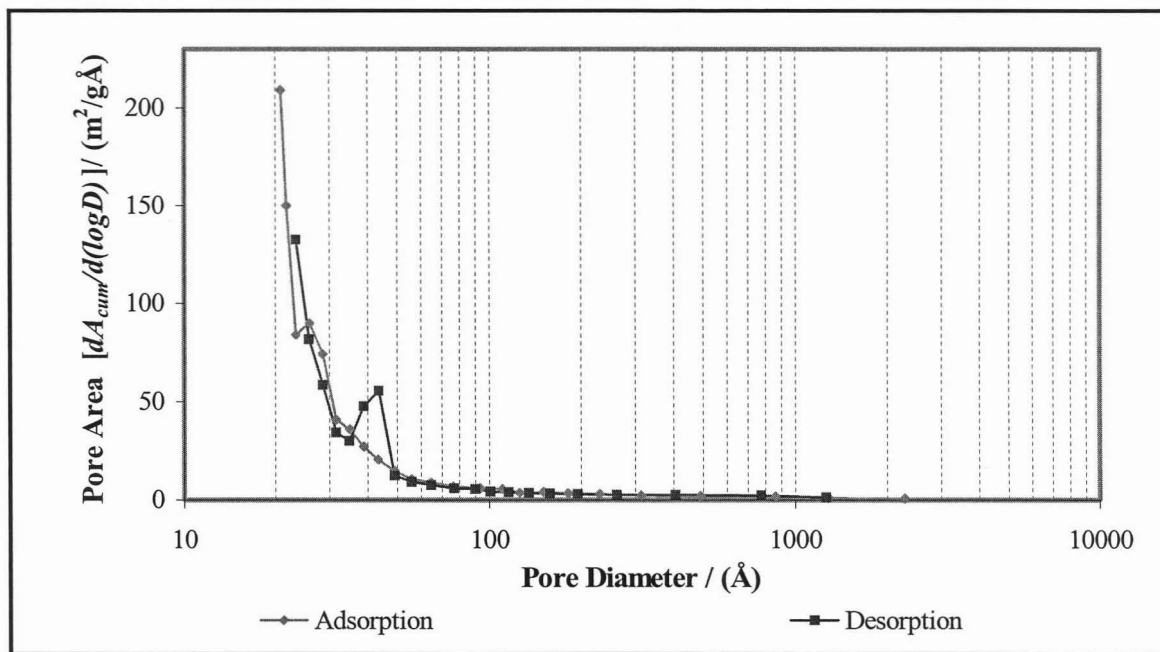
Figure C-6: BJH adsorption and desorption plots of pore area ($dA_{cum}/d(logD)$) versus pore diameter for bagasse chars produced under a nitrogen atmosphere at a heating rate of 10 ^{O}C/min to a final pyrolysis temperature of 680 ^{O}C and hold time of 1 hour.
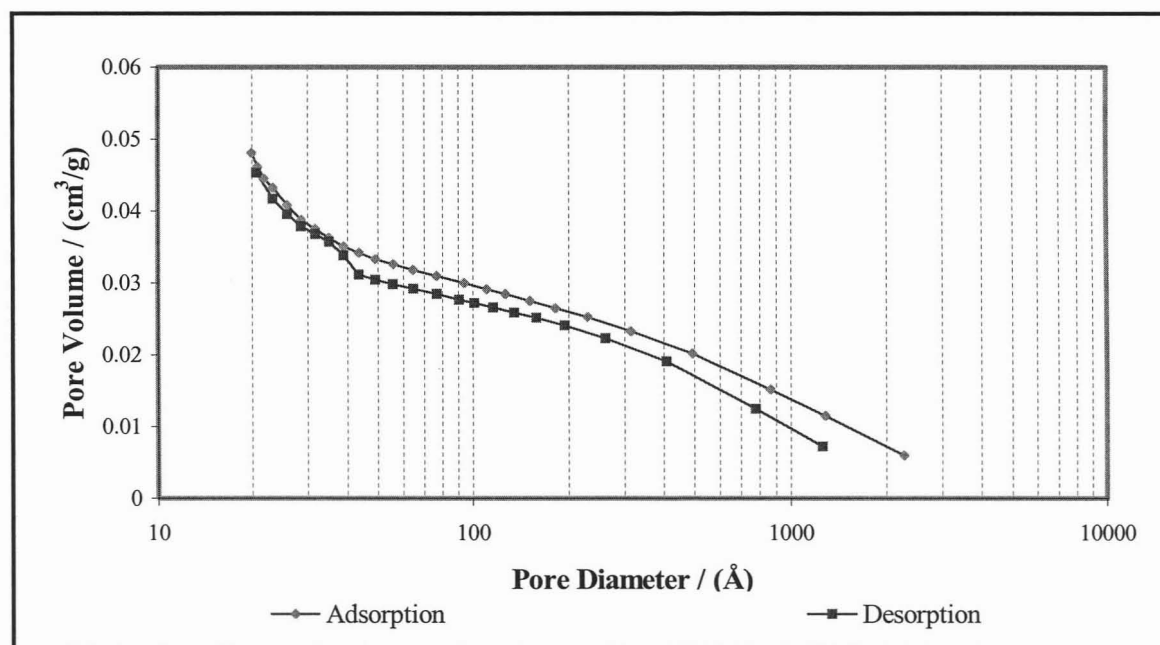
Figure C-7: BJH adsorption and desorption plots of cumulative pore volume versus pore diameter for bagasse chars produced under a nitrogen atmosphere at a heating rate of 10 ^{O}C/min to a final pyrolysis temperature of 680 ^{O}C and hold time of 1 hour.

C-2 Characterization of Activated Carbons from Sugar Cane Bagasse

C-2.1 Effect of Steam Partial Pressure on the final Activated Carbon

C-2.1.1. Total Surface Area
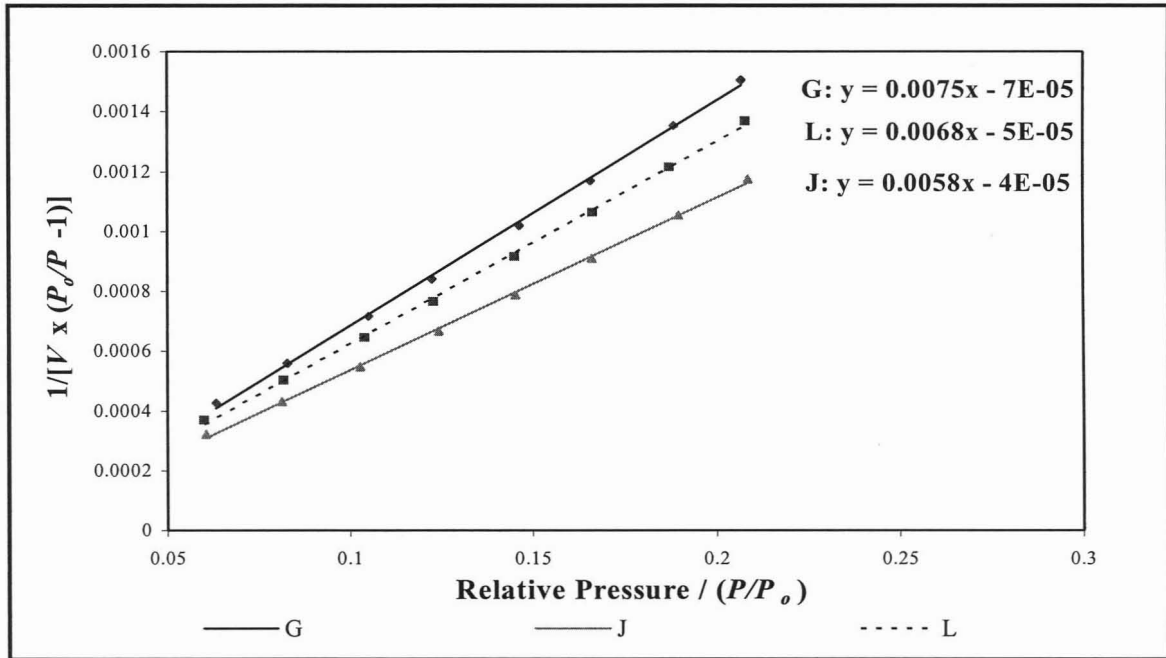
Figure C-8: BET surface area plots for bagasse activated carbons, produced at an activation temperature of 800 ^{O}C and time of 4 hours at varying steam/nitrogen ratios, (▲)J – 1:0.6, (■)L – 0.5:0.5 & (♦)G – 0.4:1.
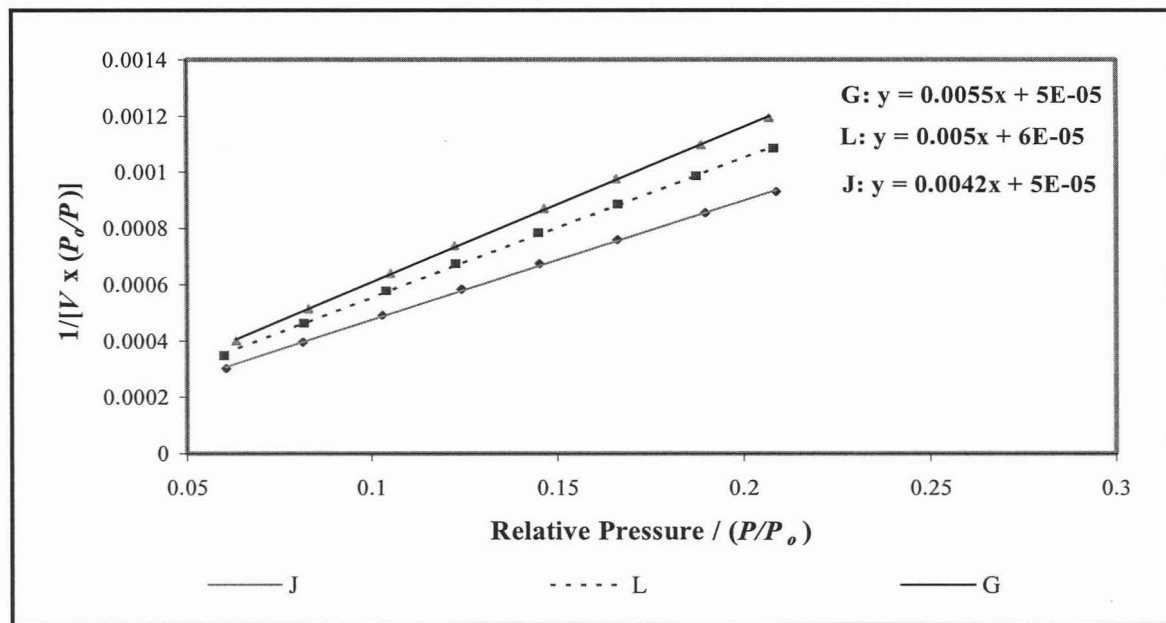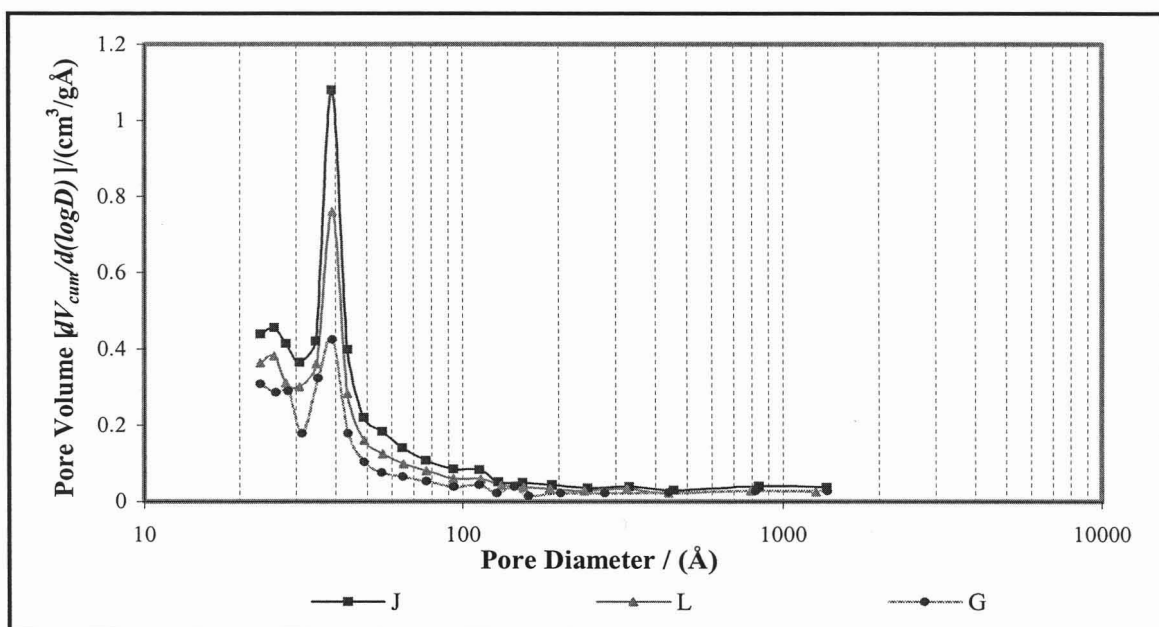

Figure C-9: Langmuir surface area plots for bagasse activated carbons produced at an activation temperature and time of 800 ^{O}C of 4 hours at varying steam/nitrogen ratios, (♦)J – 1:0.6, (■)L – 0.5:0.5 & (▲)G – 0.4:1.

C-2.1.2. External Surface Area, Micropore Area and Micropore Volume
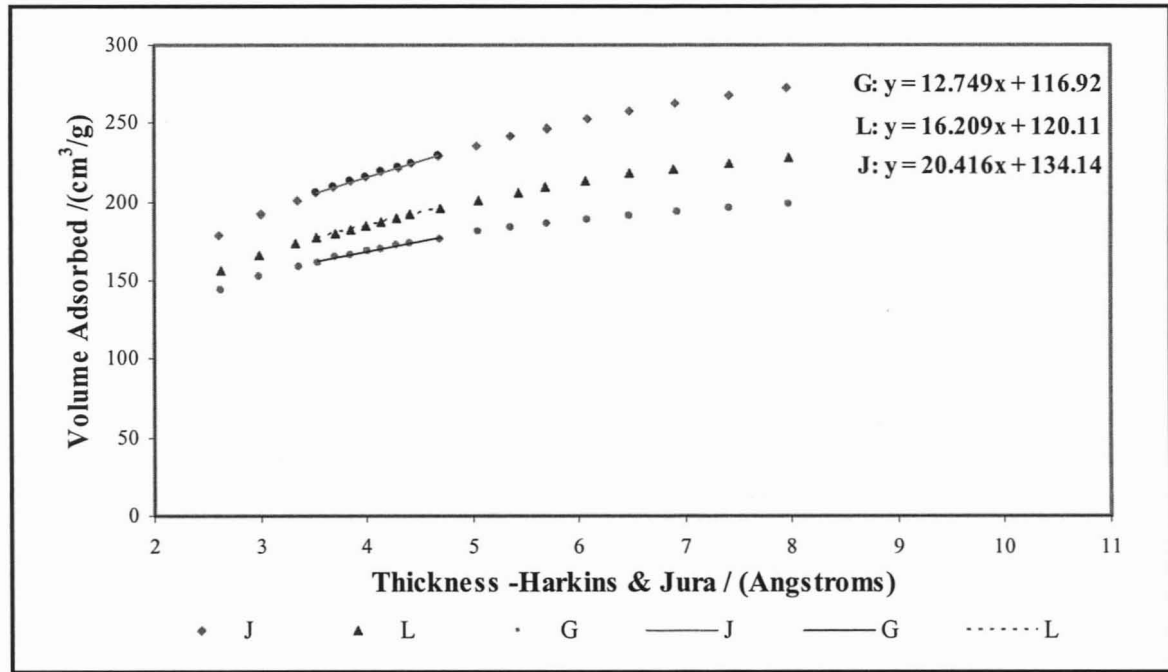
Figure C-10: t -plots to determine external surface area and micropore volume for bagasse activated carbons produced at an activation temperature and time of 800 ^{O}C and 4 hours at varying steam/nitrogen ratios: J – 1:0.6, L – 0.5:0.5 & G – 0.4:1

C-2.1.3 Meso-macropore size distributions
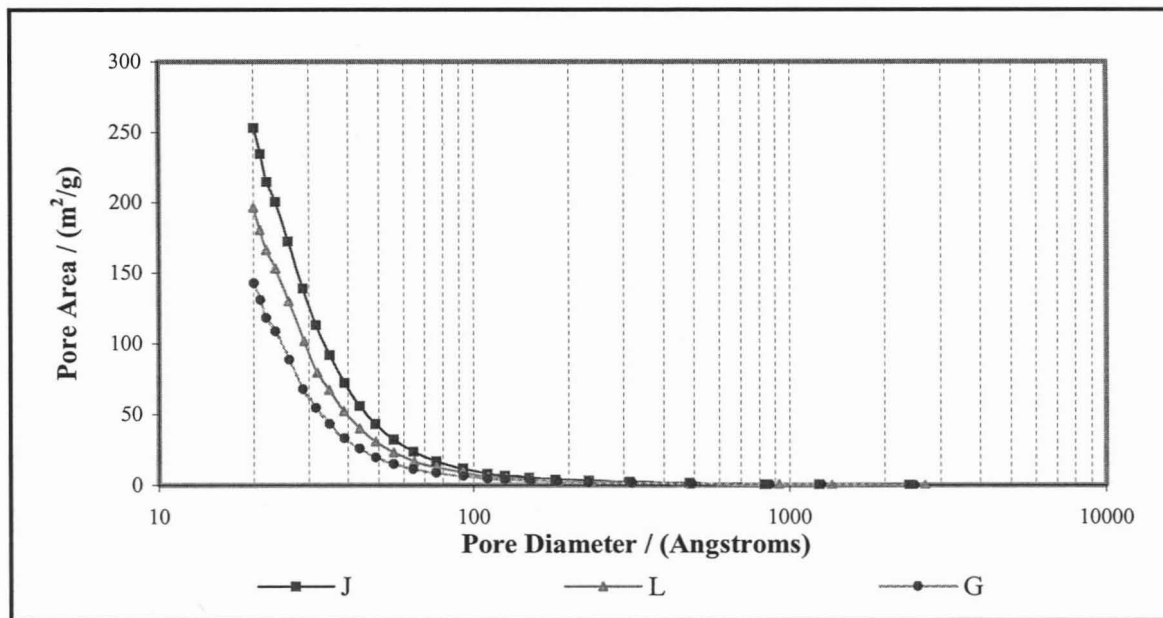
Figure C-11: BJH adsorption plots of cumulative pore area versus pore diameter for bagasse activated carbons produced at an activation temperature and time of 800 ^{O}C and 4 hours at varying steam/nitrogen ratios: J – 1:0.6, L – 0.5:0.5 & G – 0.4:1.
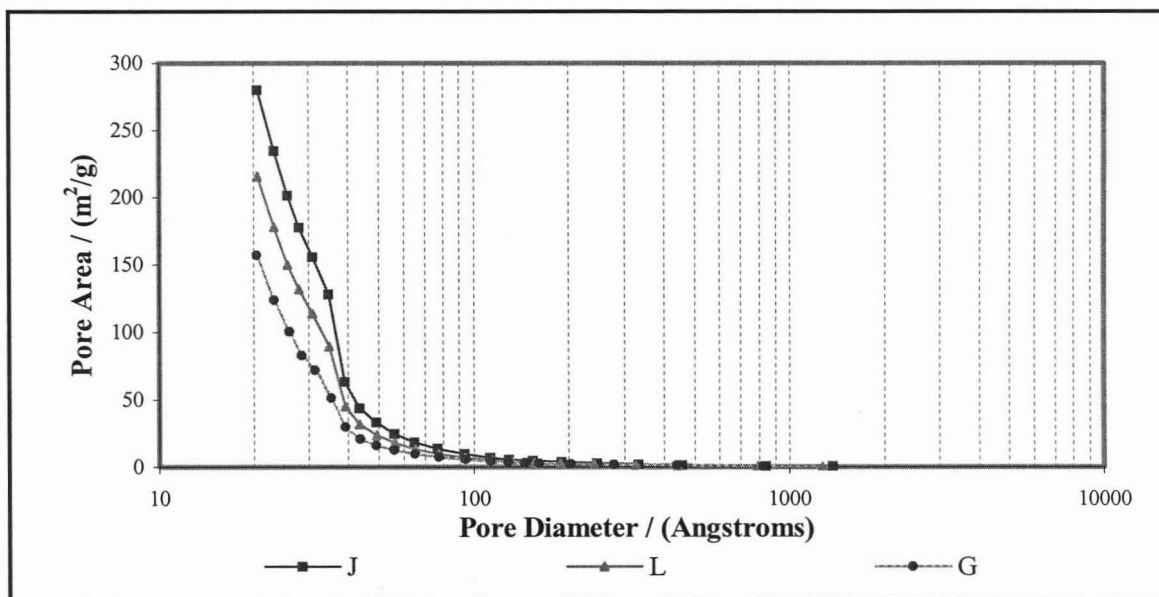
Figure C-12: BJH desorption plots of cumulative pore area versus pore diameter for bagasse activated carbons produced at an activation temperature and time of 800 ^{O}C and 4 hours at varying steam /nitrogen ratios: J – 1:0.6, L – 0.5:0.5 & G – 0.4:1.
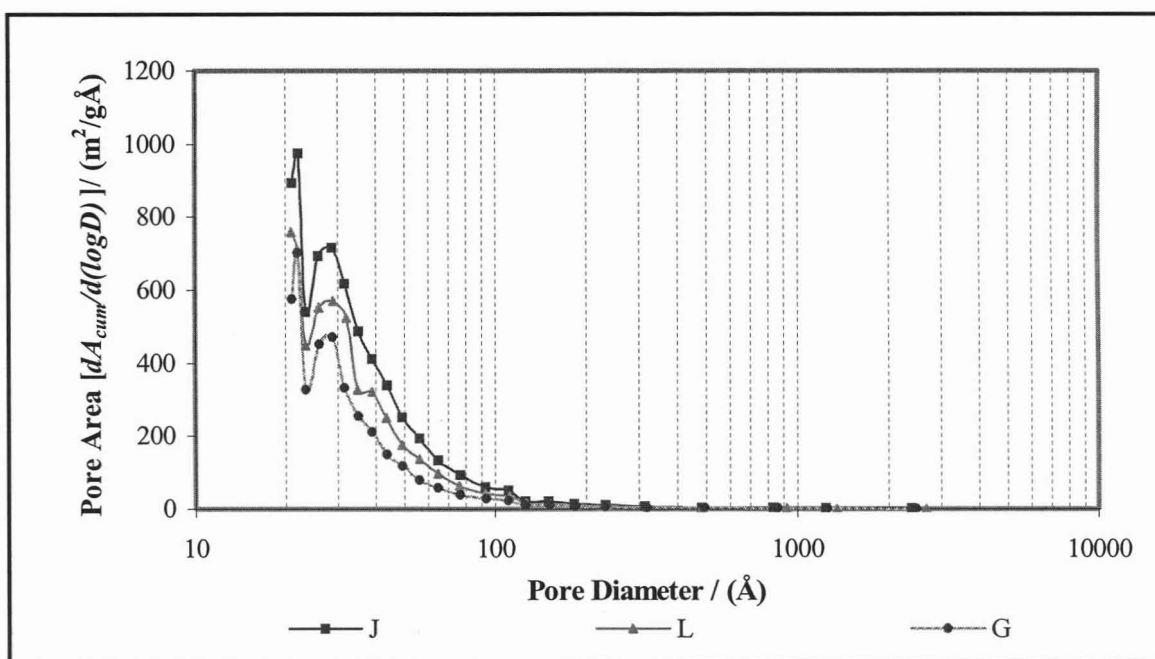
Figure C-13: BJH adsorption plots of pore area ($dA_{cum}/d(logD)$) versus pore diameter for activated carbons produced at an activation temperature and time of 800 ^{O}C and 4 hours at varying steam/nitrogen ratios: J – 1:0.6, L – 0.5:0.5 & G – 0.4:1.
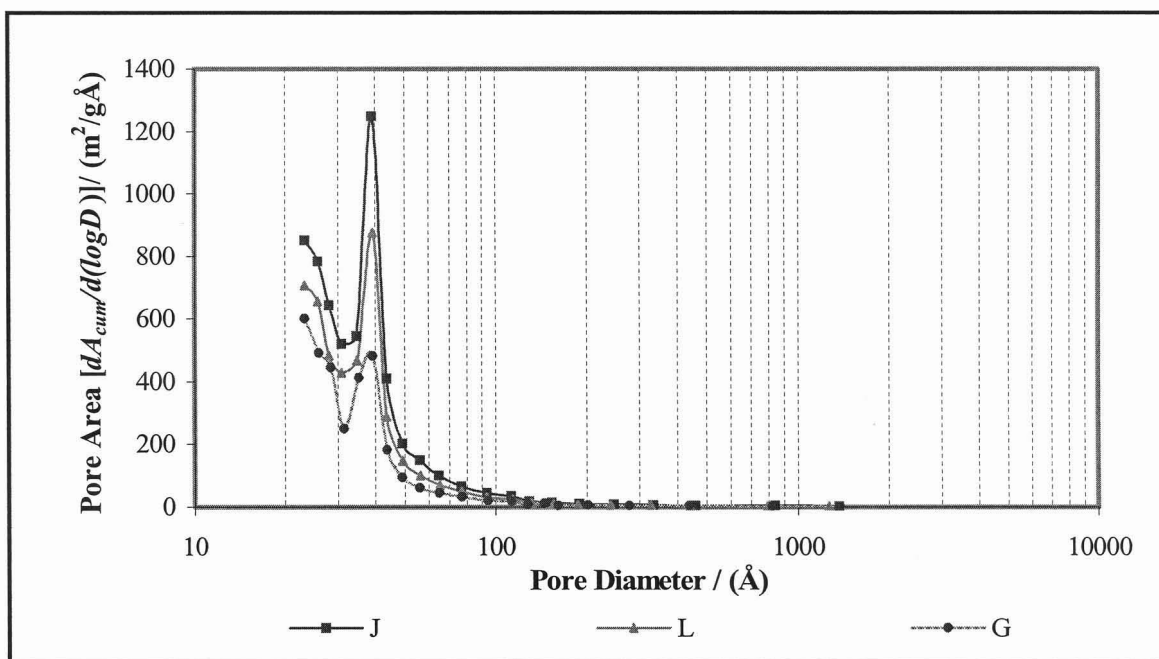
Figure C-14: BJH desorption plots of pore area ($dA_{cum}/d(logD)$) versus pore diameter for activated carbons produced at an activation temperature and time of 800 ^{O}C and 4 hours at varying steam/nitrogen ratios: J – 1:0.6, L – 0.5:0.5 & G – 0.4:1.
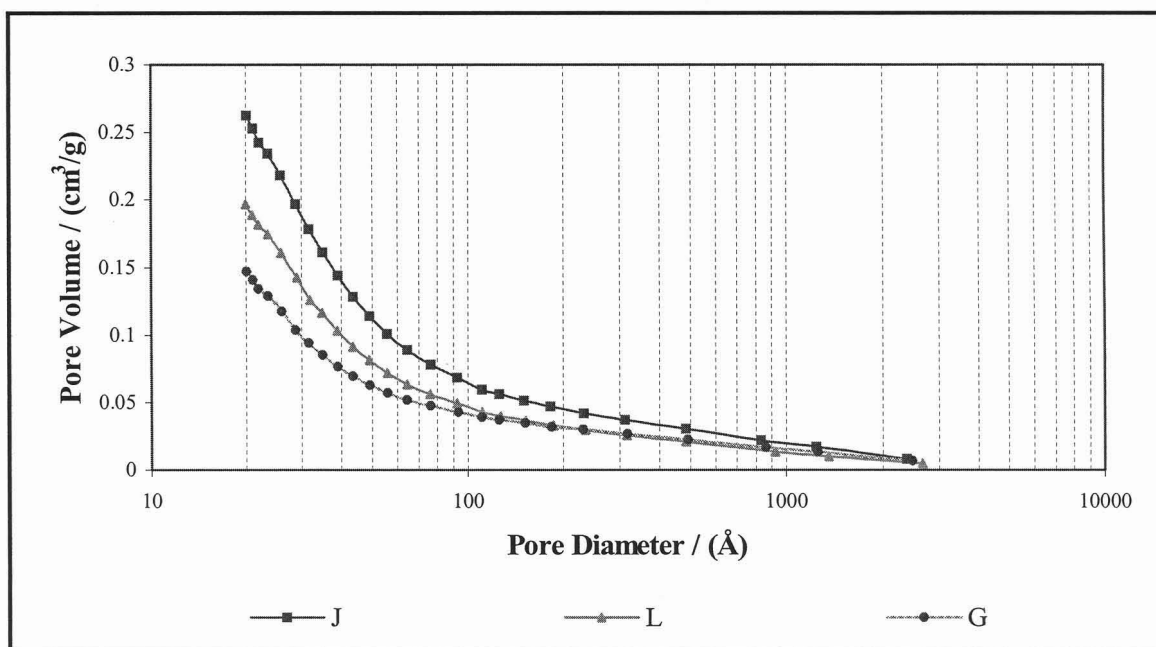
Figure C-15: BJH adsorption plots of cumulative pore volume versus pore diameter for activated carbons produced at an activation temperature and time of 800 ^{O}C and 4 hours at varying steam/ nitrogen ratios: J – 1:0.6, L – 0.5:0.5 & G – 0.4:1.
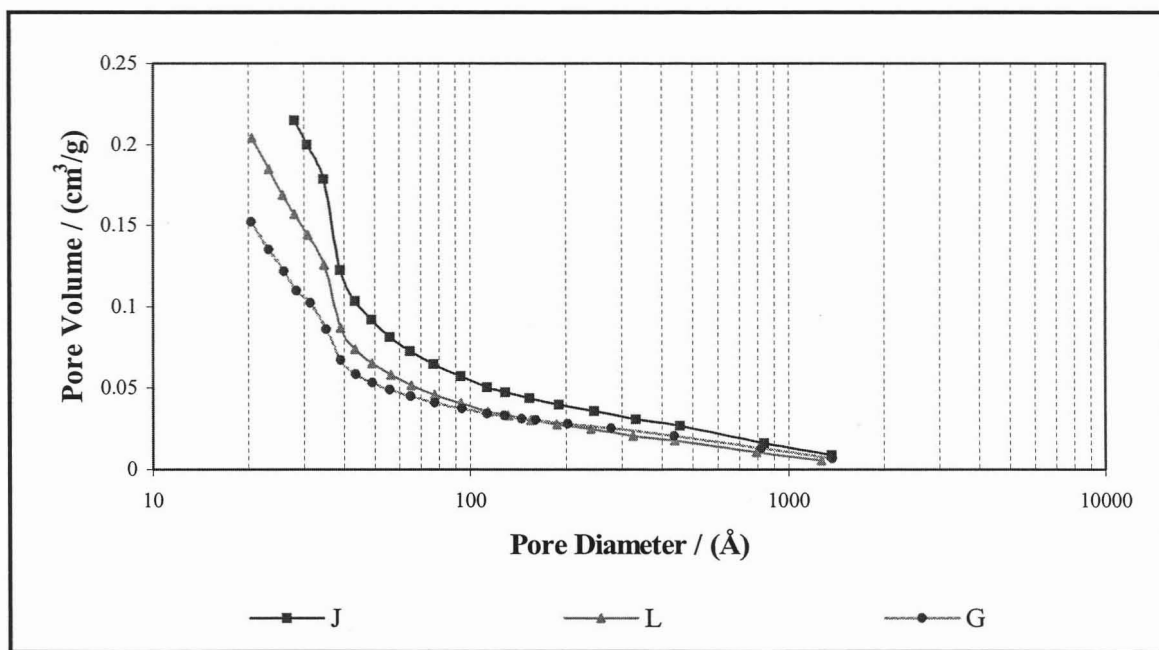
Figure C-16: BJH desorption plots of cumulative pore volume versus pore diameter for activated carbons produced at an activation temperature and time of 800 ^{O}C and 4 hours at varying steam/nitrogen ratios: J – 1:0.6, L – 0.5:0.5 & G – 0.4:1.
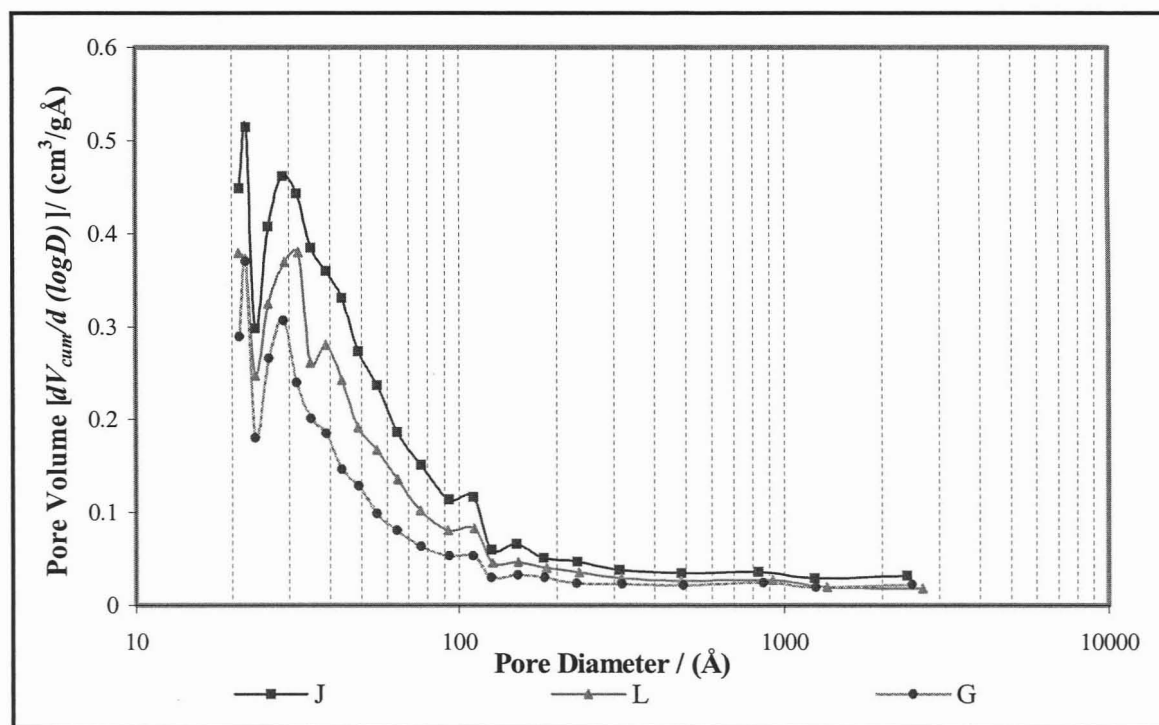
Figure C-17: BJH adsorption plots of pore volume ($dV_{cum}/d(logD)$) versus pore diameter for activated carbons produced at an activation temperature and time of 800 ^{O}C and 4 hours at varying steam/nitrogen ratios: J – 1:0.6, L – 0.5:0.5 & G – 0.4:1.

Figure C-18: BJH desorption plots of pore volume ($dV_{cum}/d(logD)$) versus pore diameter for activated carbons produced at an activation temperature and time of 800 ^{O}C and 4 hours at varying steam steam/nitrogen ratios: J – 1:0.6, L – 0.5:0.5 & G – 0.4:1.

C-2.2 Effect of Pyrolysis Exposure Time and Activation Time on the final Activated Carbon

C-2.2.1. Total Surface Area
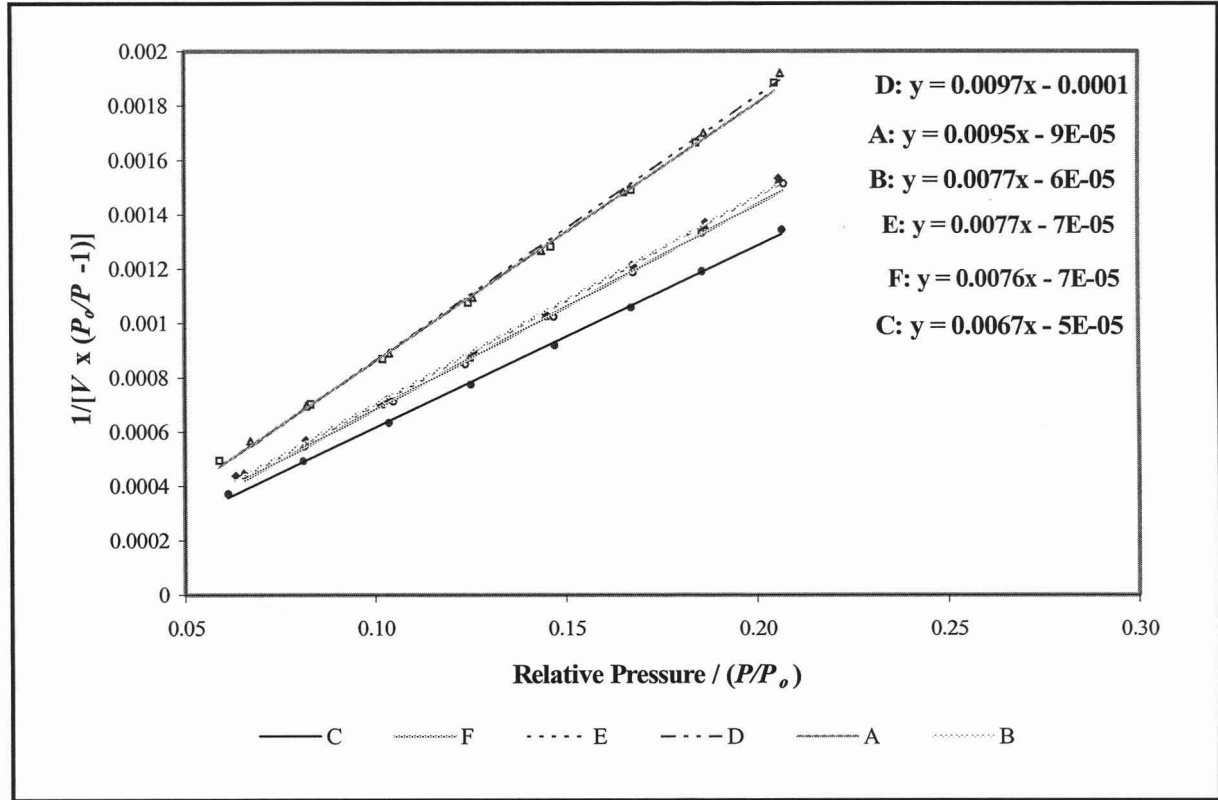
Figure C-19: BET surface area plots for bagasse activated carbons produced at an varying pyrolysis exposure times and activation times (□)A – pyrolysis time 1hr, activation time 1hr,(♦)B - pyrolysis time 1hr, activation time 3hr, (●)C - pyrolysis time 1hr, activation time 4hr, (Δ)D -pyrolysis time 2hr, activation time 1hr, (▲)E - pyrolysis time 1hr, activation time 3hr, (o)F -pyrolysis time 1hr, activation time 1hr.
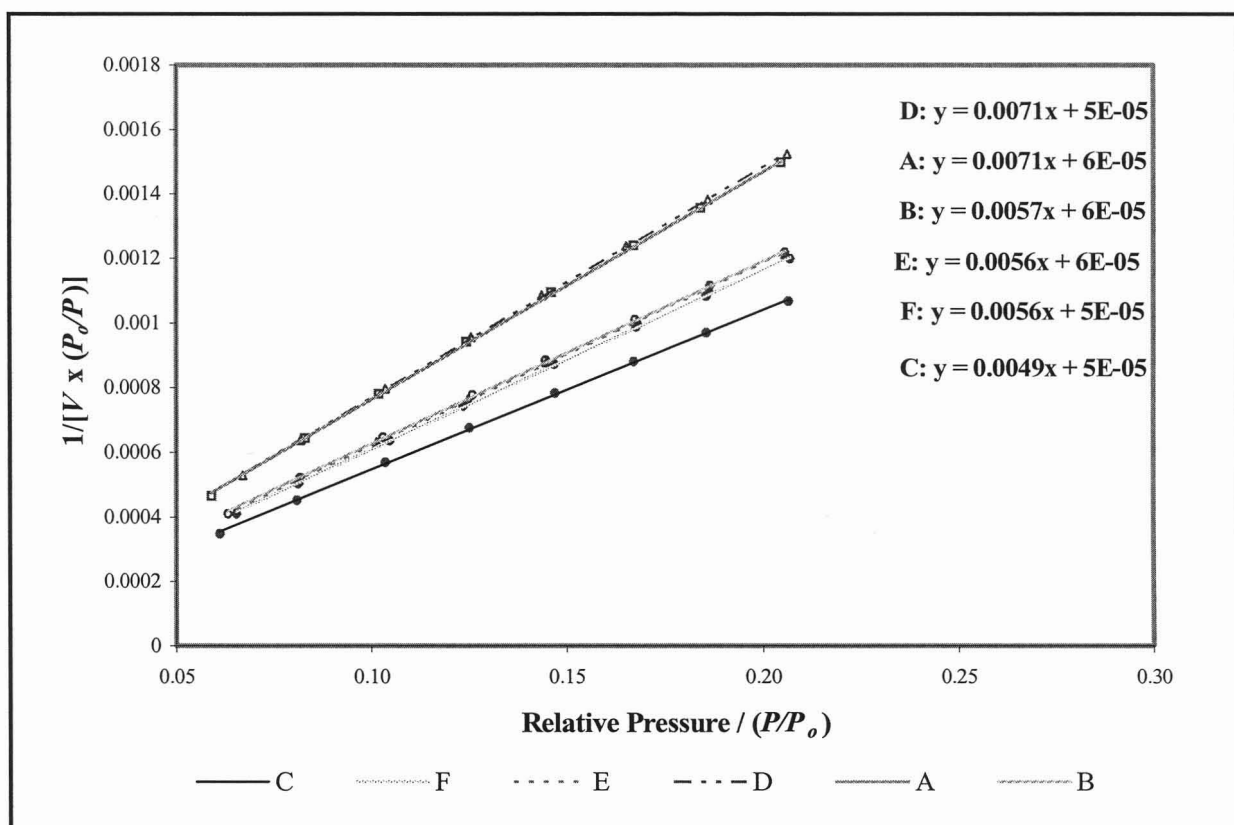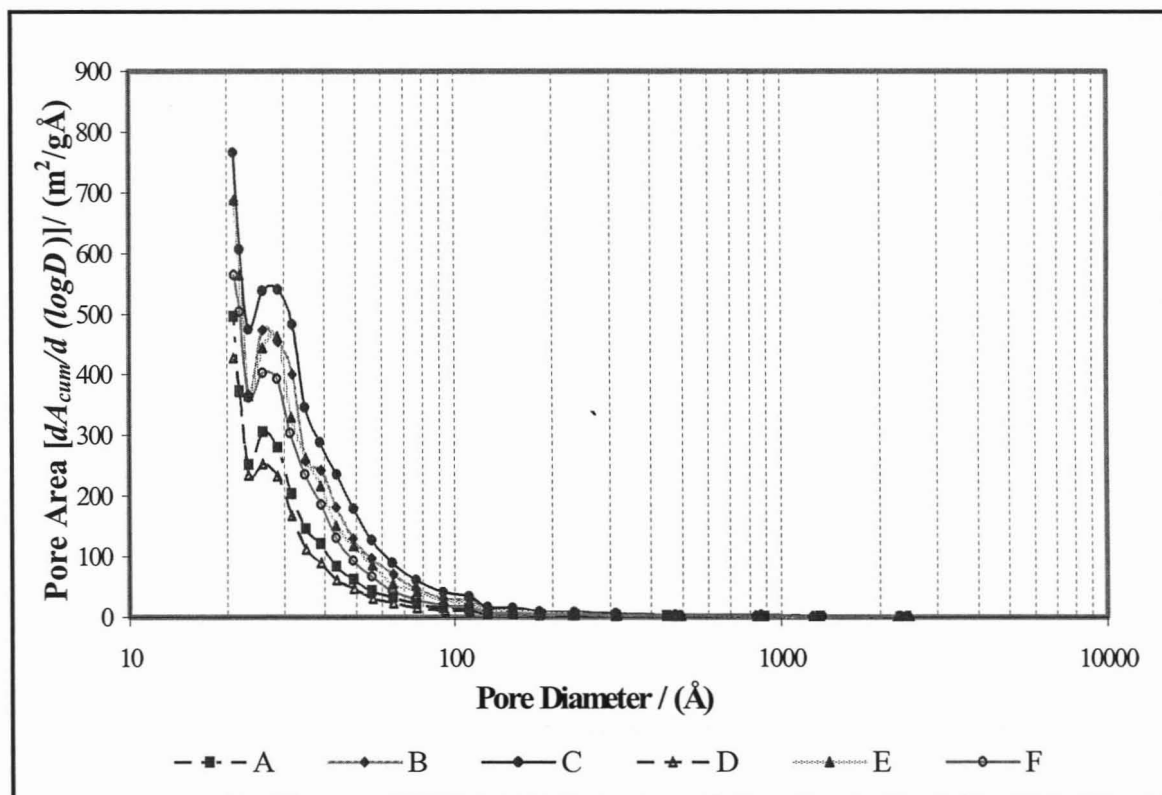
Figure C-20: Langmuir surface area plots for bagasse activated carbons produced at an varying pyrolysis exposure times and activation times (□)A – pyrolysis time 1hr, activation time 1hr,(♦)B - pyrolysis time 1hr, activation time 3hr, (●)C - pyrolysis time 1hr, activation time 4hr, (Δ)D -pyrolysis time 2hr, activation time 1hr, (▲)E - pyrolysis time 1hr, activation time 3hr, (o)F -pyrolysis time 1hr, activation time 1hr.

C-2.2.2. External Surface Area, Micropore Area and Micropore Volume

C: $y = 15.778x + 124.19$
F: $y = 11.487x + 122.13$
E: $y = 12.701x + 113.94$
B: $y = 13.321x + 110.4$
A: $y = 8.5644x + 99.081$
D: $y = 7.5326x + 102.24$
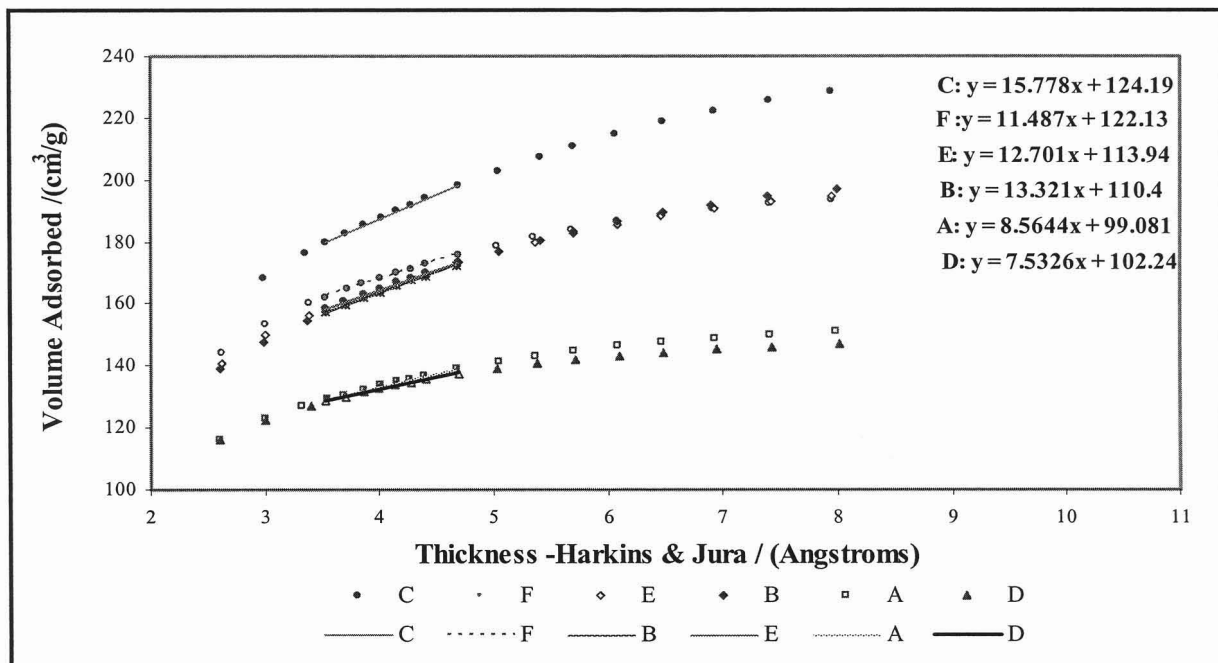
Figure C-21: t-plots to determine external surface area and micropore volume for bagasse activated carbons produced at an varying pyrolysis exposure times and activation times, A – pyrolysis time 1hr, activation time 1hr, B - pyrolysis time 1hr, activation time 3hr, C - pyrolysis time 1hr, activation time 4hr, D -pyrolysis time 2hr, activation time 1hr, E - pyrolysis time 1hr, activation time 3hr, F -pyrolysis time 1hr, activation time 1hr.
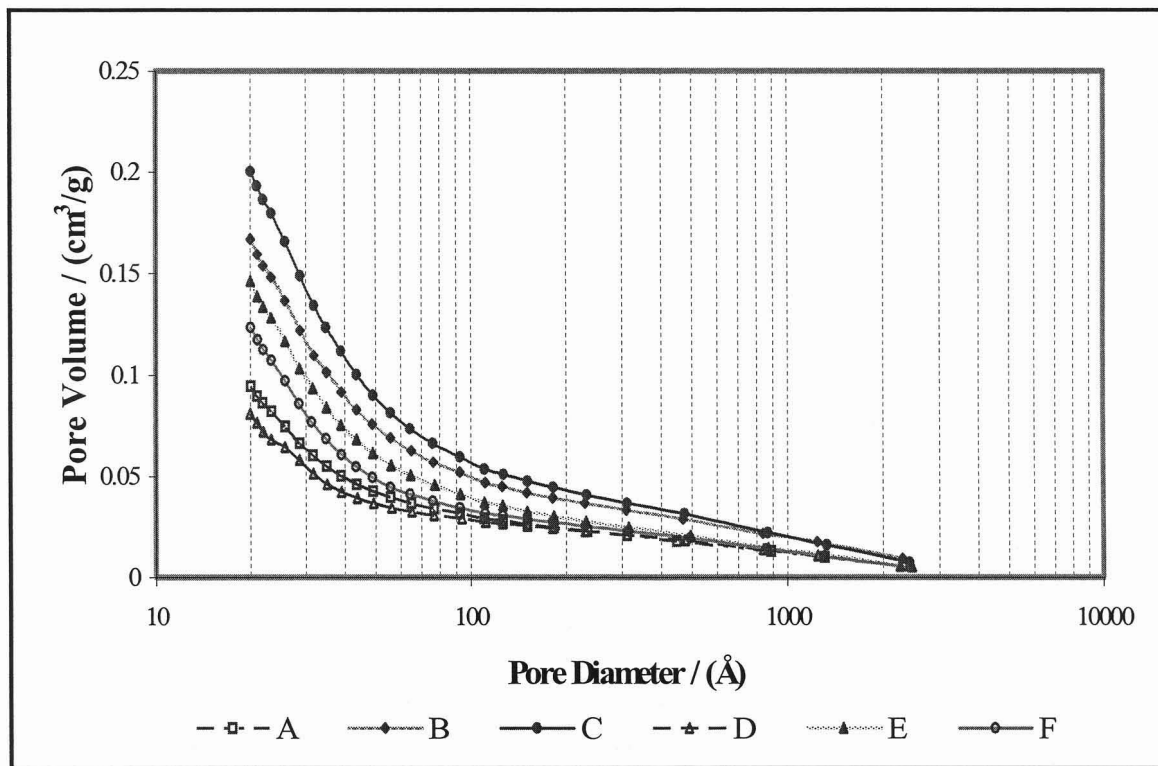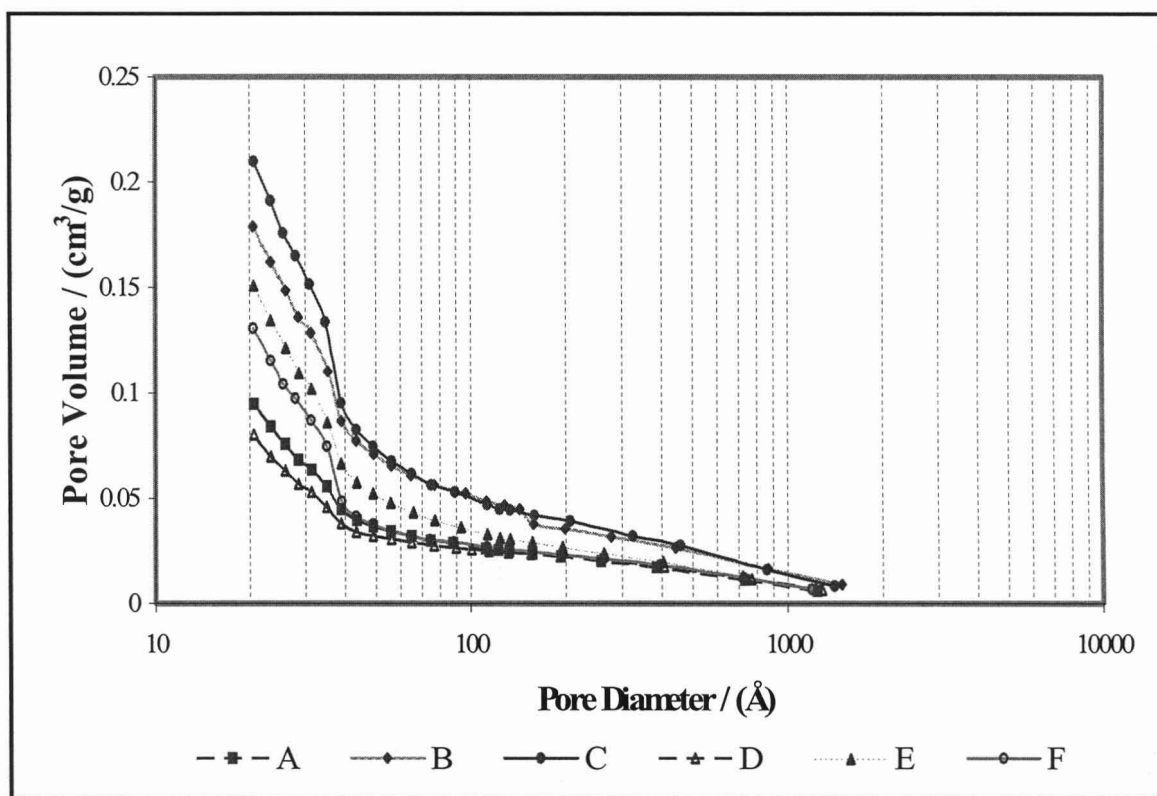
C-2.2.3 Meso-macropore size distributions
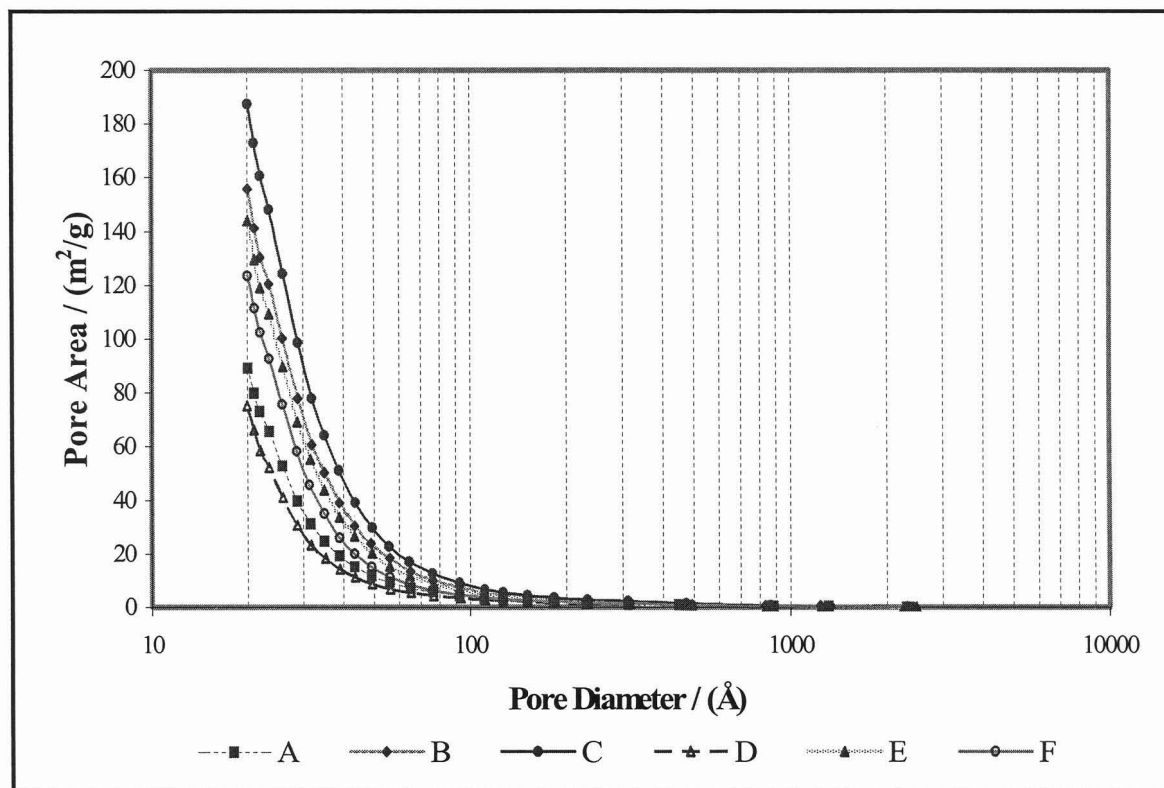
Figure C-22: BJH adsorption plots of cumulative pore area versus pore diameter for bagasse activated carbons produced at an varying pyrolysis exposure times and activation times A – pyrolysis time 1hr, activation time 1hr, B - pyrolysis time 1hr, activation time 3hr, C - pyrolysis time 1hr, activation time 4hr, D -pyrolysis time 2hr, activation time 1hr, E - pyrolysis time 1hr, activation time 3hr, F -pyrolysis time 1hr, activation time 1hr
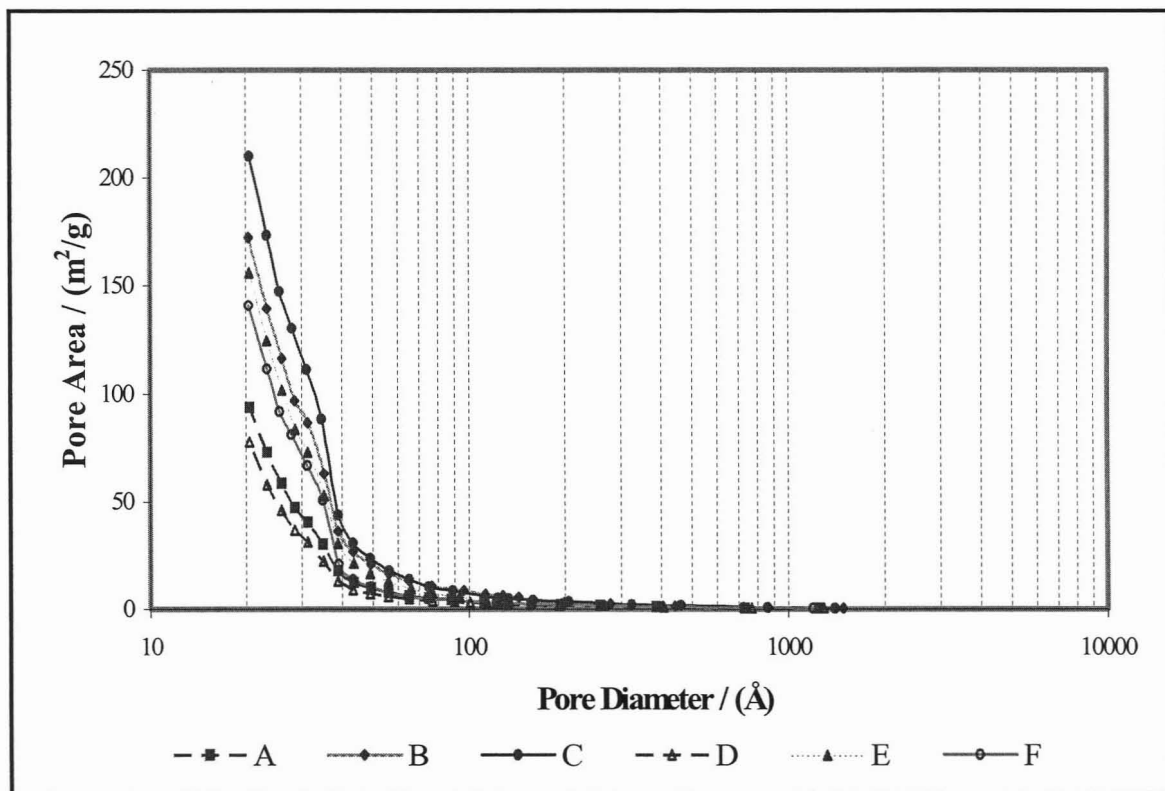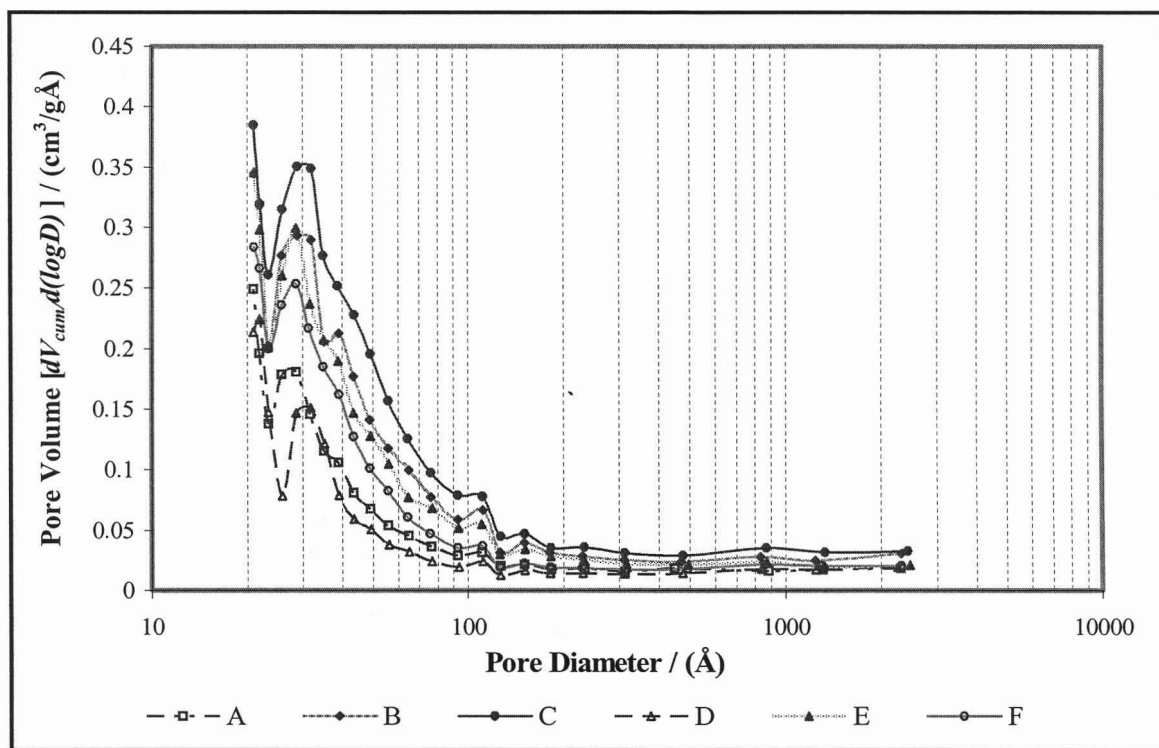
Figure C-23: BJH desorption plots of cumulative pore area versus pore diameter for bagasse activated carbons produced at an varying pyrolysis exposure times and activation times A – pyrolysis time 1hr, activation time 1hr, B - pyrolysis time 1hr, activation time 3hr, C - pyrolysis time 1hr, activation time 4hr, D -pyrolysis time 2hr, activation time 1hr, E - pyrolysis time 1hr, activation time 3hr, F -pyrolysis time 1hr, activation time 1hr

Figure C-24: BJH adsorption plots of pore area ($dA_{cum}/d(logD)$)   versus pore diameter for bagasse activated carbons produced at an varying pyrolysis exposure times and activation times A – pyrolysis time 1hr, activation time 1hr, B - pyrolysis time 1hr, activation time 3hr, C - pyrolysis time 1hr, activation time 4hr, D -pyrolysis time 2hr, activation time 1hr, E - pyrolysis time 1hr, activation time 3hr, F -pyrolysis time 1hr, activation time 1hr.
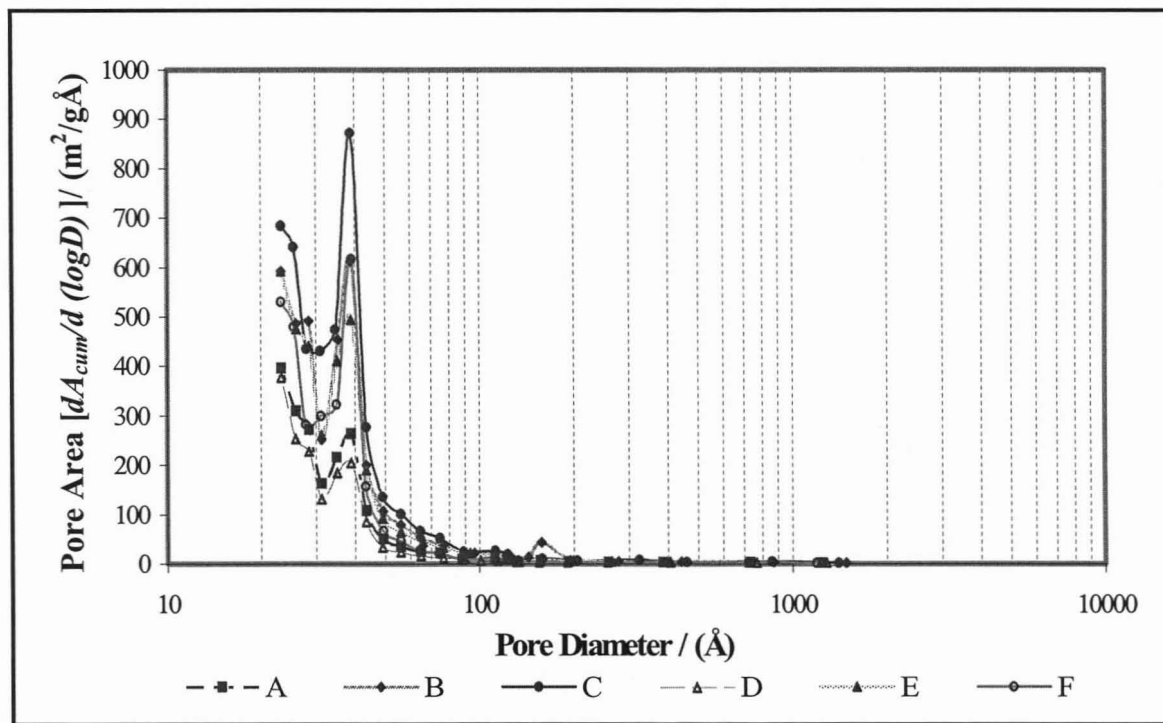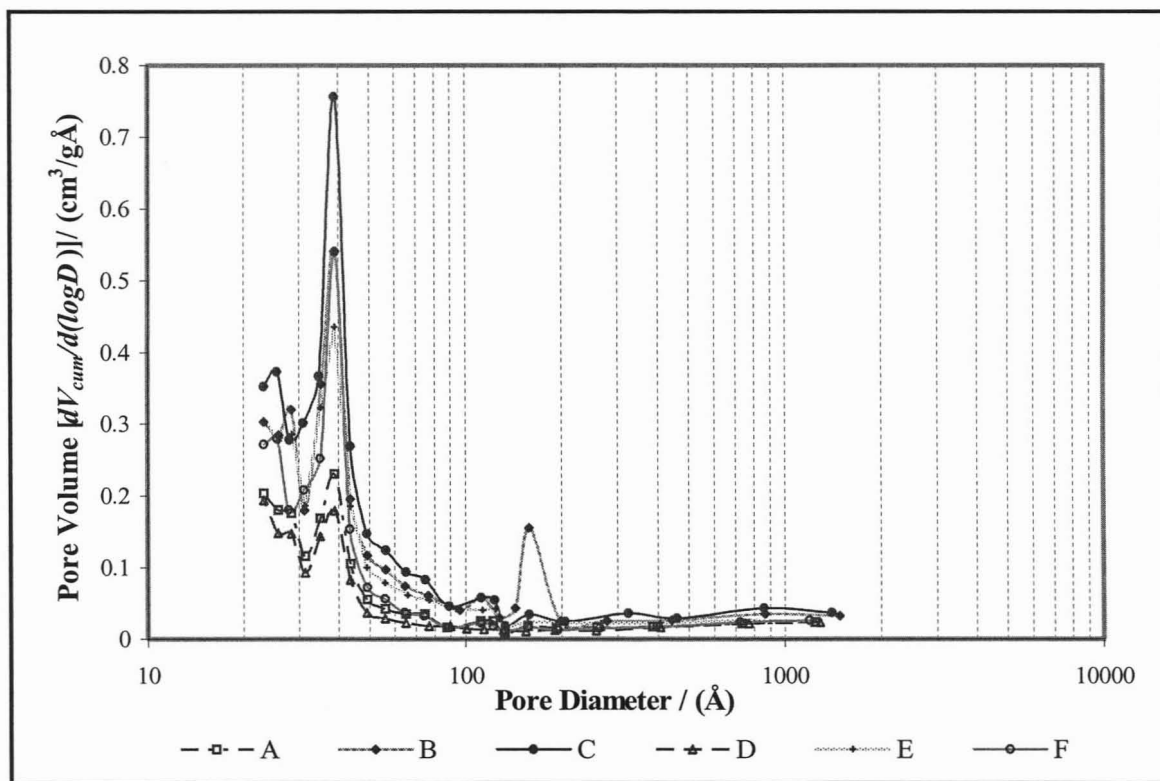
Figure C-25: BJH desorption plots of pore area ($dA_{cum}/d(logD)$) versus pore diameter for bagasse activated carbons produced at an varying pyrolysis exposure times and activation times A – pyrolysis time 1hr, activation time 1hr, B - pyrolysis time 1hr, activation time 3hr, C - pyrolysis time 1hr, activation time 4hr, D -pyrolysis time 2hr, activation time 1hr, E - pyrolysis time 1hr, activation time 3hr, F -pyrolysis time 1hr, activation time 1hr

Figure C-26: BJH adsorption plots of cumulative pore volume versus pore diameter for bagasse activated carbons produced at an varying pyrolysis exposure times and activation times A – pyrolysis time 1hr, activation time 1hr, B - pyrolysis time 1hr, activation time 3hr, C - pyrolysis time 1hr, activation time 4hr, D -pyrolysis time 2hr, activation time 1hr, E - pyrolysis time 1hr, activation time 3hr, F -pyrolysis time 1hr, activation time 1hr

Figure C-27: BJH desorption plots of pore volume versus pore diameter for bagasse activated carbons produced at an varying pyrolysis exposure times and activation times A – pyrolysis time 1hr, activation time 1hr, B - pyrolysis time 1hr, activation time 3hr, C - pyrolysis time 1hr, activation time 4hr, D -pyrolysis time 2hr, activation time 1hr, E - pyrolysis time 1hr, activation time 3hr, F -pyrolysis time 1hr, activation time 1hr

Figure C-28: BJH adsorption plots of pore volume ($dV_{cum}/d(logD)$) versus pore diameter for bagasse activated carbons produced at an varying pyrolysis exposure times and activation times   A – pyrolysis time 1hr, activation time 1hr, B - pyrolysis time 1hr, activation time 3hr, C - pyrolysis time 1hr, activation time 4hr, D -pyrolysis time 2hr, activation time 1hr, E - pyrolysis time 1hr, activation time 3hr, F -pyrolysis time 1hr, activation time 1hr.

Figure C-29: BJH desorption plots of pore volume ($dV_{cum}/d(logD)$) versus pore diameter for bagasse activated carbons produced at an varying pyrolysis exposure times and activation times   A – pyrolysis time 1hr, activation time 1hr, B - pyrolysis time 1hr, activation time 3hr, C - pyrolysis time 1hr, activation time 4hr, D -pyrolysis time 2hr, activation time 1hr, E - pyrolysis time 1hr, activation time 3hr, F -pyrolysis time 1hr, activation time 1hr.

C-2.3 Effect of Activation Temperature on the final Activated Carbon

C-2.3.1. Total Surface Area
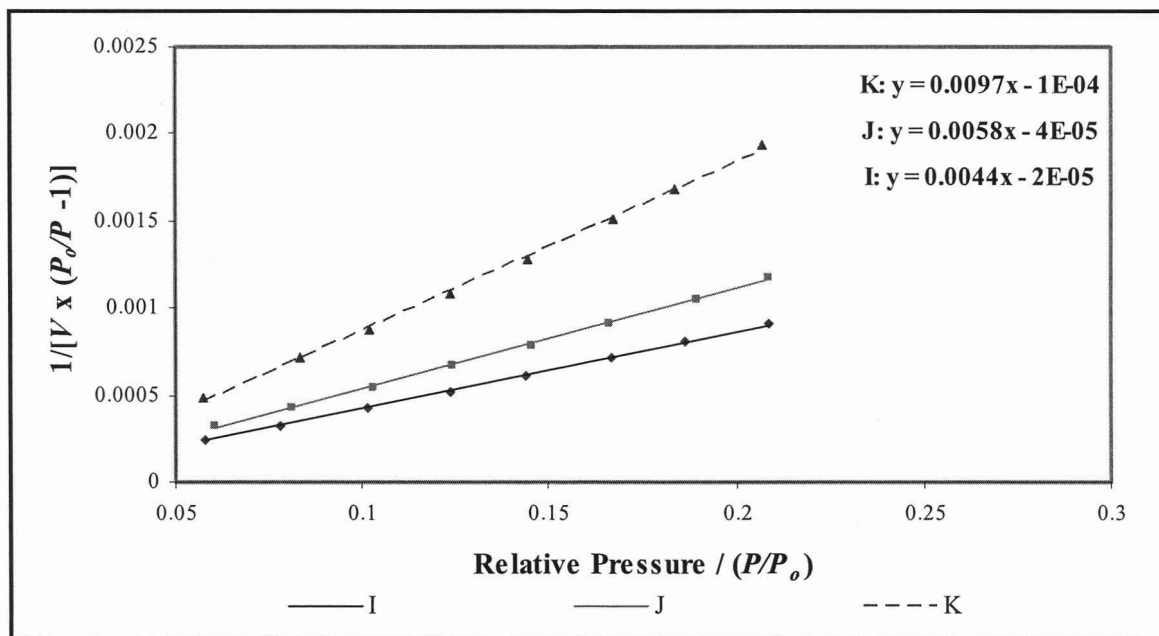
Figure C-30: BET surface area plots for bagasse activated carbons, at steam/nitrogen ratios of 1:0.6 & varying activation temperatures, (♦)I – 900 ^{O}C, 2hr, (■)J – 800 ^{O}C, 4hr & (▲)K – 700 ^{O}C, 4hr.
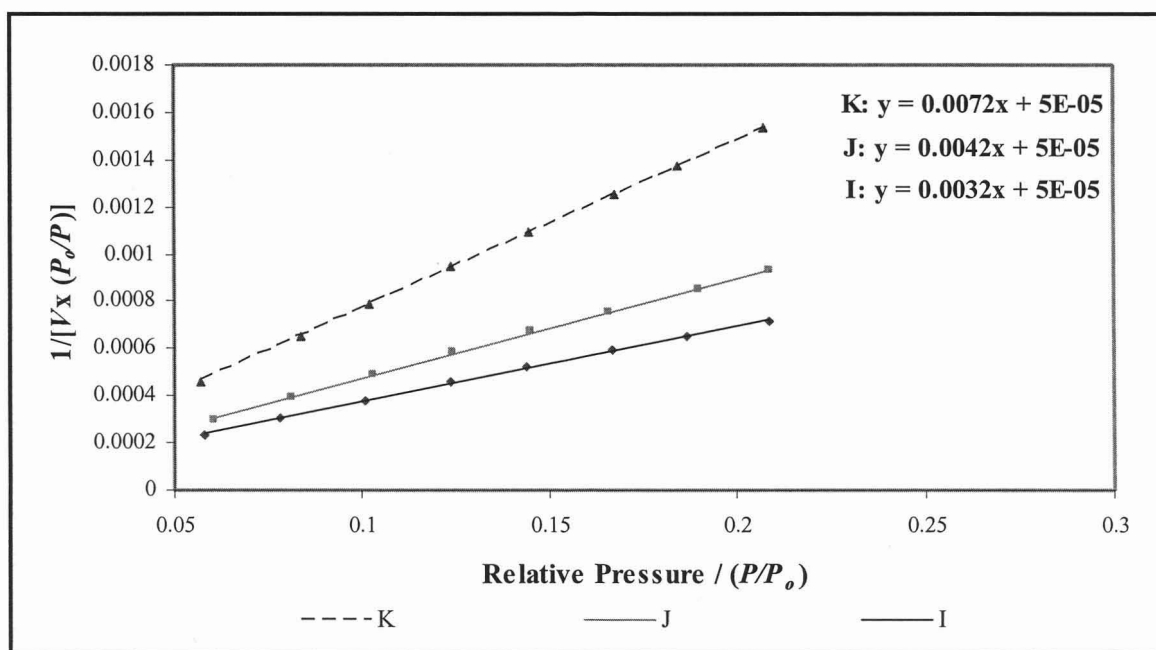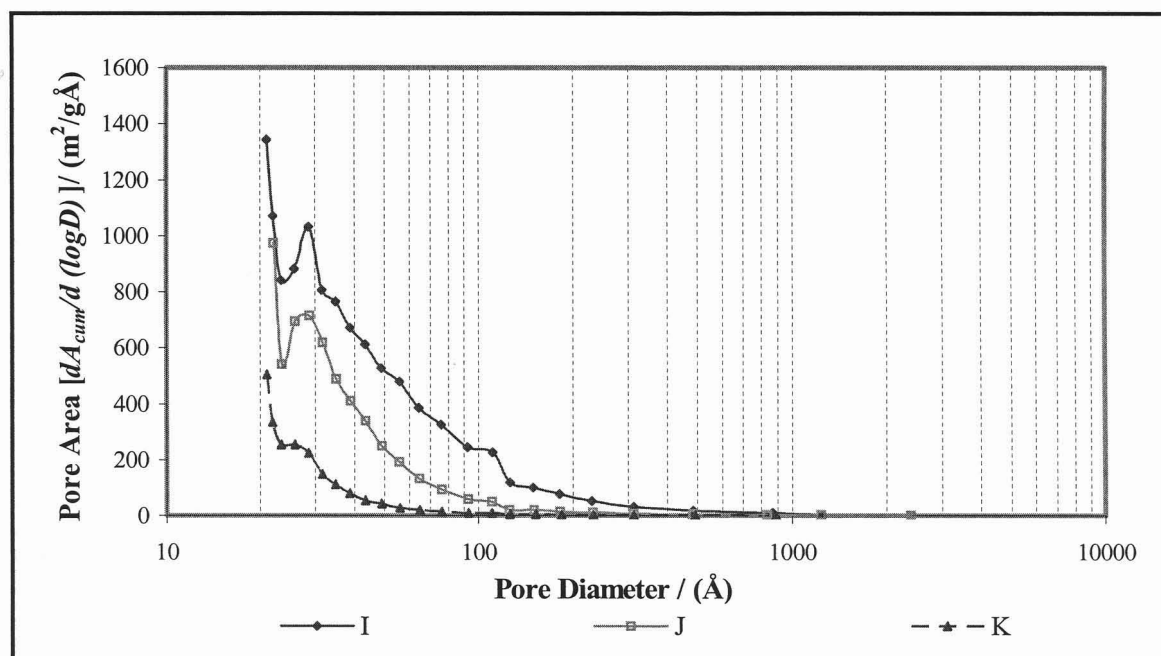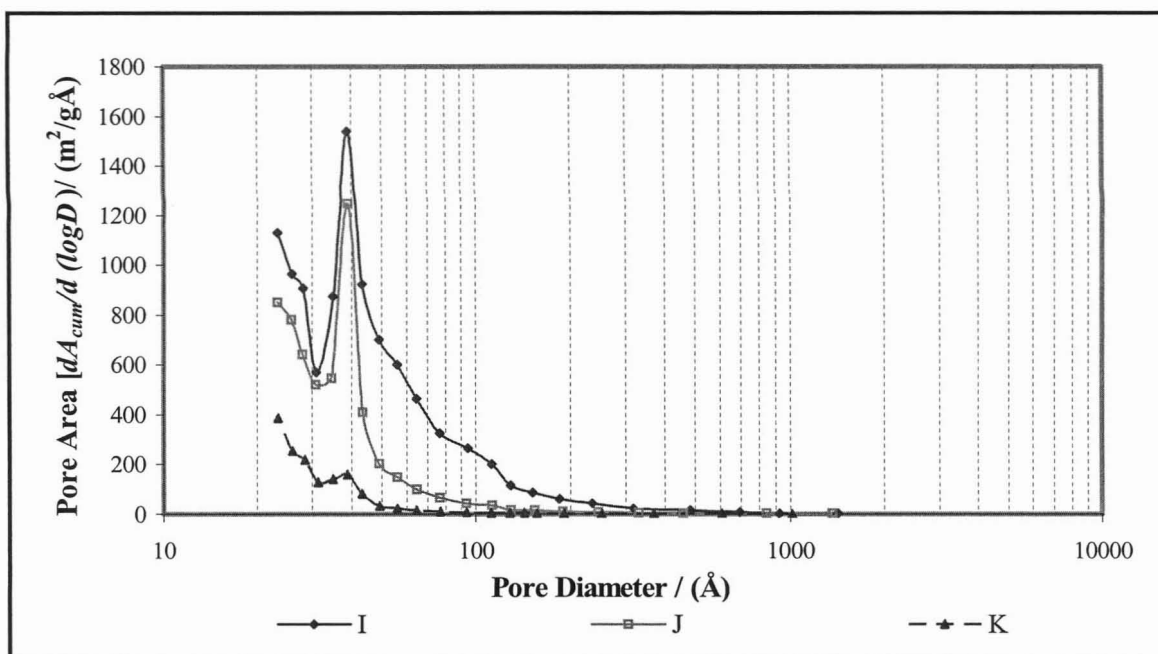

Figure C-31: Langmuir surface area plots for bagasse activated carbons, at steam/nitrogen ratios of 1:0.6 & varying activation temperatures, (♦)I – 900 ^{O}C, 2hr, (■)J – 800 ^{O}C, 4hr & (▲)K – 700 ^{O}C, 4hr.

C-2.3.2. External Surface Area, Micropore Area and Micropore Volume
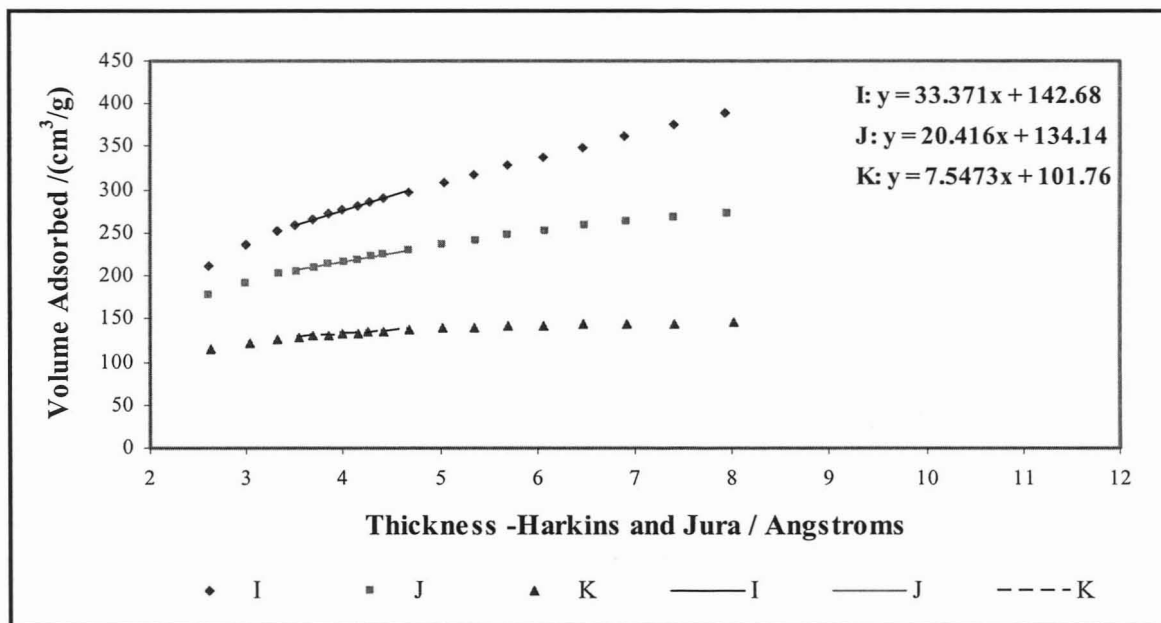
Figure C-32: t- plots to determine external surface area and micropore volume for bagasse activated carbons, at steam/nitrogen ratios OF 1:0.6 & varying activation temperatures, I – 900 ^{O}C, 2hr, J – 800 ^{O}C, 4hr & K – 700 ^{O}C, 4hr.
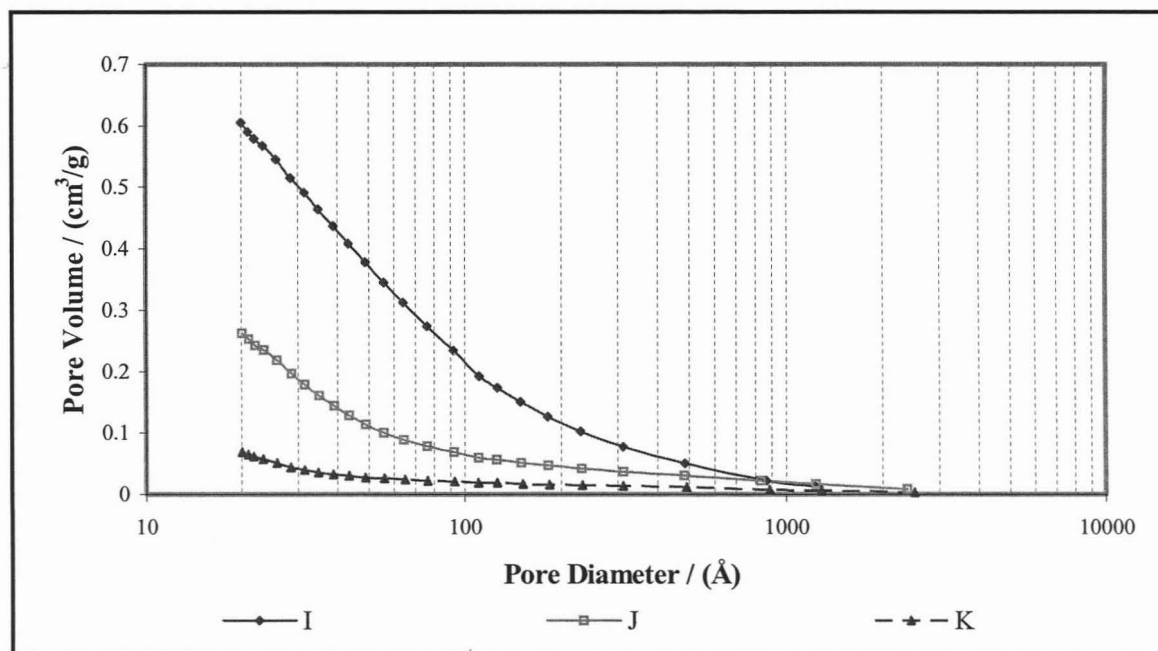
C-2.3.3. Meso-macropore size distributions
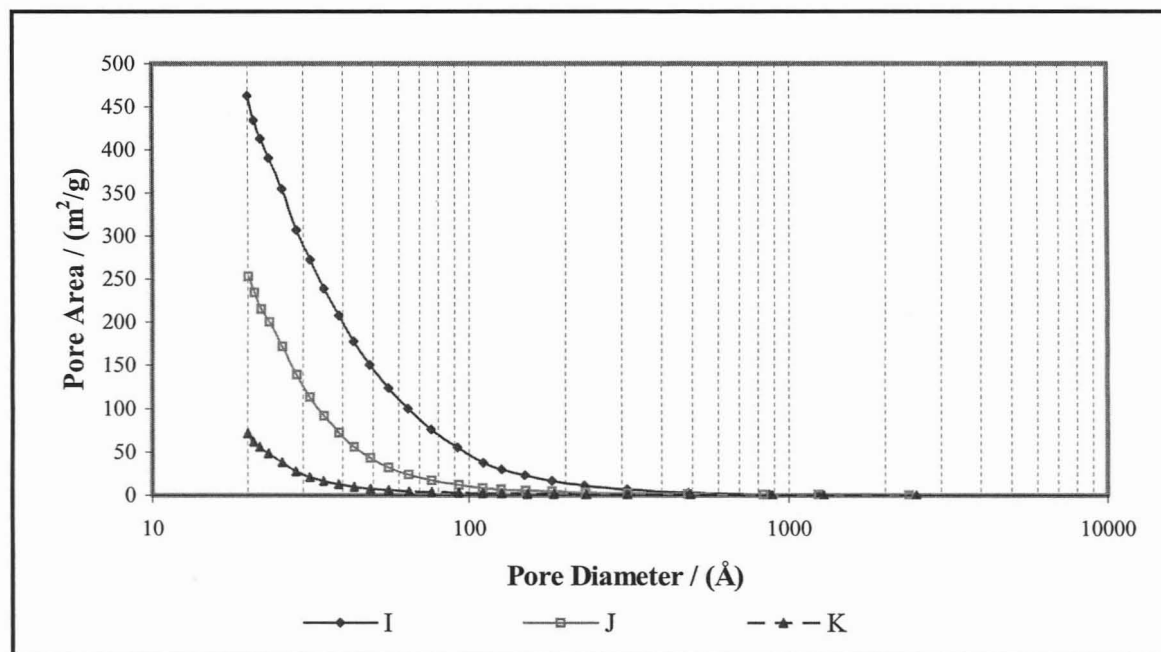
Figure C-33: BJH adsorption plots of cumulative pore area versus pore diameter for bagasse activated carbons, at steam/nitrogen ratios of 1:0.6 & varying activation temperatures, I – 900 ^{O}C, 2hr, J – 800 ^{O}C, 4hr & K – 700 ^{O}C, 4hr.
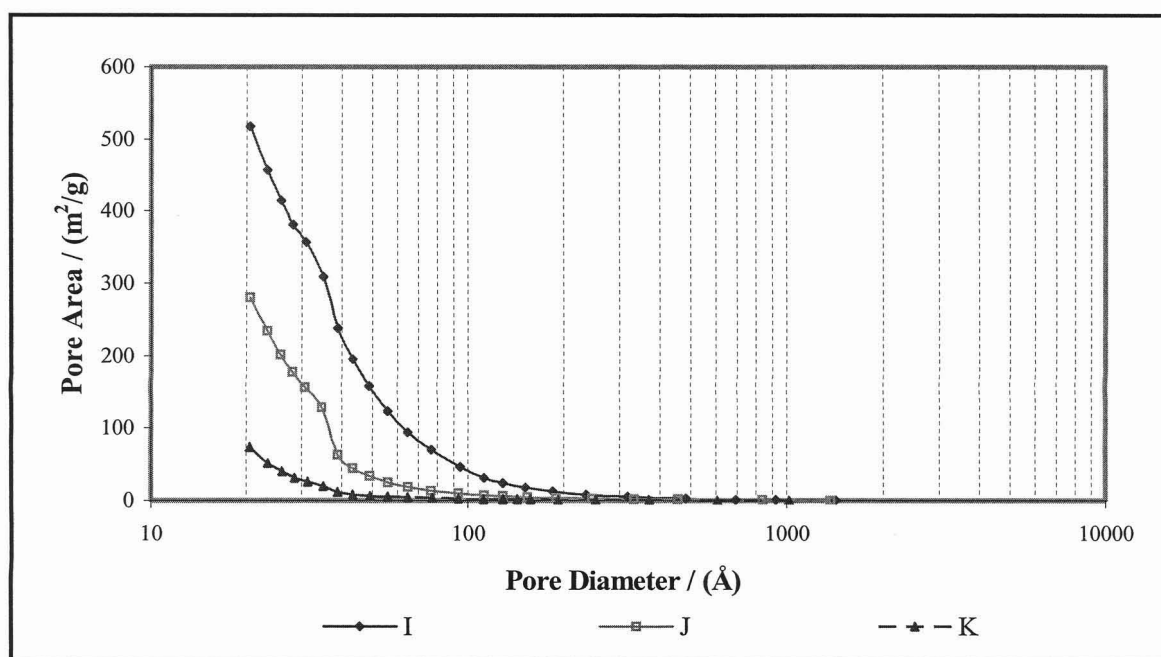
Figure C-34: BJH desorption plots of cumulative pore area versus pore diameter for bagasse activated carbons, at steam/nitrogen ratios of 1:0.6 & varying activation temperatures, I – 900 °C, 2hr, J – 800 °C, 4hr & K – 700 °C, 4hr.
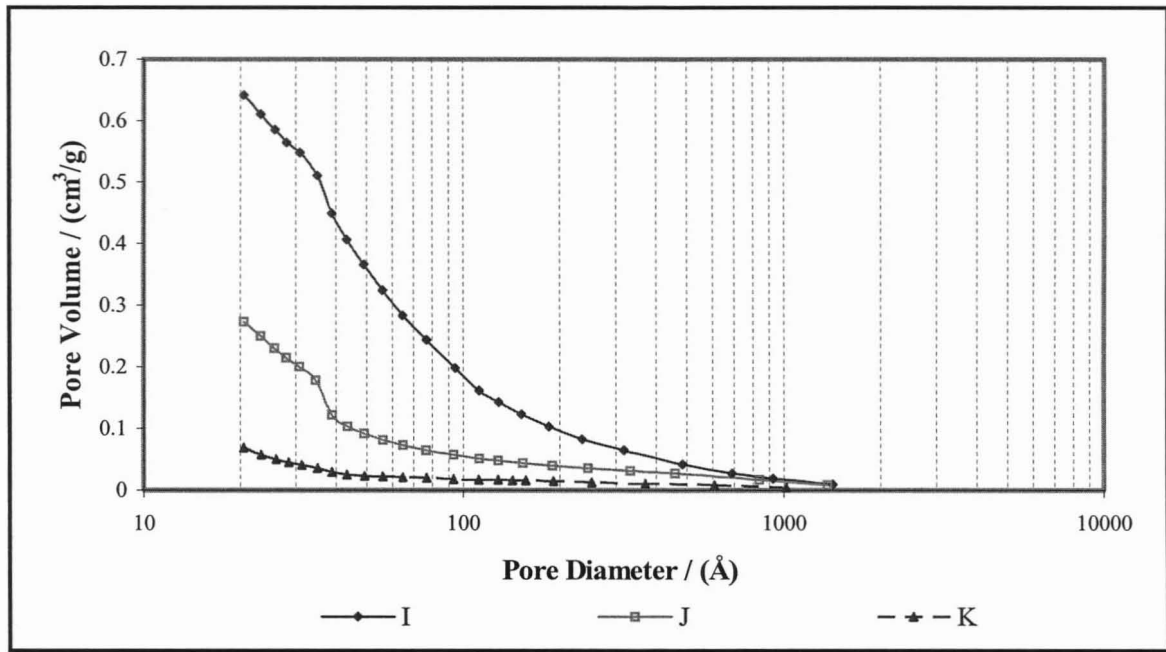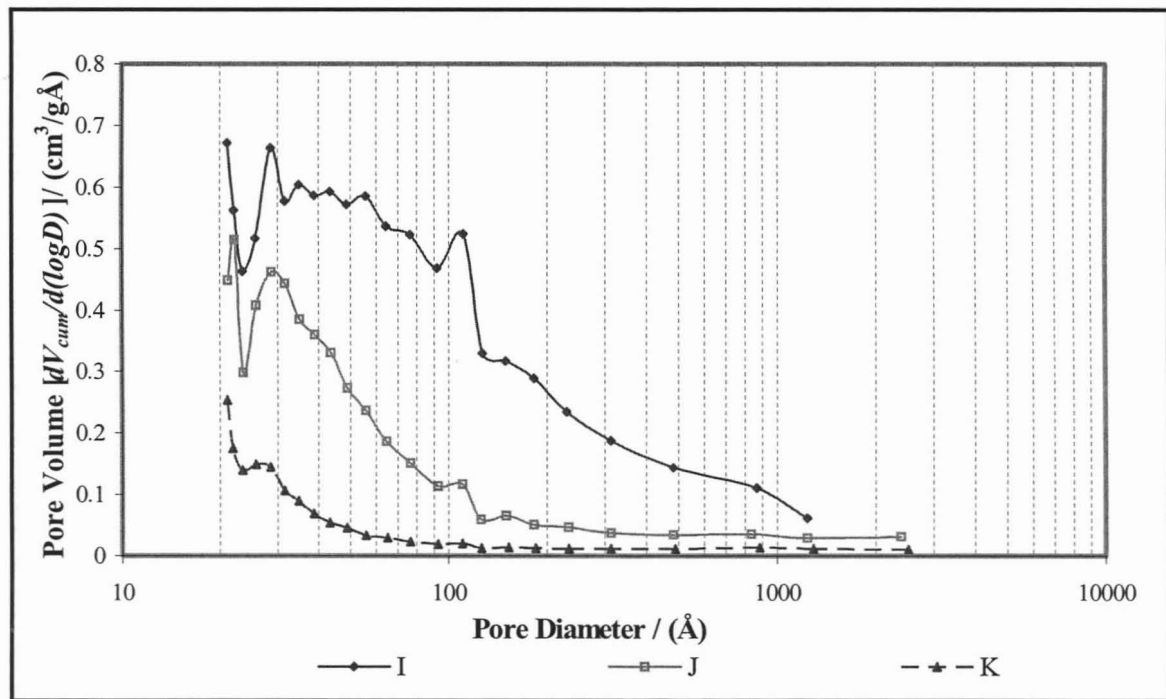

Figure C-35: BJH adsorption plots of pore area ($dA_{cum}/d(logD)$) versus pore diameter for bagasse activated carbons, at steam/nitrogen ratios of 1:0.6 & varying activation temperatures, I – 900 °C, 2hr, J – 800 °C, 4hr & K – 700 °C, 4hr.
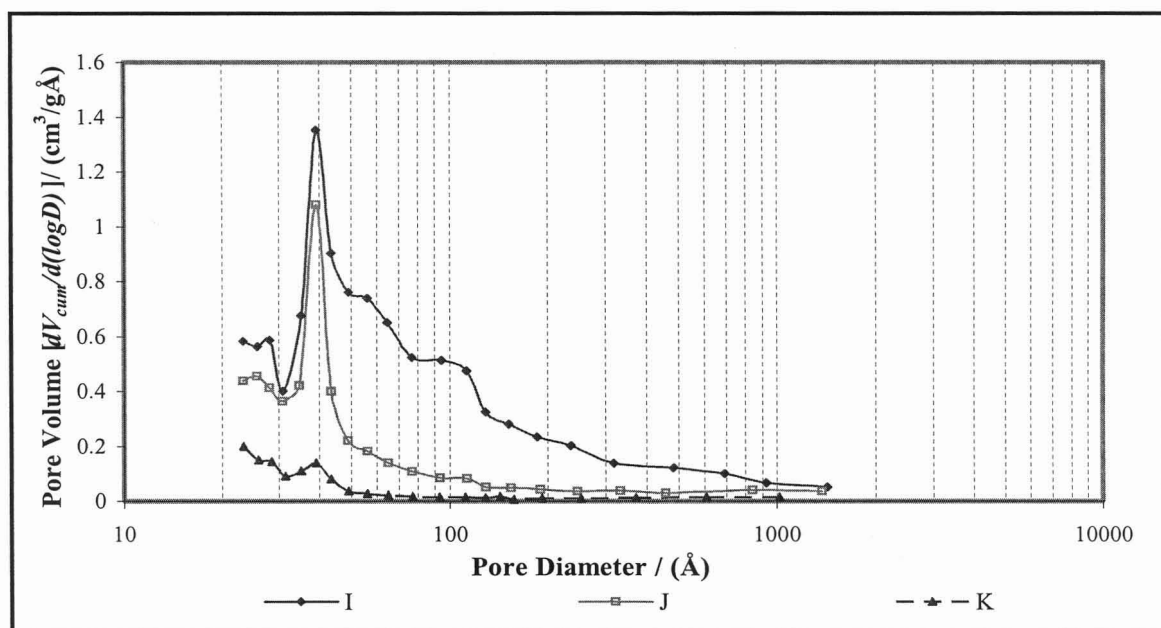
Figure C-36: BJH desorption plots of pore area ($dA_{cum}/d(logD)$)   versus pore diameter for bagasse activated carbons, at steam/nitrogen ratios of 1:0.6 & varying activation temperatures, I – 900 °C, 2hr, J – 800 °C, 4hr & K – 700 °C, 4hr.

Figure C-37: BJH adsorption plots of cumulative pore volume versus pore diameter for bagasse activated carbons, at steam/nitrogen ratios of 1:0.6 & varying activation temperatures, I – 900 °C, 2hr, J – 800 °C, 4hr & K – 700 °C, 4hr.

Figure C-38: BJH desorption plots of cumulative pore volume versus pore diameter for bagasse activated carbons, at steam/nitrogen ratios of 1:0.6 & varying activation temperatures, I – 900 $^\circ$C, 2hr, J – 800 $^\circ$C, 4hr & K – 700 $^\circ$C, 4hr.

Figure C-39: BJH adsorption plots of pore volume versus pore diameter for bagasse activated carbons, at steam/nitrogen ratios of 1:0.6 & varying activation temperatures, I – 900 $^\circ$C, 2hr, J – 800 $^\circ$C, 4hr & K – 700 $^\circ$C, 4hr.

Figure C-40: BJH desorption plots of pore volume versus pore diameter for bagasse activated carbons, at steam/nitrogen ratios of 1:0.6 & varying activation temperatures, I – 900 $^{\circ}$C, 2hr, J – 800 $^{\circ}$C, 4hr & K – 700 $^{\circ}$C, 4hr.

C-2.4 Comparison of powder and granular bagasse carbons & reference carbon

C-2.4.1.Total Surface Area
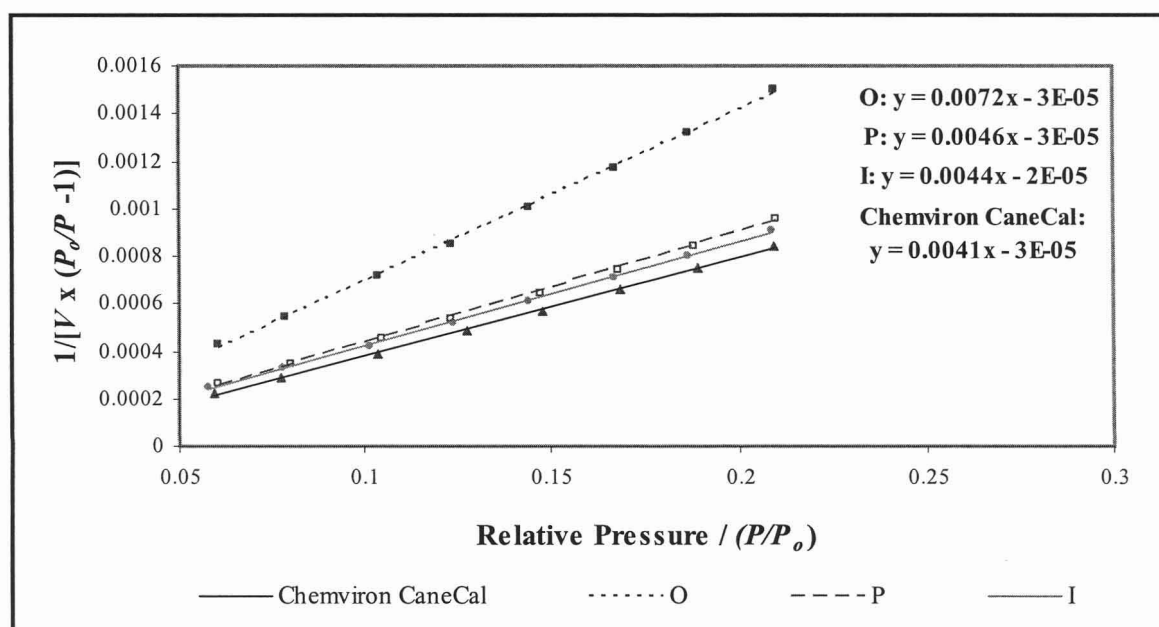
Figure C-41: BET surface area plot for bagasse activated carbons and (▲)reference Chemviron CaneCal carbon, (■)O – 56% ash, powder, (□)P – granular sugar/bagasse, (●)I – 28% ash, powder.

O: y = 0.0053x + 9E-05

P: y = 0.0034x + 4E-05

I: y = 0.0032x + 5E-05

Chemviron Canecal:
y = 0.003x + 3E-05
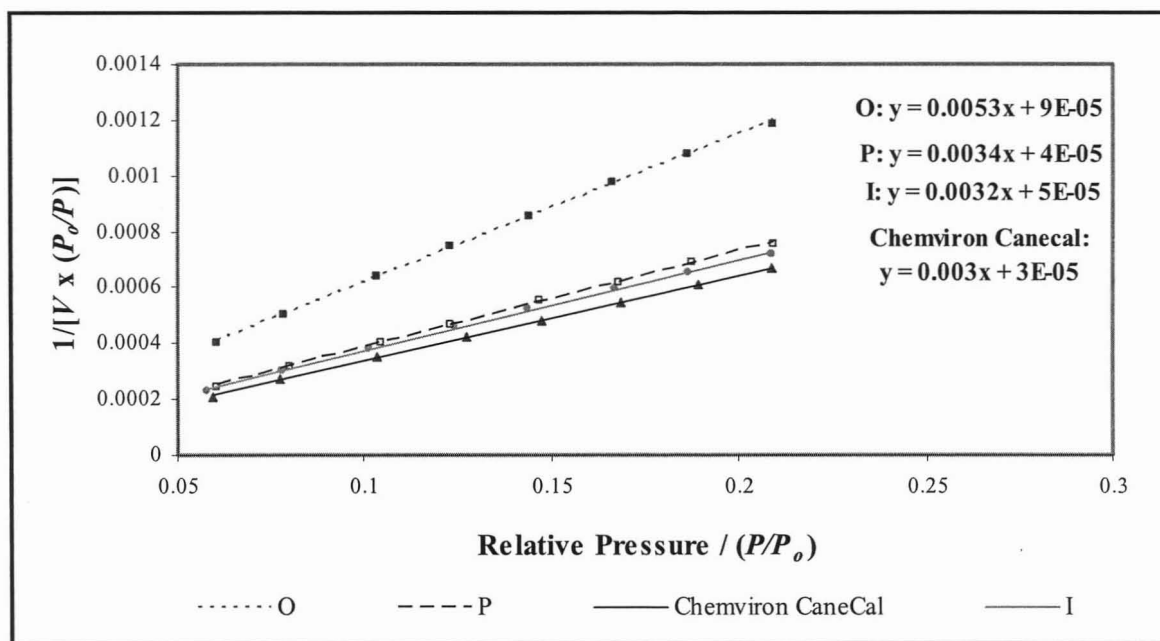
Figure C-42: Langmuir surface area plot for bagasse activated carbons and (▲)reference Chemviron CaneCal carbon, (■)O – 56% ash, powder, (□)P – granular sugar/bagasse, (●)I – 28% ash, powder.

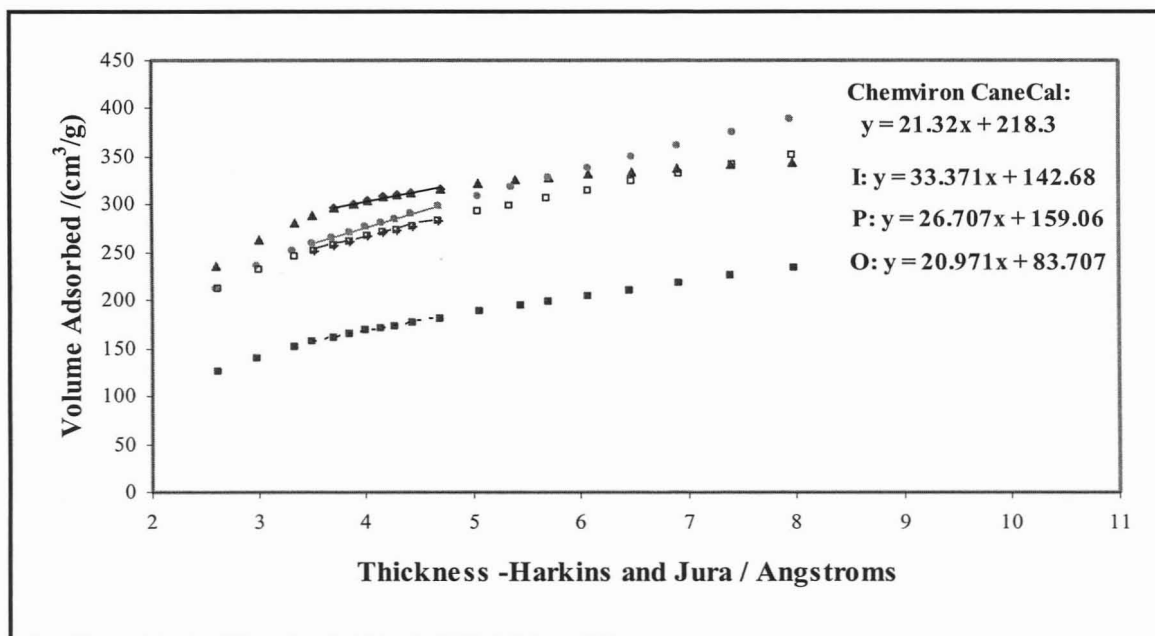## C-2.4.2. External Surface Area, Micropore Area and Micropore Volume

Chemviron CaneCal:
y = 21.32x + 218.3

I: y = 33.371x + 142.68

P: y = 26.707x + 159.06

O: y = 20.971x + 83.707

Figure C-43: t-plot to determine external surface area and micropore volume for bagasse activated carbons and (▲)reference Chemviron CaneCal carbon, (■)O – 56% ash, powder, (□)P – granular sugar/bagasse, (●)I – 28% ash, powder.

C-2.4.3 Meso-macropore size distributions
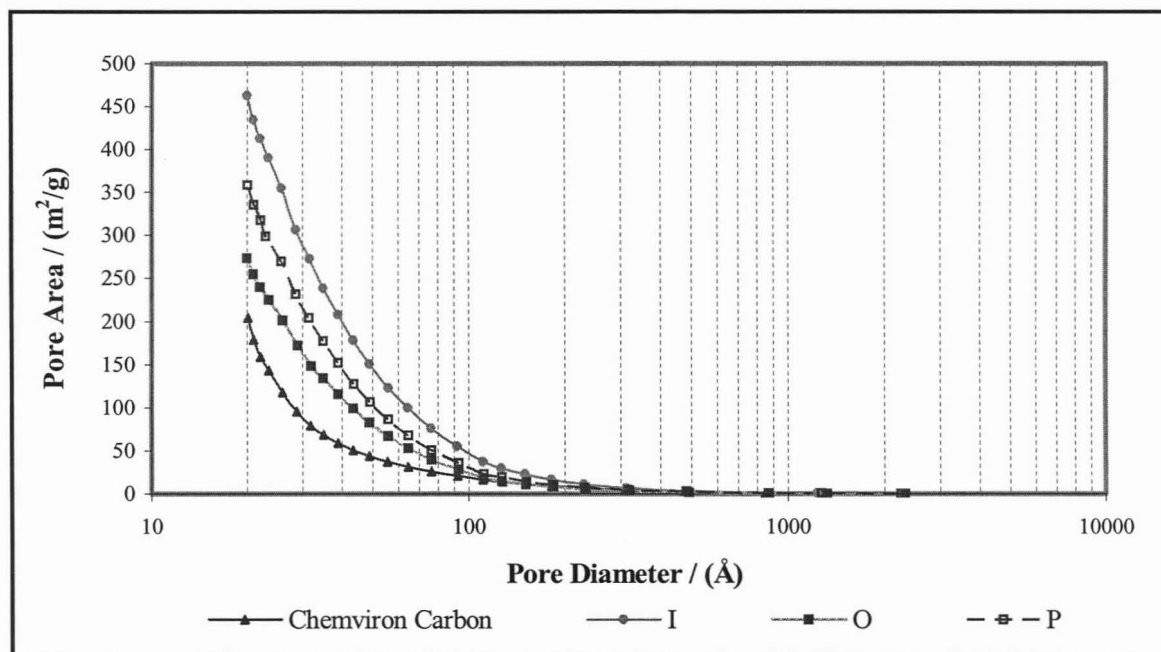
Figure C-44: BJH adsorption plots of cumulative pore area versus pore diameter for bagasse activated carbons and reference Chemviron CaneCal carbon, O – 56% ash, powder, P – granular sugar/bagasse, I – 28% ash, powder.
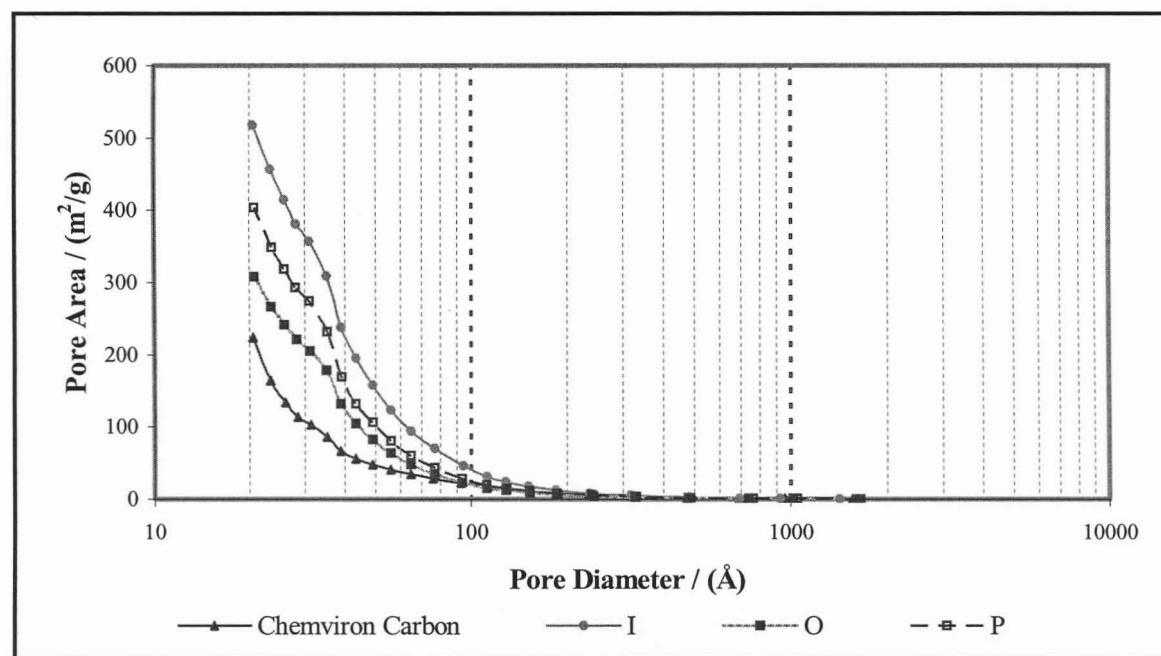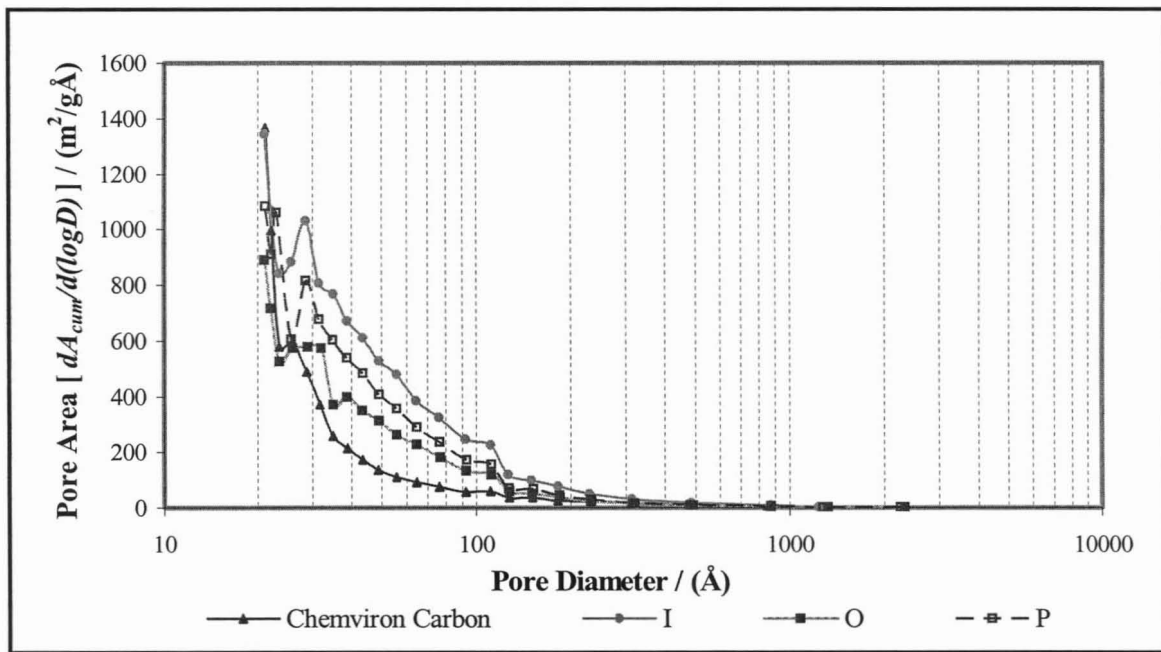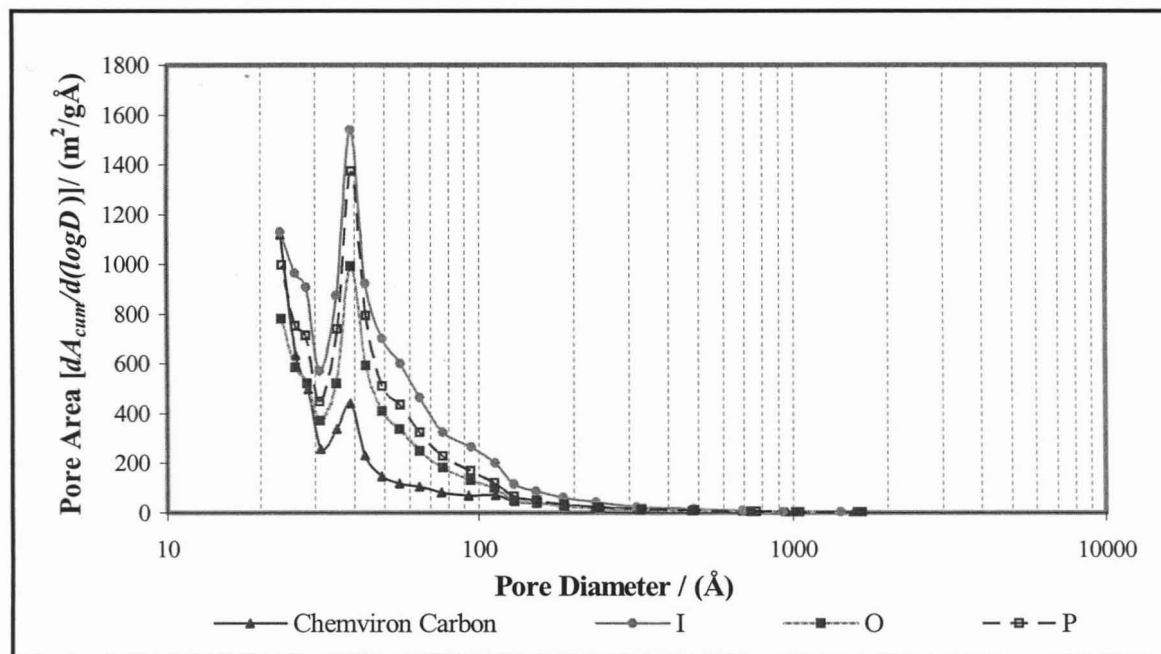

Figure C-45: BJH desorption plots of cumulative pore area versus pore diameter for bagasse activated carbons and reference Chemviron CaneCal carbon, O – 56% ash, powder, P – granular sugar/bagasse, I – 28% ash, powder.

Figure C-46: BJH adsorption plots of pore area($dA_{cum}/d(logD)$) versus pore diameter for bagasse activated carbons and reference Chemviron CaneCal carbon, O – 56% ash, powder, P – granular sugar/bagasse, I – 28% ash, powder.

Figure C-47: BJH desorption plots of pore area ($dA_{cum}/d(logD)$) versus pore diameter for bagasse activated carbons and reference Chemviron CaneCal carbon, O – 56% ash, powder, P – granular sugar/bagasse, I – 28% ash, powder.
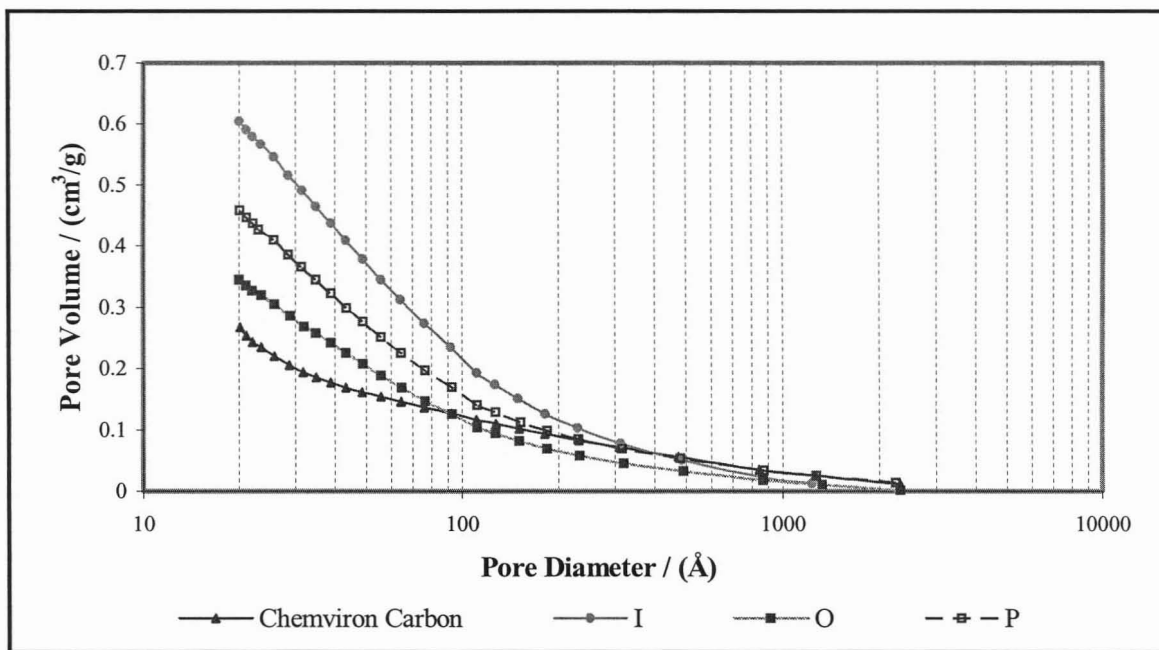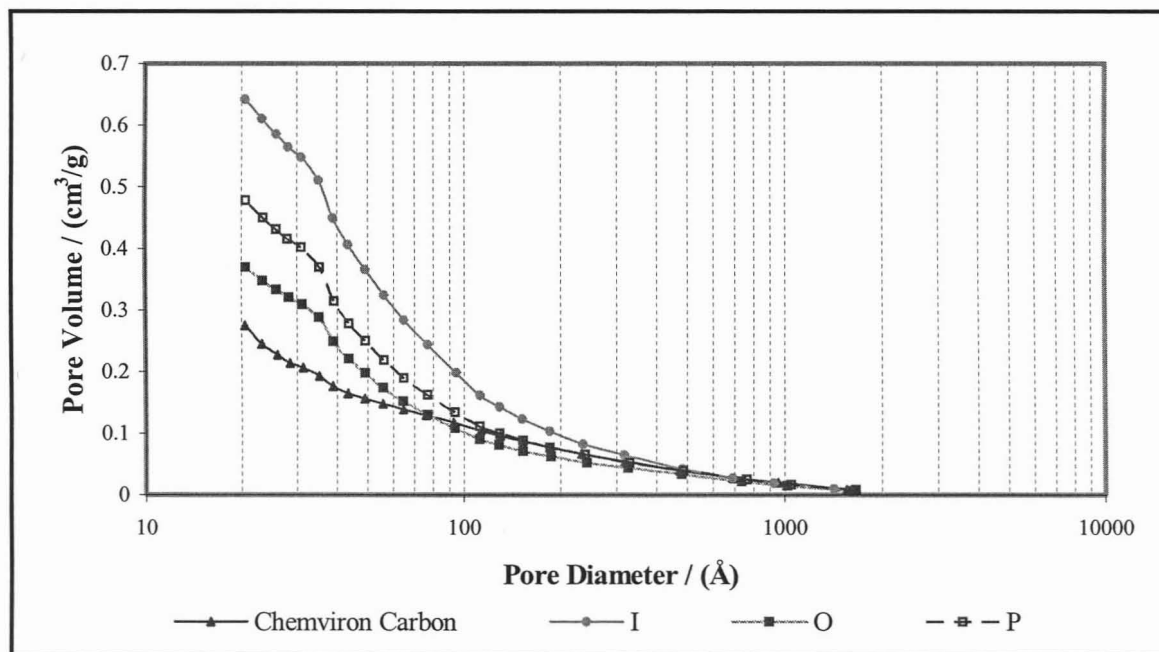
Figure C-48: BJH adsorption plots of cumulative pore volume versus pore diameter for bagasse activated carbons and reference Chemviron CaneCal carbon, O – 56% ash, powder, P – granular sugar/bagasse, I – 28% ash, powder

Figure C-49: BJH desorption plots of cumulative pore volume versus pore diameter for bagasse activated carbons and reference Chemviron CaneCal carbon, O – 56% ash, powder, P – granular sugar/bagasse, I – 28% ash, powder.
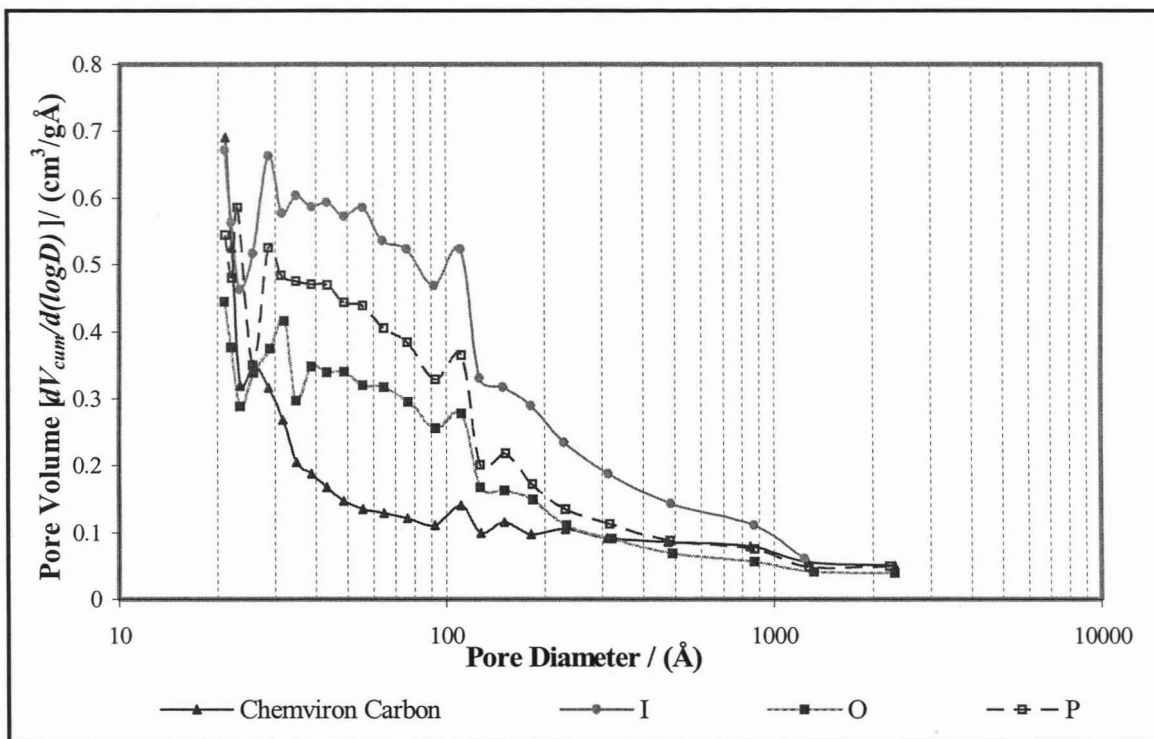
Figure C-50: BJH adsorption plots of pore volume ($dV_{cum}/d(logD)$) versus pore diameter for bagasse activated carbons and reference Chemviron CaneCal carbon, O – 56% ash, powder, P – granular sugar/bagasse, I – 28% ash, powder.
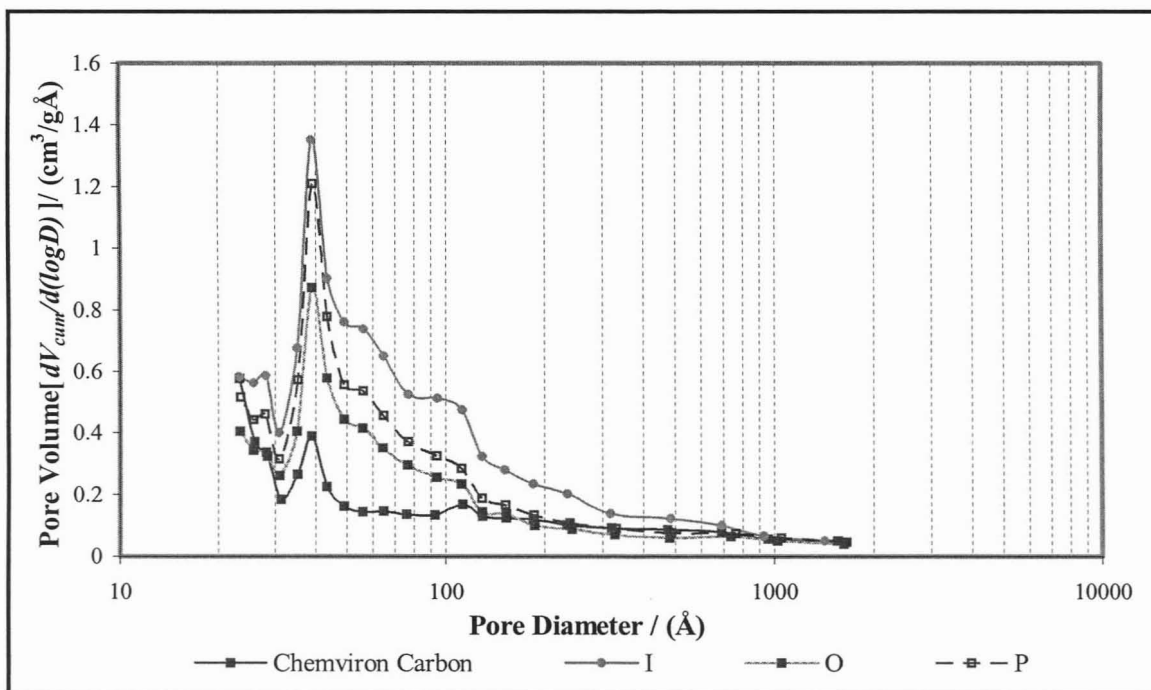

Figure C-51: BJH desorption plots of pore volume ($dV_{cum}/d(logD)$) versus pore diameter for bagasse activated carbons and reference Chemviron CaneCal carbon, O – 56% ash, powder, P – granular sugar/bagasse, I – 28% ash, powder.